Metabolic flux analysis for biosynthesis of volatile terpenoids in model *Lamiaceae* plants

Dissertation

zur Erlangung des

Doktorgrades der Naturwissenschaften (Dr. rer. nat.)

der

Naturwissenschaftlichen Fakultät I – Biowissenschaften –

der Martin-Luther-Universität

Halle-Wittenberg

Vorgelegt

von

Herrn Somnath Koley, M.Sc.

geb. am 18.07.1991 in West Bengal, Indien

Table of Contents

List of Figures

List of Tables

List of Abbreviations

AACT- acetoacetyl coenzyme-A transferase
AcCoA- Acetyl coenzyme-A
ACL- Adenosine tri-phosphate citrate lyase
ACT- aconitate
ADP- Adenosine di-phosphate
AKG- alpha-ketoglutarate
ALD- Aldolase
ARG- arginine
ASP- aspartate
ATP- Adenosine tri-phosphate
CDPMEP- cytidyldiphospho methyl erythritol phosphate
CE- Collision energy
CEST- central European standard time
CIT- citrate
CO2- carbon di-oxide
CS- citrate synthase
CXP- Collision cell exit potential
DALV- days after leaf visibility
DMAPP- dimethylallyl pyrophosphate
DMD- mevalonate pyrophosphate decarboxylase

DP- Declustering potential
DXP- deoxy xylulose phosphate
DXR-deoxy xylulose phosphate reductoisomerase
DXS- deoxy xylulose phosphate synthase
E4P- erythrose 4-phosphate
Eqn- equation
ESI- electrospray ionization
ETC- electron transport chain
F6P- fructose 6-phosphate
FBP- fructose bisphosphate
FDA- fluorescein diacetate
FPP- farnesyl pyrophosphate
FUM- fumarate
G1P- glucose 1-phosphate
G6P- glucose 6-phosphate
GAP/G3P- glyceraldehyde 3-phosphate
GAPDH- glyceraldehyde 3-phosphate dehydrogenase
GGPP- geranylgeranyl pyrophosphate
GLN- glutamine
GLU- glutamate

GPP- geranyl pyrophosphate
GPPS- geranyl pyrophosphate synthase
GT(s)- glandular trichome(s)
h- hour(s)
HIS- histidine
H6P- hexose 6 phosphate (glucose 6-phosphate and fructose 6-phosphate)
HMBPP- hydroxymethyl-but-2-enyl pyrophosphate
HMBPPR- hydroxymethyl-but-2-enyl pyrophosphate reductase
HMGCoA- 3-hydroxy-3-methylglutaryl coenzyme-A
HMGCS- 3-hydroxy-3-methylglutaryl coenzyme-A synthase
INCA- Isotopomer Network Compartmental Analysis
IPP- isopentenyl pyrophosphate
IR- interval range
ISDH- isocitrate dehydrogenase
ISOCIT- isocitrate
LB- lower bound
LEU+ILE- leucine and isoleucine
LYS- lysine
MAL- malate
MDH- malate dehydrogenase
ME- malic enzyme
MEcPP- methyl erythritol cyclodiphosphate
MEP- methylerythritol phosphate
MET- methionine
MFA- metabolic flux analysis
MID- mass isotopomer distribution
Min- minute(s)
MRM- multiple reaction monitoring
MVA- mevalonate
MVA5P- mevalonate 5-phosphate
MVAPP- mevalonate pyrophosphate
NAD- nicotinamide adenine dinucleotide

NADP- Nicotinamide adenine dinucleotide phosphate
OAA/OXA- oxaloacetate
OGA- alpha-ketoglutarate
OGDH- alpha-ketoglutarate dehydrogenase
oxPPP- oxidative pentose phosphate pathway
P5P- pentose 5-phosphate (ribulose 5-phosphate and xylulose 5-phosphate)
PDH- pyruvate dehydrogenase
PEP- phosphoenolpyruvate
PEPC- phosphoenolpyruvate carboxylase
PG- phosphoglycerate (2-phosphoglycerate and 3-phosphoglycerate)
PG6- 6-phosphogluconate
PGI- phosphoglucose isomerase
PGM- phosphoglycerate mutase
PHE- phenylalanine
PI- propidium iodide
PK- pyruvate kinase
PRO- proline
PYR- pyruvate
R5P- ribose 5-phosphate
Ru5P- ribulose 5-phosphate
Rub/RuBisCO- ribulose-1,5-bisphosphate carboxylase/oxygenase
RuBP- ribulose bisphosphate
S7P- sedoheptulose 7-phosphate
SBP- sedoheptulose bisphosphate
SDH- succinic dehydrogenase
SE- standard error
SSR- sum of squared residuals
STDEV- standard deviation
SER- serine
SUC- succinate
THR- threonine
TRP- tryptophan
UB- upper bound
X5P- xylulose 5-phosphate

Chapter I: General introduction

1.1. Natural Products

Natural products have been used for a long time to cure human diseases. Prior to the discovery of synthetic medicines, plant roots, barks and leaves were the main sources of medication. The utilization of plant-based treatment has not lost its importance in this era. For instance, approximately 60% of anticancer compounds come from a diverse source of natural products, including terpenes, flavones, phenylpropanoids and alkaloids(Cirla and Mann, 2003; Cragg et al., 2011).

Natural products are classified into primary and secondary metabolites. Primary metabolites, such as carbohydrates, proteins, fats, etc., have a direct relation in plant growth and reproduction whereas secondary metabolites like terpenes, phenols, etc., are not involved in these processes. Commercially, these plant-based secondary products are often labeled as essential oil and contains more than one natural isolates. The plant needs these secondary metabolites for several important ecological regulations. Essential oils have roles in quenching of ozone (Loreto et al., 2001), protection from ozone-induced oxidative stress (Loreto et al., 2004, 2001; Loreto and Velikova, 2001) and formation of fine particle aerosols (Kulmala, 2003; Palancar and Toselli, 2004; Peñuelas and Llusià, 2003). Moreover, they play a significant role in plant pathology by providing indirect and direct defense against pathogens (De Moraes et al., 2001; Friedman et al., 2002; Hammer et al., 2003), alluring seed disseminators (Goff and Klee, 2006) and pollinators (Buchmann and Nabhan, 1996; Dudareva et al., 2006; Dudareva and Pichersky, 2000), plant-plant signaling (Arimura et al., 2002; Kessler et al., 2006; Ruther and Kleier, 2005; Shulaev et al., 1997) and inducing tritrophic plant-herbivore-carnivore interaction (Dicke and van Loon, 2000; Hilker and Meiners, 2002; Takabayashi and Dicke, 1996).

1.2. Terpenoids

1.2.1. Importance of terpenoids

Terpenoids are the main constituents of secondary metabolites and the largest group of plant metabolites, encompassing more than 40,000 different structures (Bohlmann and Keeling, 2008). Furthermore, these are the predominant component of essential oils. Terpenoids are found in different plant parts like leaves (peppermint), fruits (orange), stems (norway spruce) and roots (Scots pine).

Essential oils of many plants such as vetiver, rosemary, thyme, basil, clove, spearmint and peppermint primarily contain terpenes that prevent the attack of flies, moths, lice and ants. Non-volatile diterpenes establish a non-penetrable physical barrier to defend directly against insect attack (Keeling and

Bohlmann, 2006; Zulak and Bohlmann, 2010). They also have an essential role in the production of phytopigments (such as carotenoids and the phytyl side chain of chlorophyll) as well as the regulation of phytohormone production (Lange and Ghassemian, 2003). Volatile terpenes, comprising monoterpene and sesquiterpene, have great value in various traditional and modern industrial practices. These compounds play an essential role in the flavor and fragrance industry. Examples include eugenol, which produces the flavor of cloves, and linalool, which produces the fragrance of coriander. Essential oils of oregano, thyme, lavender and rosemary are intensively used in cosmetics to fulfil the increasing necessity of the preservative-free, natural and skin-friendly products (Muyima et al., 2002). Volatile organic compounds of peppermint are frequently utilized in many cleansing manufactures (Anchisi et al., 2006). Additionally, volatile monoterpene and sesquiterpene provide an indirect defense against pest and microorganism. Such examples include menthol, which counters the pathogen *Staphylococcus aureus*, and oleoresin, which traps pests.

The emphasis of plant terpenes in the pharmaceutical industry has increased due to various modern innovations. These components have been utilized to cure both common and deadly human diseases. Methanol, the primary constituent of peppermint essential oil, has a cooling effect as well as properties that aid with stress relief. Artemisinin and taxol are used as anti-malarial and anti-cancer drugs, respectively (Croteau et al., 2006; Pollier et al., 2011). The activities of terpenoids as antimicrobial, antioxidant and antidiabetic have already been investigated. For instance, α- and β-pinene have antimicrobial and antioxidant activities. β-carotene and α-tocopherol are also utilized as food additives for Vitamin A and E, respectively.

1.2.2. Terpenoid biosynthesis pathways

Terpenoids are hydrocarbons which are also found in their oxygenated, hydrogenated and dehydrogenated derivatives. The chemical backbone of terpenoids is 2-methylbutane residues. This unit is usually specified as isoprene (2-methyl-1,3-butadiene) which consists of five carbons (C_5) (Breitmaier, 2006). The universal precursors of all terpenoids are two isomeric C_5 isoprene units, namely, isopentenyl pyrophosphate (IPP) and dimethylallyl pyrophosphate (DMAPP). In plants, two pathways are involved in the production of these two precursors (Ajikumar et al., 2008; Cheng et al., 2007; Rohmer, 2003). The description of these pathways is presented in Figure 1.

In earlier studies, the classical mevalonic acid (MVA) pathway has been the only terpene synthesis pathway and mevalonate has been the most important precursor of isoprenes (Chappell, 1995;

Dudareva et al., 2006). It includes seven enzymatic reactions to form IPP and DMAPP from acetyl-CoA (Ajikumar et al., 2008; Nagegowda, 2010). The pathway starts with the Claisen condensation of two molecules of acetyl-CoA (Newman and Chappell, 1999; Rohmer, 2003). In this reaction, acetoacetyl-CoA is formed from those two ester molecules by thiolase (Liao et al., 2006). Another acetyl-CoA is added to acetoacetyl-CoA by an aldol condensation reaction by 3-hydroxy-3-methylglutaryl-CoA synthase to form 3-hydroxy-3-methylglutaryl-CoA (HMG-CoA) (Langenheim, 1994). In the third step, HMG-CoA is converted to (*R*)-MVA by HMG-CoA reductase (HMGR) (Bach, 1995). This step requires two molecules of reduced NADPH. It is the vital step of this biosynthetic route and the MVA is the well-known precursor for many terpenes and sterols. In addition, HMGR is the key regulatory enzyme of this pathway and has been thoroughly investigated in many organisms including the plants, Arabidopsis (Lumbreras et al., 1995) and snapdragon (Nagegowda et al., 2010). In the next two steps, mevalonate kinase and phosphomevalonate kinase catalyze ATP-dependent phosphorylation for consecutive conversion of MVA to MVA 5-phosphate (MVA5P) and MVA5P to MVA 5-pyrophosphate (MVAPP) (Ajikumar et al., 2008). To synthesize the five-carbon compound IPP from the six-carbon compound MVAPP, the latter one loses one carboxyl carbon. This biological reaction is carried out by MVAPP decarboxylase. In the final step, IPP is interchanged to DMAPP by a stereo-specific isomerization process, catalyzed by IPP isomerase (Gershenzon and Kreis, 1999; Heaps and Poulter, 2011).

The alternate route of terpene biosynthesis is the 2-*C*-methyl-erythritol 4-phosphate (MEP) pathway also known as the 1-deoxy-ᴅ-xylulose-5-phosphate (DXP) pathway. It was recently identified in the bacteria *Escherichia coli* (Rohmer et al., 1993). This pathway, which consists of seven enzymatic biochemical reactions, is initiated with the acyloin condensation of one molecule of pyruvate and one molecule of glyceraldehyde-3-phosphate (GAP) by DXP synthase (DXS) with cofactor thiamine pyrophosphate (Dubey et al., 2003; Liao et al., 2006). As a result, DXP is formed which includes all carbons from GAP and second-third positional carbons from PYR. Like HMGR of the MVA pathway, DXS is the rate-limiting and main flux controlling enzyme of the non-mevalonate pathway (Rodríguez-Concepción and Boronat, 2015; Wright et al., 2014). In the second step, DXP is converted to MEP by the activity of DXP reductoisomerase (also known as MEP synthase). The biochemical mechanism of this step is to rearrange and successively reduce DXP by using NADPH as the electron carrier (Mac Sweeney et al., 2005; Proteau, 2004). The pathway progresses as MEP is conjugated with cytidine triphosphate by 2-*C*- methyl- ᴅ- erythritol 4- phosphate cytidylyl- transferase (MCT).

Consequently, 4-diphosphocytidyl-2-*C*-methyl-D-erythritol (CDP-ME) is synthesized and the phosphate group is released (Richard et al., 2004). In further steps, CDP-ME-2-phosphate (CDP-MEP), 2-*C*-methyl-D-erythritol2,4-cyclodiphosphate (MEcPP) and 1-hydroxy-2-methyl-2-(*E*)-butenyl 4-diphosphate (HMBPP) are biosynthesized by the respective enzymatic action of 4-(cytidine 5′-diphospho)-2-*C*-methyl-D-erythritol kinase (CMK), 2-*C*-methyl-D-erythritol 2,4-cyclo diphosphate synthase (MDS) and (*E*)-4-hydroxy-3-methylbut-2-enyl diphosphate synthase (HDS). Towards the end of the pathway, (*E*)-4-hydroxy-3-methylbut-2-enyl diphosphate reductase (HDR) catalyzes the conversion of HMBPP to IPP and DMAPP in a ratio of 5:1 (Rohdich et al., 2003; Tritsch et al., 2010). Finally, IPP isomerase regulates the balance of IPP and DMAPP ratio by stereospecific conversion of IPP to DMAPP (Tritsch et al., 2010).

These two biosynthetic pathways happen independently in two different subcellular compartments. The MVA pathway occurs in the cytosol and the DXP pathway occurs in the plastid. According to the textbook knowledge, the MVA route produces the precursor for sesquiterpene and triterpene. On the contrary, monoterpene, diterpene and tetraterpene are biosynthesized from non-mevalonate means (Dudareva et al., 2006). In higher plants, IPP produced from the cytosolic MVA pathway is also responsible for mitochondrial terpenoid biosynthesis (Dubey et al., 2003).

1.2.3. Classes of terpenoids

Terpenoids are basically synthesized by head-to-tail condensations of IPP and DMAPP as drawn in Figure 2. These biogenic reactions are catalyzed by one large family of enzymes, recognized as terpene synthases or cyclases (TPS). Initially, the monoterpene biosynthetic precursor, geranyl pyrophosphate (GPP) is formed by the addition of one molecule of IPP to one molecule of its isomer DMAPP. Likewise, farnesyl pyrophosphate (FPP) and geranylgeranyl pyrophosphate (GGPP), which are the respective precursors of sesquiterpene and diterpene, are sequentially condensed with supplementation of further IPP to GPP. Based on the number of homologous chains of isoprene units in their structure, terpenoids are classified into nine sub-classes as presented in Table 1. (Ashour et al., 2010; Martin et al., 2003; McGarvey and Croteau, 1995; Page et al., 2004) Structurally diverse cyclic or acyclic terpenoids of each class are produced through different reaction mechanism such as hydration, isomerization, conjugation, oxidation, reduction and other transformations (McGarvey and Croteau, 1995).
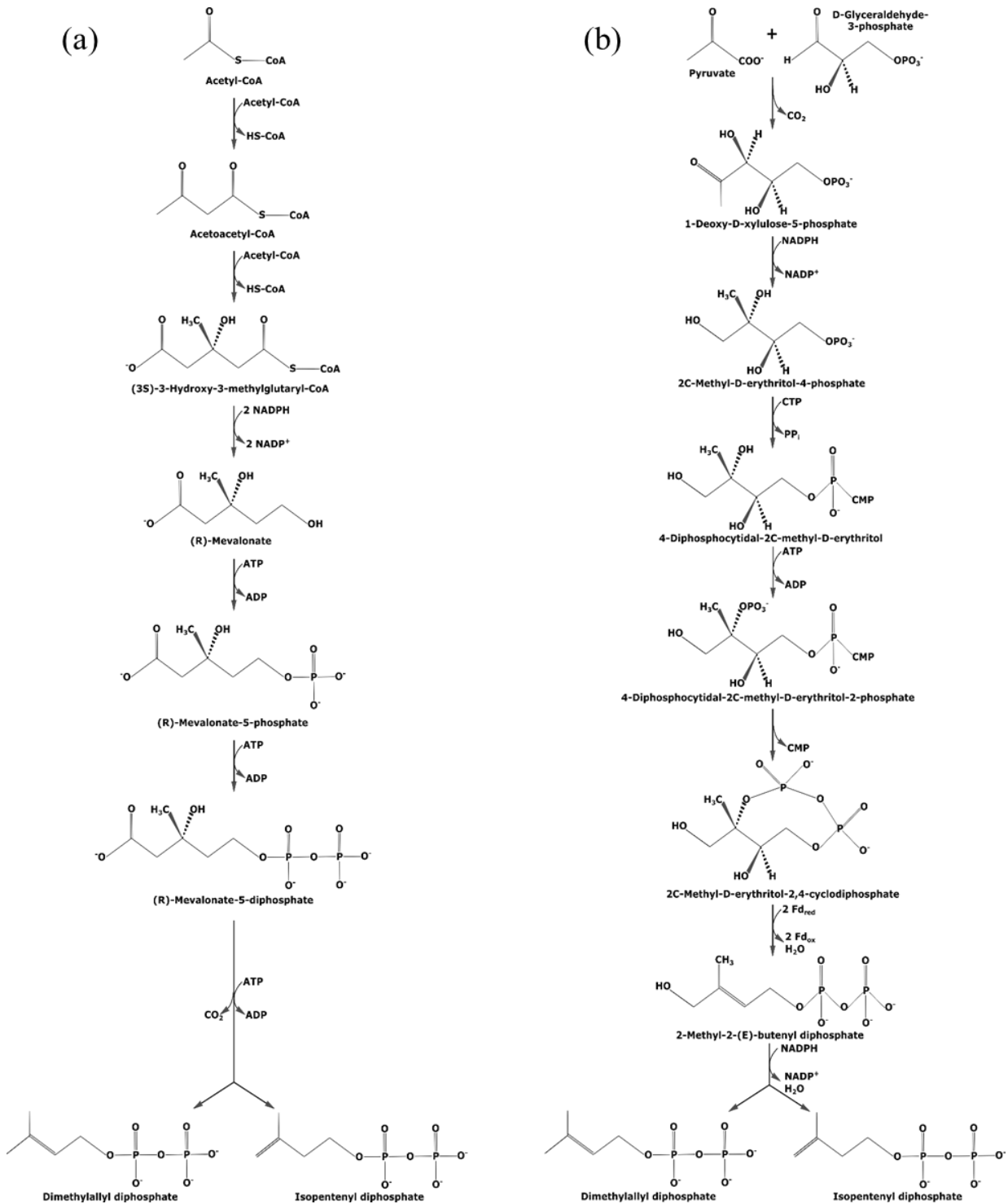
Figure 1. Biochemical reactions via two terpenoid biosynthetic pathways.

(a) MVA and (b) DXP pathway.

Table 1. Different classes of the terpene.

C_5 Isoprene (I)	Basic Formulae	Terpene Class	Precursor	Example
1×I	C_5H_8	Hemiterpene, Prenyl group	Isopentenyl pyrophosphate (IPP) or Dimethylallyl pyrophosphate (DMAPP)	Isoprene, Cytokinin
2×I	$C_{10}H_{16}$	Monoterpene	Geranyl pyrophosphate (GPP) (1 molecule of IPP and 1 molecule of DMAPP)	Menthol
3×I	$C_{15}H_{24}$	Sesquiterpene	Farnesyl pyrophosphate (FPP) (1 molecule of IPP and 1 molecule of GPP)	Artemisinin, Juvabione
4×I	$C_{20}H_{32}$	Diterpene	Geranylgeranyl pyrophosphate (GGPP) (2 molecules of IPP and 1 molecule of GPP)	Gibberellins, Taxol, Vitamin A
5×I	$C_{25}H_{40}$	Sesterpene	1 molecule of FPP and GPP	Ophiobolin A
6×I	$C_{30}H_{48}$	Triterpene	2 molecules of FPP	Squalene
8×I	$C_{40}H_{64}$	Tetraterpene	2 molecules of GGPP	Carotenoids
n×I	$C_{5n}H_{8n}$	Polyterpene	FPP or GGPP	Natural rubber
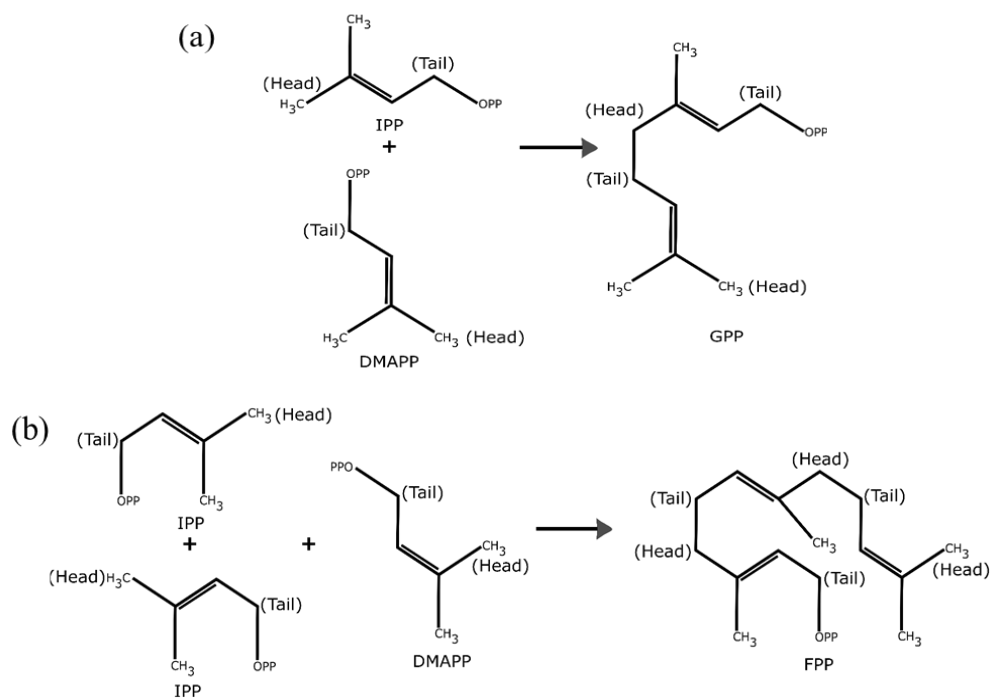
Figure 2. Head to tail condensation of isoprene units.

IPP and DMAPP are attached for the production of (a) GPP and (b) FPP.

1.2.4. Monoterpenes and sesquiterpenes in peppermint

Peppermint (*Mentha piperita*), a herb from Lamiaceae family, is commercially the most valuable essential oil producing plant for their strong aroma (Morris, 2006). The principal constituent of this essential oil is monoterpene (Rohloff, 1999). Hence, peppermint has been used as a model system for studying monoterpene biosynthesis. In addition, two sesquiterpenes are also included in the oil extract of this plant. In the course of present study, peppermint monoterpenes have been mainly emphasized.

Monoterpenes and sesquiterpenes, synthesized in this Lamiaceae plant, are listed in Figure S1. The monoterpene biosynthesis pathway is commenced by (-)-limonene synthase enzyme activity. It converts GPP to (-)-limonene (Alonso et al., 1992; Colby et al., 1993). Subsequently, (-)-limonene 3-hydroxylase catalyzes a cytochrome P450-dependent hydroxylation of (-)-limonene (Lupien et al., 1999) to form (-)-trans-isopiperitenol, which is further oxidized to (-)-isopiperitenone by (-)-trans-isopiperitenol dehydrogenase (Ringer et al., 2005; Turner and Croteau, 2004). (+)-cisisopulegone and (+)-pulegone are produced by double-bond reduction reaction (Ringer et al., 2003) and isomerization (Kjonaas et al., 1985), catalyzed by (-)-isopiperitenone reductase and (+)-cis-isopulegone isomerase, respectively. Pulegone is an important part of monoterpene biosynthesis in peppermint as it feeds into three branches. One branch directly generates the (+)-menthofuran by (+)-menthofuran synthase activity (Bertea et al., 2001). The second branch forms (-)-menthone by the action of (+)-pulegone reductase (Ringer et al., 2003). Then, menthone is converted to neomenthol and menthol by reductases (Davis et al., 2005). A similar kind of reductase activity produces isomenthone from pulegone for the (Ringer et al., 2003), which is subsequently used to synthesize isomenthol and neoisomenthol (Davis et al., 2005). Geranyl pyrophosphate also feeds into two other monoterpene branches. 1,8-cineole synthase catalyzes transformation to 1,8-cineole (Croteau et al., 1994), whereas (-)-limonene synthase also produces three side products, α-pinene, β-pinene and myrcene (Bohlmann et al., 1997). Two sesquiterpenes, namely β-caryophyllene and germacrene D, are synthesized from FPP by the action of β-caryophyllene synthase (Cai et al., 2002; Chen et al., 2003) and germacrene D synthase (Schmidt et al., 1999), respectively.

1.2.5. Trichome cell

Monoterpene and sesquiterpene biosyntheses in the mint subfamily occur inside the specialized peltate glandular trichome cells (Gershenzon et al., 1989; McCaskill et al., 1992). These cells are generally located upon the aerial surface of leaves (Amelunxen, 1965; Fahn, 1979). Peltate cells consist of a basal cell, a stalk cell, secretory cells and a sub-cuticular storage cavity (Figure 3). Eight secretory cells are present in each trichome and only these cells are capable of synthesizing monoterpenes and sesquiterpenes. Produced volatiles are released from secretory cells and are accumulated in the storage cavity. Stored volatiles can be lost from the cavity through volatilization, metabolic degradation, or other routes. However, this loss does not happen in peppermint plant (Gershenzon et al., 2000), possibly because of the presence of hard cuticle layer outside the cavity.
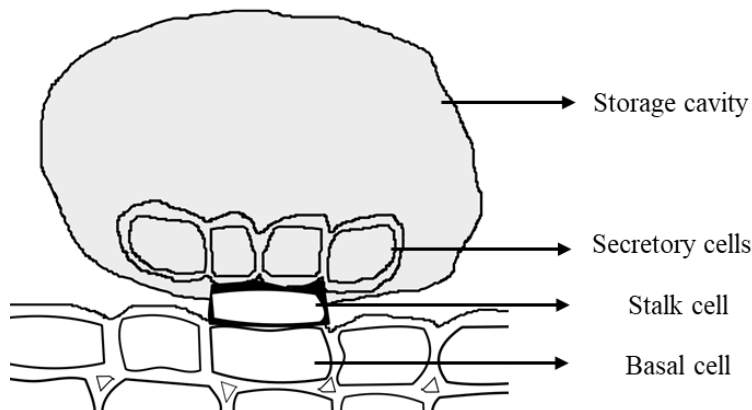
Figure 3. Diagram of peppermint peltate glandular trichome cells.
This figure is adapted from Turner et al. (1999).

1.3. Metabolic flux analysis

1.3.1. Importance of metabolic flux analysis

The ever-increasing demand for food (Ray et al., 2013; Tilman et al., 2011) coupled with increasing dependence on plants as a primary source of medicines (supplying 50% of modern drugs) (Li and Weng, 2017; Pan et al., 2013) has heightened the need to optimise plant biochemistry. Enhancing valuable end-product biosynthesis without losing the product quality is the main concern in molecular pharming. Despite the discovery of new enzymes and their regulatory controls, the specifity of pathways to cell and/or organelle, developmental stage and biotic/abiotic stress response are still very ambiguous. Also, the intracellular metabolic fluxes are adapted as per the demands and the

8

physiological state of the cell (Kruger and Ratcliffe, 2015), so information about metabolic fluxes cannot be generalized at any spatial or temporal level. Thus, additional information on metabolic fluxes is even more imperative than information on the metabolites themselves for determining an authentic metabolic phenotype (Allen, 2016; Ratcliffe and Shachar-Hill, 2005). Moreover, plants have the capability to adapt to environmental perturbations by altering their metabolism. In unfavorable conditions, their survival comes at the cost of their productivity. To increase overall yield in any adverse condition, it is imperative to understand metabolic bottlenecks involved in the production of these high-value compounds.

Quantification of biochemical fluxes is thereby necessary for metabolic engineering and functional genomics. Adduct import and product export rates of the organism are readily determined by different biochemical assays. However, the estimation of intracellular fluxes is more challenging because multiple central metabolic pathways supply identical precursors (Bonarius et al., 1997). Hereof, metabolic flux analysis (MFA) has evolved as a standard tool for visualizing metabolic phenotype, in which the fate of the importers allows us to infer more accurately the relative fluxes through different metabolic networks (Libourel and Shachar-Hill, 2008; Shachar-Hill, 2013). Flux is calculated by applying mass balances of the metabolites based on the fundamental mass conversion theory of Heinrich and Schuster (1996). Within metabolic flux, all incorporated mass must be recovered, transformed into other metabolite or remain the same. MFA determines the flow of matter through the pathway network for synthesizing the specific end product and delivering the phenotype (Ratcliffe and Shachar-Hill, 2005). Consequently, it characterizes the net flux of each pathway, such as separate biochemical fluxes of carbon di-oxide (CO_2) fixation by ribulose-1,5-bisphosphate carboxylase/ oxygenase (RuBisCo) and phosphoenol pyruvate carboxylase (PEPC).

Flux measurement is necessary to solve the plant network puzzle. It can be estimated in two ways. One strategy is quantitative analysis to determine the alteration of substrate uptake and product excretion rate. Flux balance analysis (FBA) is a well-known metabolic tool for this strategy. It is based on a linear programming approach that is inexpensive and able to compute many reactions in a single model. However, it predicts the fluxes based on the assumption that network stoichiometry is optimized for fulfilling a certain biological goal (such as growth) (Bonarius et al., 1997; Converti and Perego, 2002). The second strategy involves the qualitative analysis from the incorporation of the labeled substrate in the system where label flow is measured from isotopic patterns of intermediates

and end-products. This approach is performed by MFA which has the potential to measure all real-time fluxes simultaneously. The latter approach is more powerful as it decides the actual fluxes.

The preliminary condition for performing MFA is the metabolic steady-state of the organism. To achieve this condition, the metabolite production rate should be in linear phase during the experiment. MFA is performed via two mutually exclusive experimental approaches. Fluxes can be determined either by isotopic non-stationary state or by steady-state. $^{13}CO_2$ is incorporated into the plant system via photosynthesis for the non-stationary or dynamic procedure. It is also known as INST-MFA. The distribution of labeled carbon into the intermediate of the different pathways is analyzed at different time point until the the isotopic equilibrium phase is reached. The main advantage of INST-MFA is that it does not need isotopic steady-state, which is hard to maintain in the mixotrophic system for a long time. Consequently, non-stationary experiments are generally performed in pseudo-natural condition. It also presents kinetic properties of the included enzymes in the flux map. In contrast, the steady-state approach needs both isotopic and metabolic equilibrium phase (Roscher et al., 2000; Wiechert and Nöh, 2005) where the isotopic study is initiated with positionally labeled substrates, rather using $^{13}CO_2$. The steady-state MFA provides a large scale flux map for the primary metabolism.

1.3.2. Isotopic tracer study

Labeling information of different intermediates and end-product(s) from the isotopic study are the major input to the MFA model. Although steady-state MFA is new in this era, labeling study had been started earlier to understand the regulation of central carbon fluxes. Different isotopic tracers have been utilized to solve different pathways and fulfil certain metabolic objectives, as highlighted in Table 2. ^{13}C sugar is largely consumed for this kind of study, as every living organism needs sugar for its growth and development. Among the sugars, isotopic glucose is cheaper in price than the others and is readily available through online vendors. Selection of the labeled position in the tracer is the critical aspect and depends upon the key pathway for the study of interest. For example, $1\text{-}^{13}C_1$ glucose has been mostly used in ^{13}C-MFA investigation to understand central metabolic biochemistry. The first carbon of glucose remains in pyruvate (PYR) when the sugar is metabolized via glycolysis. However, this carbon is lost in the pentose phosphate pathway (PPP) by the activity of phosphogluconate dehydrogenase. Consequently, no label isotope is transferred into the PYR. Therefore, feeding of $1\text{-}^{13}C_1$ glucose tracer facilitates to quantify the flux distribution of PPP and glycolysis towards end-product biosynthesis.

10

Table 2. Previous reports of isotopic tracer studies in different plants.

Labeled isotope used	Objective of the study	Reference
1-, 2- and 6-$^{14}C_1$ or $^{13}C_1$ glucose	Compartmented metabolic fluxes in maize root tips	(Dieuaide-Noubhani et al., 1995)
1-$^{13}C_1$ glucose	Contribution of anapleorosis and TCA cycle to respiration and biosynthesis and to intracellular pH regulation during hypoxia in maize root tips	(Edwards et al., 1998)
U-$^{14}C_5$ choline	Glycine betaine synthesis pathway in tobacco	(McNeil et al., 2000)
U-$^{14}C_3$ glycerol, 1-$^{13}C_1$ glucose, U-$^{14}C_6$ glucose and fructose	Influence of fructose 2,6-bisphosphate on non-photosynthetic carbohydrate metabolism in plants	(Fernie et al., 2001)
U-$^{14}C_6$ leucine, 1-$^{14}C_1$ and 1-$^{13}C_1$ glucose	Stability of central metabolism and flexibility of anabolic pathways during the growth cycle of tomato cells	(Rontein et al., 2002)
L-Phenyl-$^2H_5$-alanine	Analysis of the phenylpropanoid pathway in wound-healing potato tuber	(Matsuda et al., 2003)
U-$^{13}C_6$, 1,2-$^{13}C_2$, 1-$^{13}C_1$, 6-$^{13}C_1$ and 2-$^{13}C_1$ glucose	Analysis of glycolysis and the oxPPP during embryo development stage in rapeseed	(Schwender et al., 2003)
U-$^{13}C_{12}$ sucrose	Quantification of metabolic fluxes in different subcellular compartments during embryo development stage in soybean	(Sriram et al., 2004)
L-phenyl-$^2H_5$-alanine, $^2H_7$-benzyl alcohol, $^2H_6$-benzaldehyde, U-$^{14}C_9$-phenylalanine, 1-$^{14}C_1$ acetyl CoA and 7-$^{14}C_1$ benzoyl-CoA	Understanding of *in vivo* benzenoid metabolism in petunia petal tissue	(Boatright et al., 2004)
U-$^{13}C_6$, U-$^{14}C_6$ and 1-$^{13}C_1$ glucose	Evidence of a new futile cycle for a glucose-6-phosphate to glucose turnover in maize root tips	(Alonso et al., 2005)
U-$^{13}C_6$ glucose	Recycling of glucose in tobacco plants via central carbon metabolism	(Ettenhuber et al., 2005a)
l-$^{14}C_1$ tyrosine and l-$^{14}C_1$ tyramine	Analysis of the phenylpropanoid pathway in elicitor-treated potato tuber tissue	(Matsuda et al., 2005)

Labeled isotope used	Objective of the study	Reference
$3,4\text{-}^{14}C_2$, $1\text{-}^{14}C_1$, $2\text{-}^{14}C_1$, $6\text{-}^{14}C_1$, U-$^{14}C_6$ and $1\text{-}^{13}C_1$ glucose and $1\text{-}^{14}C$ gluconate	Investigation of the impact of cold temperature in carbohydrate metabolism regulation of potato tubers	(Malone et al., 2006)
$1,2\text{-}^{13}C_2$ and U-$^{13}C_6$ glucose, U-$^{13}C_3$ and ^{15}N alanine, U-$^{13}C_5$ and ^{15}N glutamine	Understanding of the mitochondrial central carbon metabolism during embryo development stage in rapeseed	(Schwender et al., 2006)
U-$^{13}C_6$ glucose and U-$^{13}C_{12}$ sucrose	Analysis of central carbohydrate metabolism during kernel development stage in maize	(Spielbauer et al., 2006)
$1\text{-}^{13}C_1$ and $2\text{-}^{13}C_1$ glucose and U-$^{13}C_5$ glutamine	Central metabolic fluxes in developing sunflower embryos	(Alonso et al., 2007)
$1\text{-}^{13}C_1$ and U-$^{13}C_6$ glucose	Study the respiratory substrate in Arabidopsis	(Kruger et al., 2007)
U-$^{13}C_{12}$ sucrose	Understanding of effect of temperature on protein and oil biosynthesis in developing soybean cotyledons	(Iyer et al., 2008)
$1\text{-}^{13}C_1$ glucose	Central carbon fluxes in heterotrophic Arabidopsis cells	(Williams et al., 2008)
U-$^{13}C_6$ and U-$^{14}C_6$ glucose, U-$^{14}C_{12}$ sucrose, U-$^{13}C_5$ and U-$^{14}C_5$ glutamine and U-$^{14}C_4$ asparagine	The role of light in soybean seed filling metabolism	(Allen et al., 2009a)
U-$^{14}C_6$, $1\text{-}^{13}C_1$ and $2\text{-}^{13}C_1$ glucose, U-$^{14}C_6$ fructose, U-$^{14}C_5$ and U-$^{13}C_5$ glutamine	Understanding fatty acid synthesis in developing maize embryos	(Alonso et al., 2010)
U-$^{14}C_6$, $1\text{-}^{13}C$ and U-$^{13}C_6$ glucose	Central carbon fluxes in the endosperm of developing maize seeds	(Alonso et al., 2011)
U-$^{13}C_{12}$ sucrose, U-$^{13}C_6$ glucose, U-$^{13}C_5$ glutamine and U-$^{13}C_3$ alanine	Understanding subcellular primary metabolism and exchange of amino acids between compartments during embryo development stage in rapeseed	(Allen et al., 2012)
U-$^{13}C_5$ and U-$^{14}C_5$ glutamine, U-$^{13}C_4$ and U-$^{14}C_4$ asparagine, U-^{14}C sucrose, U-^{14}C and $1,2\text{-}^{13}C_2$ glucose	Understanding the carbon and nitrogen provisions for altering the metabolism in developing soybean embryo	(Allen and Young, 2013)
U-$^{13}C_5$ glutamine	Understanding the metabolism in developing soybean embryo from ^{13}C enrichment in the peptide	(Mandy et al., 2014)
U-$^{13}C_9$ phenylalanine	Assessment of lignin metabolic flux in Arabidopsis stems	(Wang et al., 2018)

1.3.3. Mass isotopomers

To get the flux map of the carbon metabolism, plant samples from the isotopically enriched tracer study are analyzed by mass spectrometry (MS) or nuclear magnetic resonance (NMR). The major analytical output for performing ^{13}C-MFA is the mass isotopomer distribution (MID) of each metabolite. Mass isotopomers are defined as isotopic isomers having the same nominal mass with identical elemental and chemical compositions, but with different positions of their isotopes. The lowest mass isotopomer is referred to as (M+0) which contains only unlabeled molecule. Succeeding mass isotopomers (M+1, M+2 …. and M+n; where n is the number of carbon atom in the molecule) are noted according to their mass differences to (M+0) due to gradual enrichment of ^{13}C isotope. In total, (n+1) different isotopomers are present for every molecule. In addition, the positional isotopomers are distinguished by the positional arrangement of the isotope. The number of positional isotopomers is equal to 2^n (Christensen and Nielsen, 1999). For instance (Figure 4), a two-carbon compound has three different mass isotopomers and four different positional isotopomers. The MID data of each metabolite is incorporated into flux analysis software where it is processed and simulated to find the global optimal solution of the carbon flux.
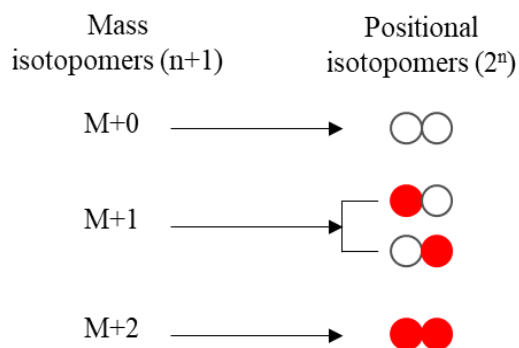
Figure 4. Mass isotopomers and positional isotopomers of the two-carbon compound.
White and red circles denote ^{12}C and ^{13}C, respectively.

1.3.4. Tools for performing MFA

A mathematical model is required to determine the unknown fluxes towards the compound of interest. Several software tools have been evolved in the past 20 years for performing MFA, as listed in Table 3. Due to the development of tandem MS and NMR, precise measurement of MID in a large number of intermediate and end metabolites is much easier and less variable than a correct assessment of

target metabolite quantity. Hence, in ^{13}C-MFA, extra metabolite information improves the accuracy of the flux measurement and increases the confidence of flux value. Therefore, ^{13}C-MFA provides a more realistic outcome of metabolism than stoichiometric MFA. Several kinds of mathematic modelling have been approached to reduce the burden of MFA, such as balancing contributions of data for isotopomers (Schmidt et al., 1997), cumomers (Wiechert et al., 1999) and bondomers (van Winden et al., 2002). Most recent approaches used for flux analysis are based on the balancing of elementary metabolite units (Antoniewicz et al., 2007a). Isotopomer Network Compartmental Analysis (INCA) (Young, 2014) is one of the software tools which is user-friendly, and this mathematical approach has also been used in the present study.

Table 3. List of software applications for MFA.

Software tools	References
13C-Flux	(Wiechert, 2001)
NMR2Flux	(Sriram et al., 2004)
FiatFlux	(Zamboni et al., 2005)
4F	(Ettenhuber et al., 2005b)
Mathematica-based program	(Selivanov et al., 2006)
METRAN	(Antoniewicz et al., 2007a)
13C-FLUX2	(Weitzel et al., 2007)
OpenFLUX	(Quek et al., 2009)
FIA	(Srour et al., 2011)
Influx_s	(Sokol et al., 2012)
INCA	(Young, 2014)

1.4. Instrumentation

1.4.1. Mass spectrometer

Highly precise measurement is required for accurate flux quantification. Stable isotopes from the labeling experiment are detected and analyzed by MS or NMR. Although NMR is the most direct way to measure the isotope enrichment, it needs a larger amount of sample and thorough knowledge of complex analysis. MS has higher sensitivity than NMR, where sample separation is performed by either gas chromatography (GC) or liquid chromatography (LC).

Injected samples for GCMS analysis are mostly liquid and they are infused into the heated liner (injector). These liquids, such as hexane and pentane, are easily volatilized. Some samples also are processed with derivatizing agents (e.g. BSTFA, MSTFA, etc) in order to increase the volatility and thermal stability of the compounds for the GCMS analysis. For faster, solvent-free and efficient extraction or injection, solid phase micro extraction fiber (SPME) has been invented. Due to its easy handling procedure, use of SPME fiber has been observed in many reports (Baranauskienė et al., 2006; Bouvier-Brown et al., 2007; Coleman III et al., 2004, 2002; Hamm et al., 2005; Johnson et al., 2004; Rohloff, 1999; Yeung et al., 2003). In the present study, SPME fiber has been used for volatile terpene extraction. The main components of the SPME instrument are the plunger, plunger retaining screw, barrel, O-ring, black adjustable depth gauge, septum piercing needle, fiber attachment needle and polymer coated fiber (Figure 5). The fiber contains one of the following stationary phases; carboxen (CAR)-polydimethylsiloxane (PDMS), only PDMS, PDMS-divinylbenzene (DVB), polyacrylate, polyethylene glycol, DVB-CAR-PDMS, carbowax (CW)-templated resin (TPR), CW-DVB, or bare fused silica.

Volatile terpenes are extracted by PDMS containing SPME fiber. The piercing needle penetrates the sample vial through the septum cap. The fiber attachment needle and coated fiber are exposed to the inside of the vial by the vertical downward movement of the plunger. At the end of the upper vertical Z- slot, the plunger is rotated to the left part of the horizontal slot where the retaining screw is fixed. This should be performed in such a manner so that the coated fiber is close to the sample, but does not come into contact with it. The SPME stand holds the SPME assembly in this position. Analytes are adsorbed into the stationary phase of the fiber from the sample matrix until equilibrium is reached. Afterward, fiber is retracted by rotating the plunger counterclockwise into the horizontal slot and moving up until the retaining screw reaches the highest position. The assembly is withdrawn from the

sample vial and then introduced into the heated GC liner where analytes are rapidly desorbed and moved into the column.
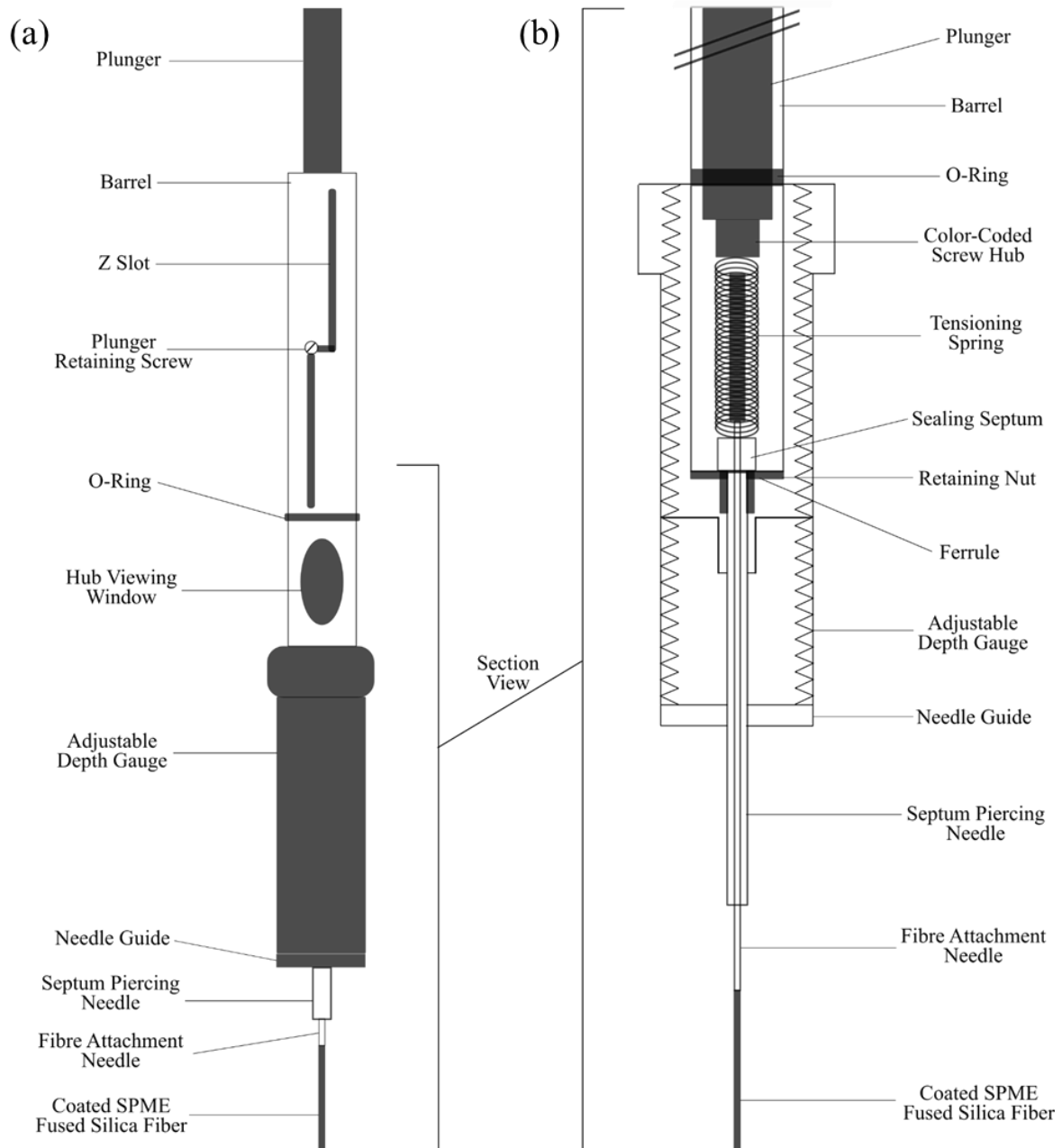
Figure 5. Diagram of SPME device.

(a) SPME fiber holder (b) cross-section of fiber assembly (Figure is adapted from Supelco Data Sheet No. T713019A, 1998)

Instrumentation

Many complex organic and biochemical mixtures (Skoog et al., 2007) are volatilized, ionized and detected by GCMS. The basic methodology of GCMS is depicted in Figure 6. Samples are vaporized by the heated liner and mixed with the carrier gas to create a high velocity of the sample. This inert gas is purified before introducing into GC component. The volatilized mobile phase is then entrained into the GC column. Fully packed coated silica particles or hollow capillary columns are used as the GC column. The stationary phase is coated onto the inner wall in the capillary column. This column is heated at a certain temperature by the GC oven for better separation of the metabolites of interest. Separated molecules are then moved to the MS component via an interface. They are ionized by the electron impact or chemical ionization source. On the basis of mass to charge ratio (m/z), ions are separated by high level of vacuum inside mass analyzer. The certain ion beam for specific m/z value is directed onto the detector lens and transformed into a spectrum signal. This signal represents different lines of fragments from the molecule in the analysis software. Tandem MS contains one extra selection of ions for increasing precision and selectivity of the compound. In this GCMS/MS, a certain mother ion is further fragmented into daughter ions. The compound is detected after these two selections on the basis of a specific daughter ion that is emerged from the specific mother ion.
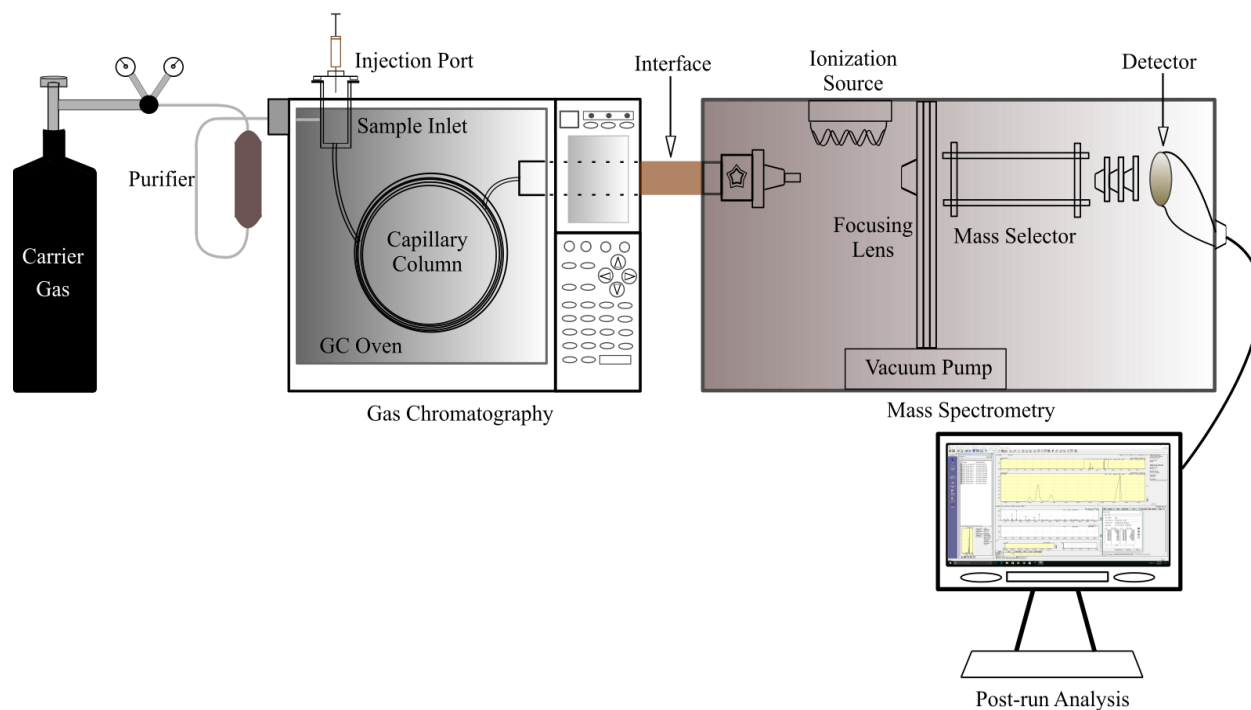
Figure 6. Schematic diagram for the basic principle of GCMS.

The main limitation of GCMS is the requirement that the gaseous samples have high thermal stability. Therefore, the utilization of GCMS is confined to relatively low molecular mass or non-polar compounds. In contrast, substances, which are dissolved in a liquid phase, can be analyzed by LCMS. The applicability of LCMS is broad from high to low polarity with a wide range of molecular weight. Derivatizing agents are also not required in LCMS for sample processing. The mobile phase(s) is selected on the basis of sample elution. In the autosampler, a specified volume of the sample is injected into the mobile phase *en route* to the column. Generally, C18 and C30 reverse phase columns are used for analysis of hydrophilic and hydrophobic metabolites, respectively. Inside the column, various metabolites interact with the stationary phase of the column and thus travel at different speeds. As a consequence, different metabolites reach the MS at a different time (retention time) depending upon their interaction with the stationary phase of the column. Unlike GCMS, the liquid phase is transferred to the MS part where it is converted to a mist of charged droplets by electrospray ionization (ESI) or atmospheric pressure chemical ionization (APCI). The basic principle of the rest MS part of LCMS is similar to the GCMS instrument (Figure 7).
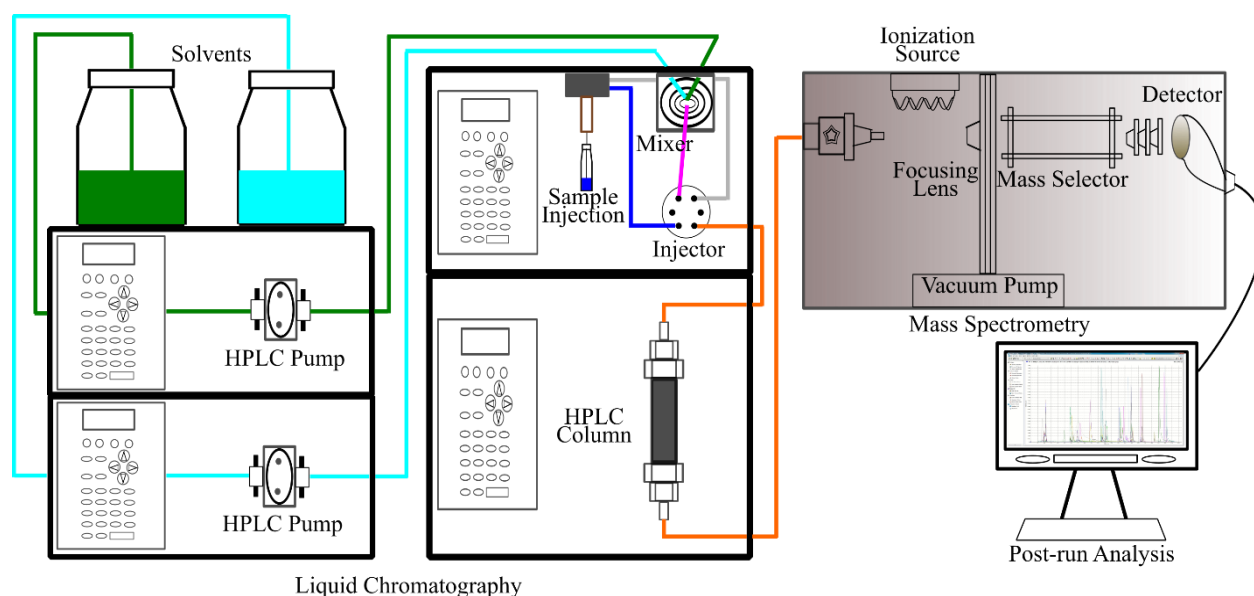
Figure 7. Schematic diagram for the basic principle of LCMS.

1.4.2. Spectrophotometer

Absorbance, transmittance and reflection of light over a specific range of wavelength are the basic phenomena of any chemical compound. This absorbance and transmittance of the electromagnetic radiation are measured by the spectrophotometer. In the present study, it has been used for measuring the chlorophyll and carotenoid content of the peppermint leaf. The spectrophotometer contains a lamp (light source), a collimator (lens), an entrance slit, a monochromator (prism), an exit slit, sample, a photoresistor and a galvanometer (amplifier) (Figure 8). It is designed by combining two main parts. First part is the spectrometer where initially light is produced from the light source, transmitted to monochromator by the lens through the entrance slit and finally dispersed into several spectra by a prism. The exit slit only selects and passes those wavelengths that are set before measurement. The second part is photometer. The selected spectrum goes through the sample solution in the cuvette. Consequently, the photoresistor detects the absorbed photons and sends a signal to the amplifier. Finally, it is digitally expressed as output.
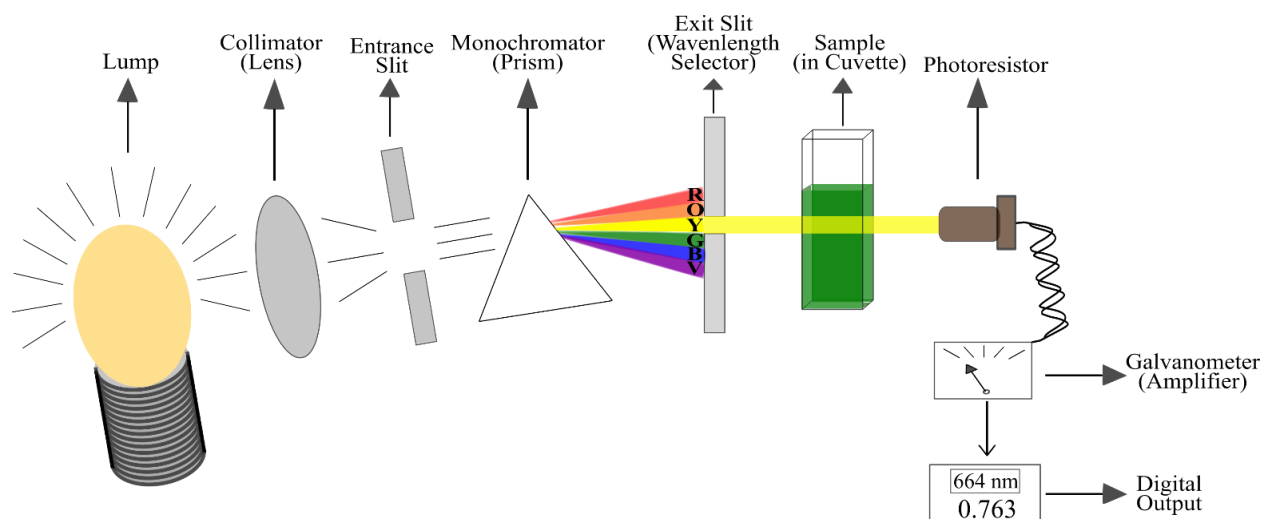
Figure 8. Schematic diagram for the basic principle of spectrophotometer.

1.5. Aims of the study

This thesis focuses on extending our knowledge of plant terpenoid biosynthesis at metabolic level by using the ^{13}C steady-state MFA technique.

Terpenoid biosynthesis in peppermint plants has been extensively studied over the last two decades due to the enrichment of monoterpenes in the leaves, which are commercially valuable as essential oils. However, overall metabolic regulation for the production of this volatile group of compounds is still not fully understood. The specific goal of the present study was to investigate the metabolism towards monoterpene biosynthesis in trichome cells. This was achieved by accomplishing the following objectives:

- Establishing a system for performing ^{13}C steady-state MFA in plant secondary metabolism. The main emphasis of this part was to obtain a culture system where the incorporation of ^{13}C isotope from the labeled source into the volatiles would be high and steadily maintained.

- Determining the participation of the two independent terpenoid biosynthetic routes for monoterpene production in peppermint GT cells. In the event, that both the terpenoid biosynthesis pathways actively participate in the production of monoterpenes, quantify the contribution of pathways towards monoterpene biosynthesis.

- Understanding the biochemistry of GT cells for synthesizing monoterpene. The intention of this investigation was to perceive the subcellular regulation of central carbon fluxes and other metabolic features inside these specialized cells.

This study was primarily based on the peppermint plant. In addition, part of this research work was validated further on another Lamiaceae plant, Oregano (*Origanum vulgarae*), which is taxonomically a close relative of the peppermint and synthesizes commercially valuable mono- and sesquiterpenes.

Chapter II: Materials and methods

2.1. Materials

2.1.1. List of chemicals, machinery and software

All the chemicals, machinery and software used for the present study were listed in Table 4, Table 5 and Table 6 respectively. LCMS and GCMS grade chemicals were used for the corresponding mass spectrometers. Some of the chemicals were collected from Dr. Gerd Balcke, a scientist from Leibniz Institute of Plant Biochemistry, Halle (DE). Updated version of the software was used for the analysis.

Table 4. List of chemicals used in this study.

Chemical Name	Company details
Nicotinamide adenine dinucleotide [$C_{21}H_{27}N_7O_{14}P_2$]	Applichem, St. Louis (USA)
U-^{13}C, 1-^{13}C, 6-^{13}C and 1,6-^{13}C$_2$ glucose [$C_6H_{12}O_6$]	Campro Scientific, Berlin (DE)
(E)-4-Hydroxy-3-methyl-but-2-enyl pyrophosphate [$C_5H_{12}O_8P_2$] Farnesyl pyrophosphate [$C_{15}H_{28}O_7P_2$] Geranyl pyrophosphate [$C_{10}H_{20}O_7P_2$] Geranylgeranyl pyrophosphate [$C_{20}H_{36}O_7P_2$] Fosmidomycin [$C_4H_{10}NO_5P$]	Cayman Chemical, Ann Arbor (USA)
MS Media	Duchefa, Haarlem (NL)
Hydrochloric acid [HCl] Hexane [C_6H_{14}] Ethanol [C_2H_5OH] Chloroform [$CHCl_3$] Dichloromethane [CH_2Cl_2] Amberlite XAD-4 resin	Merck, Burlington (USA)
Adenosine 5′-triphosphate [$C_{10}H_{14}N_5O_{13}P_3Na_2$] Adenosine diphosphate [$C_{10}H_{15}N_5O_{10}P_2$] Glucose 6-phosphate [$C_6H_{13}O_9P$] Glucose 6-phosphate dehydrogenase Hexokinase Nicotinamide adenine dinucleotide phosphate [$C_{21}H_{29}N_7O_{17}P_3$] Nicotinamide adenine dinucleotide phosphate [$C_{21}H_{29}N_7O_{17}P_3$]	Roche, Basel (CH)
Sodium hypochlorite [NaClO] Tween 20 [$C_{58}H_{114}O_{26}$] Imidazole [$C_3H_4N_2$]	ROTH, Karlsruhe (DE)

Chemical Name	Company details
Magnesium chloride [$MgCl_2$]	
Potassium chloride [KCl]	
Sodium hydroxide [NaOH]	
Dipotassium phosphate [K_2HPO_4]	
Tetrasodium pyrophosphate [$Na_4P_2O_7$]	
Phosphoenolpyruvate [$C_3H_5O_6P$]	
Fumarate [$C_4H_2O_4$]	
Malate [$C_4H_4O_5$]	
Oxaloacetate [$C_4H_2O_5$]	ROTH, Karlsruhe (DE)
Succinate [$C_4H_4O_4$]	
D-sorbitol [$C_6H_{14}O_6$]	
Polyvinylpyrrolidone 40 [$(C_6H_9NO)_n$]	
Methylcellulose [$(C_6H_7O_2(OH)x(OCH_3)y$]	
Triton™ X-100 [$C_{14}H_{22}O(C_2H_4O)_{n(n=9\text{-}10)}$]	
Acetonitrile [C_2H_3N]	
Methanol [CH_3OH]	
HEPES buffer [$C_8H_{18}N_2O_4S$]	
Isopentenyl pyrophosphate [$C_5H_{12}O_7P_2$]	
3-phosphoglycerate and 2- phosphoglycerate [$C_3H_7O_7P$]	
Aconitic acid [$C_6H_6O_6$]	
Alpha-Ketoglutarate [$C_5H_4O_5$]	
Citrate and isocitrate [$C_6H_5O_7$]	
6-Phosphogluconic acid [$C_6H_{13}O_{10}P$]	
Ribulose-5-phosphate [$C_5H_{11}O_8P$]	
Sedoheptulose 7-phosphate [$C_7H_{15}O_{10}P$]	SIGMA-Aldrich, St. Louis
Sedoheptulose 1,7-bisphosphate [$C_7H_{16}O_{13}P_2$]	(USA)
Ribulose 1,5-bisphosphate [$C_5H_{12}O_{11}P_2$]	
Nonyl acetate [$C_{11}H_{22}O_2$]	
Glucose 1-phosphate [$C_6H_{13}O_9P$]	
Glyceraldehyde 3-phosphate [$C_3H_7O_6P$]	
Fructose 6-phosphate [$C_6H_{13}O_9P$]	
Pyruvate [$C_3H_3O_3$]	
Fructose 1,6-bisphosphate [$C_6H_{14}O_{12}P_2$]	

Materials

Chemical Name	Company details
Isopentenyl pyrophosphate [$C_5H_{12}O_7P_2$] 1-Deoxy-D-xylulose 5-phosphate [$C_5H_{11}O_7P$] 2-C-Methylerythritol 4-phosphate [$C_5H_{13}O_7P$] Mevalonic acid [$C_6O_4H_{12}$] Mevalonate 5-phosphate [$C_6H_{13}O_7P$] Mevalonate 5-pyrophosphate [$C_6H_{14}O_{10}P_2$] N,O-tert-butyldimethylsilyl-group [$(CH_3)_3CSi(CH_3)_2$] Mevinolin [$C_{24}H_{36}O_5$] Dithiothreitol [$C_4H_{10}O_2S_2$] Sucrose [$C_{12}H_{22}O_{11}$] Coenzyme A [$C_{21}H_{36}N_7O_{16}P_3S$] 1-Deoxy-D-xylulose-5-phosphate [$C_5H_{11}O_7P$] Tributylamine [$C_{12}H_{27}N$] Acetic acid [CH_3COOH]	SIGMA-Aldrich, St. Louis (USA)
Amino acid standard mix	Thermo Fisher Scientific, Waltham (USA)
Ammonium formate [NH_4HCO_2]	VWR, Radnor (USA)

Table 5. List of machines and related accessories used in this study.

Machine and accessories	Machine details	Company details
GC System for QTOF QTOF GCMS System	Agilent Technologies 7890B Agilent Technologies 7200, Accurate-Mass QTOF GCMS	Agilent Technologies, Santa Clara (USA)
GC-Column for QTOF	Zebron Capillary GC-Column; ZB-Semi Volatiles (30 m × 0.25 mm × 0.25 μm)	Phenomenex, Torrance (USA)
Autosampler for QTOF	MPS-Multi Purpose Sampler	Gerstel, Mülheim an der Ruhr (DE)
GC-System GCMS-System GC- autosampler	GCMS 2010 gas chromatograph Shimadzu QP 2010 Plus GCMS Shimadzu AOC-20	Shimadzu Corporation, Kyoto (JPN)
GC-Column for Shimadzu GCMS	Supreme-5 ms column (30 m × 0.25 mm × 0.25 μm)	Chromatographie Service GmbH, Langerwehe (DE)

Machine and accessories	Machine details	Company details
LC Pump A and B	Shimadzu LC30AD	Shimadzu Corporation, Kyoto (JPN)
LC Autosampler	Shimadzu SIL30AC	
LC-Column	Nucleoshell RP 18 HPLC column (150 mm × 2 mm × 2.7 μm)	Macherey Nagel, Düren (DE)
QTRAP LCMS	AB Sciex QTRAP 5500	AB Sciex, Foster City (USA)
Vortexer	Vortex Genie 2	Scientific Industries, Bohemia (USA)
Heat Block	Block heater SBH200D	Stuart, Staffordshire (UK)
Centrifuge	Centrifuge 5418R	Eppendorf, Hamburg (DE)
Spectrophotometer	Gene Quant™ 1300 spectrophotometer	Healthcare Bio-Science AB, Uppsala (SE)
Plate Reader	ELx808 ultra microplate reader	BioTeK Inc, Winooski (USA)
Growth Chamber	CU-22L chamber	Percival Scientific Inc, Perry (USA)
SPME	100 µm polydimethylsiloxane fibre, Supelco Analytical	Sigma-Aldrich, St. Louis (USA)
Fluorescence microscope	Zeiss Axioskop 20	Carl Zeiss Light Microscopy, Goettingen (DE)
Sterile bench	Heraguard HPH18	Thermo Fisher Scientific, Waltham (USA)
Evaporator	Vapostat Version 2.1	Barkey, Leopoldshöhe (DE)
Balance Scale	Sartorius ME235P	Sartorius Weighing Technology GmbH, Göttingen (DE)
Volatile Collection Trap (VCT)	Poropak-Q filled VCT	Volatile Collection Trap LLC., Gainesville (USA)
Mixer bead mill	Retsch MM 400	Retsch GmbH, Haan (DE)
Lyophilizer	Christ Alpha 2-4 LD plus	Martin Christ freeze drying GmbH, Osterode (DE)
Phase contrast microscope	Nikon Diaphot 300	Nikon Corporation, Tokyo (JPN)

Materials

Table 6. List of software applications used in this study.

Software	Company details
GCMS Postrun Analysis (4.11 SU2)	Shimadzu Corporation, Kyoto (JPN)
Adams library (4.1) (Shimadzu version)	E-book by Adams (2007), Shimadzu Corporation, Kyoto (JPN)
Mass Hunter Qualitative Analysis (B.07.00)	Agilent Technologies, Santa Clara (USA)
Analyst (1.6.3) Multiquant (3.0.2)	AB Sciex, Foster City (USA)
Isotope Distribution Calculator and Mass Spec Plotter (www.sisweb.com/mstools/isotope.htm)	Scientific Instrument Services, Ringoes (USA)
Isotopomer Network Compartmental Analysis (INCA) (1.7)	Vanderbilt University, Nashville (USA)
MATLAB (2017a)	Math Works Inc., Natick (USA)
VANTED (2.6.5)	IPK, Gatersleben (DE)
Origin Lab (Pro 8)	Origin Lab Corporation, Northampton (USA)
Microsoft office (2016)	Microsoft Corporation, Redmond (USA)

2.1.2. Plant samples and their growth condition

Plant materials, used in the present study, were peppermint (*Mentha × piperita* var. Multimentha) and oregano (*Origanum vulgare*). Young plants were bought from Dehner garden centre (Halle, DE). They were nurtured in the growth chamber (Microclima MC1000, Snijders Lab, NL) at 25±1 °C, 65% relative humidity and 400 µmol m^{-2} s^{-1} light with 16 hr photoperiod. Young plants of the same age were obtained by vegetative propagation for the study. Therefore 8-10 cm healthy and growing shoots were scissored from the purchased plants. They were dipped into regular tap water within a beaker inside the growth chamber for 2 weeks. During this time period, new shoots and roots emerged. These shoot apices were then placed into the potting soil for further growth. The soil was bought from Klasmann-Deilmann GmbH, Geeste (DE), constituted by a blend of weakly decomposed white sphagnum peat and high-grade frozen black sphagnum peat with specific electrical conductivity (55 ± 25% mS m^{-1}), pH of 5.5-6.5 and NPK (nitrogen-phophate-potassium) ratio of 14:10:18 (2 kg m^{-3}). Sufficient amount of water was provided to the plants twice in a week. Liquid fertilizer (NPK ratio of 8:8:6), which also contained micronutrients (Boron, Copper, Iron, Manganese, Molybdenum and Zinc), was used once in a week at the dose of 1.5 µL in 1 mL of water.

2.2. Methods for culture and sample collection

2.2.1. Isolation of trichome secretory cells

Secretory trichome cell clusters were isolated according to the procedure of Gershenzon *et al.* (1992) with some modifications. Extraction buffer consisted of 25 mM HEPES (pH 7.3), 10 mM KCl, 5 mM MgCl$_2$, 0.5 mM K$_2$HPO$_4$, 0.1 mM Na$_4$P$_2$O$_7$, 5 mM DTT, 10 mM sucrose, 200 mM D-sorbitol, 10 g l^{-1} PVP 40 and 6 g l^{-1} methyl cellulose. However, at the time of preparation of isolation buffer, 2 mM sucrose was used instead of 10 mM concentration and methylcellulose was omitted to reduce the viscosity of the buffer.

Apical peppermint leaves (10-12 days old) were harvested in a glass beaker on ice. Leaves were immersed in ice-cold sterile water containing 0.01% Triton™ X-100 and left for 1 h on ice. Afterwards, soaked leaves were washed thoroughly with sterile water to remove chemicals and dirt. Cleaned leaves were placed inside a bead beater jar with 100 mL glass beads (0.5 mm) and 15 g Amberlite XAD-4 resin. The jar was filled up to full volume by extraction buffer. Leaves were extracted thrice (at 4 °C) by following the cycle of 1 min run of bead beater machine and 1 min break for cooling and setting of bead beater. The mechanism of extraction was abrasion by the low speed of bead beater. Thereafter, the mashed content was sieved through 500, 350, 200, 100 and 20 µm nylon mesh with simultaneous rinsing by pre-chilled isolation buffer. The average size of secretory cell clusters is 60 µm in diameter. Hence, cell clusters were collected upon 20 µm nylon mesh.

2.2.2. Culture of isolated trichome cell clusters

Cell clusters were washed three more times with sucrose-free isolation buffer to reduce unlabeled carbon sources for labeling study. Washed cell clusters were incubated with culture buffer which consisted of 1 mL sucrose-free isolation buffer, 1 mM NAD$^+$, 1 mM NADPH, 1.5 mM ADP, 1.5 mM ATP, 1 mM CoA and 50 mM U-^{13}C glucose (or, unlabeled glucose as control culture).

Trichome secretory cells were cultured inside 40 mL glass vial with a screw cap which had a centre hole, fixed with 3.2 mm septum (silicon cream / PTFE beige) (Figure S2). One syringe needle was directly incorporated into the cultured cell. The wide end of the needle was in ambience and attached to 0.20 µm CA-membrane filter which was further connected to regulated airflow pump. Poropak-Q filled volatile collection trap (VCT) was at another side of the screw cap. The air came from a regulated airflow and passed through a filter and needle. Cells were cultured by vigorous bubbling,

which then produced monoterpenes. Air containing volatiles exited and passed through the volatile collection trap, where monoterpenes were trapped into the poropak-Q.

The VCT was conditioned every time after use. It was repetitively washed with dichloromethane and dried in an oven at 150 °C for 3 hr. After cooling down of the VCT to room temperature, both ends were wrapped with aluminium foil and stored until reuse. Aluminium foil was removed just before initiation of the experiment. All other glass components of the system were washed with chloroform to remove traces of volatiles, sticking to the inner glass surface. Vial cap, filter and syringe needle were always altered at the initiation of every cell culture.

2.2.3. Shoot-tip culture

Shoot-tip culture of Peppermint and oregano plant was performed with slight modifications from the method, described by Holm et al. (1989). Tissue culture process was entirely performed under the laminar air flow bench. Explants were taken from 5-6 weeks of the healthy growing plant to retain the same vegetative growth and refrain from the reproductive stage of the plant. About 1 cm long shoot apices containing one nodal portion were cut from the growing plant. Those plant parts were sterilized with 70% ethanol for 60 seconds. Sterilized plant parts were further disinfected with 0.5% sodium hypochlorite solution, containing few drops of Tween 20, for 7 min. Those treated plant parts were rinsed with autoclaved water four times to clean them off any residual bleach or ethanol solution. Then the end of the stem was taken apart, as this part was dead (blackened) due to its exposure to sterilization and washing solutions. All the leaves were also trimmed away for the study of shoot-tip culture without leaf. The final apex (about 5-7 mm) with none and/or one developing leaf pair was used for culture. Those explants were cultured within Magenta box (Sigma-Aldrich, Germany) into 2 ml of liquid media containing half concentration of MS media (Murashige and Skoog, 1962) with B5 vitamins, supplemented with 2% glucose. No extra hormones and antibiotics were added to the medium. pH of the medium was adjusted to 5.7 by the addition of 0.1N sodium hydroxide or 0.1N hydrochloric acid. The medium was filter sterilized with 0.20 μm CA-Membrane filter (Heinemann Labortechnik GmbH, Duderstadt, Germany). Shoot-tip cultures were cultivated in the growth chamber (CU-22L, Percival Scientific Inc., USA). The climatic condition of the growth chamber was set at 25±2 °C and 16hr light/8hr dark photoperiodic condition with different light intensities as per the requirement of the experiments.

2.2.4. Study of light intensity on shoot-tip culture

Four different light intensities (5, 10, 20 or 30 µmol m^{-2} s^{-1}) were tested in peppermint shoot-tip culture to understand the satisfactory growth condition with high isotope enrichment into terpenes. The light was provided by Osram cool white fluorescence lamps (Lumilux T8 L18W/840, DE). Measurements of qualitative and quantitative characteristics of shoot-tip culture from different light intensities were the objective of this study. For qualitative measurement, U-^{13}C glucose was supplemented with basal medium, whereas unlabeled (^{12}C) glucose was used for control culture and for quantitative analysis. Samples were collected on the 15th or 20th day after first leaf visibility (DALV) as most of the monoterpene biosynthesis enzyme activity was highest at 15 days leaf age and total monoterpene content was statistically maximum around 20 days leaf age (McConkey et al., 2000). The layout of this study was presented in Figure 9.
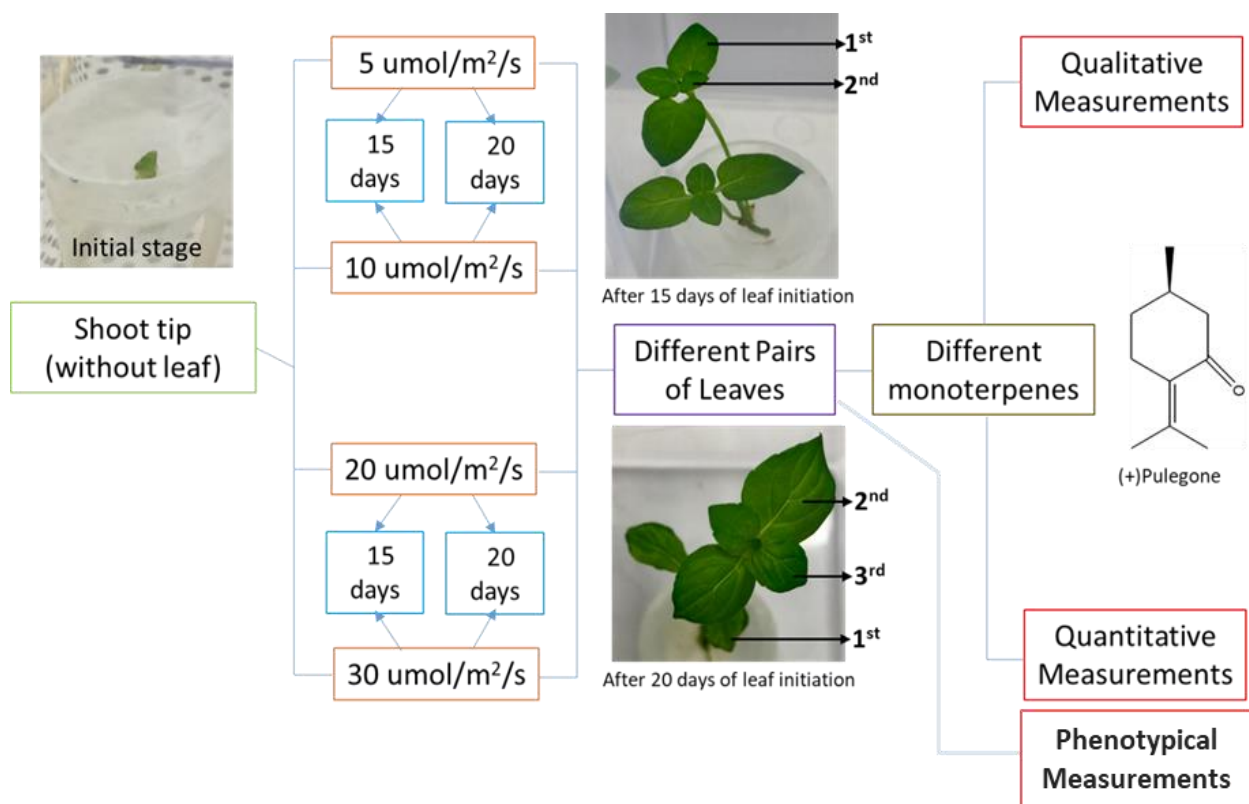
Figure 9. Layout of the light-study.

The effect of different light intensities on the monoterpene (qualitatively and quantitatively) was designed. Qualitative (^{13}C) and quantitative measurements were taken from U-^{13}C$_6$ and unlabeled (^{12}C) glucose fed culture, respectively.

2.2.5. Determination of steady-state in shoot-tip culture

Shoot-tip cultures of peppermint and oregano plants were cultivated under 5 and 10 µmol m^{-2} s^{-1} light intensity, respectively for flux analysis. For determining the metabolic steady-state, the culture was initiated with unlabeled glucose. Different aged first pair leaves (from 13 to 18 days old) were collected for quantitative analysis. The total amount of mono- and sesquiterpenes from oregano culture and total monoterpenes from peppermint culture were determined by GCMS instrument.

Isotopic steady-state was performed by analyzing average isotope enrichment in the monoterpenes and sesquiterpenes. In this case, U-^{13}C$_6$ glucose was supplemented into the basal media and used for the culture. First pair leaves of 14, 15 and 16 DALV old were collected for qualitative analysis.

2.2.6. Positional isotopic tracer study for MFA
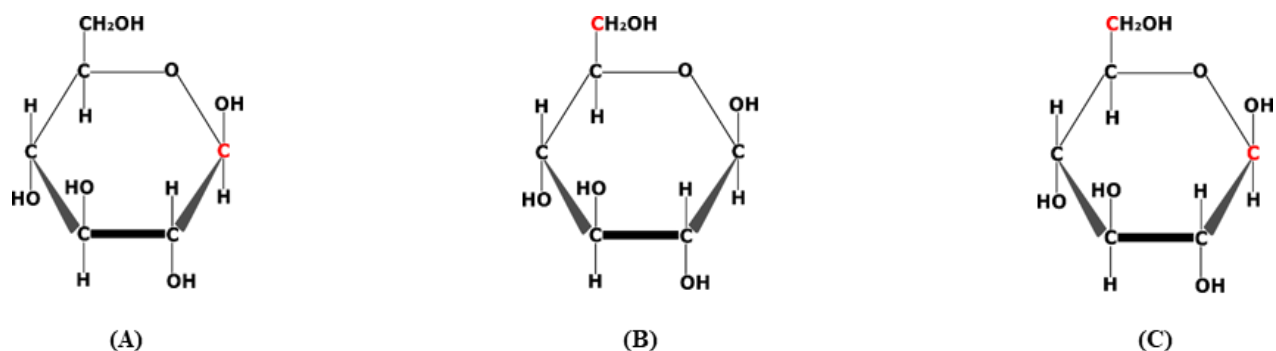
Figure 10. Positionally labeled glucoses used for isotopic study
Label carbon (^{13}C) is coloured in red. (A) 1-^{13}C$_1$, (B) 6-^{13}C$_1$ and (C) 1,6-^{13}C$_2$ glucose.

The isotopic study was performed to understand the metabolic fluxes after fulfilling the pre-requisite of MFA (steady-state of volatile production). Positionally labeled glucose (1-^{13}C$_1$, 6-^{13}C$_1$ or 1,6-^{13}C$_2$ glucose; Figure 10) was supplemented in the basal MS medium as the sole carbon source. The shoot apices were cultivated into the medium and left to grow at 5 and 10 µmol m^{-2} s^{-1} for peppermint and oregano, respectively. Continuous culture was maintained up to the steady-state growth phase (15 DALV). After this duration, first pair leaves were collected for volatile analysis. Besides, all the leaves were stored together for LCMS analysis.

2.2.7. Inhibition study of terpenoid biosynthetic pathway

Different concentrations of fosmidomycin (FSM) (at 0, 10, 20, 30 and 40 µM) were used for the inhibition of DXP pathway in peppermint shoot-tip culture under 5 µmol m^{-2} s^{-1} light intensity. FSM was added to the culture media which was supplemented with unlabeled glucose. Fifteen days old leaves were collected and measured for photosynthetic content.

Labeling pattern and enrichment into pulegone (monoterpene) of 15 days old leaves were also assessed after the partial inhibition of the non-mevalonate pathway by 10 µM FSM. As a sole carbon source, 1-^{13}C$_1$ glucose was supplemented into the inhibitor containing culture media. The control culture was reared in the same isotopic media without treatment of the inhibitor.

2.2.8. Leaf sample collection

Definite time for initiation of the culture (14.00 -15.00 h CEST) and collection of the leaf sample (10.00 -11.00 h CEST) were scheduled to get constant influence of diurnal rhythm for every replication of the shoot-tip culture, which is proven to have a role for the non-mevalonate pathway (Covington et al., 2008; Wiberley et al., 2009). For label enrichment analysis in volatiles and metabolic steady-state, different pairs of leaves were collected separately. However, total leaves were stored collectively for other quantitative and physiological analysis. Plant leaf samples were rapidly frozen in liquid nitrogen and stored at -80°C for further investigation. Before analysis, frozen leaf samples were grounded in liquid nitrogen with the help of micro pestles within the Eppendorf tube.

2.3. Methods for biochemical assay

2.3.1. Viability test of trichome cell

Duo staining with fluorescein diacetate (FDA) and propidium iodide (PI) emit green or red color for viable or dead cells, respectively. To prepare a stock solution, 50 mg of FDA was dissolved in 1ml acetone. The stock of PI was bought at a concentration of 1mg/ml of water. These two stocks were further diluted in cell culturing buffer to get a working concentration of 2.5 µg FDA and 10 µg PI in 1 ml. Finally, 1 ml of the working solution was mixed with 1 ml cell suspension and incubated for 5 minutes at room temperature in dark.

The vitality of the cells was observed under an Axioskop 20 fluorescence microscope with an AxioCam MRc camera. Software for image acquisition was Axiovision Rel. 4.6. The filter combination for fluorescence microscopy of FDA-signal was a Zeiss filter-set 9 (450-490 nm excitation/510 nm beam splitter/515 nm emission) and PI-signal was Zeiss filter-set 15 (546 nm excitation/580 nm beam splitter/590 nm emission). Some of the fluorescent images were made as a combination of FDA-fluorescence and bright field microscopy (very low intensity of light) to observe the position of the cells.

2.3.2. Quantitative measurement of phytopigments

Chlorophyll and carotenoid measurements were performed according to the procedure, described by Lichtenthaler (1987). Fresh weight (FW) of the leaf was recorded after collection under liquid nitrogen. Weighted samples were further pulverized using micro pestles. Two mL of 95% (v/v) ethanol was added to the homogenized tissue and samples were vortexed for 30 seconds. These tubes were then left overnight at room temperature after wrapping with aluminium foil to prevent photo-bleaching of the analyzed pigments. Samples were vortexed again on the next morning and allowed to stabilize for 10 min. The final measurement was conducted with 1 mL clear supernatant. Distilled water and 95% ethanol were used as blank and for the normalization of the light spectrophotometer. Chlorophylls and total carotenoids were estimated from the absorbance value at 470 (A_{470}), 649 (A_{649}) and 664 (A_{664}) nm. Additionally, the analysis was also accomplished at 750 nm to correct the measurement error. The content of individual pigments was calculated by the equation (eqn.) 1 to 3.

$$Cholorophyll\ a\ (C_a) = \frac{(13.36\ A_{664} - 5.19\ A_{649}) \times 2}{FW} \qquad \dots (1)$$

$$Cholorophyll\ b\ (C_b) = \frac{(27.43\ A_{649} - 8.12\ A_{664}) \times 2}{FW} \qquad \dots (2)$$

$$Carotenoids\ (C_{x+c}) = \frac{(4.785\ A_{470} + 3.657\ A_{664} - 12.76\ A_{649}) \times 2}{FW} \qquad \dots (3)$$

2.3.3. Measurement of glucose uptake rate

After 15 DALV, the amount of the remaining medium from each peppermint shoot-tip culture set up was noted and stored at -20 °C. Glucose uptake was evaluated using the modified version of the original protocol (Bondar and Mead, 1974; Kunst, 1984). A buffer containing 100 mM imidazole-HCl (pH 6.9), 5 mM MgCl$_2$, 2.25 mM NAD, 1mM ATP as final concentrations was used for the measurement of soluble sugars using microplate reader at 340 nm. The temperature of the plate reader was set at 30 °C. Further addition of auxiliary enzymes such as hexokinase and glucose 6-phosphate dehydrogenase allowed the conversion of glucose to gluconate-6-phosphate and NADPH, respectively. The amount of NADPH formed was measured spectrophotometrically at 340 nm to determine glucose amounts in the leftover MS medium. A calibration curve with different concentrations of glucose was also used for accurate measurement of glucose concentrations. Glucose uptake was further determined by deducting the leftover glucose from the total supplemented glucose.

2.3.4. Measurement of isotope enrichment in protein hydrolysates

Proteins were hydrolyzed by overnight incubation of the pulverized leaf samples with concentrated HCl, as per the protocol of Klapa et al. (2003) and Schwender et al. (2003). Fresh weight of the leaf samples was noted. These samples were further homogenized with 1 mL protein buffer (0.01 M Na$_3$PO$_4$, pH 7.5 adjusted by NaOH and 0.5 M NaCl) into a cooled glass homogenizer by a pestle. Homogenate was transferred into a 2 mL Eppendorf tube. Mortar and pestle were washed with 1 mL hexane: diethyl ether (1:1, v/v) and the solution was added to the homogenate. The sample was vortexed, kept cool for 30 min and centrifuged at $16900 \times g$ (4 °C, 10 min). Upper phase containing the lipids was removed from the tube. Addition of hexane-diethyl ether mixture was repeated, followed by removal of the lipophilic phase after centrifugation. Lower phase and interphase containing proteins were separated into a new tube for the process of protein hydrolysis. Trichloroacetic acid (50% w/v in H$_2$O) was added to a final amount of 10% (v/v) to the amount of protein extract and incubated for 30 min on ice. Thereafter, the samples were centrifuged for 10 min. The supernatant was then discarded. The remaining pellet was washed thrice with 1 mL of ethanol:

ether (1:1, v/v) by subsequent vortexing and centrifugation. The pellet was dried under N_2 fumigation (at 0.5 L/min). Thereafter, 1 mL of 6N HCl was added to the dry pellet. The solution was incubated overnight (16 h) in a shaker (600 rpm) at 99 ° C. Subsequently, the samples were stored at -80 °C until further analysis.

Prior to GCMS measurement, the solvent was removed from the aliquot under the stream of N_2 at 60°C. These amino acids were derivatized to N,O-tert-butyldimethylsilyl (TBDMS) derivatives. Samples were mixed in 50 µL of pyridine followed by addition of 50 µL of N-methyl-N-(tert-butyldimethylsilyl) trifluoroacetamide (MTBSTFA). This derivatizing process was automatically performed in GCMS by online derivatization method. Amino acids in these storage proteins were analyzed by Agilent QTOF GCMS. The sample was splitlessly injected in 250 °C heated liner. Zebron Capillary GC-Column was used for analytical separation. The helium carrier gas was provided at a constant flow of 1 mL/min. The oven temperature was initially held at 60 °C for 2 min, then increased to 280 °C at the rate of 20 °C /min and finally held for another 5 min. Mass spectrometer had a 230 °C heated source with an ionization potential of 70 eV. Amino acids were detected at scan mode in the range of 50-550 amu at the rate of 5 spectra/s. List of measured fragments was presented in Table 7. Data were evaluated by Agilent Mass Hunter Qualitative Analysis software.

Table 7. **Details of measured amino acids and their fragments.**

Measured amino acids	Source intermediate(s)	Compartments (Dersch *et al.*, 2016)	Analyzed fragments
Tyrosine (Tyr)	Phosphoenolpyruvate and Erythrose 4-phosphate	Plastid	364 (M-57)
Serine (Ser)	3-phosphoglyceric acid	Cytosol	362 (M-85)
Alanine (Ala)	Pyruvate	Cytosol	232 (M-85)
Lysine (Lys)	Oxaloacetic acid	Cytosol	431 (M-57)
Proline (Pro)	α-ketoglutarate	Mitochondria	258 (M-85)

2.3.5. Qualitative and quantitative measurement of volatile terpenes from the culture

Volatile terpene from the trichome cell culture was extracted from Poropak-Q by washing the VCT with 100 µL hexane twice. This hexane was collected in GC vial. Prior to using for the cell culture, VCT was also washed with hexane which was treated as a blank. One µL of the sample was manually injected into the GCMS machine.

In the case of shoot-tip culture, pulverized leaf sample was placed into a 1.5 mL SPME (Solid Phase Micro Extraction) vial for qualitative (^{13}C) analysis of terpenoids. A 100 µm polydimethylsiloxane SPME fibre was exposed to the headspace of the peppermint sample for 2 min at room temperature (~24°C). The only modification for terpenoid extraction from oregano and FSM-treated peppermint leaf was 15 min exposure of SPME fibre into the sample vial due to the presence of less amount of volatiles in these leaves. For quantitative analysis of the terpenoids, the fresh weight of the sample was determined prior to homogenization. Thereafter, 300 µL of hexane containing 10 ng/µL of nonyl acetate (as internal standard) was added to the ground sample. This mixture was shaken overnight at 25°C. Then, the mixture was allowed to stabilize at room temperature for 10 min. Afterward, the supernatant was collected and assessed in GCMS.

Qualitative and quantitative study of terpenoids were performed in a GCMS 2010 gas chromatograph, coupled to GCMS-QP 2010 Plus mass spectrometer. To estimate the quantity of terpenoids, a split injection was used with a ratio of 1:5, whereas the unloading of the SPME fibres was carried out in splitless mode for an understanding of labeling pattern into terpenoids. Analytic separation was performed in Supreme-5 ms column. Hydrogen was used as a carrier gas with a flow rate of 1 mL/min. Injector and interface temperature were set to 220 °C and 250 °C respectively, with an ionization potential of 70 eV and a scan range of 50–350 amu. The oven temperature was held at 50 °C for 3 min, then increased with 7 °C/min to 150 °C followed by a rate of 100 °C/min up to 300 °C, which was held for 2 min. Sampling and solvent cut time were adjusted to 1 and 1.5 min, respectively.

2.3.6. Procedure of labeled data interpretation

The GCMS Postrun Analysis software was used to analyze the chromatograph. The Adams library (Adams, 2007) was integrated into the software for the detection of peaks. Terpenoids were identified from control (unlabeled) samples by the mass spectral library. Peaks from the labeled samples were identified by comparing retention time with the control mass spectra. In the case of qualitative interpretation, the intensity of each mass isotopomer, *i.e.* (M+0) to (M+10) isotopomers for each monoterpene (C_{10} compound) was corrected for theoretical natural abundance. Corrected Abundance (C) of each mass isotopomer was normalized to MID which was the percentage of corrected abundance for each isotopomer as a fraction of the total abundances for all isotopomers. MID was defined by the eqn. 4. For instance, eqn. 5 shows the calculated MID of (M+0) mass isotopomer.

Methods for biochemical assay

$$MID_{(M+n)} = \frac{C_{(M+n)}}{\sum_{i=0}^{n} C_{(M+i)}} \qquad \ldots (4)$$

$$MID_{(M+0)} = \frac{C_{(M+0)}}{\sum_{i=0}^{n}(M+i)} \qquad \ldots (5)$$

Here, the number of carbon atoms present in the compound were symbolized by n. Average ^{13}C enrichment was enumerated by summing up each MID after multiplying with their extra ^{13}C atom number as the fraction of a total atom (eqn. 6).

$$Average\ 13C\ Enrichment = \frac{\{MID_{(M+0)} \times 0\} + \{MID_{(M+1)} \times 1\} + \ldots + \{MID_{(M+n)} \times n\}}{n} \qquad \ldots (6)$$

To determine scrambling of the label due to external carbon dioxide fixation and presence of unlabeled carbon in initial biomass of 5-7 mm shoot-tip, ^{13}C enrichment was recalculated after correcting not only natural abundance but also 1% U-[13]C_6 glucose impurity (purity of ^{13}C in labeled glucose was 99%, sold by the chemical vendor). After these two corrections, the average dilution of labeling was measured by eqn. 7.

$$Average\ dilution\ of\ labelling = 100\% - Corrected\ 13C\ Enrichment \qquad \ldots (7)$$

2.3.7. Isotopomer network and MFA

The MID measurements of the most abundant peppermint monoterpenes (i.e. pulegone, isopulegone and menthofuran) from three parallel tracer studies (1-[13]C_1, 6-[13]C_1 and 1,6-[13]C_2) were used for MFA. The flux was estimated based on the mean value of three biological replicates from each tracer. Thus, a total of 9 monoterpene fragments resulting in 99 MID signals was input for parallel ^{13}C-MFA (Table S2, Table S3, Table S4). To account for the effect of natural isotopes, the raw MS data was corrected for natural isotope abundance (Fernandez et al., 1996). Additionally, the fragments were carefully screened with respect to measurement precision (i.e. natural vs. theoretical isotope abundance ratio). The machine precision (0.03 unit) was used as a threshold value (i.e. minimum standard deviation) for the standard deviation of all mass isotopomers (Abernathy et al., 2017; Allen et al., 2009b).

Isotopic steady-state ^{13}C-MFA was performed using the MATLAB-based INCA software (Young, 2014), which applies the EMU framework (Antoniewicz et al., 2007a; Young et al., 2008) for isotopomer analysis. Using a Levenberg-Marquardt optimization algorithm (Dennis and Schnabel, 1983), metabolic fluxes were estimated by least-squares regression of isotope labeling measurements of above-mentioned three monoterpenes from three tracers fed culture study. For the integrated [13]C-

MFA approach (also known as parallel ^{13}C-MFA), the labeling data sets were simultaneously fitted to a single flux model.

All flux estimations were accomplished by defining the monoterpene excretion rate to 1 (arbitrary unit). In addition, the upper bound of ^{13}C-glucose uptake was constrained to 3 (arbitrary unit) based on preliminary flux balance analysis computations, which predicted a minimal requirement of 1.67 mol glucose for the biosynthesis of 1 mol monoterpene. As it was observed from experimental result that average ^{13}C enrichment into monoterpene from 15 days old leaves was 0.5% (Chapter IV: Assessment of metabolic fluxes in secretory trichome), the upper bound of the unlabeled glucose uptake was constrained to 0.01. This value was about 0.5% of labeled glucose uptake. To quantify the energy and redox requirements for monoterpene biosynthesis, the respective reactions for ATP, NADH and NADPH import were left unconstrained.

To identify a global best-fit solution, flux estimations were repeated at least 100 times starting from random initial values. The ^{13}C-MFA results were subjected to a χ^2-statistical test to assess the goodness-of-fit between experimental data and model. Given a number of degrees of freedom (DOF) of 56, the estimated fluxes were considered acceptable when the obtained variance-weighted sum of squared residuals (SSR) was below the χ^2 at a 95% confidence level ($\chi^2_{95\%, 60} = 83.3$). The statistical uncertainty (at 95% CI) in the best fit flux value was assessed by evaluating the sensitivity of the SSR to parameter variation (Antoniewicz et al., 2006). Flux precision (i.e. standard error; SE) was determined as formulated by Antoniewicz *et al.* (2006) and presented in eqn. 8.

$$Flux\ precision\ (SE)\ =\ [(flux\ UB_{95}) - (flux\ LB_{95})]\ /3.92 \qquad\qquad \dots (8)$$

All flux calculations were performed on a 40-core Dell EMC PowerEdge R640 server running Ubuntu LTS 16.04.4 and MATLAB R2017a. Initial flux maps were generated using the Fluxmap add-on (Rohn et al., 2012) of the visualization software VANTED (Junker et al., 2006).

2.3.8. Extraction of the hydrophilic metabolites from the whole leaf

Central carbon and terpenoid biosynthetic intermediates were extracted by following the procedure from Balcke et al. (2014) with some modifications. The first pair leaves of 15 DALV old were obtained from growing shoot-tips under 5 µmol m^{-2} s^{-1} light intensity. Leaf sample was flash frozen in 2 mL Eppendorf tube, filled with two steel beads (3 mm) and 100 mg of glass beads (0.5 mm).

Leaves were slightly crushed by shaking of the tube in the presence of steel beads at -80°C temperature. Thenceforth, 900 µL dichloromethane: ethanol (2:1 v/v, -80°C), followed by 200 µL of 50 mM aqueous ammonium formate buffer (0 °C, pH 3.0) was added to each sample tube. Total two rounds of extraction were pursued by Retsch mill bead beating to increase the extraction efficiency of the intermediates. Each round contained three cycles (first cycle at -80°C, second and third cycle at subsequent room temperature) for 30 s each at a frequency of 30 Hz. Phase separation was achieved by centrifugation at 15,000×*g* for 4 min (4 °C). Roughly, 150 µL of the upper phase was achieved from the first round of extraction, which was collected in a separate tube. The full round of bead beating was repeated with the addition of another 100 µL ammonium formate buffer. After the second centrifugation, further 150-160 µL aqueous phase was gained and combined with the previous collection. This separated upper phase was centrifuged for 2 min and then filtered through a 0.2 mm PVDF membrane filter to completely discard the lower hydrophobic phase and proteins. To get a concentrated sample, aqueous extract was lyophilized overnight in LC vial. Freeze dried samples were stored at -80°C for the future investigation.

2.3.9. Determination of the compound dependent parameter for central metabolites

Declustering potential (DP), collision energy (CE) and collision cell exit potential (CXP) of the metabolites were determined at negative ionization mode of AB SCIEX QTRAP 5500 mass spectrometer. The list of measured analytes is presented in Table S14. Standard solutions (50 µM) of these compounds were prepared in the mixture of water: methanol (1:1; v / v) solvent and injected directly into the MS at a flow rate of 10 µL/min by syringe-pump configuration. For the maintenance of the machine, some parameters were always fixed, such as curtain gas, ion spray voltage, source temperature, gas stream 1 and 2 (Table 8). The scan rate of 200 Da/s and a minimum 100 cycles for each scan were set. Precursor ion was detected by Q1 MS scan within 50 to 500 Da range in negative polarity mode. Multiple fragment ions from specific Q1 ion and their MS parameters were detected in product ion (MS2) scan mode by ramping of collision energy from -5 to -100 V, followed by ramping of DP (from 0 to -150 V) and CXP (from 0 to -55 V).

2.3.10. Assessing the precision and accuracy of the metabolites in LCMS/MS

To understand measurement biases due to the extraction procedure and matrix effect of the actual sample, 15 DALV aged leaf samples from unlabeled glucose study were extracted. Chromatographic

and mass spectrometric details were presented in Table 8 and multiple reaction monitoring (MRM) details for the measurement of those metabolites are presented in Table S13. Freeze dried samples were diluted with 50 μL solvent A and 10 μL solvent B. Injection volume for each technical replication was set to 2 μL. Area of each mass isotopomer was estimated by using AB Sciex Multiquant software. Accuracy and precision of mass isotopomer measurement were determined by comparing natural and theoretical abundance from 10 repetitive injections from one sample within a day as described in equation 9 and 10. To verify the reproducibility of the measurement, 10 more injections was repeated in the next week.

$$Measurement\ accuracy = Experimental\ \frac{MID_{(M+n)}}{MID_{(M+n-1)}} - Theoretical\ \frac{MID_{(M+n)}}{MID_{(M+n-1)}} \quad \dots (9)$$

$$Measurement\ precision = Standard\ deviation\ of\ \frac{MID_{(M+n)}}{MID_{(M+n-1)}} \quad \dots (10)$$

Table 8. Compound independent chromatographic and mass spectrometric details of LCMS/MS

Chromatographic details	
Solvent A	10 mM aqueous tributylamine (pH = 6.2, adjusted by acetic acid)
Solvent B	Acetonitrile
Solvent gradient flow	Solvent B flow of total flow: 0 min: 2%, 2 min: 2%, 18 min: 36%, 21 min: 95%, 25.5 min: 95%, 25.51 min: 2%, 31 min: 2%
Equilibration time	4 min
Injection volume	25 μL
Flow rate	0.4 mL/min
Column temperature	40°C
Autosampler temperature	4°C
Needle cleaning solvent	Methanol : water (1:1, v/v)
Mass spectrometric details	
Ion source temperature	450 °C
Gas stream 1 / 2	60 / 70 psi
Curtain gas	40 psi
Ion spray voltage	-4500 V
Integrated Valco valve position (A to MS and B to waste)	0 min: A, 23 min: B, 27 min: A

Chapter III: Establishment of the experimental set-up for performing MFA

3.1. Introduction

Positionally labeled ^{13}C substrates have been key players towards the development of the carbon-based MFA approach in plants. Recently, there has been substantial progress in ^{13}C tracer studies, however, usually isolated plant tissues with homogenous cell populations and long metabolic steady-state has been extensively investigated using this technique. Central metabolic fluxes were characterised in cultured oilseeds, developing embryos of Arabidopsis and Brassica genotypes to imply on potential metabolic engineering targets towards improved yield and better seed composition (Allen and Young, 2013; Alonso et al., 2011; Hay et al., 2014; Lonien and Schwender, 2009). Likewise, differentiated systems such as plant hairy root cultures of *Catharanthus roseus* and tobacco were also studied to understand the impact of genetic and environmental changes on metabolic fluxes (Masakapalli et al., 2014; Sriram et al., 2007).

One of the major challenges for steady-state ^{13}C-MFA in plants is the accomplishment of the steady-state at both the isotopic and metabolic level. The time factor required to achieve both steady states has to be short to avoid significant metabolic shifts, which might further lead to a misconception of the ^{13}C-MFA study (Schwender, 2008). This is the reason why the general focus of MFA mainly revolves around central core metabolism where a steady-state for metabolites can be established within seconds to several minutes or hours (Arrivault et al., 2009; Masakapalli et al., 2010; Stitt et al., 1983). However, studies involving secondary metabolism networks require much longer experimental periods to establish metabolic steady-state. In such cases, transient isotope labeling approaches were used to estimate accurate metabolic fluxes as the conventional steady-state approach lacks conviction (Boatright et al., 2004; Heinzle et al., 2007). Another challenge for steady-state ^{13}C-MFA is the application to plant tissues, which is limited by a high heterogeneity of the involved cell types and, furthermore, a number of subcellular compartments. Studies on developing maize seeds have used tissues that have been cultured separately or in pairwise combination to study central metabolic fluxes (Alonso et al., 2011, 2010). However, in such heterogeneous systems, the actual metabolism is difficult to determine. It becomes even more critical when studying growing plant system using isotopic sugars, where photosynthesis has the capacity to limit the label enrichment of the metabolites. Feeding the system with $^{13}CO_2$ substrate instead of the sugars allows quantifying photoautotrophic metabolic fluxes, however only at the transient state of isotope incorporation, as the steady-state will be achieved for the independent flux distribution (Ma et al., 2014; Shastri and Morgan, 2007). Thus, conventional ^{13}C-MFA study is capable of quantifying heterotrophic and

mixotrophic fluxes as shown by several studies within the literature. To improve the practicability of the steady-state MFA on growing plants, the discussed constraints are needed to be addressed.

When high label enrichments should be achieved in mixotrophic tissues such as sink leaves, it is crucial to decrease photosynthetic carbon fixation without affecting other physiological processes. In order to maintain sink tissue as a net importer for a longer time, light irradiation can be reduced. Light correlates positively with plant growth, however negatively with label enrichment from ^{13}C sugar tracers by regulating photosynthetic rate (Baly, 1935). A recent study showed the ^{13}C enrichment in Arabidopsis sink leaves for short dark periods (4 hrs), where label enrichment from U-$^{13}C_6$ sucrose feeding was up to 34.8% in different amino acids (Dethloff et al., 2017). In that study, a conventional shoot culture method with the presence of source leaves as explant were explored for central metabolism. However, label amounts can even be further increased by minimizing the initial biomass prior to the experiment.

Peppermint has been a model system for studying monoterpene biosynthesis which is confined into specialized glandular trichome (detailed description in Chapter I: General introduction). In this part of the investigation, it was initially attempted to establish a method for high isotope enrichment in trichome cell culture, as this is the conventional approach for steady-state MFA in the plant. However, this endeavour was not successful due to the incorporation of a very low degree of label ^{13}C inside the cell. In the next step, a system was introduced to increase the potential for long-term isotopic steady-state labeling to probe intact plant entity for a better understanding of secondary metabolism. The confounding effect of growing plant system to perform steady-state MFA has been addressed here using a shoot-tip culture system. The method was also extended to oregano (*Origanum vulgare*), another member of the Lamiaceae family with high essential oil content, to ascertain this strategy further. The procedure is economically feasible, robust and easy to use and represents a high labeling percentage for longer periods. Besides, an interesting strategy was devised to alter light intensity, which further inhibited the rate of light-dependent reactions and thus obtain a very high labeling efficiency in growing plant system. The system was also validated for primary metabolism with maximum 6% deviation of label enrichment between proteinogenic amino acids and secondary metabolites, even after a leaf growth period of 15 days. Thereby, the foundation was laid to trace ^{13}C for studying sink leaf metabolism and to further increase the accuracy of estimations of metabolic fluxes within growing plants for longer durations.

3.2. Results

The development of a ^{13}C incorporation method on monoterpene of peppermint was focused by two approaches; trichome cell culture and shoot-tip culture. Stable isotope labeling experiments were performed on such a culture system by feeding with exogenous labeled glucose to synthesize labeled monoterpenes. Monoterpenes are C_{10} compounds having (M+0) to (M+10) mass isotopomers, for example, the molecular weight of (M+0) to (M+10) mass isotopomer of pulegone is 152.23 to 162.23 Da. On using the source of entirely unlabeled glucose, theoretically, the lowest mass isotopomer (M+0) depicts the highest accumulation, while in case of uniformly labeled glucose source, the highest mass isotopomer (M+10) exhibits the highest accumulation. Here, various approaches are first explicitly described that were employed towards achieving and maintaining high ^{13}C label enrichment in monoterpene and the application of this method was finally discussed in studying ^{13}C-MFA via sink leaf metabolism.

3.2.1. Establishment of the ^{13}C enriched trichome cell culture

Secretory cells of GTs were isolated from young peppermint leaves (10-12 days aged) and observed under light microscopy. Both early and matured stage trichome cells were found in the isolated sample. Eight secretory cells of one trichome formed cell cluster which was surrounded by the cuticle layer (Figure 11). The viability of the trichome cell was examined by FDA-PI staining. Although cells were intact in nature and looked alive, they did not emit either green or red colour in the presence of fluorescence light during the assay. It was suspected that the staining solution could not enter into the trichome cell due to the hard outer layer.

In the next step, isolated cells were cultured in U-^{13}C$_6$ glucose (as the sole source of carbon) containing media along with the external supply of energy sources. Culture method was developed by supplying external airflow into the system. Simultaneously, air along with monoterpenes was emitted from the culture and volatiles were trapped into Poropak-Q. The measurement was taken at 1, 2, 6 and 12 hrs after culture initiation by changing VCT consecutively at each time point. Label enrichment was analysed from three monoterpenes which were found to be the highest from the culture (Table 9). Unfortunately, a very low amount (1 - 2.4%) of isotope incorporation was observed in all measured volatiles. The enrichment was not statistically altered over the time. However, cells maintained their shape and intactness during the experiment.

As the high label enrichment was unattainable from the specialized cell culture, ^{13}C MFA method for studying monoterpene biosynthesis was aimed to be designed into the growing plant culture in the successive step. Thereby, peppermint shoot-tip was adopted and optimized for a higher degree of isotope inclusion into monoterpene.
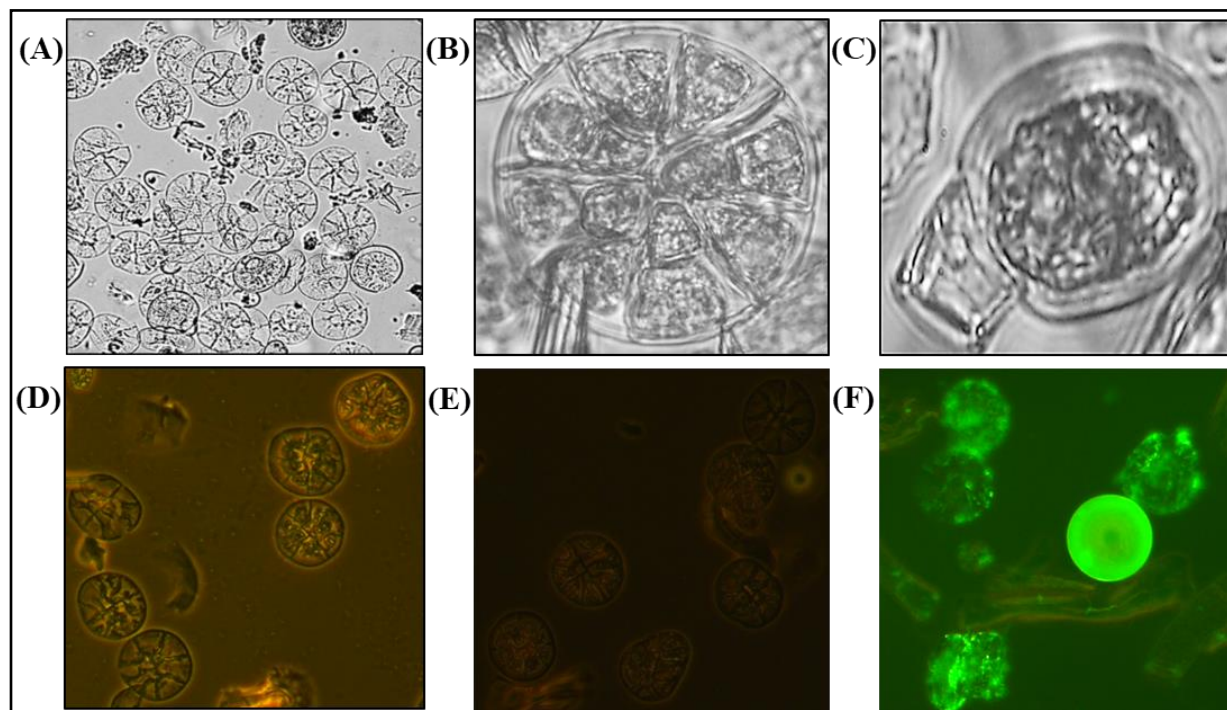
Figure 11. Images of the isolated trichome cells.

Images of (A)-(C) were captured with a phase contrast microscope and images of (D)-(F) were taken with a fluorescence microscope. (A) Overview of isolated trichome cells before culture, (B) matured cell after 12 hrs culture, (C) early-aged cell after 12 hrs culture, (D) light-induced fluorescent image of trichome cell, (E) fluorescent image of trichome cell where no emission of green or red colour and (F) fluorescent image of positive control where green colour emission from the other viable cells from the isolation.

Table 9. Average label enrichment into monoterpenes from trichome cell culture.

Three replications were studied in three successive days (mean ± standard error, n=3).

Monoterpenes	^{13}C enrichment (%) at different time point				
	Control	1 h	2 h	6 h	12 h
Limonene	0.2 ± 0.1	1.7 ± 0.4	1.6 ± 0.2	1.3 ± 0.2	1.7 ± 0.2
Pinene β	0.3 ± 0.1	2.4 ± 0.5	1.7 ± 0.3	1.4 ± 0.4	1.4 ± 0.6
Pinene α	0.2 ± 0.1	1.9 ± 0.4	1 ± 0.2	1.2 ± 0.2	1.8 ± 0.4

Results

3.2.2. Establishment of the ^{13}C enriched shoot-tip culture

The shoot-tip culture studies were performed in liquid medium as compared to solid agar medium, because of the convenience of maintaining the required glucose concentration over time. Each explant was cultivated in a 3.5-4.0 ml liquid medium. In the basal MS medium, glucose was used as a sole carbon source. Growth hormones and antibiotics were not added to the basal medium to minimize the dilution of ^{13}C by unlabeled ^{12}C in the culture system.
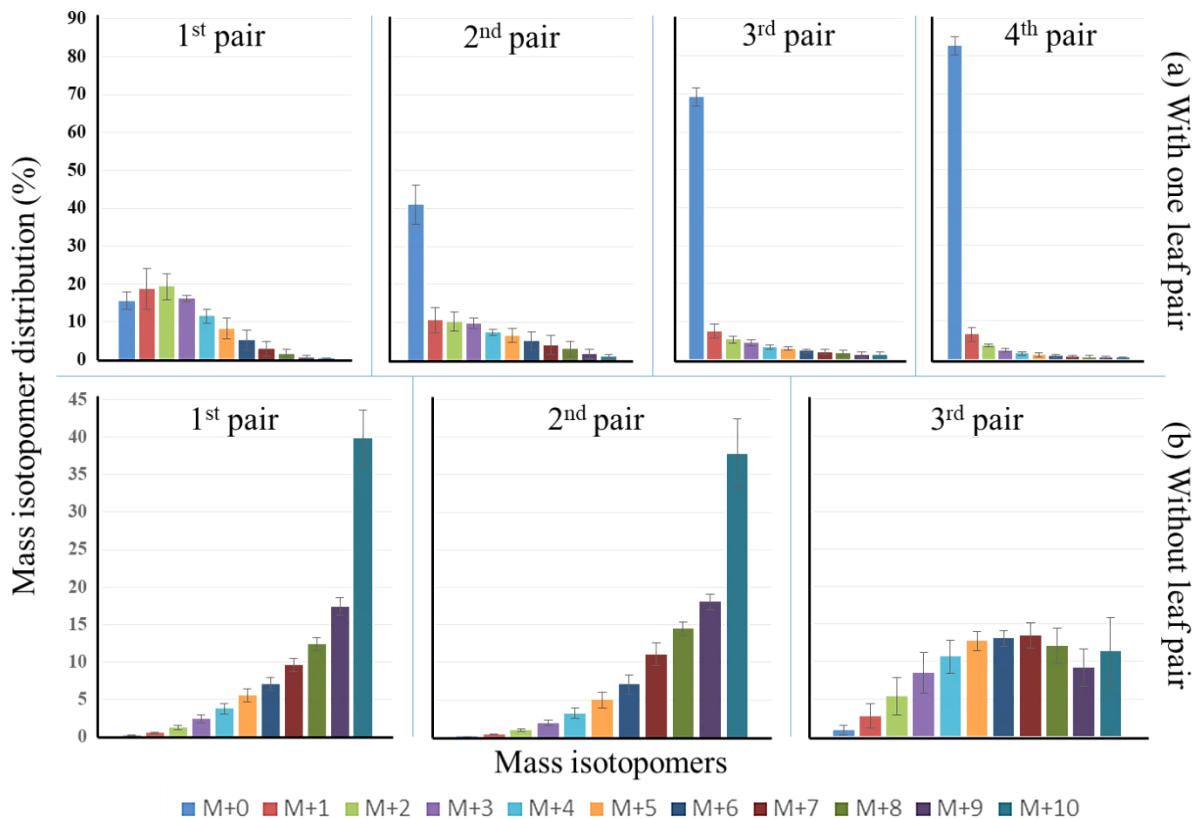
Figure 12. MID of pulegone in each leaf pair at 30 µmol m^{-2} s^{-1} light intensity.

(a) Shoot-tip culture initiated with one developing leaf pair and after 15 days of culture total four leaf pairs (older than 6 days) were observed. (b) Shoot-tip culture started without leaves and at 15 DALV total three leaf pairs (older than 6 days) were observed (mean ± standard error, n=5).

The critical part in the establishment of a predominantly labeled biological system was to minimize the primary unlabeled carbon source. Two strategies were devised in order to find the optimal starting material as an explant for the shoot-tip culture system. Firstly, the shoot-tip culture study (Figure 12a) was initiated with one existing leaf pair and monitored for MIDs after 15 days of the cultivation at 30 µmol m^{-2} s^{-1} light intensity. In spite of feeding shoot-tip with U-^{13}C$_6$ glucose, the (M+10) distribution

of the monoterpene pulegone was the lowest in each pair of leaves, whereas (M+0) isotopomer was the highest in three new pairs of leaves (2nd to 4th pair). This indicated that label incorporation was insufficient and diluted over time with newer leaf pairs. As a consequence, ^{13}C enrichment (Figure 13a) was only 27% in the first leaf pair and gradually decreased in newer leaf pairs. However, higher label incorporation is desirable for better interpretation of ^{13}C-MFA. Therefore, a second strategy was established wherein existing leaf pairs were excised and the explant was raised in similar conditions as described previously. The removal of existing leaves meant that the unlabeled source of carbon was reduced from the explant. After 15 DALV, (M+10) isotopomer was the highest in the first and second leaf pair (Figure 12b). Labeled carbon was more diluted in the newest (3rd) pair of leaves. Similar kind observations were made in other monoterpenes (Figure S3, Figure S4). It was very evident that ^{13}C was highly enriched (61% to 82%) in the second strategy compared to the first (5% to 27%) (Figure 13a, Figure 13b). Thus, it was concluded that the shoot-tip culture method without previously existing leaves was more suitable for ^{13}C-MFA and was used for further analysis within the scope of this investigation.
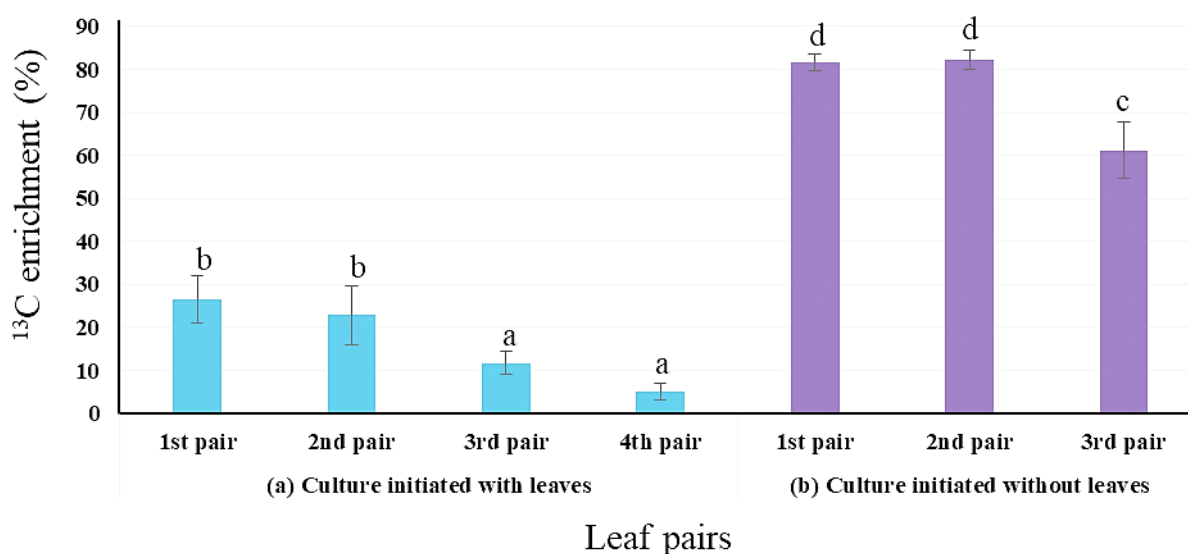
Figure 13. Average ^{13}C enrichment into pulegone of each leaf pair at 30 µmol m^{-2} s^{-1} light intensity.

(a) Shoot-tip culture initiated with one developing leaf pair and after 15 days of culture total four leaf pairs (older than 6 days) were observed. (b) Shoot-tip culture started without leaves and at 15 DALV total three leaf pairs (older than 6 days) were observed. For statistics, data were evaluated by one-way Anova, followed by Tukey HSD test and statistical difference (p<0.05) was indicated by different letters (a to d) (mean ± standard error, n=5).

3.2.3. Determining optimal light conditions through phenotypical characterisation

Light has indirect influence on unlabeled CO_2 fixation from ambient air to plant. Hence, the effects of different light intensities (5, 10, 20 and 30 µmol m^{-2} s^{-1}) on ^{13}C enrichment were studied to increase the label incorporation even beyond the maximum observed from aforementioned shoot-tip culture method establishment. Leaves were harvested at either 15 or 20 DALV since monoterpene biosynthesis and total monoterpene content was noted to be pronounced at this respective leaf age (Gershenzon et al., 2000). The highest glucose uptake was 55 mg per shoot-tip explant under studied light intensities for 15 DALV (Table S1). Hence, the basal medium (3.5-4.0 ml) was supplemented with 2% w/v (70-80 mg) glucose, which was more than the required amount of the culture. Growing explants were morphologically and physiologically characterised to gain a deeper understanding of their growth status under different light intensities. Two morphological traits (Table 10), the total leaf weight and the number of leaves, were determined. The lowest selected light intensity for the culture was 5 µmol m^{-2} s^{-1}. Explants, grown at lower than 5 µmol m^{-2} s^{-1} light intensity, showed no visible leaf emergence. Leaf pairs, which were visible for more than three days, were counted. After 15 DALV, the total number of leaf pairs (2 pairs) remained the same for 5-20 µmol m^{-2} s^{-1} light intensity (Table 10, Figure S5). However, the explant grown at 30 µmol m^{-2} s^{-1} light intensity, showed the development of an extra pair of leaves (3rd pair). Total leaf weight was also observed to increase with increasing light intensity and was significantly highest under 30 µmol m^{-2} s^{-1} light.

In order to better understand the physiological status of these explants under different light intensities, amounts of chlorophyll a, b and carotenoids were quantified for both the shoot-tip cultures as well as normal soil-grown peppermint plants in growth rooms. As presented in Table 11, chlorophyll a and b was notably higher at 30 µmol m^{-2} s^{-1} than at 5-10 µmol m^{-2} s^{-1} light. The normal plant (*in vivo*) also demonstrated similar chlorophyll a and b contents to these shoot-tip explants. The chlorophyll a to b ratio was also computed to get a better understanding of the adaptive response of the light-harvesting complex. Significantly higher chlorophyll a to b ratio was noted in the lower two light intensities, compared to the maximum two cultured light conditions. In addition, carotenoid contents were unaffected at different light intensities.

Table 10. Phenotypic traits of peppermint shoot-tip culture under different light intensities.

The measurement was taken at 15 DALV growth stage. For statistics, data were evaluated by one-way Anova, followed by Tukey HSD test and statistical difference (p<0.05) was indicated by different letters (mean ± standard error, n=5). Zero standard error of leaf number was calculated, as all observations of the same treatment were identical.

Light intensities	Total leaf weight (mg)	Total number of leaves
5 µmol m^{-2} s^{-1}	41.92 ± 3.55 [a]	2 pairs
10 µmol m^{-2} s^{-1}	43.44 ± 6.76 [a]	2 pairs
20 µmol m^{-2} s^{-1}	59.36 ± 3.05 [b]	2 pairs
30 µmol m^{-2} s^{-1}	90.89 ± 4.60 [c]	3 pairs

Table 11. Production of phytopigments (mg g^{-1} leaf fresh weight) in 15 DALV old shoot-tip culture.

Shoot-tip culture reared under different light intensities (mean ± standard error, n=5). For statistics, data were evaluated by one-way Anova, followed by Tukey HSD test and statistical difference (p<0.05) was indicated by different letters.

Light intensities	Chlorophyll (mg g-1)			Chl (a/b)	Carotenoids (mg g-1)
	Chl a	Chl b	Total (a+b)		
5 µmol/m^2/s	1.11 ± 0.09 [a]	0.66 ± 0.02 [a]	1.77 ± 0.11 [a]	1.68 [b]	0.23 ± 0.02 [a]
10 µmol/m^2/s	1.15 ± 0.04 [a]	0.76 ± 0.08 [a]	1.91 ± 0.11 [a]	1.52 [b]	0.20 ± 0.01 [a]
20 µmol/m^2/s	1.27 ± 0.05 [ab]	1.12 ± 0.04 [b]	2.38 ± 0.04 [b]	1.13 [a]	0.20 ± 0.02 [a]
30 µmol/m^2/s	1.46 ± 0.11 [b]	1.20 ± 0.07 [b]	2.66 ± 0.09 [c]	1.21 [a]	0.22 ± 0.05 [a]
In vivo condition	1.53 ± 0.03 [b]	1.00 ± 0.07 [b]	2.54 ± 0.09 [bc]	1.54 [b]	0.31 ± 0.02 [b]

On the basis of this limited morpho-physiological characterisation, it can be deduced that the best development of plant was detected under higher light intensity, however, lower light intensity did not show any adverse effects on plant growth and its physiological status.

3.2.4. Establishing optimal light conditions for the highest and stable ^{13}C incorporation

Once the establishment of optimal light conditions for satisfactory growth of explants in the shoot-tip culture system was achieved, it was now imperative to optimise the conditions for higher and stable ^{13}C incorporation in the plant terpenoids, which were the main focus of this scientific research. Previously it was shown that volatile terpenes cannot be detected in peppermint leaves younger than 7 days (Gershenzon et al., 2000), hence the leaves older than 6 days were further analysed for the terpene content. Qualitative and quantitative analyses were accomplished for eleven monoterpenes and one sesquiterpene from these shoot-tip cultures under different light intensities (Figure 14).

Results

Pulegone was the most abundant monoterpene in the leaves followed by menthofuran and isopulegone. The relative amounts of other monoterpenes and sesquiterpene were very limited. Interestingly, most of the monoterpenes (except pulegone, cineole, sabinene hydrate and germacrene D) were apparently produced in higher amounts under the lowest light intensity. The maximum accumulation of the total volatile terpenoids per unit of leaf weight was also observed under 5 µmol m^{-2} s^{-1} light intensity. Compared to the *in vivo* condition, the total amount of volatiles was not statistically altered, however, menthol and cineole were more abundant under natural light than the studied light intensities.
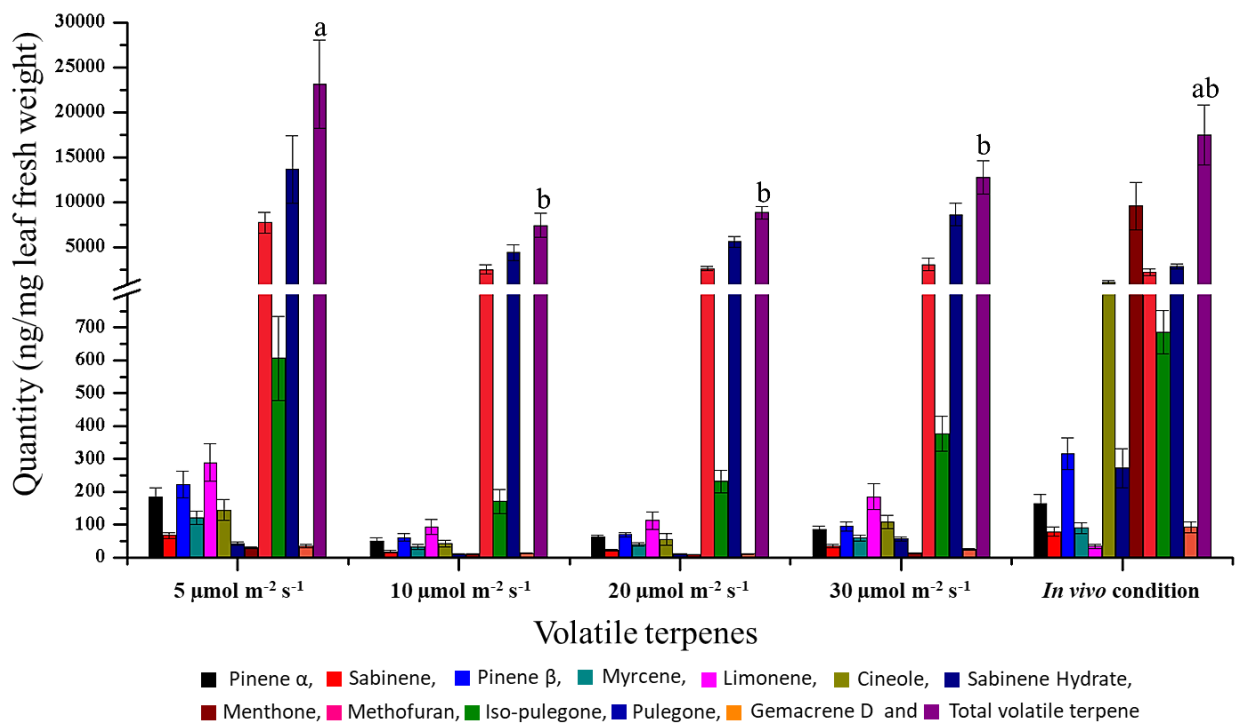
Figure 14. Comparison of volatile terpenes (ng/mg leaf fresh weight) produced under four studied light intensities and in vivo condition.

11 monoterpenes, one sesquiterpene (germacrene D) and total of those volatiles were found in 15 DALV old leaves. For statistics, total terpene amounts were evaluated by one-way Anova, followed by Tukey HSD test. Statistical difference ($p<0.05$) was indicated by different letters (a to b) (mean ± standard error, n=5).

Higher amounts of pulegone, allowed it to be selected as a prime candidate for further MID analysis. As a control, unlabeled glucose was used as a sole carbon source and the label distribution in (M+0) isotopomer after natural abundance correction was accounted to be 99.74% (Figure S6). Uniformly labeled glucose (U-$^{13}C_6$) replaced unlabeled glucose into the shoot-tip culture medium to study the

label incorporation patterns through the MIDs within pulegone. The highest accumulation of the (M+10) isotopomer of pulegone in all pairs of leaves was observed under 5 µmol m^{-2} s^{-1} light condition, irrespective of their age (Figure 15a). Such a desirable pattern of isotopomer distribution was also noticed in explants grown under 10 µmol m^{-2} s^{-1} light until 15 DALV (Figure 15b). The shoots exposed to 20 and 30 µmol m^{-2} s^{-1} light intensities showed varied dilution of the labeled carbon within several mass isotopomers of pulegone (Figure 15c and d).

While exploring the leaves of different age, it was apparent that the labeling percentage was decreased with the increasing age of shoot culture. For instance, the contribution of (M+10) isotopomer of the second pair of leaves at 5 µmol m^{-2} s^{-1} was slightly declined from 89% to 80% with increasing age from 15 DALV to 20 DALV (Figure 15a). Similarly, this dilution of the label was even more prominent under 10 µmol m^{-2} s^{-1} light (Figure 15b). The amount of decreasing percentage in (M+10) isotopomer was 13% and 50% in the first and second pair of leaves respectively (Figure 15b) with advancing leaf age. No significant effects were observed within the (M+10) isotopomer in the specific leaf pair from 15 to 20 DALV (Figure 15c and d) under two higher light intensities.

Comparison between different leaf pairs revealed that the newest leaf pair (3rd pair) always had the lowest abundance of (M+10) isotopomer. Among pulegone of different leaf pairs found at 5 µmol m^{-2} s^{-1} light after 20 DALV, accumulation of highest isotopomer (M+10) was markedly lower in third leaf pair (50%) (Figure 15a). Moreover, this accumulation was continuously attenuated with each newer leaf pair of 20 DALV aged plant under 10 and 20 µmol m^{-2} s^{-1} light intensities (Figure 15b and c). Although the first two leaf pairs from tested under highest light intensity had significantly indifferent (M+10) distribution, however, the third leaf pair had the least accumulation (Figure 15d). Thus, the accumulation of label showed a significant difference between the leaf pairs for the plants exposed to different light intensities. The only exception to this comparison at a specific age was 15 DALV aged plants exposed to 5 and 10 µmol m^{-2} s^{-1} light intensities (Figure 15a and b).

^{13}C enrichment and label dilution were calculated for more accurate and precise measurement of the label incorporation into pulegone. Correction of 1% ^{12}C impurity in U-^{13}C$_6$ glucose was considered to determine the dilution of labeling appropriately. Measured dilutions were derived from either unlabeled carbon of initial explant or externally unlabeled CO$_2$ exchange through photosynthesis. At 15 DALV (Figure 16a, Figure 17a), each leaf pairs from lower two light intensities had the best amount of label enrichment (~ 100%) and equivalently the least amount of dilution. Indeed, unlabeled

carbon fixation constantly enhanced with increasing light intensity, increasing leaf age and into the newer leaves. As a consequence, higher ^{13}C dilution (35% to 45%) were observed in the 3rd leaf pair at 20 DALV under higher light intensities (20 and 30 μmol m^{-2} s^{-1}) (Figure 17b).

Real-time measurement of CO_2 assimilation rate in 15 days old leaves from these cultures was also assessed for better understanding of the isotopic dilution due to the fixation of ambient CO_2 (Table 12). Peppermint plants consumed less ambient carbon under reduced light conditions (5 and 10 μmol m^{-2} s^{-1}). The assimilation was relatively escalated at high light intensities (20 and 30 μmol m^{-2} s^{-1}). Furthermore, the net CO_2 uptake was invariable under different light intensities between shoot-tip culture and natural peppermint plants.

Table 12. Photosynthetic assimilation rates of 15 days old leaves.

The measurement was taken from the shoot-tip cultures and normal plants. The measurements were taken using the LI-6400XT portable gas exchange system (Li-Cor Inc., Lincoln, NE, USA) (mean ± standard error, n=5).

Light intensity (μmol m^{-2} s^{-1})	Assimilation rate (μmol $_{(CO2)}$ m^{-2} $_{(leaf area)}$ s^{-1})	
	Shoot cultures	Normal plants
5	-0.402 ± 0.094	-0.482 ± 0.114
10	-0.129 ± 0.089	-0.101 ± 0.056
20	0.433 ± 0.082	0.461 ± 0.123
30	0.518 ± 0.077	0.661 ± 0.112

3.2.5. Establishing the effects of different light intensities on glucose consumption

The glucose uptake was determined in these shoot-tip culture experiments, in order to understand the biosynthetic demand of carbon from sugar in the basal media rather than environmental CO_2 fixation. After 15 DALV, 987 and 1084 μg glucose was consumed by the cultured explants under 5 and 10 μmol m^{-2} s^{-1} light, respectively, to produce one mg leaf. However, glucose uptake amounts were progressively reduced at 20 μmol m^{-2} s^{-1} light intensity followed by further reduction at the highest light condition (Figure 18A). Analysing the glucose demands at 5 μmol m^{-2} s^{-1} light intensity across different developmental stages of the shoot indicated that 14 mg of glucose was consumed by each explant up to leaf initiation stage. Afterwards, the uptake rate was increased and 41 mg was consumed up to 15 DALV (Figure 18B).
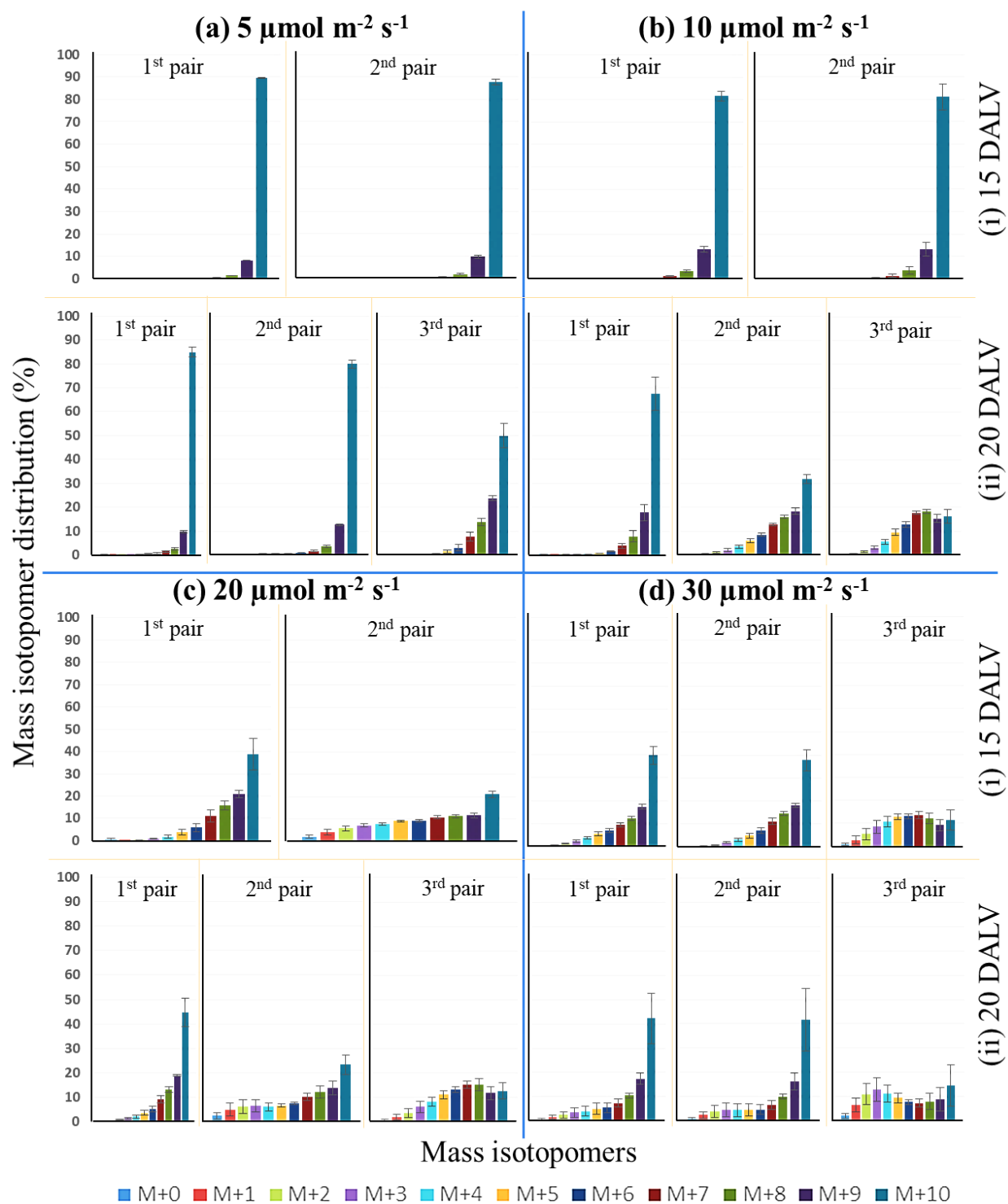
Figure 15. MIDs of pulegone in different leaf pair observed under different light intensities.

(a) shoot-tip culture at 5 μmol m^{-2} s^{-1} light intensity, (b) shoot-tip culture at 10 μmol m^{-2} s^{-1} light intensity, (c) shoot-tip culture at 20 μmol m^{-2} s^{-1} light intensity and (d) shoot-tip culture at 30 μmol m^{-2} s^{-1} light intensity. Measurement was taken on (i) 15 DALV and (ii) 20 DALV for each light intensity (mean ± standard error, n=5).
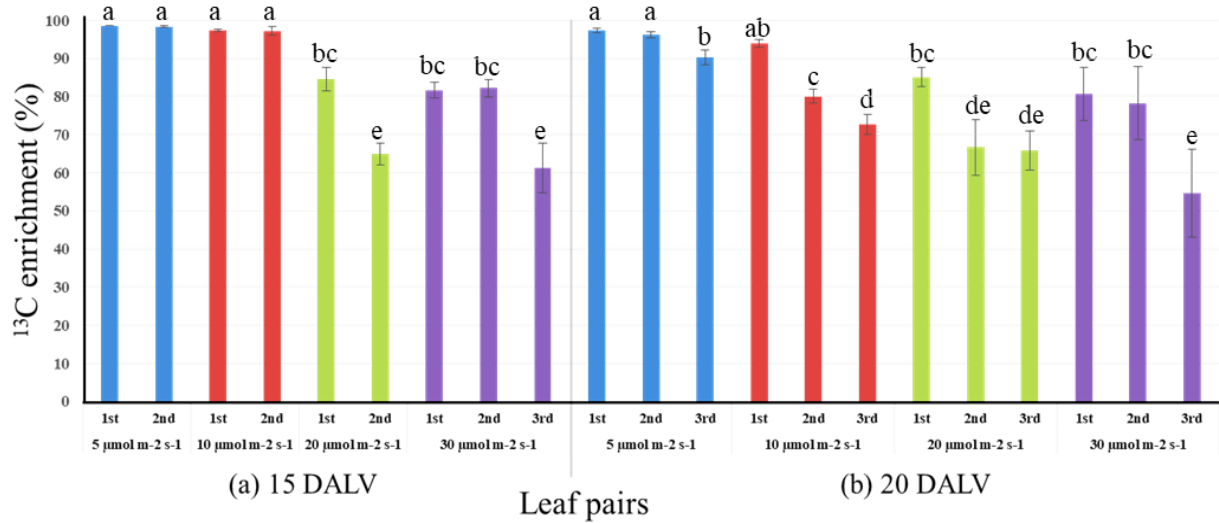
Figure 16. Average ^{13}C enrichment into pulegone in different leaf pair observed under four investigated light intensities.

The measurement was taken from the shoot-tip culture of (a) 15 DALV and (b) 20 DALV. For statistics, data were evaluated by one-way Anova, followed by Tukey HSD test and statistical difference ($p<0.05$) was indicated by different letters (a to e) (mean ± standard error, n=5).
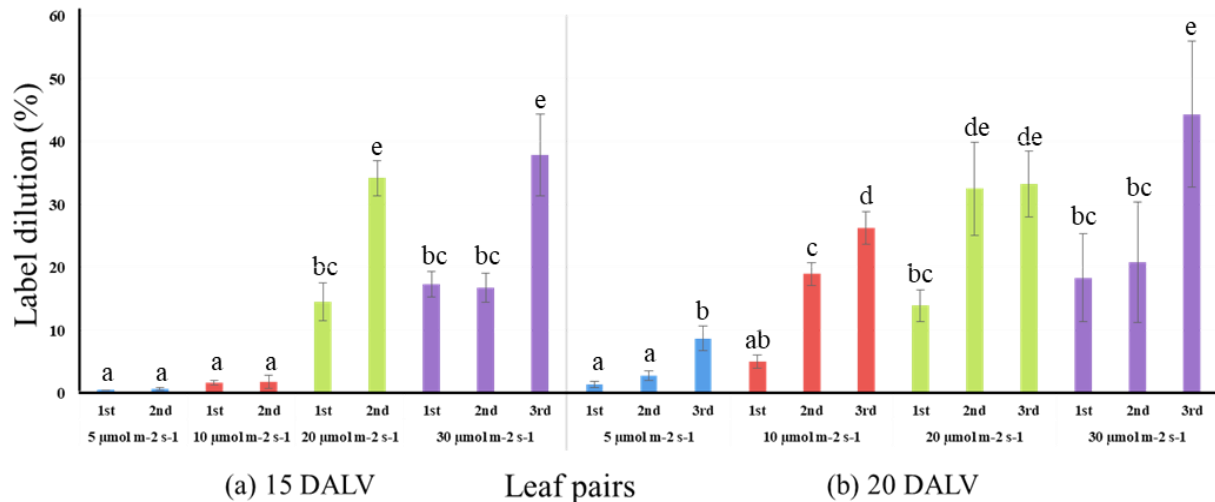
Figure 17. Average isotope dilution into pulegone in different leaf pair observed under four investigated light intensities.

The measurement was taken from the shoot-tip culture of (a) 15 DALV and (b) 20 DALV. For statistics, data were evaluated by one-way Anova, followed by Tukey HSD test and statistical difference ($p<0.05$) was indicated by different letters (a to e) (mean ± standard error, n=5).
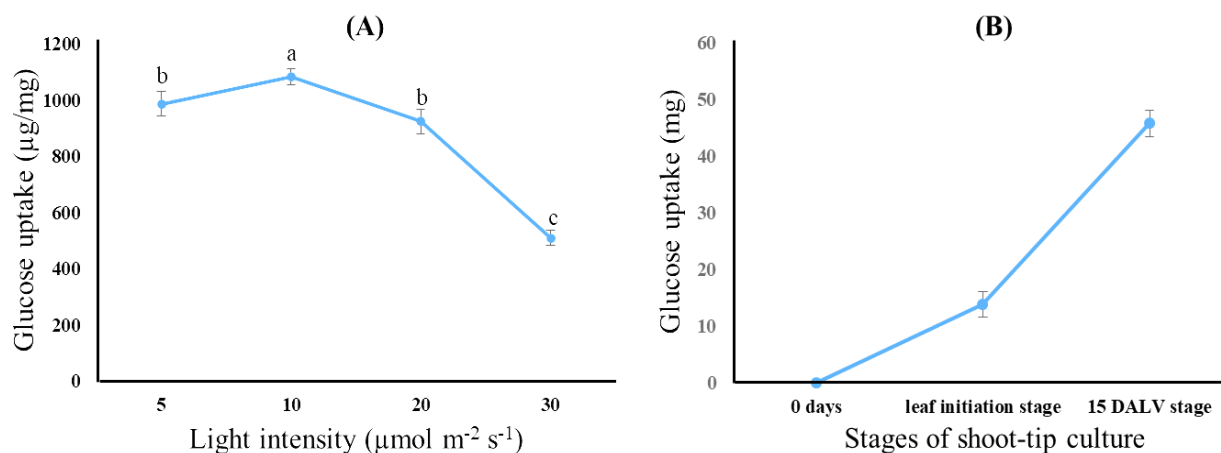
Figure 18. Biosynthetic demand of glucose by shoot-tip culture.

(A) Comparison of glucose uptake (µg/mg leaf fresh weight) at 15 DALV growth of the shoot-tip culture under different light intensities, (B) requirement of glucose (mg) per shoot-tip culture during different growth stages up to 15 DALV at 5 µmol m^{-2} s^{-1} light intensity. (Mean ± standard error, n=5). For statistics in the first case, data were evaluated by one-way Anova, followed by Tukey HSD test and statistical difference (p<0.05) was indicated by different letters (a to c).

Validation of the method:

Throughout the growth and development of a biological system, amino acids are produced from different parts of the central carbon metabolism such as glycolysis, PPP and tricarboxylic acid cycle (TCA) (Table 7) (Dersch et al., 2016). These amino acids are translated into proteins. Thus, label incorporation throughout the whole system could be validated by the isotope inclusion into such proteinogenic amino acids. ^{13}C enrichment in five protein-bound amino acids was evaluated using uniformly labeled glucose in the medium under best labeling condition (Figure 19). Enrichment of labeled carbon was robust, varying from 94% to 99%. This validated the result of monoterpenes and confirmed that mint shoot culture under low light intensity was predominantly dependant on the supplied glucose. The sources of unlabeled carbon in amino acids were anticipated to be due to the fraction (1%) of ^{12}C impurity from the labeled glucose, photosynthetically fixed atmospheric carbon and (or) translocation of unlabeled amino acids from the initial explant shoot to the new sink leaves.

The shoot-tip culture strategy was also further validated in oregano plant under 10 µmol m^{-2} s^{-1} light intensity. These explants showed no visible leaf emergence at lower light intensities. Dilution of ^{13}C isotope into monoterpene was found to be limited (1.36% to 1.83%) in growing shoot-tips at 15 DALV (Table 13).
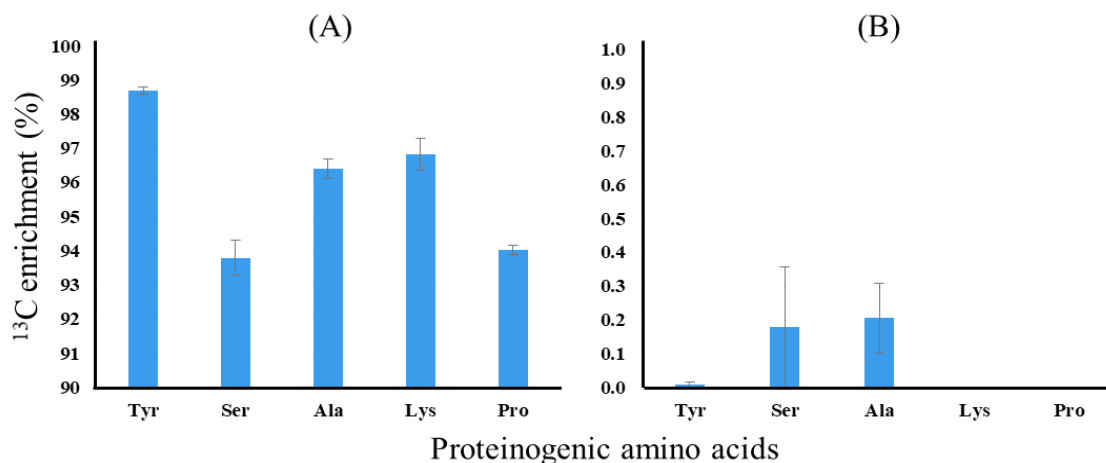
Figure 19. *Average ^{13}C enrichment into proteinogenic amino acids in leaves of 15 DALV.*

(A) Cultured with U-$^{13}C_6$ glucose and (B) cultured with ^{12}C glucose (control) at 5 µmol m^{-2} s^{-1} light intensity (mean ± standard error, n=5).

Table 13. *Average isotope dilution into sabinene hydrate in two leaf pairs of oregano shoot-tip.*

The culture was reared under 10 µmol m-2 s-1 light intensity and measurement was taken at 15 DALV. (Mean ± standard error, n=5).

Leaf pair	Label dilution (%)
First	1.83 ± 0.19
Second	1.36 ± 0.05

3.3. Discussion

Maintaining high isotope enrichment for steady-state MFA is rather easy in cell culture, compared to a growing green plant. Indeed, the establishment of a culture system is crucial and determined by cellular structure and biochemistry. Mint GTs are non-photosynthetic cells, hence they depend on external carbon source for their metabolism. However, they could not uptake adequate amount of labeled glucose in the present investigation (Table 9). Over 12 h of the cultivation period, label inclusion was not significantly enhanced. Interestingly, these specialized cells neither uptake FDA nor PI dye (Figure 11). Even if FDA could not pass the hard layer of the living cell, yet PI must enter through the ruptured outer membrane of any dead cells. These observations suggested that isolated cells were perhaps alive, however prone to be impermeable to ^{13}C glucose or FDA stain. Nevertheless, it has been previously exhibited that isolated trichomes from peppermint plant have been successfully cultured by supplying radioisotopic sucrose (Johnson et al., 2017; McCaskill et al., 1992; McCaskill

and Croteau, 1995). [13]C labeled sucrose was not a feasible option to use for establishing a culture method as it costs nearly 100 times more than the price for the same amount of ^{13}C-glucose.

3.3.1. A metabolic sink system with enriched carbon isotope content

The main concept of sink and source leaves is that sinks are net importers, while the latter ones are net exporters of carbon assimilates (Larson and Dickson, 1973; Turgeon and Webb, 1975). There are two kinds of the sink, namely utilization sinks (meristem, immature leaves) and storage sinks (tuber, embryo, and seed). The utilization sinks are metabolically active and can also be referred to as metabolic sinks. When fed with isotopic tracers, these metabolic sinks provide a unique system to study changes in plant metabolic networks. Firstly, when one or more source leaves existed in the short-term ^{13}C tracer study using the shoot-tip culture system, a larger dilution effect from the unlabeled biomass of the already existing leaves towards ^{13}C enrichment was observed (Figure 12a, Figure 13a). The reason for such a negative effect in the new sink leaves was mainly due to the additional import of unlabeled carbon from the existing source leaves. In the latter strategy without any source leaf, the newly developed immature leaves showed high label enrichment as there were no initial source leaves, except for 0.5 cm of shoot explant, which otherwise could have led to label dilution. Therefore, the biomass of the first leaf pair was nearly exclusively built from the externally supplied, labeled glucose. This technique of initiation of a culture without any existing (source) leaves exhibited more than three-fold higher label enrichment in monoterpenes, compared to the system with previously existing leaves (Figure 13).

3.3.2. A system for further simplification of ^{13}C-MFA in plant

In a growing plant, photosynthetic activity of the leaf increases with its age (Jeong et al., 2004). Through this system, it was proved that modulating the intensity of light had a respective effect on external CO_2 fixation. In this study, leaves grown under the highest experimental light intensity indirectly exhibited ambient CO_2 consumption, even at half leaf expansion stage (15 DALV). Previous observations demonstrated that peppermint leaves expanded to half size after 15 days and to full size after 21 days (Turner et al., 2000). Thereupon, isotopic dilution due to unlabeled CO_2 fixation was varied from 17% to 38% (Figure 17a). This result was supported by the previous reports about the transition from predominantly sink leaves to predominantly source leaves after 30% to 60% of the leaf age (Fellows and Geiger, 1974; Turner et al., 2000). Within this transition, leaves change

Discussion

from net carbon importers to net carbon exporters. However, label dilution due to fixation of unlabeled CO_2 was very limited under the lower two light conditions at half leaf expansion stage (Figure 17a). It can be concluded that the first pair of leaves at these two reduced light conditions acted as metabolic sinks due to a limitation of light reactions. The amount of sucrose available in source leaves for transporting to sink tissues depends on photosynthetic activity (Lemoine et al., 2013), which is quite identical at higher light (30 µmol m^{-2} s^{-1}) intensity. This is in contrast to reduced light conditions (5 or 10 µmol m^{-2} s^{-1}). Transported sugars from pre-mentioned sources (first leaf pair after 15 DALV) to new sinks (second leaf pair after 15 DALV) was mostly made from external ^{13}C glucose under low light. The glucose consumption data also indicated that at a higher light intensity, the shoot-tip explants employed photosynthesis to satisfy their carbon demands partly, whereas at lower light intensities they showed increased dependence on the externally supplied glucose (Figure 18). Previous studies confirmed that upregulation of hexose content causes downregulation of photosynthesis (Herold, 1980; Paul and Driscoll, 1997; Paul and Foyer, 2001; Turgeon, 1989). This was further corroborated with real-time measurement of photosynthetic rate via carbon dioxide assimilation studies on 15 days old leaves (Table 12). Peppermint plants showed negligible carbon dioxide uptake rates under reduced light conditions (5 and 10 µmol m^{-2} s^{-1}). However, at a higher light intensity (20 and 30 µmol m^{-2} s^{-1}) they showed increased carbon dioxide assimilation. Thus, this low light shoot-tip system can avoid photosynthetic label scrambling for ^{13}C MFA in plants.

This system also displayed competent growth as new leaves emerged, although at a slower rate, however with similar volatile and pigment content, compared to the plants grown at ambient light conditions (Figure 14, Table 11). Despite the fact that low light ensured a reduction in photosynthesis over two weeks, the amount of various phytopigments remained very similar under different light intensities. In addition, statistically similar chlorophyll a/b ratio at normal and 5 µmol m^{-2} s^{-1} light was indicating that the peppermint plants could adapt to the low light. In addition, no remarkable differences were observed in the terpenoid content. This suggested that the shoot-tip culture system was very stable over time and that altering the light intensity did not negatively affect the growth capacity of the explant while simultaneously resulting in a high label enrichment.

The high label in hydrolysed amino acids further proved the efficacy of the shoot-tip system to be used as an *in vitro* system for ^{13}C MFA. Label in different amino acids was varied up to only 5%. It might be possible that some amount of unlabeled amino acids were transported from the explant

shoot-tip to the sink tissue for the initial growth of shoot culture (Lonien and Schwender, 2009; Williams et al., 2010). Hence, the amount of ^{13}C in serine and lysine are slightly different from the label in tyrosine. Amino acids are produced by different metabolic pathways and in different compartments of the cell. For instance, the label amount in tyrosine, which is produced in the plastid (Dersch et al., 2016; Rippert et al., 2009) strongly represents the effect of photosynthesis. More than 98.5% label in tyrosine suggested that this culture system relied on external glucose over 15 days of leaf growth, rather than CO_2 fixation (Figure 19). Tyrosine, serine, alanine, lysine and proline are also synthesised from different intermediates of several primary metabolic pathways as described in Table 7. In addition, these amino acids are produced in different cellular compartments such as cytosol, plastids and mitochondria. A very high percentage of isotopic inclusion in proteinogenic amino acids (Figure 19) illustrated high ^{13}C enrichment throughout the plant metabolic network and various subcellular compartments. This result strongly recommends the use of this system in carbon-based MFA to study the metabolism of developing leaves.

Plants have a complex metabolic system where the matrix effect of interaction between various inter- or intra-compartment metabolic pathways at the cell level are apparent (Heinig et al., 2013; Sweetlove and Fernie, 2013). Indeed, investigation of concerned metabolic pathways in the normal and continuously growing plant is much more realistic than in the specific organ culture. Secondary metabolite production requires a longer time period. Maintaining high ^{13}C enrichment and isotopic steady-state over longer time periods are challenging for steady-state MFA, due to impoverished labeling amounts on exposure to light. Therefore, on previous occasions, time-course labeling experiments were undertaken for instationary MFA study on plant secondary metabolism (Boatright et al., 2004). Here in this study, the shoot-tip culture system enabled us to maintain the growing plants for over two weeks with virtually 100% isotopic enrichment in monoterpenes, thereby extending the area in steady-state flux analysis of plant secondary metabolism. Interestingly, this system can also be implemented in other plants, however, it may warrant other necessary alterations in light intensities or growth hormone addition. For instance, oregano plant grown under this shoot-tip culture system with 10 µmol m^{-2} s^{-1} light intensity showed very low isotopic dilution (Table 13).

3.3.3. A system to study sink-source transition in leaves

Young leaves are mixotrophic, growing partially depending on the carbohydrates imported from other organs of the same plant. Mature leaves, on the other hand, are autotrophic, producing an excess of photo-accumulates and acting as the plant's major sources for transportable sugar (Turgeon, 1989). As the young leaves develop into mature leaves, the effect of photosynthesis increases and carbohydrate metabolism is switched from catabolic to anabolic pathways. During ontogeny, leaves undergo a developmental transition from net importers (sink) to net exporters (source) of photo-assimilates (Harn et al., 1993). In this transition, minimum three different phases are observed. At an early immature phase, the leaves are fully dependent on the source for their carbon need and act predominantly as sink tissue. After some days, at a late immature phase, the leaves are capable to make their own carbon with increasing photosynthetic activity, although they are still mostly dependent on other source leaves and remain as a sink. Finally, immature leaves become mature and transform themselves to become the source tissue for new sink leaves due to their own photosynthetic assimilation (Turgeon, 1989). In this system, it was observed that the leaves after 15 DALV at 5 and 10 µmol m^{-2} s^{-1} light (Figure 16a) behaved like the first phase of sink tissue where they were almost fully dependent on the external isotopic carbon source. The best portrait of photosynthetic activity in the middle phase of sink-source transition could be demonstrated in leaves of 20 DALV age at the lowest light intensity (Figure 16b). At this stage, the cultured plant started to make photoaccumulates and therefore isotopic enrichment was decreased; nevertheless labeled glucose was still the major source for carbon supplies. The effect of photosynthesis was also observed on the final phase when ^{13}C enrichment of monoterpene in the third leaf pair at 30 µmol m^{-2} s^{-1} light intensity was reduced to 54% (Figure 16). A plausible idea is suggested here that the first pair of leaves, which had started to photosynthesize, acted as source leaves by transporting the sugars to the 3rd pair of leaves and thereby diluting the labeled carbon. This finding indicated that the U-^{13}C$_6$ glucose study with altering the light intensity allowed us to gain a deeper understanding of the sink to source transition of developing mint leaves. This system, therefore, provides an excellent tool for investigating sink leaf metabolism (Malinowski, 2013; Nakayama and Kuhlemeier, 2009).

Concerning the principal objective of the present endeavor, this culture strategy enlightened a concrete step for performing steady-state ^{13}C MFA towards peppermint monoterpene biosynthesis.

Chapter IV: Assessment of metabolic fluxes in secretory trichome cells

---

4.1. Introduction

Plants have two independent pathways for supplying precursors of terpene biosynthesis: the plastidic DXP and the cytosolic MVA pathway. These pathways are compartmentally separated inside the plant cell; however, they synthesize common isomeric isoprenoid units, namely IPP and DMAPP. It is widely accepted that the DXP pathway provides the substrates for mono-, di- and tetraterpenes, while the MVA pathway provides the substrates for sesqui- and tri-terpenes production (Rodríguez-Concepcíon, 2005) (Figure 20). Plant species have evolved several committed organs and cells for the storage of these secondary metabolites at the surface or internally (Tissier, 2018). GTs are one such dedicated extracellular structures and found in 30% of vascular plants (Glas et al., 2012). GTs of the Lamiaceae family exclusively produce and accumulate various volatile terpenes (Lange, 2015).

The essential oil of peppermint, commercially the most valuable for its strong aroma, has monoterpenes as the principal constituent. This volatiles are synthesized and accumulated inside the peltate type GTs to about 88% of their total biomass (Gershenzon et al., 1989; McCaskill et al., 1992). Meta-analysis of mint GTs showed that these cells also exhibited a high degree of metabolic specialization towards terpene biosynthesis (55% of all GT transcripts) (Zager and Lange, 2018). Due to their high biosynthetic activity, these specialized cells of peppermint have been extensively used as a model system for terpene biosynthesis during the last three decades.

Previous studies indicated that the DXP pathway is the exclusively responsible for monoterpene biosynthesis in peppermint GTs (Eisenreich et al., 1997; McCaskill and Croteau, 1995). These studies were based on the feeding of isotopic central carbon intermediate tracer, where ^{13}C incorporation and position of labels in monoterpenes were observed to determine the interaction between the DXP and the MVA pathways. Although the MVA and DXP pathways function in two different subcellular compartments, growing evidence of cross-talk between these two terpene biosynthetic pathways has been reported in other plants, such as the DXP pathway for sesquiterpene production in chamomile (Adam et al., 1999), snapdragon (Dudareva et al., 2005) and cotton (Opitz et al., 2014). This interaction was also shown for sterol biosynthesis in tobacco bright yellow-2 cells (Hemmerlin et al., 2003) and Arabidopsis (Kasahara et al., 2002). The participation of the MVA pathway for producing C_{10} terpenes was also reported previously (Bartram et al., 2006; Hampel et al., 2007; Mendoza-Poudereux et al., 2015; Opitz et al., 2014; Piel et al., 1998; Schuhr et al., 2003).
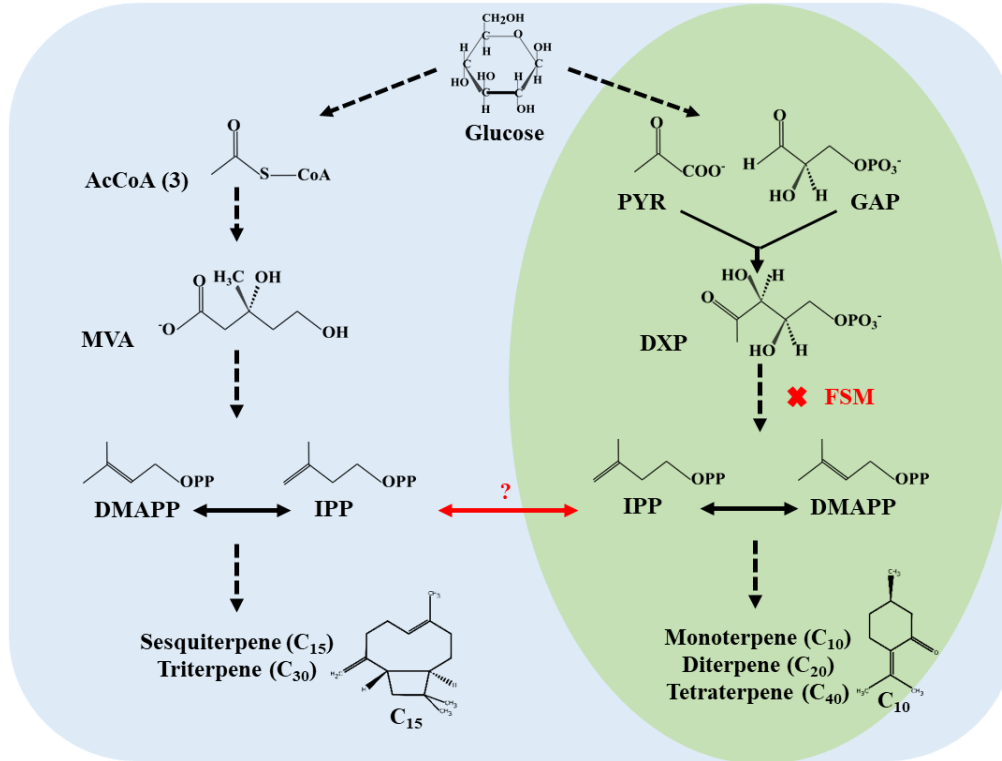
Figure 20. Terpenoid biosynthesis in plants by the means of DXP and MVA pathways
Blue and green area indicate the cytosolic and plastidic organelle of the plant cell, respectively. DXP pathway can be inhibited by fosmidomycin (FSM).

The use of alternative approaches such as inhibitor studies, incorporation of labeled precursors and transgenic methods have resulted in the lack of a consolidated view on the interaction between these two pathways. Studies, to address such interaction, indicated a major role of common isoprenoid precursors such as IPP, GPP, FPP, GGPP (Liao et al., 2006). Mostly, labeled intermediates of the MVA and DXP pathways were utilized in these studies to understand the communication of these two routes for specific terpene production. However, isotopic steady-state of terpenes would hardly be achieved by using pathway intermediates, as the isotope of ^{13}C MVA or ^{2}H DXP are continuously diluted by the incorporation of unlabeled central metabolites into the terpene biosynthetic pathways. Thereby, this strategy might not provide real interpretation. Additionally, increasing the metabolic pool size of these intermediates for a short duration leads to the undesirable upregulation of their respective pathway. While in the case of studies using a longer duration, labeled secondary metabolic intermediates are scrambled with those from the existing unlabeled primary metabolic pool. In inhibitor studies, a complementation effect exhibited by one pathway due to the inhibition of other has also been observed (Laule et al., 2003). These strategies resulted in interaction shifts (increase or

decrease) between pathways for the certain terpene synthesis. For instance, ^{13}C enrichment into sesquiterpenes and monoterpenes from respectively labeled MVA and DXP varies from 3-95% and 0-90% in the above-mentioned cross-talk studies, while those being the classical biosynthetic means for corresponding terpenes. Thus, such investigations suggest a more unnatural outcome. Part of the problem in such approaches were the use of detached organs, tissues and cell cultures instead of an intact growing plant system (Opitz et al., 2014). Another problem was the lack of a technique for maintaining high isotope enrichment with continuous feeding of labeled substrate for longer duration to track the terpene production right from the start of its biosynthesis. Due to these issues, relative fluxes of the DXP and MVA pathways and the holistic know-how towards specific terpene biosynthesis remains undefined in any plant species.

In addition to the previous concern, sole observation of the isotopic status in the product from the feeding of ^{13}C central metabolite would provide indecisive quantification of cross-talk. Also, prior to the secondary metabolism, the labeling position from such primary ^{13}C sources are rearranged through different cyclic pathways involved in central carbon metabolism. In other words, *de novo* biosynthesis of monoterpenes from a primary carbon source (sugar) would provide a higher degree of freedom to the system by allowing modulation and interaction between both the classical and the alternative pathways of terpene production.

Furthermore, the central carbon flux of GTs is important to be studied for understanding overall regulation toward the final product at the subcellular level. The cloning and characterization of biosynthetic genes inside these specialized cells were described in the past years (Croteau et al., 2005; Jin et al., 2014; Lange and Turner, 2013; Tissier, 2012). However, unlike secondary metabolism, the understanding of central metabolism in GTs is still very ambiguous, except few recent comprehensive reports in peppermint and tomato plant (Balcke et al., 2017; Johnson et al., 2017; Zager and Lange, 2018). From there, a tentative understanding of the carbon transfer and redox requirements for the terpene biosynthesis has been gained. Such information would be valuable to speculate on cellular biochemistry. However, those investigations were principally based on transcriptomic and genomic data sets, which alone are insufficient to deduce the cellular metabolism.

A comprehensive metabolomics view is desired to draw the further-reaching conclusion about the cross-talk between two terpene biosynthetic routes and the flux regulation inside GTs. For this, ^{13}C-MFA would be the best method of choice to generate a flux map of the GT's biochemistry for volatile

terpene production inside the compartmented network. A parallel MFA approach was implemented by simultaneously fitting data sets of peppermint monoterpenes from three different tracer studies (1-$^{13}C_1$, 6-$^{13}C_1$ and 1,6-$^{13}C_2$ glucose) to a single, compartmentalized flux model. This study offers new insights into peppermint GT metabolism by (1) providing evidence for the contribution of the alternate MVA pathway to monoterpene biosynthesis and (2) allowing quantification of the cross-talk between DXP and MVA pathway along with the central carbon metabolism of peppermint GT towards C_{10} isoprenoid production. To strengthen the understanding of GT metabolism, flux analysis was also accomplished in oregano which is taxonomically from the same mint subfamily.

4.2. Results

4.2.1. Establishing pre-requisites of steady-state ^{13}C MFA
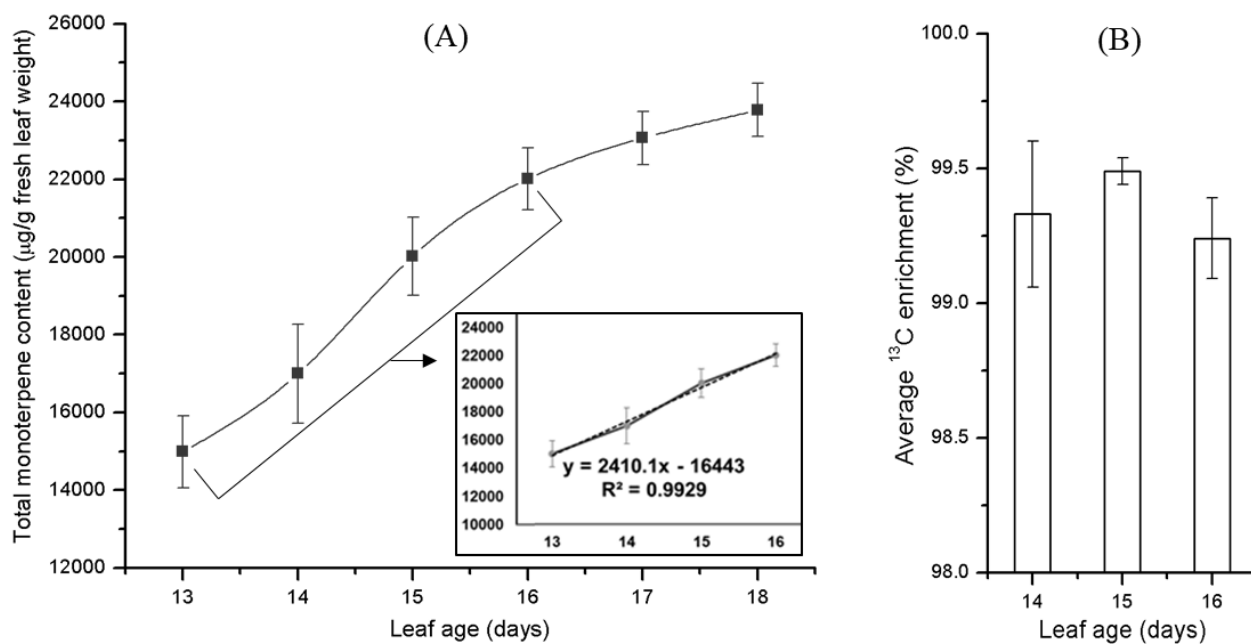
Figure 21. Steady-state determination in the first leaf pair of peppermint shoot-tip culture.
(A) Establishment of metabolic steady-state by quantifying total monoterpene and (B) isotopic steady-state by assessing average ^{13}C enrichment. The culture was grown under 5 µmol m^{-2}s^{-1} light intensity in the basal media containing (A) unlabeled and (B) U-$^{13}C_6$ glucose (mean ± SE, n=5).

The basic requirement for performing steady-state MFA investigation is the metabolically and isotopically stable condition of the studied organism. Steady monoterpene production in the present study was achieved by using the culture method described in Chapter III: Establishment of the experimental set-up for performing MFA. The linear accumulation phase of monoterpene was observed between 13 and 16 days (Figure 21A) which indicated steady monoterpene production

inside the peppermint GTs. Isotopic enrichment into monoterpene was stable during 14 to 16 days age of the leaf-pair (Figure 21B). In addition, as the shoot culture was initiated from the labeled glucose containing media and the leaf emerged using the isotopic carbon source, the initial and maximum ^{13}C enrichment in the leaf could be 100%. The average label incorporation (99.5%) in 15 days old leaf-pair was close to the maximum possible, indicating the isotopically unchanged condition of the GTs. The fifteen day old leaf-pair was selected for further studies.

4.2.2. Tracer analysis
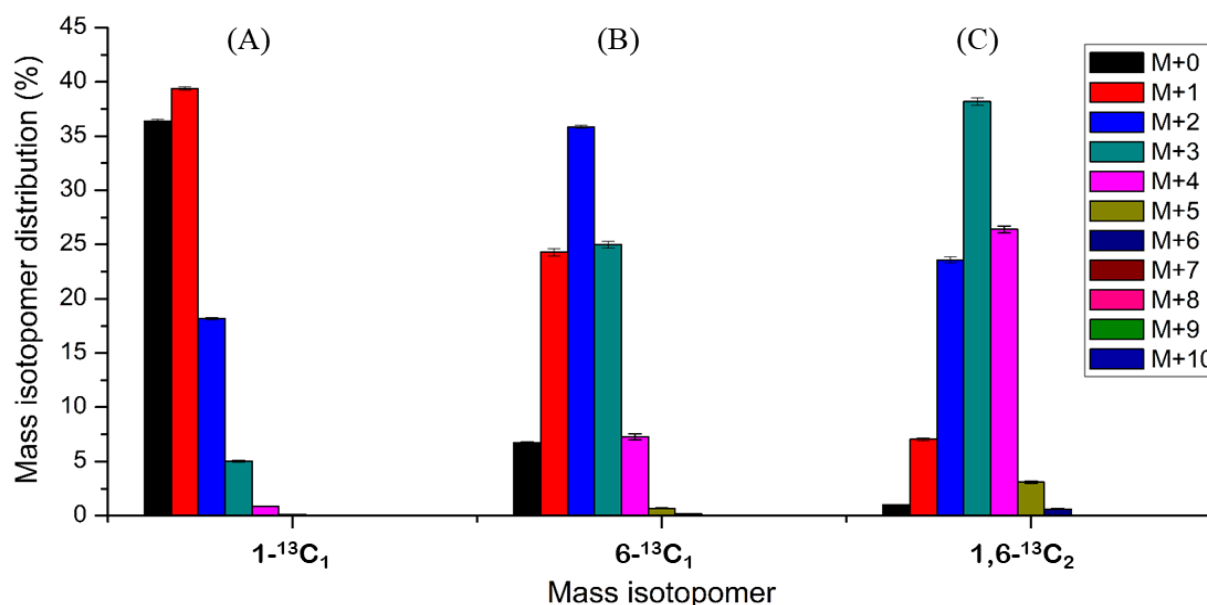
Figure 22. MID of pulegone in the first leaf pair from three different tracer analysis.

Peppermint shoot-tip culture was grown under 5 µmol m^{-2} s^{-1} light intensity in the basal media containing (A) 1-$^{13}C_1$, (B) 6-$^{13}C_1$ and (C) 1,6-$^{13}C_2$ glucose as the sole carbon source (mean ± SE, n=3). Similar MID was also found in other monoterpenes (Table S3 and Table S4).

Integrated MFA predicts much more realistic fluxes than single tracer based MFA. Thus, three different positionally labeled glucose substrates were chosen for interpreting pathways of interest. The pattern of MIDs into monoterpene (pulegone) was dissimilar between two $^{13}C_1$ glucose feeding studies (Figure 22A and B). The abundances of (M+0) and (M+1) mass isotopomers were predominantly higher in 1-$^{13}C_1$ hexose fed culture. From 6-$^{13}C_1$ glucose, (M+2) was more prominent than other mass isotopomers. This pattern of the highest ^{13}C enrichment into the next higher masses was continued in 1,6-$^{13}C_2$ tracer study, where (M+3) was the most enriched mass isotopomer. In addition, average ^{13}C enrichment into monoterpene from 6-$^{13}C_1$ glucose (20.5%) was two times higher than the enrichment observed in 1-$^{13}C_1$ glucose study (9.5%). This isotopic difference was

confirmed as the average label inclusion into this monoterpene from $1,6\text{-}^{13}C_2$ glucose fed culture (29.4%) was virtually equal to the sum of enrichments from two $^{13}C_1$ tracer studies. Furthermore, (M+5) and (M+6) isotopomers were observed from $1,6\text{-}^{13}C_2$ glucose study. Two other monoterpenes (menthofuran and isopulegone) also showed similar isotopic patterns to pulegone (Table S3 and Table S4). To make an explicit interpretation of the tracer studies and quantifying the fluxes of different pathways, MFA was carried out as described in the following sections.

4.2.3. ^{13}C MFA in peppermint GTs

Steady-state ^{13}C MFA (Ratcliffe and Shachar-Hill, 2006; Schmidt et al., 1997; Wiechert and Wurzel, 2001; Zupke and Stephanopoulos, 1994) was carried out using isotopic information from the tracer studies described above. Prior to performing MFA, a GT-specific model was reconstructed.

Reconstruction of the model

A compartmentalized model network of monoterpene essential oil biosynthesis of secretory cells within non-photosynthetic GTs of peppermint during the secretory phase was defined for MFA study. In the step-wise process of network reconstruction, initially central pathways involved in monoterpene biosynthesis were identified by surveying the respective biochemical literature (Ahkami et al., 2015; Gershenzon et al., 1989; Johnson et al., 2017) and online databases such as BRENDA (Placzek et al., 2017), MetaCyc (Caspi et al., 2018) and PlantCyc (Dreher, 2014). In the next step, the model was refined in an iterative data-driven process based on a comparative analysis of alternative model versions. Variations tested in a different version of the models comprised (1) in-/exclusion of certain reactions/pathways (e.g. fermentation and cytosolic oxPPP), (2) different degrees of compartmentalization (e.g. isoenzymes and lumped metabolite pools), and (3) model simplifications (e.g. lumping of unnecessary reactions in linear pathways). These network formulations were necessary to produce an accurate metabolic flux map based on the provided labeling information.

The final ^{13}C-MFA model is comprised of 37 biochemical reactions and 12 transport processes across four different compartments (cytosol, mitochondria, leucoplast and extracellular medium) (Table S5). In addition to two terpene biosynthetic routes, the compartmentalized metabolic network was composed of glycolysis, the TCA cycle, the PPP, the RuBisCO bypass and multiple ana-/cataplerotic reactions. Imported carbon (unlabeled or labeled glucose) was converted to precursors for monoterpene biosynthesis via glycolysis (cytosolic and plastidic) and the oxidative/non-oxidative branch of PPP. The resulting trioses, namely, plastidic glyceraldehyde-3-phosphate (GAP) and

pyruvate (PYR) served as precursors for the DXP pathway. Alternatively, plastidic PYR could be synthesized via the plastidic NADP-dependent malic enzyme (NADP-ME). Cytosolic acetyl-CoA (AcCoA), the precursor of the MVA pathway, was obtained via the citrate-shuttle. In the mitochondrial TCA cycle, citrate (CIT) was produced by citrate synthase and then transported into the cytosol where it was cleaved to oxaloacetate (OXA) and AcCoA by the cytosolic ATP-citrate lyase (ACL). To replenish the carbon withdrawn from the TCA cycle, malate and pyruvate were produced from the anaplerotic reaction, catalyzed by phosphoenolpyruvate carboxylase (PEPC), malate dehydrogenase (MD), malic enzyme (ME) and pyruvate kinase (PK) in the cytosol. RuBisCO, which had demonstrated high expression in peppermint GT (Ahkami et al., 2015), was included in the model as a potential mechanism to recycle CO_2. To account for the energy and redox-related processes involved in monoterpene biosynthesis, the model integrates ATP, NADH and NADPH production and consumption. Oxidative phosphorylation was defined based on the stoichiometry of 2.5 ATP per NADH (Hinkle, 2005). Assuming an unbalanced network behavior of the model with respect to energy and redox metabolism, the model integrated the exchange of these co-factors with the extracellular medium. Thereby, the model was named as the open_redox version.

Necessary simplification of subcellular compartmentation had been completed during the process of reducing model complexity. The compartmentation of upper glycolysis (G6P to GAP) had not been considered in the final model. Since preliminary versions demonstrated that metabolic fluxes of upper glycolysis could not be precisely resolved based on the provided labeling input, however, the median flux values were relatively unchanged. Furthermore, monoterpene production was confined to the plastid as the first step of monoterpene biosynthesis (from GPP to limonene) takes place exclusively in plastids (Alonso et al., 1992; Colby et al., 1993).

For further improvement of the biochemical network, the exchange of intermediates was restricted to PYR, MAL and CIT between the cytosol and mitochondria, and G6P, GAP, PYR, MAL and IPP between the cytosol and plastid. The inclusion of triose phosphate and hexose phosphate transporters was verified which did not change the carbon flux. IPP was used as the means of cross-talk between cytosolic and plastidic terpene biosynthetic pathways as this is the first common intermediate of these pathways and the C_5 unit or C_5 derivative of this unit was reported to be transported between the compartments (Henry et al., 2018). Along with labeled tracer, uptake of unlabeled glucose was integrated into the network to account for the dilution from the unlabeled carbon source. Further details of the peppermint GT model are provided in Table S5.

4.2.4. Metabolic fluxes in non-photosynthetic peppermint GTs

The flux analysis provided a statistically acceptable fit with the resulting minimized SSR of 79.2 which was in the range of the expected lower (40.5) and upper bound (83.3) for the 95% confidence region of SSR. The metabolic flux map representing the best-fit solution is presented in Figure 23 and Table S7. Additionally, all the necessary relative fluxes are enumerated in Table 14. Most of the central carbon and both terpene biosynthesis metabolic fluxes had good precision with low relative SE. Some low and zero fluxes, such as non-oxPPP were also well resolved; however, those fluxes had high relative SE due to the corresponding high fluxes in oxPPP and glycolysis.

Cross-talk between DXP and MVA pathway for monoterpene biosynthesis

Contrary to textbook knowledge, the flux analysis confirmed that the MVA pathway contributed to monoterpene biosynthesis in peppermint GTs. IPP produced in the cytosol was transported into the plastid for the production of GPP, the precursor of monoterpene synthesis. Flux analysis indicated that 13% of monoterpenes were synthesized via the MVA pathway and 87% via the DXP pathway (Table 14-1). The role of MVA was significant as 9.5% lower bound of MVA was determined at 95% CI in MFA. Furthermore, this outcome is true at a 99.9% confidence level where the interval between 6.9% and 20% contained the true value of the MVA flux for monoterpene biosynthesis (Table S6).

Central carbon fluxes towards monoterpene biosynthesis

The precursors of the classical plastidic DXP pathway are GAP and PYR. These two trioses were predominantly synthesized via the joint route of glycolytic bypass (oxPPP) and RuBisCO. This central metabolic route fulfilled the entire PYR demand for DXP pathway; however, a small portion (5%) of GAP precursor was predicted to be supplied solely from glycolysis (Table 14-2). No flux was observed for substrate production by the activity of the plastidic malic enzyme (NADP-ME).

Imported glucose into the secretory cells was largely directed towards the oxidative branch of the PPP (62%), due to the fact that the main monoterpene biosynthesis pathway (DXP) takes place in the plastid (Table 14-3). Among the remaining sugar (38%), 7% was metabolized by plastidic non-oxPPP and rest 31% flowed solely through glycolysis for synthesizing trioses. Since there was no transport process within the lower glycolytic metabolites (PG or PYR), it could be simplified that 11% of total glycolytic GAP (equivalent to 3% of total glucose uptake) was used by the plastidic DXP pathway, while the cytosolic MVA route utilized the rest (equivalent to 28% of total glucose uptake) (Table

14-4). In the essence from the upper central metabolism in GTs, the relative flux analysis pointed that cells operated minimum 28% or maximum 31% (when 3% was transported to plastid for DXP pathway) of carbon by cytosolic glycolysis. Furthermore, the flux map also portrayed that RuBisCO carboxylated Ru5P of oxPPP (86%) and non-oxPPP (14%) to triose phosphate (PG) (Table 14-5).

Figure 23. Metabolic flux map of central and monoterpene metabolism of secretory cells in non-photosynthetic peppermint GTs during the secretory phase.

Parallel MFA (open_redox version) was assessed from ^{13}C labeling patterns of monoterpenes (pulegone, menthofuran and isopulegone) from $1\text{-}^{13}C_1$, $6\text{-}^{13}C_1$ and $1,6\text{-}^{13}C_2$ glucose incorporation (SEM, n = 3). Molar amounts of fluxes (in red color) are presented after normalization to a net monoterpene production rate of 1 mol per unit time. Arrows indicate the direction of net flux, arrow widths are proportional to the magnitude of relative fluxes, and dashed arrows indicate zero flux value.

Table 14. Relative contribution of metabolic fluxes in peppermint GTs for monoterpene production.

The unit of the flux value is molar amount of the metabolite per mol of the monoterpene production. Relative values are enumerated from the outcome of open_redox version of peppermint GTs. Relative flux in Sl. no. 2 and 4 are predicted from the GAP pool by observing the relative pools of cytosolic and plastidic PG.

Sl. no.	Metabolic fluxes	Total flux	Relative flux	Relative flux (%)
1	**Total IPP for monoterpene biosynthesis**	2		
	From DXP pathway		1.742	87%
	From MVA pathway		0.258	13%
2	**GAP source for DXP pathway**	1.742		
	Produced by glycolysis		0.086	5%
	Produced by oxPPP + RuBisCO		1.656	95%
3	**Glucose conversion**	2.347		
	Converted by sole oxPPP		1.464	62%
	Converted by sole glycolysis		0.726	31%
	Converted by sole non-oxPPP		0.157	7%
4	**Glycolytic GAP for terpene biosynthesis**	1.453 (31%)		
	For plastidic DXP pathway		0.165	11% (3%)
	For cytosolic MVA pathway		1.288	89% (28%)
5	**Ru5P source for RuBisCO flux**	1.699		
	Produced by oxPPP		1.464	86%
	Produced by non-oxPPP		0.235	14%
6	**Mitochondrial CIT flux**	1.288		
	Export to cytosol		0.773	60%
	Used for lower TCA cycle		0.515	40%
7	**Carbon conversion**	14.082		
	Carbon converted into biomass		10	71%
	Carbon released as CO_2		4.082	29%
8	**Total CO_2 production**	7.069		
	Total CO_2 fixation		2.987	42%
	Total CO_2 release		4.082	58%
9	**CO_2 fixed by RuBisCO**	1.699		24%
	Emerged from oxPPP		1.464	21%
	Emerged from other pathway		0.235	3%
10	**NADPH source**	7.743		
	Produced by oxPPP		2.928	38%
	Produced by cytosolic NADP-ME		1.288	17%
	Consumption from external source		3.527	46%

Sl. no.	Metabolic fluxes	Total flux	Relative flux	Relative flux (%)
	NADH source	7.564		
	Produced by glycolysis		1.288	17%
11	Produced by TCA cycle		3.606	48%
	Produced by monoterpene biosynthesis		1	13%
	Consumption from external source		1.67	22%
	NADH requirement	7.564		
12	Requirement for ATP conversion		3.847	51%
	Requirement for other pathways		3.717	49%

Flux analysis indicated that cytosolic PG was converted to cytosolic AcCoA through the TCA cycle and malate-citrate shuttle. The TCA cycle was fueled by the import of cytosolic PYR and malate. Mitochondrial citrate flux had two functions such as, (1) mostly (60%) exported from the mitochondria to sustain monoterpene biosynthesis, and (2) moved (40%) into the lower part of TCA cycle for the production of energy and redox equivalent (Table 14-6).

Carbon conversion efficiency and redox requirements for monoterpene biosynthesis

Secretory cells of GTs were highly efficient for conversion of substrate to the final end-product. For each mol of C_{10} terpene production, this cell imported 2.35 mol of C_6 sugar, resulting in 71% carbon conversion efficiency (CCE) of GTs (Table 14-7). It was observed that 42% of the total CO_2, produced by different metabolic pathways, was accumulated again inside GTs (Table 14-8). Besides the role in supplying metabolites for monoterpene biosynthesis, the RuBisCO bypass was also important for fixation of metabolic CO_2, generated in central and monoterpene metabolism. The flux map estimated that RuBisCO assimilated 24% of the produced CO_2 by GT metabolism, thereby strongly contributing to the CCE in peppermint GTs (Table 14-9). Moreover, high flux through oxPPP produced a high amount of CO_2 that was predicted to be fully consumed by RuBisCo. It could also fix 3% of CO_2 produced from other biochemical pathways of GT. In addition, the amount of CO_2 released by the activity of ME was carboxylated again by PEPC, due to the presence of futile anaplerotic cycle (Figure 23 and Table S7).

The interpreted flux values from the open_redox model were basically computed based on the carbon transfer between metabolites. However, the production and consumption of co-factors (ATP, NADH and NADPH) up to pulegone (monoterpene) biosynthesis was included in the network with an open consumption source of external origin. The flux map demonstrated that 7.74 mol NADPH was

required for 1 mol pulegone biosynthesis (Table S7). A higher extent (46%) of reductant was imported from external sources which are not included in the present network map (Table 14-10). Inside the GT, NADPH was produced from oxPPP (38%) and by cytosolic NADP dependent ME (17%). The other electron carrier (NADH) was provided by the TCA cycle (48%), an external source (22%), glycolysis (17%) and the monoterpene biosynthetic route (13%) (Table 14-11). Although cells consumed external NADH, they possibly needed it for converting into ATP. The metabolic network predicted that 51% of the total required NADH was used for ATP synthesis (Table 14-12). Along with this source, GTs mainly satisfied energy requirement by themselves.

Advanced MFA version with the closed network for redox balance inside GTs

It was anticipated that there could be the other sources of energy and redox than the currently considered metabolic networks. However, another version of the MFA model (close_redox version) was generated where all three co-factors were exclusively produced inside the cell. The metabolic network remained the same in this version, except skipping the import of redox equivalents (see the legend of Table S5). The main aim of this advanced version was to observe the flux changes for supplying enough electron carriers that were imported from an outer source in the open_redox version. The flux values and network map are presented in Table S8 and Figure S7, respectively. Due to the higher demand of NADPH by two terpene biosynthetic pathways and also for monoterpene biosynthesis, the glucose was transported exclusively via oxPPP. In addition, the direction of non-oxPPP was reversed from the previous version for fueling oxPPP to a greater extent. Except for this initial metabolic shift, other fluxes were relatively similar. For instance, the MVA route had 10% participation in monoterpene production. Since, this version was principally based on redox balance, it eventuated in the reduction of CCE to 59%, compared to the carbon-based flux of 71%.

4.2.5. Validation of the GT metabolism

Inhibition study to prove cross-talk between MVA and DXP pathway in peppermint GTs

The role of the MVA pathway for the production of DXP pathway-derived compounds in peppermint was validated by the inhibition study. Like monoterpenes, carotenoids and the phytol side chain of chlorophyll are traditionally produced via the DXP pathway, however not inside GTs. Fosmidomycin (FSM) is a potent inhibitor of the DXP reductoisomerase. Four different concentrations of FSM were tested to observe the effect of the inhibitor on synthesis of total chlorophyll and carotenoid. It was

assessed that 20, 30 and 40 µM FSM showed the similar and highest amount of inhibition for phytopigment production (Table 15 and Figure S8). Nevertheless, a relatively low quantity of carotenoids and chlorophylls were still produced. Additionally, biosynthesis of the photosynthetic pigments was observed to be partially blocked at 10 µM FSM.

Table 15. Production of phytopigments from fosmidomycin treated shoot-tip.
15 days old leaf pairs were obtained from growing shoot-tip cultivated in culture media containing 0 (control), 10, 20, 30 or 40 µM fosmidomycin (FSM) (mean ± standard error, n=5).

Phytopigments	Fosmidomycin concentration				
(mg/g fresh weight)	0 µM	10 µM	20 µM	30 µM	40 µM
Total chlorophyll	1.75 ± 0.19	0.20 ± 0.02	0.06 ± 0.02	0.05 ± 0.02	0.07 ± 0.01
Total carotenoid	0.25 ± 0.02	0.06 ± 0.01	0.02 ± 0.01	0.02 ± 0.01	0.02 ± 0.01
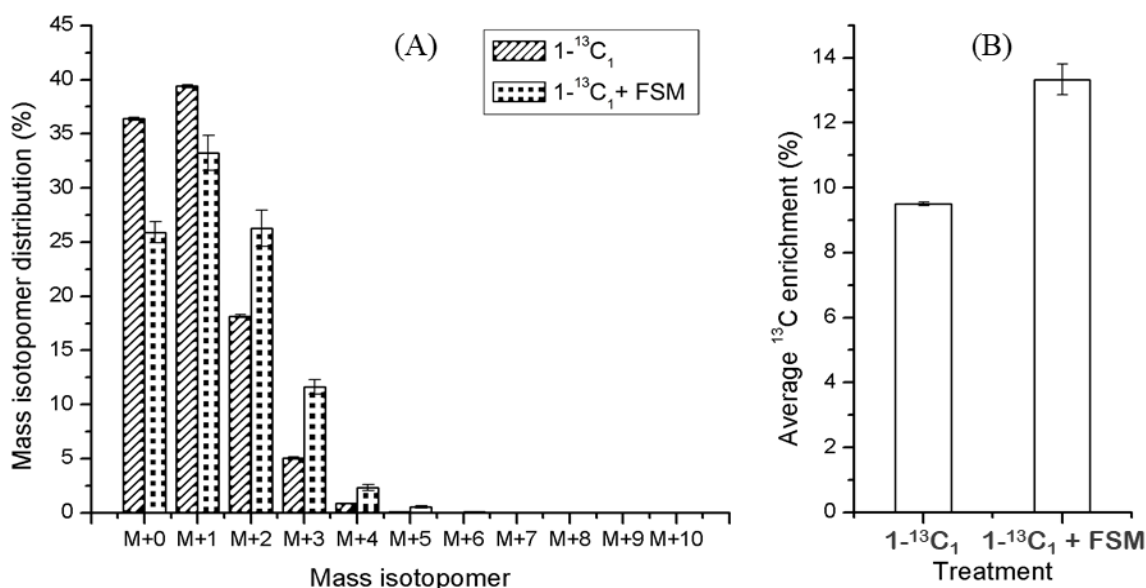
Figure 24. Labeling study after partial inhibition of the DXP pathway.
15 days old leaf pairs were obtained from growing shoot-tip cultivated in culture media without (only $1\text{-}^{13}C_1$ glucose) or with ($1\text{-}^{13}C_1$ glucose + FSM) 10 µM fosmidomycin (FSM). (A) MID and (B) average ^{13}C enrichment of pulegone were assessed from the control and inhibited culture (mean ± SE, n=3).

To understand the effect of the inhibitor on monoterpene biosynthesis inside GTs, the partial inhibition concentration of FSM (10 µM) was used for a labeling study of monoterpene, since a certain amount of metabolite is necessary for precise analysis of MIDs. The hypothesis of this investigation was that the isotope distribution and enrichment into pulegone should be unchanged between control and inhibited GTs after partial blockage of plastidic terpene biosynthesis pathway, if monoterpene is

exclusively produced by DXP pathway. However, the change in isotope inclusion proves the role of the alternate MVA pathway in monoterpene synthesis (Figure S13). From the comparison study (Figure 24), the pattern of MIDs was noted to be significantly altered. The lower mass isotopomers, such as (M+0) and (M+1) were reduced after inhibition, whereas (M+2) to (M+5) mass isotopomers were increased, compared to the control. The average ^{13}C enrichment into monoterpene was also increased in inhibited GTs (13%) than in control (9.5%).

Metabolic fluxes of GTs in oregano

The present understanding of GT biochemistry was further extended to oregano plant which belongs to the same taxonomic hierarchy of peppermint plant and makes their volatiles in similar peltate GTs (Crocoll et al., 2010). Oregano produces both monoterpenes and sesquiterpenes which are classically originated from DXP and MVA pathways, respectively. Thus, this plant was used to validate the trend of central metabolism of peppermint GTs and assess the cross-talk between two terpene biosynthetic means when both the pathways have their own end products. In addition to the open_redox model version of peppermint GT, the oregano model was extended for the inclusion of sesquiterpene production from cytosolic IPP and transport of plastidic IPP for sesquiterpene production. Details of the model construction and reaction network are presented in Data S1, Data S2 and Table S9.

Two pre-requisites of steady-state MFA were fulfilled by 15-day-old leaf where the production of monoterpenes and sesquiterpenes was metabolically and isotopically stable (Figure S9, Figure S10). Average ^{13}C enrichment in oregano volatiles (98.6% of monoterpene to 99.5% of sesquiterpene) was similar to peppermint (99.5%). In addition, the ratio between amount of total production of monoterpene and sesquiterpene was 88% to 12%. These two factors were taken into consideration while constraining oregano MFA. Sabinene hydrate ($C_{10}H_{18}O$) and bisabolene ($C_{15}H_{24}$) were the respective highest synthesized monoterpene and sesquiterpene. Those were used as the representative of their corresponding isoprene class. To avoid low signal to noise ratio and low precision of the data, other low content volatiles were not used for further labeling and flux analysis.

In the next step, the isotopic investigation from three different tracers (1-^{13}C$_1$, 6-^{13}C$_1$ and $1,6$-^{13}C$_2$ glucose) was performed (Figure S11 and Figure S12). The higher mass isotopomers were more abundant from the consecutive change of tracer from 1-^{13}C$_1$ to 6-^{13}C$_1$ and 6-^{13}C$_1$ to $1,6$-^{13}C$_2$ glucose. Alike peppermint monoterpene, MIDs from two ^{13}C$_1$ tracers were different from each other. Moreover
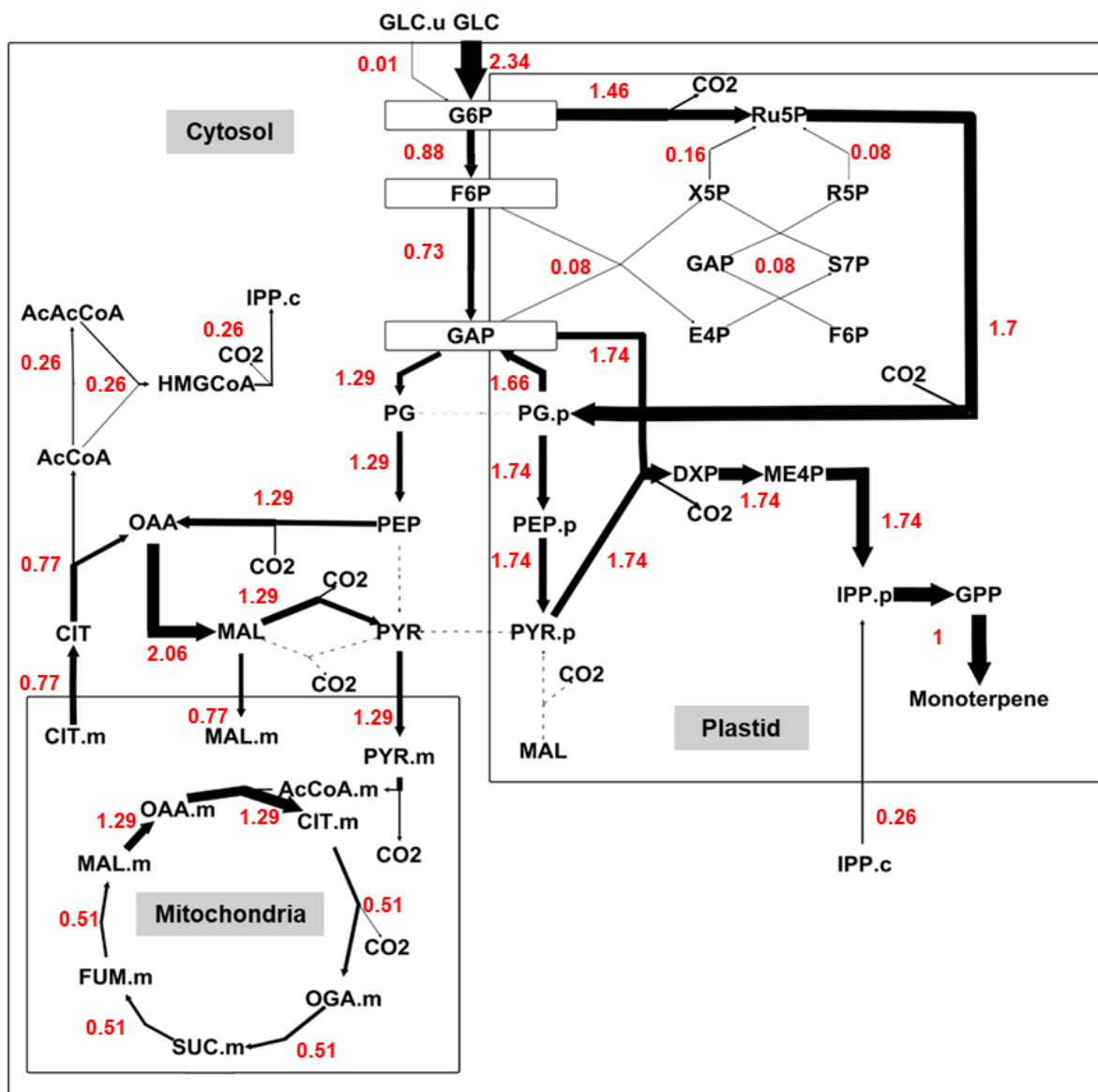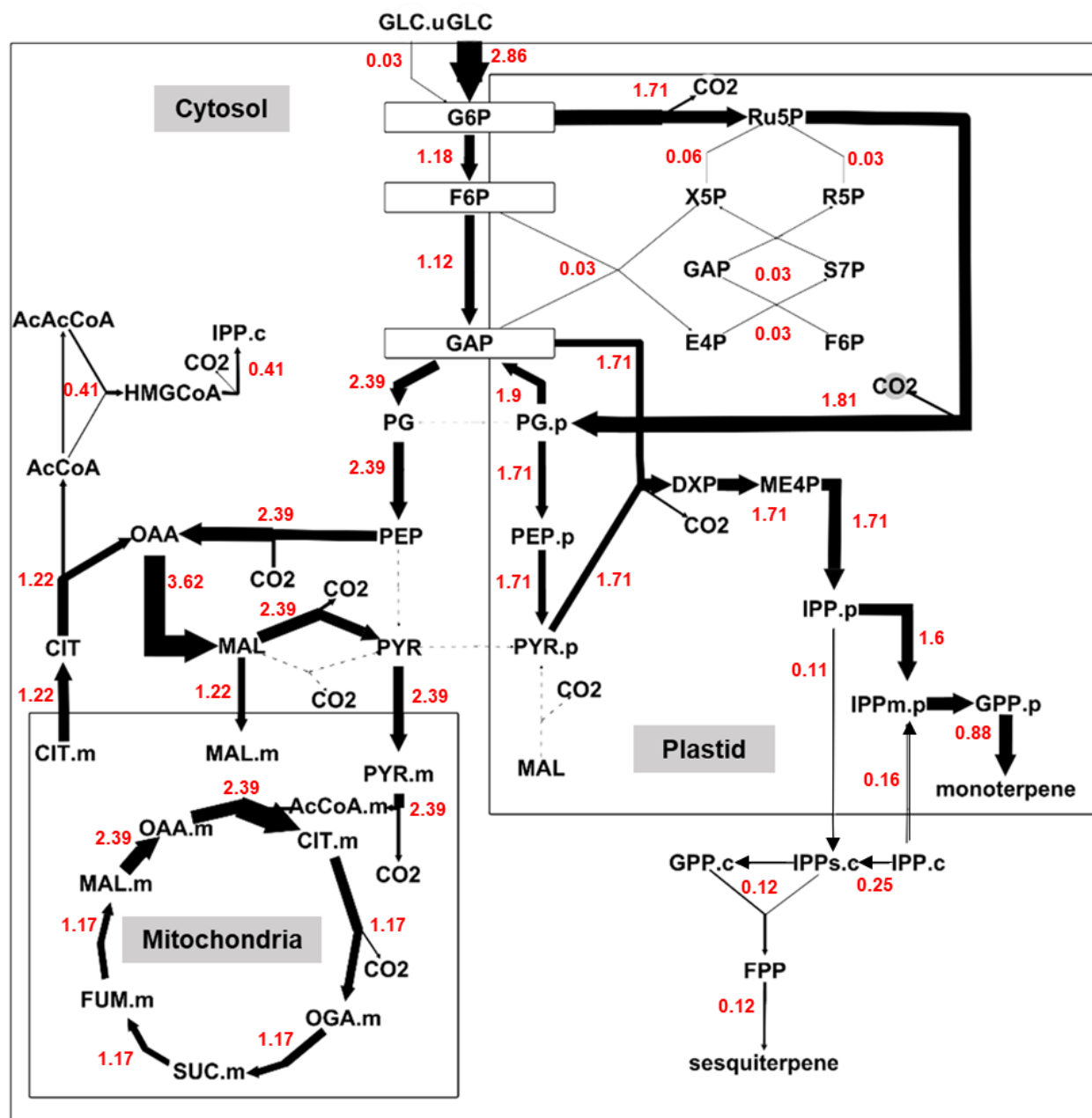
Figure 25. Metabolic flux map of central and monoterpene metabolism of secretory cells in non-photosynthetic oregano GTs during the secretory phase.

Parallel MFA was assessed from ^{13}C labeling patterns of monoterpene (sabinene hydrate) and sesquiterpene (bisabolene) from $1\text{-}^{13}C_1$ and $6\text{-}^{13}C_1$ glucose incorporation (SEM, n = 3). Mol amount of fluxes (in red color) are presented after normalization to a net monoterpene and sesquiterpene production rate of 0.88 and 0.12 mol, respectively. Arrows indicate the direction of net flux, arrow widths are proportional to the magnitude of relative fluxes, and dashed arrows indicate zero flux value.

Table 16. Relative contribution of metabolic fluxes in oregano GTs for mono- and sesquiterpene production.

The unit of the flux value is mol amount of the metabolite per mol of the volatile production (0.88 mol monoterpene and 0.12 mol sesquiterpene). Relative values are enumerated from the outcome of oregano GTs' MFA. Relative flux in Sl. no. 4 is predicted from the GAP pool by observing the relative pool of cytosolic and plastidic PG.

Sl. no.	Metabolic fluxes	Total flux	Relative flux	Relative flux (%)
1	**Total IPP for monoterpene synthesis**	1.76		
	From DXP pathway		1.604	91%
	From MVA pathway		0.156	9%
2	**Total IPP for sesquiterpene synthesis**	0.36		
	From DXP pathway		0.109	30%
	From MVA pathway		0.251	70%
3	**Glucose conversion**	2.894		
	Converted by sole oxPPP		1.714	59%
	Converted by sole glycolysis		1.119	39%
	Converted by sole non-oxPPP		0.061	2%
4	**Source of cytosolic PG for MVA pathway**	2.394		
	Produced by entire glycolytic GAP		2.238	93%
	Produced by RuBisCO bypass		0.156	7%
5	**Ru5P source for RuBisCO flux**	1.805		
	Produced by oxPPP		1.714	95%
	Produced by non-oxPPP		0.091	5%
6	**Mitochondrial CIT flux**	2.394		
	Export to cytosol		1.223	51%
	Used for lower TCA cycle		1.171	49%
7	**Carbon conversion**	17.364		
	Carbon conversion into biomass		10.6	61%
	Carbon released as CO_2		6.764	39%
8	**Total CO_2 production**	10.963		
	Total CO_2 fixation		4.199	38%
	Total CO_2 release		6.764	62%
9	**CO_2 fixed by RuBisCO**	1.805		16%
	CO_2 originated from oxPPP		1.464	15%
	CO_2 originated from other pathway		0.235	1%
10	**NADPH source**	5.954		
	NADPH produced by oxPPP		3.428	58%
	NADPH produced by cytosolic NADP-ME		2.394	40%
	NADPH consumption from external source		0.132	2%

(M+5) and (M+6) mass isotopomer were also observed in monoterpenes of oregano. For better understanding, flux analysis was performed using the best fitting labeling information from the tracers (Table S10 and Table S11). Fluxes of oregano GT are presented in Figure 25 and Table 16.

Cross-talk between two terpene biosynthetic pathways was also prominent in the oregano GT model. For instance, the MVA pathway contributed 9% of the monoterpene flux (Table 16-1). The amount of cross-talk was increased for the sesquiterpene biosynthesis when the participation of alternate route (DXP) was 30% (Table 16-2).

The pattern of carbon flow in central metabolism was similar in GT fluxes of both the plants. However, all of the cytosolic and mitochondrial fluxes were slightly higher compared to peppermint GTs due to the extra production of sesquiterpenes at the cytosol compartment in oregano. The fate of glucose through oxPPP (59%) was also substantial in oregano trichomes. Glycolysis (39%) and reductive non-oxPPP (2%) also played a role in sugar metabolism (Table 16-3). The precursors for the DXP pathway were predicted to be supplied exclusively by the joint route of PPP and RuBisCO bypass (Figure 25). Thus, the entire glycolytic GAP along with 7% of total cytosolic PG from RuBisCO was perhaps utilized for the substrate production of MVA pathway (Table 16-4).

In addition, with the increasing MVA flux, CO_2 emission was increased due to the relatively increasing TCA cycle. Thence, the CCE of oregano cells was reduced to 61% from 71% observed in peppermint GTs (Table 16-7). The oregano model also predicted that ATP and NADH requirements were satisfied internally (Table S12). A very low amount of NADPH (2%) was imported from the external source. Nevertheless, oxPPP played an eminent role in redox metabolism by supplying 58% of the total NADPH requirement of oregano GTs (Table 16-10).

4.3. Discussion

The present study demonstrated the metabolic map of peppermint GTs for monoterpene production which was partly synthesized by the unconventional MVA route. Central carbon metabolism of these secretory cells revealed that the imported sugar was mainly catabolized by the glycolytic bypass. In addition, GT cells convert carbon efficiently due to the presence of the RuBisCO bypass.

MFA is a powerful approach for quantifying metabolic fluxes at the subcellular level. Both steady-state and instationary MFA have been often used for unravelling primary metabolism in many plants (Table 2). Few instances with instationary MFA were also reported for interpreting secondary

Discussion

metabolism of plants (Boatright et al., 2004; Heinzle et al., 2007). However, to the best of the author's knowledge, this is the earliest instance of performing steady-state MFA for the secondary metabolism of plants as well as carbon flux quantification towards terpene biosynthesis in plant GTs. In this investigation, the volatile monoterpenes portray the exclusive metabolism of peppermint secretory cells, as they are entirely produced inside the trichome cells. However, isotopic measurement of trichome-specific central carbon, DXP and MVA pathway intermediates from the peppermint leaf was unattainable for MFA due to the following reason. Unlike trichome isolation from tomato by brushing under liquid nitrogen (Balcke et al., 2017), the isolation of peppermint GTs is not achievable within a few seconds. This procedure takes more than an hour by using the protocol of Gershenzon et al. (1992), within which the labeling pattern and concentration of metabolites inside GTs would undesirably be renovated at room temperature. Thus, this exclusive GT model is entirely based on the labeling study of different monoterpenes.

This study uncovered that the MVA pathway was partly involved for monoterpene production in peppermint plants. The DXP pathway, the traditional means for monoterpene biosynthesis in plants, was preferentially involved for the production of these C_{10} terpenes. The MVA pathway contribution (13%) was statistically significant from this model (Table 14). The truthfulness of this statement was also manually calculated at 99.9% CI, where the significant lower bound (6.9%) of the MVA pathway was monitored (Table S6). It validated the null hypothesis of cross-talk between two terpene biosynthetic pathways. In oregano GTs, the relatively similar amount of cross-talk between two pathways was detected for the production of C_{10} isoprene and the contribution of the alternate pathway was more extensive for the synthesis of C_{15} isoprene. Furthermore, by deeper insights of possible labeling patterns into monoterpenes from the fed tracers (Figure 26), it was identified that (M+0) to (M+4) mass isotopomers of monoterpene were conceivably emerged from both DXP and MVA pathway, whereas (M+5) and (M+6) mass isotopomers were produced exclusively by the MVA pathway. Those two mass isotopomers could be produced by the DXP pathway, only when anapleorosis after the repetition of complete respiration cycle would provide (M+2) or (M+3) PYR. This would then subsequently result in the presence of more than (M+4) mass isotopomer of monoterpene via the DXP pathway. However, the absence of PYR transport from cytosol to plastid in the present study diminished this possibility (Figure 23). Hence, a significant amount of (M+5) and (M+6) in this investigation from 1,6-$^{13}C_2$ tracer indicated the activity of a cytosolic isoprene synthetic pathway for monoterpene (Figure 22).
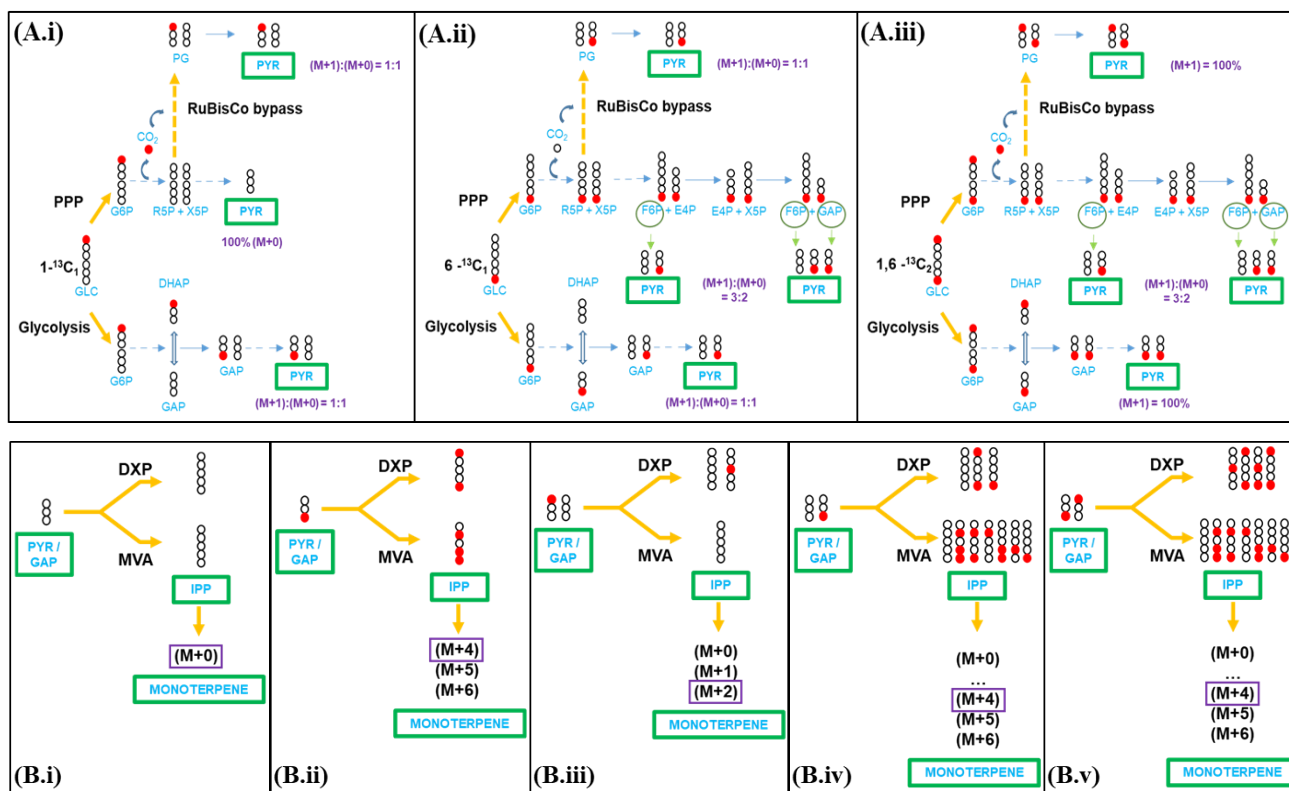
Figure 26. Theoretical overview of label carbon flow from three isotopic glucose.

This is a simplified scheme of ^{13}C (in red) flow from $1-^{13}C_1$, $6-^{13}C_1$ and $1,6-^{13}C_2$ glucose via (A.i-iii) glycolysis, PPP and RuBisCo bypass. PYR and GAP, produced from these three routes, are transferred through the DXP and MVA pathway (B.i-v) for monoterpene production. The highest possible mass isotopomer of monoterpene, synthesized independently via the DXP pathway, is marked by a violet box.

The active participation of the MVA pathway was further proved by the inhibition study. The considerable quantity of carotenoids (C_{40} isoprenoid) and chlorophyll (C_{20} isoprenoid side chain) after the highest possible level of DXP pathway inhibition could illustrate the interaction of two terpene biosynthetic pathways in peppermint leaf (Table 15). Due to the fact that FSM is a competitive inhibitor of the DXP pathway (Koppisch et al., 2002) and phytopigments are not produced in GTs, the additional labeling study of monoterpene was carried out in the presence of inhibitor. Alteration of the labeling pattern and isotopic enrichment between control and FSM-treated shoot-tip confirmed the role of the MVA pathway in monoterpene production (Figure 24). Overall, these results differ from the previous concepts of peppermint GTs (Eisenreich et al., 1997; McCaskill and Croteau, 1995), where the exclusive role of the DXP pathway for monoterpene biosynthesis was mentioned. However, some labeling information from those reports could also be interpreted as low participation from the MVA pathway. For example, less ^{13}C incorporation in the 2nd and 6th carbon position of

monoterpene suggested the activity of alternate MVA pathway in the first study (Eisenreich et al., 1997). In other one (McCaskill and Croteau, 1995), the significant label incorporation into monoterpene from ^{14}C-MVA (catabolized after the activity of HMGR enzyme) supported the present outcome. However, scientists mentioned this result as a biased outcome considering the result from other tracer investigations. It could be assumed that the rate-limiting HMGR enzyme (Chappell, 1995) limited the conversion of a central labeled intermediate into monoterpene during that short period of study. Another report (McCaskill et al., 1992) also demonstrated low levels of incorporation of radioisotopic acetate into monoterpenes in peppermint GTs. Moreover, the role of unconventional means (MVA) for monoterpene was also detected in other plant species, such as *Hedera helix* (Piel et al., 1998), *Catharanthus roseus* (Schuhr et al., 2003), *Phaseolus lunatus* (Bartram et al., 2006), *Fragaria sp.* (Hampel et al., 2007), *Gossypium hirsutum* (Opitz et al., 2014) and *Lavandula latifolia* (Mendoza-Poudereux et al., 2015). Quantification of MVA pathway participation could not be specified by the amount of inhibition or label incorporation from intermediate into monoterpene in those reports, but was demonstrated by MFA in the present research.

The oxPPP is an alternative route of glycolysis for metabolism of hexose to triose. This path has been expected to be abundant in oilseeds where NADPH is required for fatty acid biosynthesis (Eastmond and Rawsthorne, 2000; Glas et al., 2012; Kang and Rawsthorne, 1996). The flux map of GTs exhibited that the oxPPP was the main sugar metabolic route to supply precursors for monoterpene. The phosphogluconate flux (62%) was twice as large as the total glycolytic fluxes (31%) (Table 14) in the peppermint GTs. This biochemical trend was also observed for volatile production in oregano. As an alternative proof of the active oxPPP in GTs, isotopic abundance in different mass isotopomers was different between 6-^{13}C and 1-^{13}C glucose fed cultures. The label was more incorporated in monoterpene from 6-^{13}C glucose compared to the latter one (Figure 22). Furthermore, the larger difference of (M+0) mass isotopomer between those two tracers denoted the larger oxPPP flux than glycolysis flux, as observed from the simplified scheme of carbon flow (Figure 26). The abundance of oxPPP was also observed in GTs from spearmint (Jin et al., 2014), peppermint (Lange et al., 2000; Tissier, 2012; Zager and Lange, 2018) and tomato (Balcke et al., 2017).

Theoretically, the DXP and MVA pathways require three and two units of NADPH, respectively, for one unit of IPP production from their precursors (PYR/GAP and AcCoA) (Johnson et al., 2017). Additionally, the biosynthetic steps from GPP to pulegone use extra two units of NADPH. It could be predicted that the reason for the high oxidative branch of the glycolytic bypass was due to this high

demand of reducing agent for monoterpene biosynthesis. Hence, in the close_redox MFA version of peppermint GTs (Figure S7), oxPPP was certainly increased compared to the open_redox MFA version. The cells also used this pathway as an exclusive means for sugar metabolism. The other source of NADPH in GTs was the catabolic reaction by NADP-ME for production of PYR from MAL. The abundance of NADP-ME was noticed in spearmint (Jin et al., 2014) and tomato GTs (Balcke et al., 2017). The flux map indicated the presence of a cytosolic version of this anaplerotic enzyme. Nonetheless, upper part of glycolysis is also capable of producing an electron carrier (NADH) which is independent of NADPH and used as an oxidizing agent in the catabolic reaction (Alberts et al., 2002). In this way, glycolysis could not replace the active oxPPP in GTs. The other source of NADH production in secretory cells was the TCA cycle. Apparently, these NADHs generate ATP by the ETC to satisfy the high energy requirement for monoterpene metabolism. Furthermore, oregano GTs imported fewer redox equivalents from the outer source than peppermint GTs because they lack the demand for reductant during the GPP to volatile conversion.

In the present study, precursors of the DXP pathway were mainly provided by the RuBisCO bypass (Table 14-2). Non-photosynthetic cells generally prefer the joint route of non-oxPPP and RuBisCO which results in the increase of carbon conversion for producing one unit AcCoA (Schwender et al., 2004). However, as interpreted above, oxPPP was the integral part of central carbon metabolism in GT-like non-photosynthetic cells where the reductive pathway (terpene biosynthesis) produced the end-product (monoterpene). To fix the high amount of CO_2 as a fate of oxPPP, the biochemical need of cells for being carbon efficient was through the RuBisCO bypass. Net non-oxPPP flux was limited and produced the pentose, rather than the glycolytic triose and hexose (Table S7). These characteristics of GTs (high RuBisCO and less non-oxPPP) were well supported by the labeling pattern of monoterpene from $6\text{-}^{13}C_1$ and $1,6\text{-}^{13}C_2$ glucose studies (Figure 22). It was observed that the distribution of (M+0) to (M+3) from $6\text{-}^{13}C_1$ glucose was roughly equal to (M+1) to (M+4) distribution from $1,6\text{-}^{13}C_2$. This one-shift MID pattern is only possible when metabolite from oxPPP was moved through the RuBisCO bypass. This is due to the fact that the same amount of label carbon from these two tracers flows through the non-oxPPP, however, one extra ^{13}C from $1,6\text{-}^{13}C_2$ glucose was moved via the RuBisCO bypass (Figure 26).

Two benefits of the futile anaplerotic cycle could be foreseen from the present flux map: (1) extra supply of NADPH in GTs (as discussed above) and (2) indirect participation for the precursor's

supply in the MVA pathway. Hence, the flux by PEPC was equal to the flux by cytosolic NADP-ME and the amount of cytosolic MAL transported to mitochondria was the amount of cytosolic OAA produced by CIT (Figure 23). In detail, cytosolic MAL was transferred to mitochondria; subsequently, it produced citrate with the addition of AcCoA in mitochondria, which was then exported to the cytosol where it produced the invariable amount of AcCoA. This two-carbon intermediate is impermeable to the membrane and thus its cytosolic version was synthesiszied by ACL (Fatland et al., 2002). Presence of this enzyme in GTs was found in tomato (Balcke et al., 2017). Function of this enzyme was also mentioned to breakdown CIT in plant fatty acid biosynthesis studies (Junker et al., 2007; Schwender et al., 2006) where cytosolic AcCoA increased the oil production.

Earlier studies suggested that carbon can be independently fixed in GTs, addition to the carbon import from leaf tissue (Kandra and Wagner, 1988; Keene and Wagner, 1985; McDowell et al., 2011). Peppermint GTs are highly efficient in carbon conversion (71%) from source to the end product (Table 14-7). The flux map suggested that the amount of CO_2 fixed by PEPC was equivalent to the CO_2 produced by NADP-ME. It could be predicted that CO_2, a fate from hexose to pentose production, was fixed by RuBisCO. High carbon efficiency (more than 70%) of developing seed from the different plant was observed in previous reports (Alonso et al., 2011; Goffman et al., 2005; Lonien and Schwender, 2009). In addition, the amount of CO_2 release is related to satisfying the demand of reductant in these highly metabolically active cells, which was suggested from the comparison of two flux versions of peppermint GTs (Table S7, Table S8). Hence, CCE was reduced in the close_redox MFA version to produce the extra reductant at the cost of losing carbon via oxPPP. Previous literature confirmed that GTs are capable of releasing CO_2 (Johnson et al., 2017) in spite of importing this gas (Balcke et al., 2017). The reason for this distinct feature of GTs could be to maintain cellular homeostasis by avoiding the over-saturation of CO_2.

From the essence of GT models of two plants, it could be anticipated that glycolytic GAP (possibly in the cytosol compartment) supplied precursor to the MVA pathway. Hence, the amount of glycolytic contribution was escalated in oregano GTs compared to peppermint GTs, where the MVA pathway was also required for part of sesquiterpene synthesis (Table 14 and Table 16). This biochemical characteristic can be well explained by the deeper insights of labeling pattern from the inhibited plant. Increasing distribution in higher mass isotopomers of the monoterpene was observed in the FSM-treated culture, resulting in increased average isotope enrichment (Figure 24). The DXP pathway was started from the condensation of the two trioses (GAP and PYR), whereas the MVA pathway was the

fate of net three trioses. When precursor trioses emerge from glycolysis, one more label carbon from 1-^{13}C glucose is always transferred towards monoterpene through the MVA compared to the DXP pathway (Figure S13). After the partial blockage of the DXP pathway, net ^{13}C incorporation was more enriched into pulegone as the MVA pathway involvement was relatively increased. However, this hypothesis could not be concluded if glucose was highly metabolized through the joint route of oxPPP and RuBisCO for the precursor of MVA pathway, as a result of which 1-^{13}C glucose converted mainly into (M+0) mass isotopomer of monoterpene via the mevalonate route (Figure 26). In non-inhibited GTs, the DXP pathway was the largest contributor for monoterpene production. Therefore, regulation of glucose was higher by plastidic oxPPP. However, the labeling pattern of inhibitor-treated shoot-tip suggested that FSM inhibited the plastidic route of monoterpene production leading to consequent reduction of oxPPP and relative increase of glycolytic flux. This predicted regulatory link between oxPPP and DXP pathway in the plastid of GTs could be of interest for future studies.

Previous studies showed that no effect of light was observed on the metabolism of peppermint GTs, due to their non-photosynthetic nature (Zager and Lange, 2018). In other hand, trichomes metabolize mostly as self-supporting organ and depend on leaf for sugar (Schilmiller et al., 2008). Therefore, it was anticipated that reduced light had no adverse effect on the metabolism of GTs in the availability of sufficient amount of sugars. In addition, raffinose is most likely imported into GTs as the primary carbon source in many Lamiaceae (Büchi et al., 1998; Olennikov and Tankhaeva, 2007). As no commercial source for the ^{13}C raffinose was available, labeled glucose (which is formed in raffinose catabolism) was utilized in the present labeling experiments. Feeding isotopic glucose in the culture media was also the means of some past investigations to understand the isoprenoid biosynthesis of different plants (Lichtenthaler et al., 1997; Skorupinska-Tudek et al., 2008). Furthermore, the author was concerned that the feeding of alternate pathway intermediate (such as ^{13}C MVA) along with unlabeled glucose for the shorter duration would be difficult for establishing isotopic steady-state and would also result in an imbalance of normal metabolic pool size. Undesirably, it could increase the activity of the respective pathway and result in increasing interaction between pathways for the end product synthesis. This could hinder actual flux quantification. For these reasons, glucose was selected as the sole carbon source in the media and supplied throughout the practical investigation.

Chapter V: Establishment of LCMS/MS acquisition method for analyzing the isotopic status of central carbon and terpenoid biosynthetic intermediates

5.1. Introduction

An accurate flux model requires sufficient information about the underlying biochemistry of the investigated organism. Central metabolites play an important role in MFA analysis as they are the principal source for growth, development and reproductive processes. Therefore, a major task for solving complex metabolism by MFA is to get an accurate isotopic status of as many metabolites as possible. Protein-bound amino acids provide excellent metabolic information about longer periods as they are abundant and stable in the cell (Fischer et al., 2004; Schellenberger et al., 2012; Zamboni et al., 2009). However, they need more turnover time. Consequently, they can not provide sufficient information for non-stationary isotopic analysis where real-time incorporation of labeled carbon into metabolites from ^{13}CO2 is demanded for each short span (Ma et al., 2014). This perturbation can be solved by assessing the fast turnover metabolites. Thereby, to increase our understanding of the live metabolic process, there is an urgency to measure the intermediates of central pathways and free amino acids (Katharina and Wolfgang, 2006; Toya et al., 2006).

MIDs from the metabolites during dynamic and steady-state growth are analyzed by mass spectrometry. Among the primary metabolites, proteogenic amino acids have been measured by GCMS machine. However, central carbon metabolism intermediates are difficult to measure in this instrument due to their low abundance, lack of stability and rapid transformations (Millard et al., 2014). In this context, LCMS has several applied leverages for its higher sample throughput, softer ionization and ability to measure non-volatile and thermally fragile molecules (Lu et al., 2010; McCloskey et al., 2015). Hence, LCMS is an important analytical tool in ^{13}C MFA by providing more information about instantaneous cell metabolism.

Besides measurement of the analytes, the other major concern for the input of MS data in MFA is the requirement of precise assessment of MIDs (Allen and Ratcliffe, 2009), which is necessary to be administered during the establishment of the acquisition method for each sample matrix. Here, an acquisition method was developed for quantifying MIDs of primary metabolites by LCMS/MS. First, compound dependent parameters and different fragments of each metabolite were identified from the injection of each respective standard. The list of possible MIDs for each fragment was created. Afterwards, MS parameters along with the respective fragment were integrated into one multiple reaction monitoring (MRM) scan type. The method was validated for the isotopic analysis from the peppermint leaf extraction by testing the reproducibility and sensitivity of each fragment.

Furthermore, MIDs of the analytes from two positional labeling studies of peppermint shoot-tip culture were measured and evaluated for correlation with each other. This isotopic investigation provided the biochemical overview of 15 day old shoot-tip culture by the deeper insights of label incorporation. It helped to perceive the central metabolism from the whole leaf under low light condition, compared to the previously interpreted non-photosynthetic GT's biochemistry.

5.2. Result

5.2.1. Acquisition method development

Intermediates from the central metabolism play an integral part of any end product synthesis. The initial aim was to establish a mass spectrometric technique for quantifying central metabolites including free amino acids which come from glycolysis, PPP/Calvin cycle and TCA cycle. This task was further extended for measuring intermediates from the DXP and MVA pathways. The compound dependent parameters of each metabolite and their fragments were detected in negative mode of ESI by Q1 and Q3 MS scan through direct injection of the standard solution into the MS. The MRM method was created based on the compound-independent parameters from the literature (Balcke et al., 2014) and our compound-dependent parameter assessment. To generate the detection library of the metabolites, the standard mix was injected into the LCMS using the gradient flow of buffers through a C18 column. The retention time of each compound was confirmed by measuring different concentrations (10, 50 and 100 µm) of standards. The scheduled MRM was created to maximize dwell time and to increase the data quality. Enabling this time restriction for scanning each fragment is crucial for inclusion of many mass transitions in a single analytical run. The details of the determined compounds and their parameters are listed in Table S14 and Table S13.

5.2.2. Optimization and validation of acquisition method for the isotopic study

The isotopic abundance of mass isotopomers for each compound is the fundamental input in MFA software. Therefore, a list of all possible mass transitions was constructed. In the acquisition method, a total of 656 mass transitions were included from 61 fragments that came from 45 metabolites (Table S13). In this part of the investigation, the above-mentioned set of analytes and their fragments were sequestered from the peppermint leaf sample by two-step screening. Initially, compounds of no peak, relatively lower abundance and higher abundance with bad quality were removed (Table S14 and Figure 27). A bad quality peak was defined as a peak that overlapped another peak, representing overloading or larger peak-tailing.

Result

Table 17. Accuracy and precision of the LCMS fragments from peppermint leaf sample.
The analysis was performed based on the initial mass isotope ratio, as higher than (M+1) isotopomers have no value in many cases. A fragment was accepted when peak fulfilled all three criteria: absolute accuracy and SD should not be greater than 0.005 (Antoniewicz et al., 2006) and RSD should be under 15% (Food and Drug Administration, 2018).

Compound	Theoretical (M+1)/(M+0)	Experimental (M+1)/(M+0)	Measured SD	Measured RSD (%)	Absolute accuracy
Accepted fragments					
H6P-1	0.07	0.071	0.003	4.596%	0.001
H6P-3	0.07	0.067	0.002	3.418%	0.003
FBP-1	0.072	0.07	0.003	4.125%	0.002
PG	0.036	0.036	0.001	3.034%	0
PEP-1	0.036	0.04	0.001	2.173%	0.004
PEP-2	0.036	0.038	0.001	2.779%	0.002
P5P	0.059	0.058	0.001	2.46%	0.001
S7P	0.082	0.078	0.005	5.882%	0.004
RuBP	0.06	0.059	0.001	2.467%	0.001
SBP	0.083	0.086	0.001	1.496%	0.003
CIT-1	0.069	0.064	0.002	3.049%	0.005
CIT-3	0.069	0.064	0.004	6.488%	0.005
CIT-4	0.069	0.068	0.002	2.323%	0.001
ISOCIT	0.069	0.068	0.001	1.778%	0.001
AKG	0.057	0.06	0.001	1.947%	0.003
MAL-1	0.046	0.048	0.002	3.35%	0.002
MAL-2	0.046	0.051	0.005	9.926%	0.005
MAL-4	0.046	0.046	0.001	2.12%	0
ASP	0.049	0.053	0.003	6.726%	0.004
GLU	0.064	0.065	0.003	4.911%	0.001
GLN	0.061	0.062	0.005	7.745%	0.001
HIS	0.078	0.076	0.004	5.469%	0.002
PHE	0.103	0.1	0.004	4.217%	0.003
SER	0.038	0.038	0.001	3.827%	0
DXP-1	0.058	0.061	0.003	4.95%	0.003
MEcPP	0.059	0.059	0.001	1.596%	0
IPP/DMAPP	0.059	0.056	0.002	2.71%	0.003
Rejected fragments					
GAP	0.036	0.035	0.007	18.064%	0.001
FBP-2	0.072	0.065	0.006	8.126%	0.007
CIT-5	0.069	0.06	0.003	4.834%	0.009
ACT	0.068	0.057	0.008	11.173%	0.011
ARG	0.082	0.087	0.014	16.563%	0.005
LYS	0.075	0.055	0.002	3.089%	0.02
TRP	0.13	0.25	0.009	7.226%	0.12
MVAPP-1	0.071	0.088	0.001	1.982%	0.017
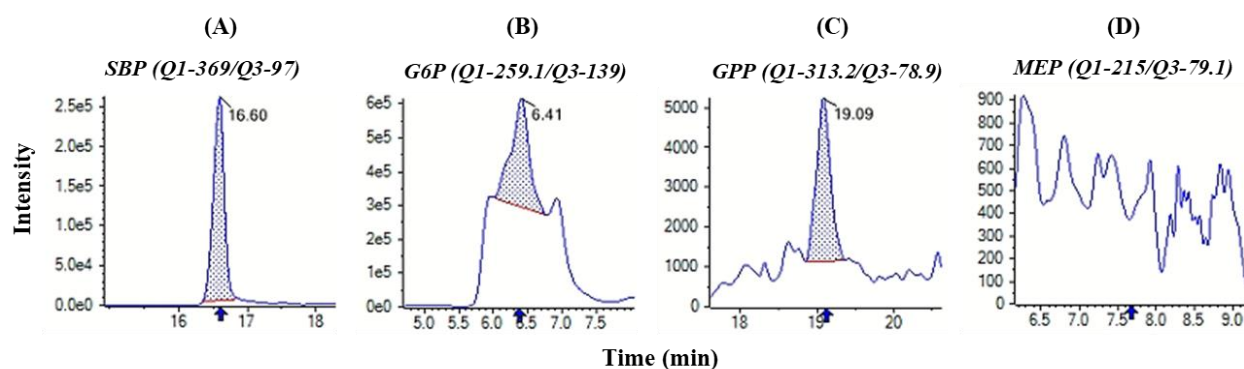
Figure 27. Examples of initial peak screening from the peppermint leaf extraction.

(A) A high abundance peak with good quality, (B) a high abundance peak with bad quality, (C) a low abundance peak and (D) no peak found. All the peaks represent (M+0) mass isotopomer of the corresponding metabolite. See the Table S14 for the full screening information of each analyte.

By this scrutiny, 27 fragments were excluded from the existing method. This selection process could be varied from sample to sample of different organisms. In the second step, the precision and accuracy of MIDs from each fragment were monitored (Table 17). One hydrophilic phase of peppermint leaf extraction was repetitively injected into LCMS for 20 times (10 times each for two sequential days). Twenty seven fragments, that exhibited high accuracy, sensitivity and reproducibility, were finally confirmed for further isotopic study of peppermint leaf metabolism and presented in Figure S14.

5.2.3. Central metabolic overview of peppermint leaf

Affirmatory test of the validated method was performed by the isotopic study of peppermint shoot-tip culture. The glimpse of label dilution was observed in proteinogenic amino acids at 15 DALV aged growing plant, reared under 5 µmol/m^2/s light intensity (Chapter III: Establishment of the experimental set-up for performing MFA; Figure 19). By this method, the MIDs of central metabolites from positionally labeled glucose fed shoot-tip culture was expected to be diverse, especially after feeding positionally labeled glucose. Indeed, closely produced metabolites with similar carbon number could correlate with each other respective to their ^{13}C inclusion, in case the established acquisition method was accurate and precise. Moreover, MIDs of each fragment were interpreted to predict the impact of unlabeled and labeled CO_2 fixation and possible regulation of the central biochemistry in the whole peppermint leaf. As a single leaf pair from the shoot-tip culture provided very small sample size, all the leaf pairs were collected together to obtain a more concentrated sample.

Result

5.2.4. Isotopic enrichment in central carbon metabolites and free amino acids:

Theoretically, the isotope enrichment in $1\text{-}^{13}C_1$ and $1,6\text{-}^{13}C_2$ glucose (99% purity) is 16.5% and 33%, respectively. In this part of the investigation (Figure 28A), label enrichment in H6P and FBP were roughly 14% and 29.5% from the corresponding two tracer studies. Label incorporation was further increased (32%) into PG and PEP from $1,6\text{-}^{13}C_2$ glucose study. However, the isotope amount remained similar in the upper and lower parts of glycolysis from $1\text{-}^{13}C_1$ glucose feeding. Free amino acid SER portrays the isotopic status of PG. ^{13}C enrichment of this amino acid was 12.5% and 27.5% from the corresponding one- and two-carbon labeled tracer study.
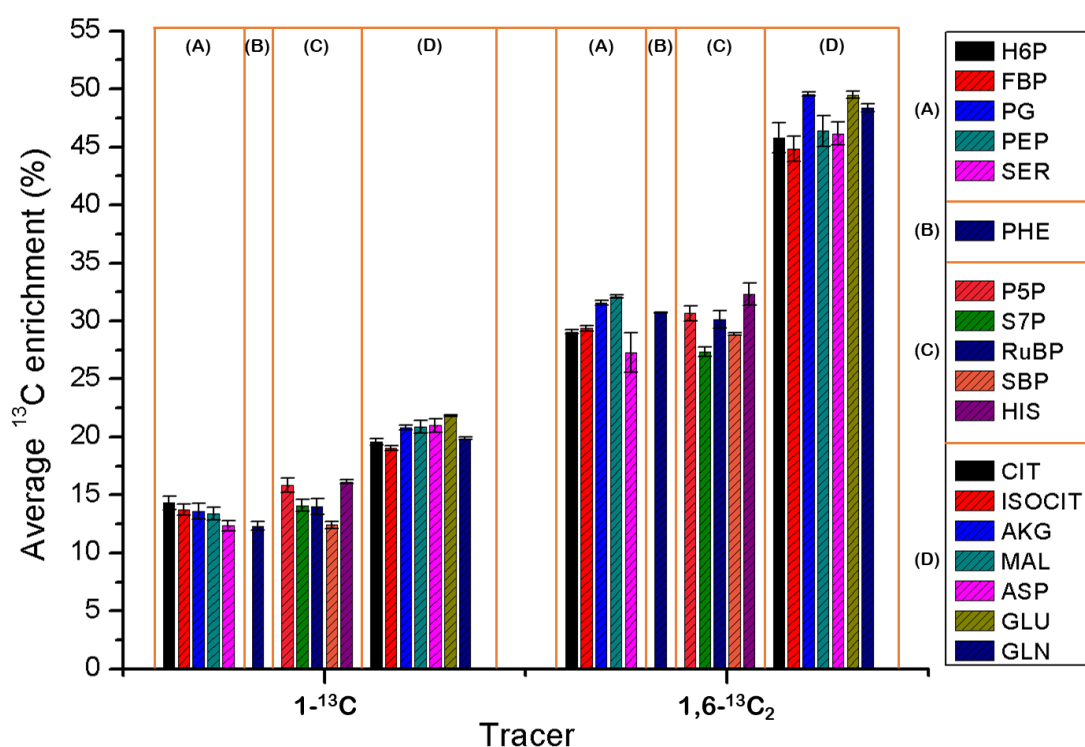
Figure 28. Average isotope enrichment in central metabolites and free amino acids.

The chosen metabolites are involved in the following pathways, namely (A) glycolysis, (B) glycolysis and PPP/Calvin cycle, (C) PPP/Calvin cycle and (D) TCA cycle (mean ± standard error; n=3). The metabolites were measured in ESI negative mode of LCMS.

Isotopic enrichment from the intermediates of PPP and/or Calvin cycle (Figure 28C) was apparently similar to the average ^{13}C amount of the glycolytic intermediates. Isotope incorporation in P5P was respectively 15.5% and 30.5% from $1\text{-}^{13}C_1$ and $1,6\text{-}^{13}C_2$ glucose fed culture. This observation was also supported by one free amino acid (HIS) which is produced from the P5P. RuBP also appeared to be identical with the pentose. However, S7P had lower label inclusion compared to P5P, which was

clearly evident from $1,6\text{-}^{13}C_2$ glucose study. SBP, the intermediate of Calvin cycle, was also evaluated to understand the contribution of ambient CO_2 fixation. However, the enrichment in this analyte was not drastically changed from other metabolites. PHE is synthesized by the joint action of glycolysis and PPP. This amino acid from the respective $1\text{-}^{13}C_1$ and $1,6\text{-}^{13}C_2$ tracer study had 12.5% and 31% ^{13}C enrichment, which was less than 1% from PEP (Figure 28B).

Four metabolites were estimated from the citric acid cycle (Figure 28D). These were CIT (C_6), ISOCIT (C_6), AKG (C_5) and MAL (C_4). Isotope enrichment in these metabolites varied from 19-21% and 45-49.5% in the case of $1\text{-}^{13}C_1$ and $1,6\text{-}^{13}C_2$ glucose fed culture, respectively. Higher ^{13}C incorporation was observed in AKG compared to CIT and ISOCIT. This enrichment was decreased again during MAL production. Furthermore, GLU and GLN discerned similar label statuses to AKG, as these two free amino acids are converted from that 5C compound without any change in carbon positioning. ASP, the carbon mimic of OAA, was also deduced in the present assay and depicted to be isotopically analogous to MAL. Moreover, the isotopic status of released CO_2 during conversion of C_6 to C_5 from $1,6\text{-}^{13}C_2$ glucose study was attempted to be calculated by the simplified concept (Data S3). It was determined that 50% of this carbon loss was labeled.

5.2.5. Label distribution in central carbon metabolites and free amino acids

Isotopic carbon distribution from the central metabolites and free amino acids depicted the high amount of label scrambling in the whole leaf due to the cycling of metabolic pathways throughout shoot-tip growth. Analysis of upper glycolytic metabolites (H6P and FBP) demonstrated (M+1) and (M+2) mass isotopomer as the highest from the respective $1\text{-}^{13}C_1$ and $1,6\text{-}^{13}C_2$ glucose treatment (Figure 29A and B). Lower and higher isotopomers were also found for these metabolites, for instance, (M+0) and (M+2) from the $1\text{-}^{13}C_1$ glucose feeding study. A similar trend was also found from the other tracer study, as two lower isotopomers and one higher isotopomer than (M+2) were present in these hexose phosphates. Among these, the distribution of lower mass isotopomers was increased in FBP, compared to H6P. Moreover, carbon allocation of (M+0) and (M+1) isotopomer in the trioses (PG and PEP) were the highest from the corresponding $1\text{-}^{13}C_1$ and $1,6\text{-}^{13}C_2$ glucose source (Figure 29C and D). The label scrambling effect was also noted due to the presence of (M+2) mass isotopomer in these trioses.
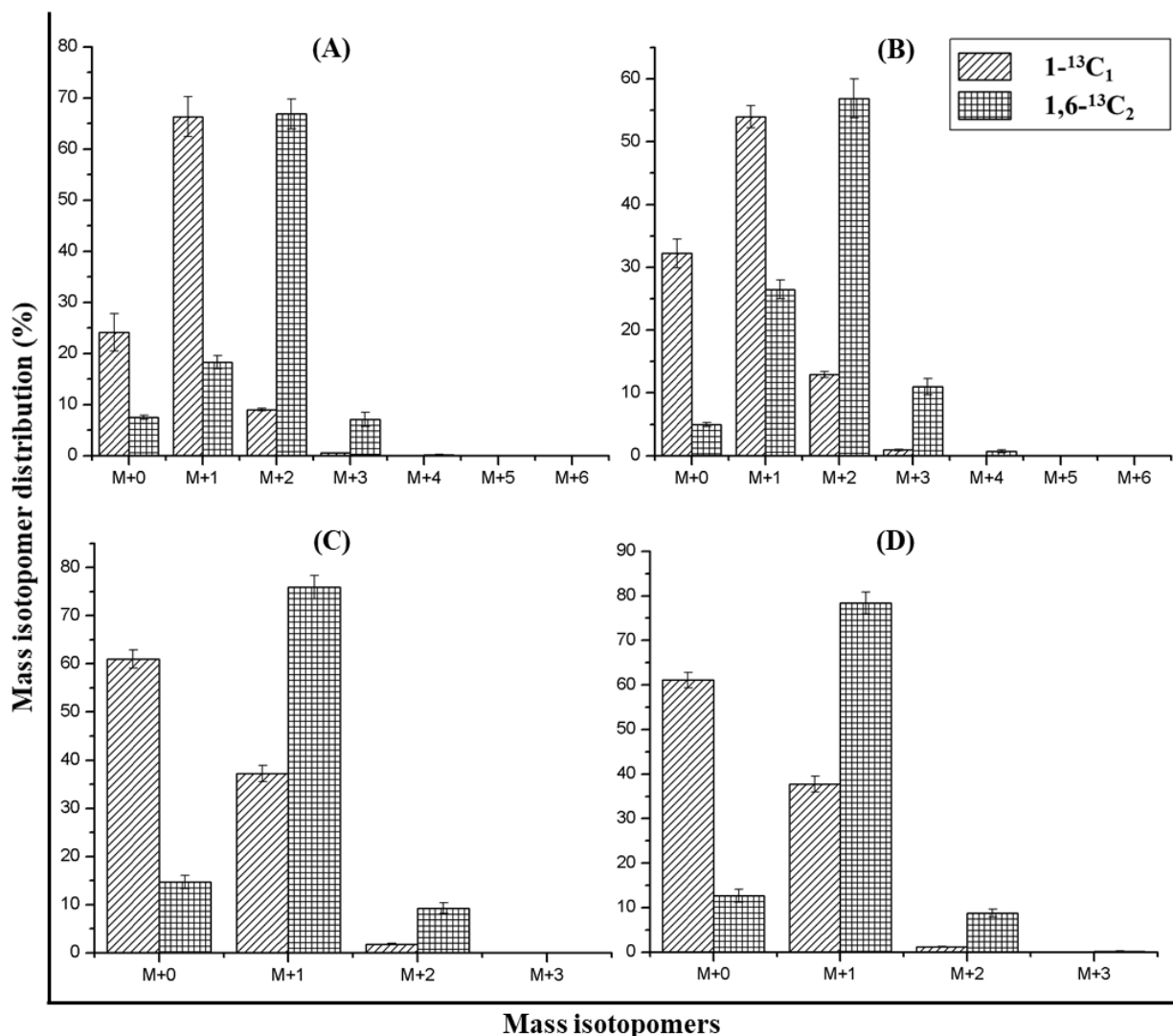
Figure 29. MID of glycolytic intermediates.

(A) H6P, (B) FBP, (C) PG and (D) PEP (mean ± standard error; n=3). The metabolites were measured in ESI negative mode of LCMS.

Four common metabolites of PPP and Calvin cycle were assessed in the present investigation (Figure 30). The highest mass isotopomers in these intermediates, found from the respective $1\text{-}^{13}C_1$ and $1,6\text{-}^{13}C_2$ glucose study, were (M+1) and (M+2). The nearest abundant mass isotopomer was (M+0) and (M+1) from the corresponding tracer study. The eminent amount of (M+2) and (M+3) from $1\text{-}^{13}C_1$, and (M+3) and (M+4) from $1,6\text{-}^{13}C_2$ glucose were also detected in all of these four metabolites.

In the TCA cycle intermediates (Figure 31), redistribution of the label was highly evident. As a consequence, all isotopomers, except the highest possible mass isotopomer, were observed in the $1,6\text{-}^{13}C_2$ glucose study. (M+3) of six carbon compound, both (M+2) and (M+3) of five carbon compound,

and (M+2) of four carbon compound were the most abundant isotopomer(s) from this tracer fed culture. As a fate of $1\text{-}^{13}C_1$ glucose incorporation, (M+1) isotopomer was statistically higher than others in each metabolite of this respiratory cycle. Additionally from this tracer, (M+0) and (M+2) had a similar distribution in CIT and ISOCIT; however, the lowest mass isotopomer was more enriched with the loss of CO_2 in the latter part of the Krebs cycle. Simultaneously, the degree of (M+2) isotopomer dropped from 28% (in ISOCIT) to 17% (in MAL).
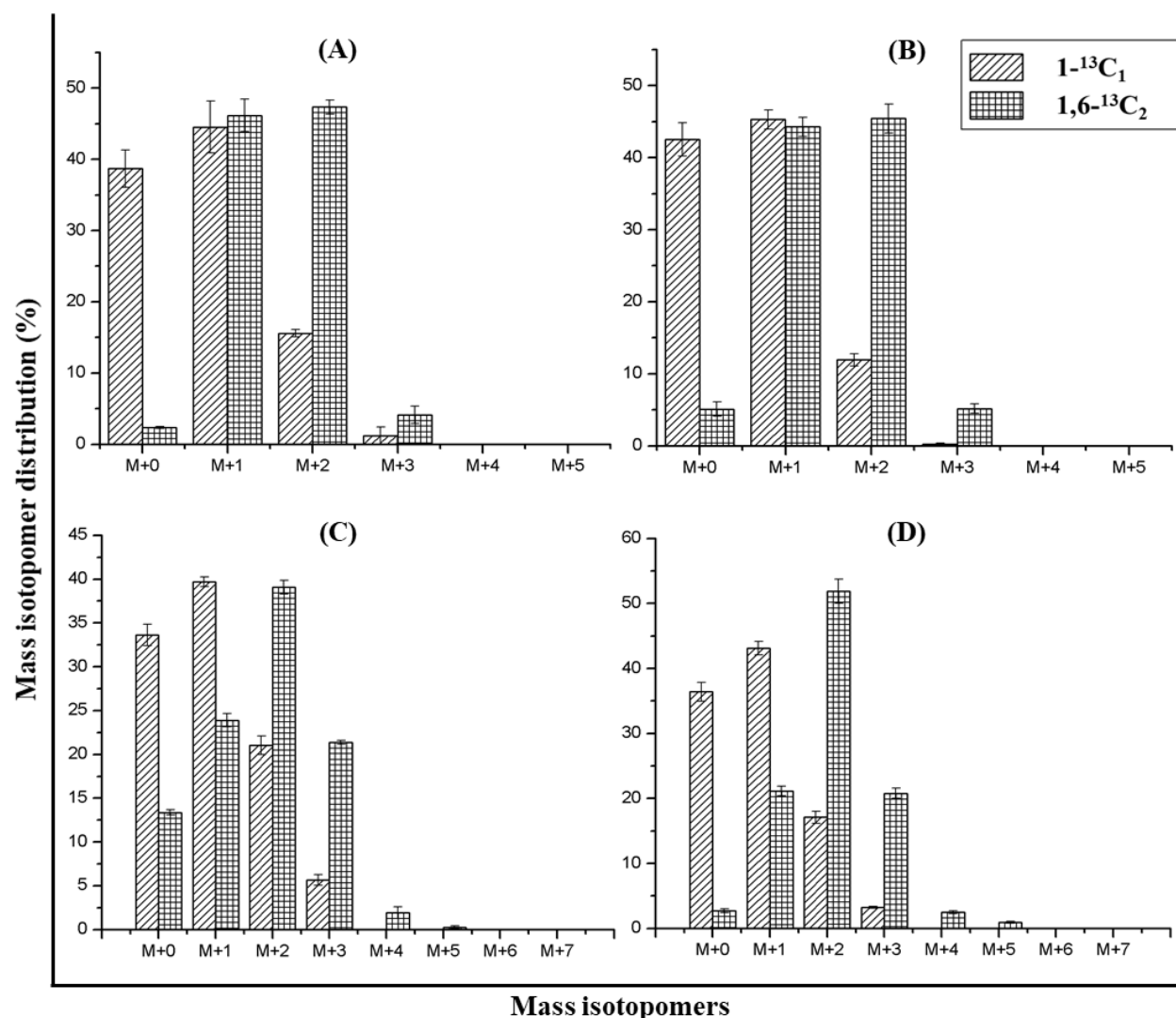
Figure 30. MID of PPP and Calvin cycle intermediates.

(A) P5P, (B) RuBP, (C) S7P and (D) SBP (mean ± standard error; n=3). The metabolites were measured in ESI negative mode of LCMS.
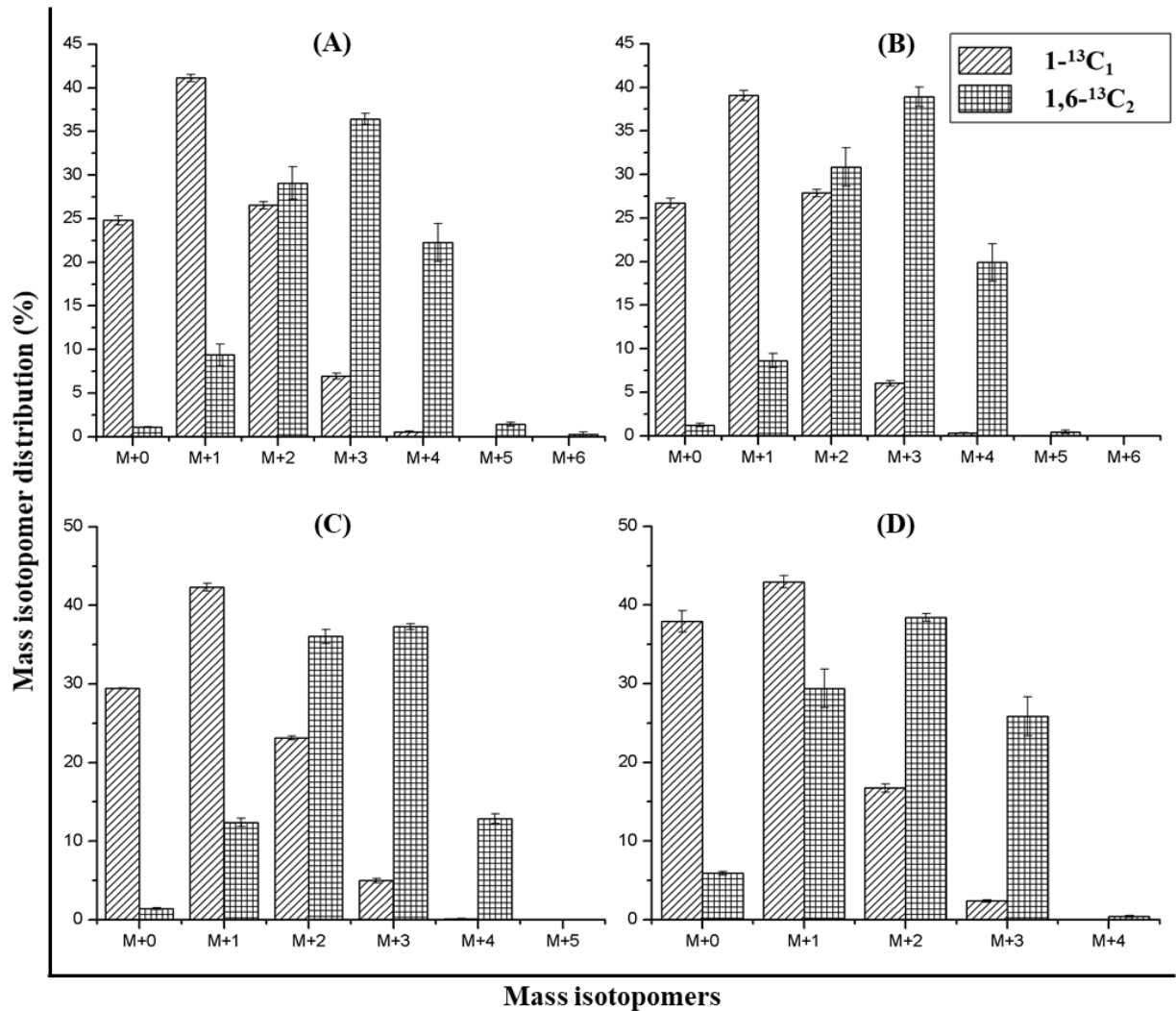
Figure 31. MID of TCA cycle intermediates.
(A) CIT, (B) ISOCIT, (C) AKG and (D) MAL (mean ± standard error; n=3). The metabolites were measured in ESI negative mode of LCMS.

The pattern of MIDs in SER was similar to PG and PEP; however, the amount of (M+0) isotopomer was slightly increased in amino acids than trioses (Figure 32). It was also noticed that (M+0) and (M+1) of $1\text{-}^{13}C_1$ glucose were virtually equal to the respective (M+1) and (M+2) isotopomer of $1,6\text{-}^{13}C_2$ glucose. In the case of PHE, the label was enriched to the highest level in (M+1) or (M+3) from the corresponding one- or two-position(s) labeled tracer study. (M+3) from $1\text{-}^{13}C_1$ glucose and (M+4) from $1,6\text{-}^{13}C_2$ glucose were also noticed. The carbon distribution of HIS demonstrated a similar trend to P5P. However, (M+3) isotopomer of this amino acid from $1,6\text{-}^{13}C_2$ glucose was higher than P5P at a cost of decreasing (M+1). This observation was also relevant from $1\text{-}^{13}C_1$ glucose study, as a comparable amount of (M+2) isotopomer was increased and (M+0) isotopomer was decreased.
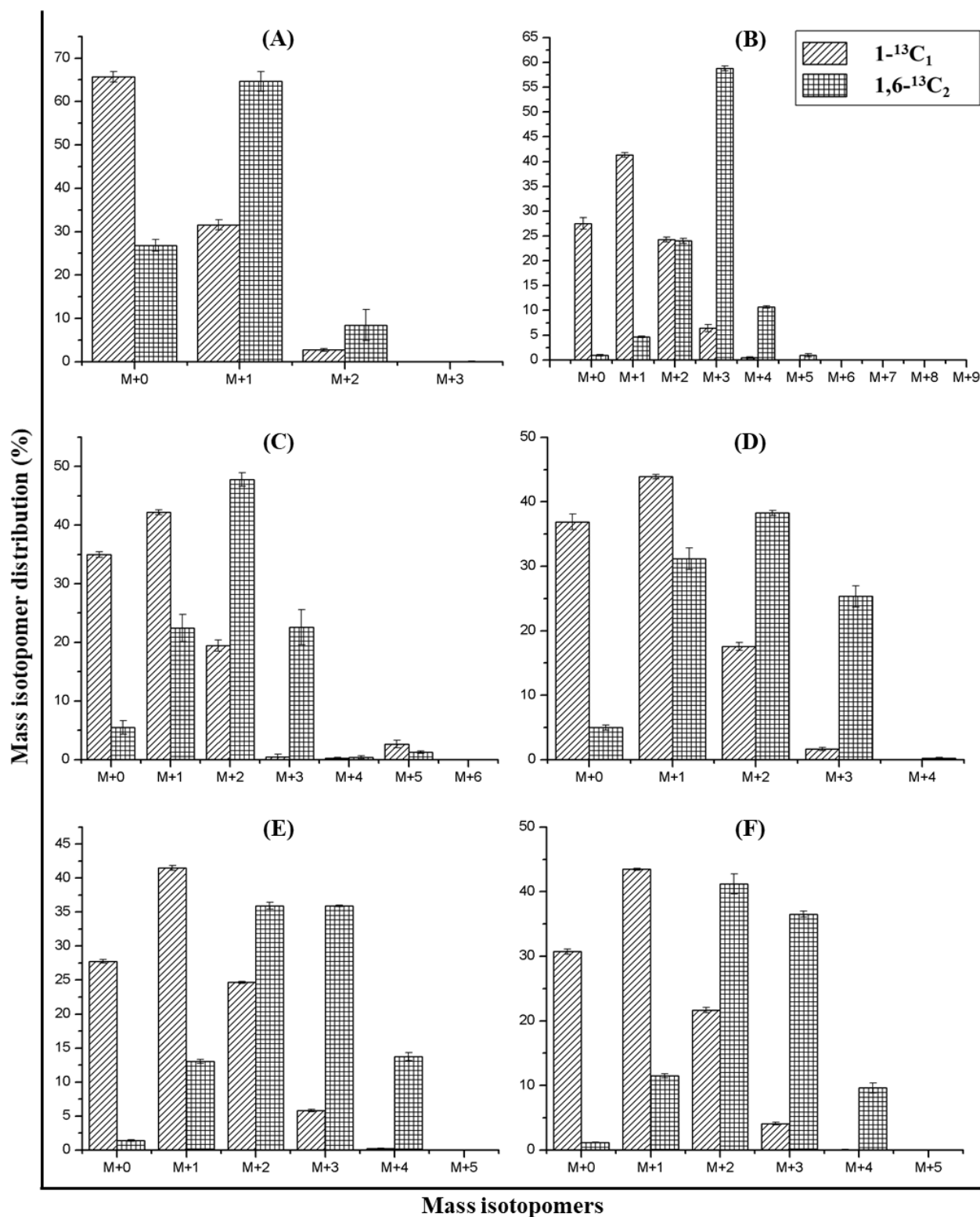
Figure 32. MID of free amino acids.

(A) SER, (B) PHE, (C) HIS, (D) ASP, (E) GLU and (F) GLN (mean ± standard error; n=3). The metabolites were measured in ESI negative mode of LCMS.

Result

OAA from Krebs's cycle also produces amino acids, such as ASP. Although measurement of OAA was not precise in our mass spectrometry analysis, MAL was considered to show similar isotope characteristics. It was heeded that ^{13}C distribution of ASP matched with that of MAL. The other TCA cycle precursor for amino acid production is AKG, from which GLU and GLN are synthesized. As expected, carbon status from both of these amino acids was the replica of AKG.

5.2.6. Overview of terpene biosynthetic pathways from peppermint leaf

Two DXP pathway intermediates (DXP and MEcPP) and the first common intermediate (IPP or DMAPP) from DXP and MVA were analyzed from the whole peppermint leaf. Unfortunately, MVA pathway intermediates could not be measured due to the low abundance and precision. From the ^{13}C enrichment analysis of $1-^{13}C_1$ glucose fed culture, MEcPP and DXP contained an average of 12.5% isotope whereas enrichment was increased in IPP (15.3%) (Figure 33). This trend was also identified from the investigation of the other tracer. Furthermore, (M+3) and (M+4) mass isotopomers of IPP were noticed from the respective C_1 and C_2 tracer studies at a lower extent (Figure 34). These isotopomers were totally absent in DXP pathway intermediates. Feeding of $1,6-^{13}C_2$ glucose resulted in higher (M+3) isotopomer in IPP than DXP and MEcPP. This observation was relevant to (M+2) isotopomer from $1-^{13}C_1$ glucose.
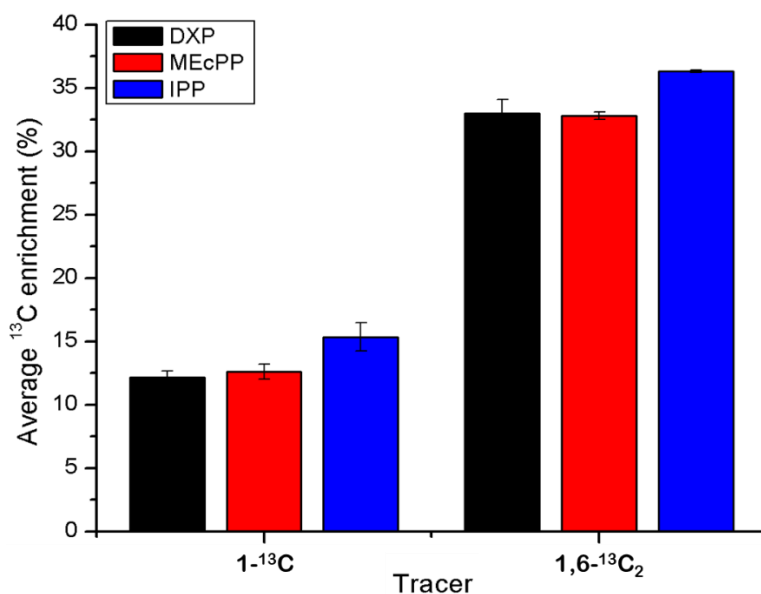
Figure 33. Average isotope enrichment in terpene biosynthetic intermediates.
DXP and MEcPP were produced via the DXP pathway and IPP was produced via both DXP and MVA pathway (mean ± standard error; n=3). The metabolites were measured in ESI negative mode of LCMS.
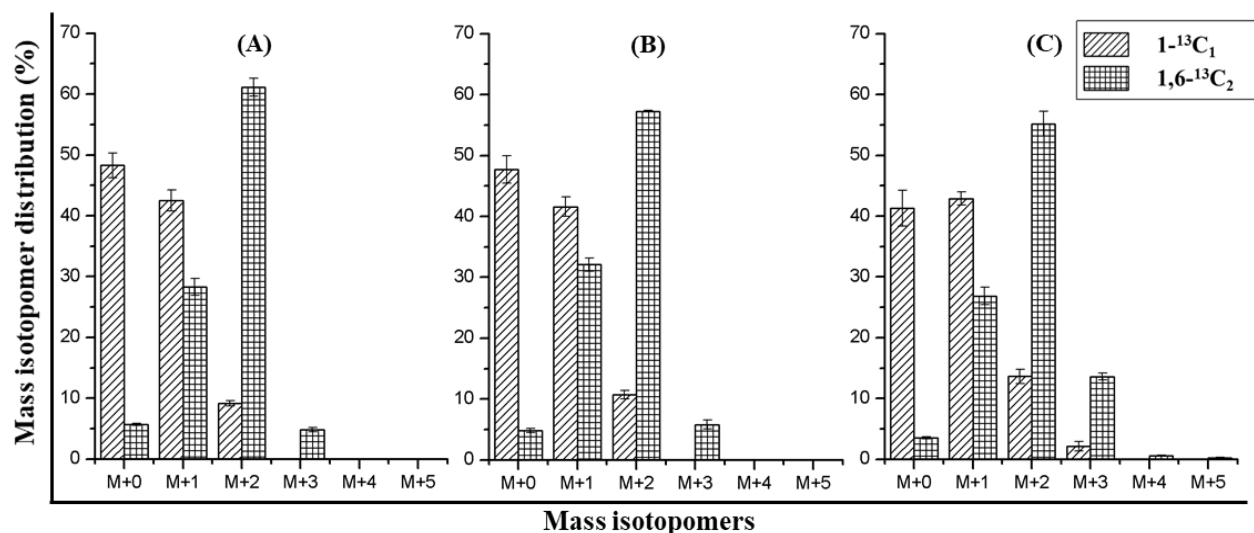
Figure 34. MID of terpene biosynthetic intermediates.

(A) DXP, (B) MEcPP and (C) IPP (mean ± standard error; n=3). The metabolites were measured in ESI negative mode of LCMS.

5.3. Discussion

Accessing metabolite data points from key pathways improves the understanding of cellular biochemistry (McCloskey et al., 2016). Central carbon metabolism regulates the isotope scrambling in the labeling experiment. In this part of the study, an acquisition method in ESI negative ionization mode was established for measuring isotopomer distribution of free amino acids and the intermediates from glycolysis, Calvin cycle, PPP and TCA cycle. MRM detection window (220 s) and target scan time (0.7 s) were also minimized to increase dwell time as it is necessary for maximizing the number of fragment isotopomers in a single run (Rühl et al., 2012). In the next step (Table 17), MIDs of each fragment needed to be precise and accurate to diminish the possibility of wrong flux presumption due to machine error (Jaiswal et al., 2018; McCloskey et al., 2016). Therefore, one hydrophilic phase of peppermint leaf extraction was repetitively injected into LCMS ten times. The same validation procedure was followed for a total two different days to understand the reproducibility of the system. In the initial part of the selection (Figure 27), low abundant peaks were also necessarily screened to avoid the disturbance of low signal to noise ratio due to the significant background chemical interference (Bergner and Lee, 1995; Fagerquist et al., 1999). Simultaneously, bad peaks were excluded because these mass transitions either overlapped with other unknown signals or, were overloaded, resulting in an inaccurate ceiling value. This rejection is necessary to obtain accurate flux values with high precision (Antoniewicz et al., 2007b; Kruger et al., 2007). Many previous reports

detected a different range of precision and accuracy values (Dauner and Sauer, 2000; Klapa et al., 2003b; Patterson et al., 1993). However, small measurement error culminates low confident flux values in MFA (Antoniewicz et al., 2006). Therefore, the error value was desired to be less than 0.5% (Antoniewicz et al., 2007b). It was imperative to develop one MRM method for hydrophilic analytes in LCMS for the detailed analysis of any living organism's biochemistry. In the future, it will be worthwhile to extend this method for other hydrophilic compounds and to create acquisition details for measuring MIDs of lipids and hydrophobic metabolites in atmospheric pressure chemical ionization mode.

In the latter part of this investigation, the validated method was successfully applied to assess the isotopic pattern of intracellular metabolites from the low-light shoot-culture condition. The label scrambling was evident in the central metabolites from the whole peppermint leaf at 15 DALV (Figure 28). This was expected due to the recycling of ^{13}C label via PPP and TCA cycle throughout this growth period. The ^{13}C abundance of upper glycolytic intermediates (H6P and FBP) was reduced to an average of 14% and 29% from the respective 16.5% and 33% ^{13}C-enriched imported glucose. This scenario was also noticed in PG, PEP, P5P, S7P, RuBP and SBP. Compared to the previous result (chapter III, Figure 19), the lower effect of unlabeled carbon was also found in proteogenic amino acids. Isotopic dilution could be possible by two ways; (1) unlabeled source of existing initial shoot-tip or ambient CO_2 and (2) loss of ^{13}C in the form of CO_2 during the central pathway recycling which could not be refixed. Although the first possibility can not be ignored, the negative CO_2 assimilation (chapter III, Table 12) strengthens the second option. Furthermore, ^{13}C enrichment in PG and PEP from 1,6-$^{13}C_2$ glucose was relatively higher than the glycolytic and PPP analytes and little more (2%) than RuBP (Figure 28). This biochemical feature exhibited $^{13}CO_2$ fixation in the peppermint leaf.

PG is a crucial intermediate of central metabolism as it is produced not only via glycolysis but also from the activity of RuBisCo fixation. Thus, the presence of (M+2) isotopomer in PG from both the tracers signified the contingency of $^{13}CO_2$ fixation inside the leaf. This kind of fixation was also visible in all other glycolytic and PPP intermediates, for instances, 7% (M+3) of H6P, 11% (M+3) of FBP and 9% (M+2) of PEP (Figure 29). From the theoretical interpretation, it was observed that (M+2) could not be present when carbon from these tracers flows either through glycolysis or through the joint action of oxPPP and non-oxPPP (Figure 26). Among the two possible routes (oxPPP and reductive non-oxPPP) of supplying the precursor for RuBisCo, reductive non-oxPPP seemed to be

mostly happening in the peppermint leaf (Figure S15). As an alternate proof, $^{13}CO_2$ fixation after oxPPP, which could result only in the change in label position of PG, does not generate (M+2) mass isotopomer (Chapter IV, Figure 26). Therefore, it could be anticipated that carbon was metabolized via the upper part of glycolysis, non-oxPPP and then RuBisCO in the peppermint shoot-tip culture. The effect of $^{13}CO_2$ fixation in H6P and FBP might also be due to the reversible reaction by transaldolase (Calvin cycle) or, transketolase (reductive PPP). The other circumstance to obtain higher mass isotopomers in upper glycolytic intermediates could be through gluconeogenesis after anaplerotic production of PYR from MAL. However, the average ^{13}C enrichment of malate (46% from $1,6-^{13}C_2$ glucose) was totally unmatched with the enrichment of glycolytic intermediates (29% - 32% from $1,6-^{13}C_2$ glucose), which denied the presence of fully reversed glycolysis (Figure 28).

Interpreting the isotopic status of TCA cycle is sophisticated work due to the presence of stereospecific interconversion of fumarate and malate. It leads to escalating disorientation and the amount of label carbon with the accomplishment of each round of cycle. Thus, the amount of isotopic abundance in TCA cycle intermediates was distinctively compared to the above-discussed biochemical pathways. Nonetheless, the analytes of this repetitive cycle were more or less correlated with each other. Interestingly, the isotope enrichment in AKG increased compared to CIT or ISOCIT (Figure 28). The release of CO_2 from CIT for the production of AKG seemed to be 50% unlabeled (Data S3). However, the lost carbon from AKG to MAL was predicted to be highly labeled, as the average ^{13}C inclusion was decreased during this transition. Because of the absence of extra ^{13}C, (M+0) of MAL was higher than the other TCA cycle metabolites (Figure 31D). This labeled and unlabeled carbon could be refixed by RuBisCO and simultaneously produce lower and higher mass isotopomers than expected from the tracer (for example, M+0 and M+2 of PG). In addition, the isotopic status of AKG was supported by GLU and GLN whereas MAL was analogous to ASP (Figure 32).

By comparing the assessments from two tracers, it could be confirmed that leaf from shoot-tip culture did not have high flux via the joint route of oxPPP and non-oxPPP. This was also implied by ^{13}C enrichment in all the analytes from $1,6-^{13}C_2$ glucose fed culture, which was nearly two (1.8-2.5) times higher than that from $1-^{13}C_1$ glucose (Figure 26). Biochemically, oxPPP is required to prevent oxidative stress due to high light (Juhnke et al., 1996; Krüger et al., 2011; Stincone et al., 2015) and to supply electron carrier (NADPH) for anabolism (Neuhaus and Emes, 2000) such as fatty acid or terpene biosynthesis. In the present case, a leaf from the low-light adapted plant should not have the

issue of oxidative stress and might not require a high amount of NADPH. Due to the restriction of illumination, peppermint shoot-tip cultures could not consume a high amount of ambient CO_2 and were also unable to produce light-induced ATP. Indeed, for maintaining energetic homeostasis, the low light adapted plant required more mitochondrial ETC flux by repetitions of TCA cycle (Beckers et al., 2016; Cheung et al., 2015; Kramer and Evans, 2011). This process produced a high amount of CO_2. Therefore, the plant would consider reassimilating this CO_2 by the joint route of non-oxPPP and RuBisCO rather than by the carbon costly path (oxPPP). This was suggested in rapeseed where the developing embryo used non-oxPPP route followed by RuBisCO fixation (Schwender et al., 2004).

The assessment from terpene biosynthetic pathway intermediates suggested the presence of MVA pathway activity in the peppermint leaf (including GTs). Hence, the isotope was more enriched in IPP compared to DXP and MEcPP (Figure 33). Higher ^{13}C abundance in higher mass isotopomers of IPP also proved this hypothesis (Figure 34). Enrichment was assumed to be higher via the MVA route as the precursor for this pathway was produced from highly enriched CIT by the catabolism of ATP-CIT lyase. For the DXP pathway, two C_3 substrates came from relatively low enriched glycolytic intermediates, as suggested by average labeling status of DXP pathway intermediates, which were analogues to C_3 metabolites of glycolysis.

This part of the research was done to establish and verify acquisition methods in LCMS for analysis of central and terpenoid biosynthetic intermediates. However, flux analysis on LCMS-based result from leaf tissue was not performed, because (1) the main aim of the thesis was to interpret the terpenoid metabolism of GT cells for their high commercial value, rather than primary metabolism of leaf tissue; (2) metabolic steady-state of both primary and secondary metabolism together are difficult to achieve at a specific time due to extensive biochemical network of the leaf; and (3) leaf-based MFA requires the additional labeling information of the primary metabolic end-product (such as, ^{13}C distribution in protein, starch or lipid), their individual production rate and active-inactive pool size of the intermediates. Therefore, leaf-based model of primary metabolism, which has less importance for peppermint compared to monoterpene metabolism, was not considered to be addressed in the course of this thesis.

Summary

Peppermint plant has evolved to protect itself against natural aggressors by producing secondary metabolites on its surface. Essential oils of this Lamiaceae plant, mainly consisting of monoterpenes, have huge industrial value due to their commercial relevance in aromatic, fragrance, cosmetic, nutraceutical and therapeutic purposes. Hence, this plant has been a model system for studying monoterpene biosynthesis. *In vivo*, terpenes are produced by two independent pathways, namely, cytosolic MVA and plastidic DXP. In the postulated view, the cytosolic route supplies the precursors for sesqui- and triterpenes production whereas the plastidic route provides the precursors for processing mono-, di- and tetraterpenes. The volatile terpenes (mono- and sesquiterpenes) are synthesized in specialized and highly active cells, known as glandular trichome (GT) secretory cells. These cells in the peppermint plant are characterized as non-photosynthetic cells. Monoterpene biosynthesis is classically operated by the DXP pathway in the leucoplast of these cells. The present study tracks not only the secondary metabolism but also the primary metabolism to gain a more complete and deeper understanding of monoterpene biosynthesis in peppermint GT cells.

A better understanding of the physiological and metabolic status of plants can only be obtained when metabolic fluxes are accurately assessed in a growing plant. Steady-state ^{13}C-MFA has been established as a routine method for analysis of fluxes in plant primary metabolism. However, the experimental system needs to be improved for continuous carbon enrichment from labeled sugars into metabolites for longer periods until complex secondary metabolism reaches steady-state. Therefore, the initial objective of this study was to establish a new culture condition where isotopic carbon incorporation would be high and stable during steady monoterpene production for the successful implementation of ^{13}C-MFA.

An in vitro tissue culture strategy was developed for peppermint plant to minimize unlabeled carbon fixation. The growing shoot-tip was strongly dependent on labeled glucose for its carbon necessity. The light conditions were optimized in the process of system advancement to maintain satisfactory plant growth while at the same time achieving high volatile terpene production. Analysis of label incorporation into monoterpene after continuous U-^{13}C$_6$ glucose feeding revealed nearly 100% ^{13}C, even at 15 days after first leaf visibility. Label enrichment gradually scrambled with increasing light intensity and leaf age. The proof of validation for this system was recapitulated through high levels of label enrichment in proteinogenic amino acids and in oregano plant.

Summary

This shoot-tip culture describes a method in achieving long term, stable and a high percentage of label accumulation in secondary metabolites within a fully functional growing plant system. It recommends the potential application for the investigations of various facets of plant metabolism by steady-state ^{13}C-MFA. Primary metabolism does not demand long-term experiments, and in this study, the ^{13}C incorporation level in proteinogenic amino acids was exceptionally high already after two weeks. Therefore, this system also provides an alternative approach for studying steady-state fluxes in primary metabolism for shorter time periods. This strategy of achieving high label into the metabolites in 15 days leaf also provides a greater potential to study sink leaf metabolism. The culture set-up is economically feasible (70-80 mg labeled glucose per replicate), robust and allows parallel operation without any requirement of specialized equipment during cultivation. Using this approach, performing ^{13}C-MFA in the plant can be less challenging and more effective to quantify the contribution of different pathways for various end-products. Additionally, the carbon economy of the plant can also be conceived. Overall, this investigation introduces a potential approach to accurately describe complex metabolic phenotypes in a growing plant.

The metabolism of GT cells for monoterpene biosynthesis was depicted by using this culture strategy in low light. Integrative MFA was performed by simultaneously fitting data sets of three different tracer studies to a single, compartmentalized metabolic network. The flux analysis offers new insights into peppermint GT metabolism by demonstrating the participation of an alternate MVA route to monoterpene biosynthesis and quantifying the amount of cross-talk between the two terpenoid biosynthesis pathways. These findings have been confirmed by inhibition study of the DXP pathway and in-depth theoretical analysis of ^{13}C labeling data. In addition, the flux analysis provided a quantitative description of the central carbon metabolism of peppermint GT towards monoterpene production. MFA supported a prominent role for the oxidative branch of the PPP in providing reductants for monoterpene biosynthesis and for RuBisCO in refixing metabolic CO_2 thereby contributing to the CCE in peppermint GTs. The relative fluxes also allowed speculation at the connection of glycolysis with the MVA pathway in GTs. Additionally, flux analysis of oregano using the same culture system, reiterated the trend of central metabolism in GTs. Both the terpenoid biosynthetic pathways contributed for mono- and sesquiterpene production in oregano, however the cross-talk between the pathways was more evident for the latter one.

To the best of my knowledge, this is the first time that steady-state ^{13}C MFA has been successfully applied to map monoterpene biosynthesis in peppermint GTs. This study reveals the potential of ^{13}C MFA to ascertain previously unquantified metabolic insights of the trichome cell. It can advance the metabolic engineering of these cells by uncovering the biochemical bottleneck for further increasing the productivity of these valuable compounds inside these highly active cells.

References

Abernathy, M.H., Yu, J., Ma, F., Liberton, M., Ungerer, J., Hollinshead, W.D., Gopalakrishnan, S., He, L., Maranas, C.D., Pakrasi, H.B., Allen, D.K., Tang, Y.J., 2017. Deciphering cyanobacterial phenotypes for fast photoautotrophic growth via isotopically nonstationary metabolic flux analysis. Biotechnol. Biofuels 10, 273.

Adam, K.-P., Thiel, R., Zapp, J., 1999. Incorporation of 1-[1-13C] deoxy-D-xylulose in chamomile sesquiterpenes. Arch. Biochem. Biophys. 369, 127–132.

Adams, R.P., 2007. Identification of essential oil components by gas chromatography/mass spectrometry. Allured publishing corporation Carol Stream, IL.

Ahkami, A., Johnson, S.R., Srividya, N., Lange, B.M., 2015. Multiple levels of regulation determine monoterpenoid essential oil compositional variation in the mint family. Mol. Plant 8, 188–191.

Ajikumar, P.K., Tyo, K., Carlsen, S., Mucha, O., Phon, T.H., Stephanopoulos, G., 2008. Terpenoids: opportunities for biosynthesis of natural product drugs using engineered microorganisms. Mol. Pharm. 5, 167–190.

Alberts, B., Johnson, A., Lewis, J., Raff, M., Roberts, K., Walter, P., 2002. Catalysis and the Use of Energy by Cells. Mol. Biol. Cell 4th Ed.

Allen, D.K., 2016. Quantifying plant phenotypes with isotopic labeling & metabolic flux analysis. Curr. Opin. Biotechnol. 37, 45–52.

Allen, D.K., Laclair, R.W., Ohlrogge, J.B., Shachar-Hill, Y., 2012. Isotope labelling of Rubisco subunits provides in vivo information on subcellular biosynthesis and exchange of amino acids between compartments. Plant Cell Environ. 35, 1232–1244.

Allen, D.K., Ohlrogge, J.B., Shachar-Hill, Y., 2009a. The role of light in soybean seed filling metabolism. Plant J. Cell Mol. Biol. 58, 220–234.

Allen, D.K., Ohlrogge, J.B., Shachar-Hill, Y., 2009b. The role of light in soybean seed filling metabolism. Plant J. 58, 220–234.

Allen, D.K., Ratcliffe, R.G., 2009. Quantification of Isotope Label, in: Schwender, J. (Ed.), Plant Metabolic Networks. Springer New York, New York, NY, pp. 105–149.

Allen, D.K., Young, J.D., 2013. Carbon and Nitrogen Provisions Alter the Metabolic Flux in Developing Soybean Embryos. Plant Physiol. 161, 1458–1475.

Alonso, A.P., Dale, V.L., Shachar-Hill, Y., 2010. Understanding fatty acid synthesis in developing maize embryos using metabolic flux analysis. Metab. Eng. 12, 488–497.

Alonso, A.P., Goffman, F.D., Ohlrogge, J.B., Shachar-Hill, Y., 2007. Carbon conversion efficiency and central metabolic fluxes in developing sunflower (Helianthus annuus L.) embryos. Plant J. Cell Mol. Biol. 52, 296–308.

Alonso, A.P., Val, D.L., Shachar-Hill, Y., 2011. Central metabolic fluxes in the endosperm of developing maize seeds and their implications for metabolic engineering. Metab. Eng. 13, 96–107.

Alonso, A.P., Vigeolas, H., Raymond, P., Rolin, D., Dieuaide-Noubhani, M., 2005. A new substrate cycle in plants. Evidence for a high glucose-phosphate-to-glucose turnover from in vivo steady-state and pulse-labeling experiments with [13C]glucose and [14C]glucose. Plant Physiol. 138, 2220–2232.

Alonso, W.R., Rajaonarivony, J.I., Gershenzon, J., Croteau, R., 1992. Purification of 4S-limonene synthase, a monoterpene cyclase from the glandular trichomes of peppermint (Mentha x piperita) and spearmint (Mentha spicata). J. Biol. Chem. 267, 7582–7587.

Amelunxen, F., 1965. Elektronenmikroskopische untersuchungen an den drüsenschuppen von mentha piperita L. 1. Planta Med. 13, 457–473.

Anchisi, C., Meloni, M.C., Maccioni, A.M., 2006. Chitosan beads loaded with essential oils in cosmetic formulations. J. Cosmet. Sci. 57, 205–214.

Antoniewicz, M.R., Kelleher, J.K., Stephanopoulos, G., 2007a. Elementary metabolite units (EMU): a novel framework for modeling isotopic distributions. Metab. Eng. 9, 68–86.

Antoniewicz, M.R., Kelleher, J.K., Stephanopoulos, G., 2007b. Accurate assessment of amino acid mass isotopomer distributions for metabolic flux analysis. Anal. Chem. 79, 7554–7559.

Antoniewicz, M.R., Kelleher, J.K., Stephanopoulos, G., 2006. Determination of confidence intervals of metabolic fluxes estimated from stable isotope measurements. Metab. Eng. 8, 324–337.

Arimura, G., Ozawa, R., Nishioka, T., Boland, W., Koch, T., Kühnemann, F., Takabayashi, J., 2002. Herbivore-induced volatiles induce the emission of ethylene in neighboring lima bean plants. Plant J. 29, 87–98.

Arrivault, S., Guenther, M., Ivakov, A., Feil, R., Vosloh, D., van Dongen, J.T., Sulpice, R., Stitt, M., 2009. Use of reverse-phase liquid chromatography, linked to tandem mass spectrometry, to profile the Calvin cycle and other

References

metabolic intermediates in Arabidopsis rosettes at different carbon dioxide concentrations. Plant J. Cell Mol. Biol. 59, 826–839.

Ashour, M., Wink, M., Gershenzon, J., 2010. Biochemistry of terpenoids: monoterpenes, sesquiterpenes and diterpenes. Biochem. Plant Second. Metab. 2, 258–303.

Bach, T.J., 1995. Some new aspects of isoprenoid biosynthesis in plants—a review. Lipids 30, 191–202.

Balcke, G.U., Bennewitz, S., Bergau, N., Athmer, B., Henning, A., Majovsky, P., Jiménez-Gómez, J.M., Hoehenwarter, W., Tissier, A., 2017. Multi-omics of tomato glandular trichomes reveals distinct features of central carbon metabolism supporting high productivity of specialized metabolites. Plant Cell 29, 960–983.

Balcke, G.U., Bennewitz, S., Zabel, S., Tissier, A., 2014. Isoprenoid and Metabolite Profiling of Plant Trichomes, in: Rodríguez-Concepción, M. (Ed.), Plant Isoprenoids: Methods and Protocols, Methods in Molecular Biology. Springer New York, New York, NY, pp. 189–202.

Baly, E.C.C., 1935. The kinetics of photosynthesis. Proc. R. Soc. Lond. Ser. B-Biol. Sci. 117, 218–239.

Baranauskienė, R., Venskutonis, P.R., Dewettinck, K., Verhé, R., 2006. Properties of oregano (Origanum vulgare L.), citronella (Cymbopogon nardus G.) and marjoram (Majorana hortensis L.) flavors encapsulated into milk protein-based matrices. Food Res. Int. 39, 413–425.

Bartram, S., Jux, A., Gleixner, G., Boland, W., 2006. Dynamic pathway allocation in early terpenoid biosynthesis of stress-induced lima bean leaves. Phytochemistry 67, 1661–1672.

Beckers, V., Dersch, L.M., Lotz, K., Melzer, G., Bläsing, O.E., Fuchs, R., Ehrhardt, T., Wittmann, C., 2016. In silico metabolic network analysis of Arabidopsis leaves. BMC Syst. Biol. 10.

Bergner, E.A., Lee, W.-N.P., 1995. Testing gas chromatographic/mass spectrometric systems for linearity of response. J. Mass Spectrom. 30, 778–780.

Bertea, C.M., Schalk, M., Karp, F., Maffei, M., Croteau, R., 2001. Demonstration that menthofuran synthase of mint (Mentha) is a cytochrome P450 monooxygenase: cloning, functional expression, and characterization of the responsible gene. Arch. Biochem. Biophys. 390, 279–286.

Boatright, J., Negre, F., Chen, X., Kish, C.M., Wood, B., Peel, G., Orlova, I., Gang, D., Rhodes, D., Dudareva, N., 2004. Understanding in vivo benzenoid metabolism in petunia petal tissue. Plant Physiol. 135, 1993–2011.

Bohlmann, J., Keeling, C.I., 2008. Terpenoid biomaterials. Plant J. 54, 656–669.

Bohlmann, J., Steele, C.L., Croteau, R., 1997. Monoterpene synthases from grand fir (Abies grandis). cDNA isolation, characterization, and functional expression of myrcene synthase, (-)-(4S)-limonene synthase, and (-)-(1S,5S)-pinene synthase. J. Biol. Chem. 272, 21784–21792.

Bonarius, H.P.J., Schmid, G., Tramper, J., 1997. Flux analysis of underdetermined metabolic networks: the quest for the missing constraints. Trends Biotechnol. 15, 308–314.

Bondar, R.J., Mead, D.C., 1974. Evaluation of glucose-6-phosphate dehydrogenase from Leuconostoc mesenteroides in the hexokinase method for determining glucose in serum. Clin. Chem. 20, 586–590.

Bouvier-Brown, N.C., Holzinger, R., Palitzsch, K., Goldstein, A.H., 2007. Quantifying sesquiterpene and oxygenated terpene emissions from live vegetation using solid-phase microextraction fibers. J. Chromatogr. A 1161, 113–120.

Breitmaier, E., 2006. Terpenes: flavors, fragrances, pharmaca, pheromones. John Wiley & Sons.

Büchi, R., Bachmann, M., Keller, F., 1998. Carbohydrate metabolism in source leaves of sweet basil (Ocimum basilicum L.), a starch-storing and stachyose-translocating labiate. J. Plant Physiol. 153, 308–315.

Buchmann, S.L., Nabhan, G.P., 1996. The forgotten pollinators.

Cai, Y., Jia, J.-W., Crock, J., Lin, Z.-X., Chen, X.-Y., Croteau, R., 2002. A cDNA clone for beta-caryophyllene synthase from Artemisia annua. Phytochemistry 61, 523–529.

Caspi, R., Billington, R., Fulcher, C.A., Keseler, I.M., Kothari, A., Krummenacker, M., Latendresse, M., Midford, P.E., Ong, Q., Ong, W.K., Paley, S., Subhraveti, P., Karp, P.D., 2018. The MetaCyc database of metabolic pathways and enzymes. Nucleic Acids Res. 46, D633–D639.

Chappell, J., 1995. Biochemistry and molecular biology of the isoprenoid biosynthetic pathway in plants. Annu. Rev. Plant Biol. 46, 521–547.

Chen, F., Tholl, D., D'Auria, J.C., Farooq, A., Pichersky, E., Gershenzon, J., 2003. Biosynthesis and emission of terpenoid volatiles from Arabidopsis flowers. Plant Cell 15, 481–494.

Cheng, A.-X., Lou, Y.-G., Mao, Y.-B., Lu, S., Wang, L.-J., Chen, X.-Y., 2007. Plant Terpenoids: Biosynthesis and Ecological Functions. J. Integr. Plant Biol. 49, 179–186.

Cheung, C.Y.M., Ratcliffe, R.G., Sweetlove, L.J., 2015. A Method of Accounting for Enzyme Costs in Flux Balance Analysis Reveals Alternative Pathways and Metabolite Stores in an Illuminated Arabidopsis Leaf. Plant Physiol. 169, 1671–1682.

Christensen, B., Nielsen, J., 1999. Isotopomer analysis using GC-MS. Metab. Eng. 1, 282–290.

Cirla, A., Mann, J., 2003. Combretastatins: from natural products to drug discovery. Nat. Prod. Rep. 20, 558–564.

Colby, S.M., Alonso, W.R., Katahira, E.J., McGarvey, D.J., Croteau, R., 1993. 4S-limonene synthase from the oil glands of spearmint (Mentha spicata). cDNA isolation, characterization, and bacterial expression of the catalytically active monoterpene cyclase. J. Biol. Chem. 268, 23016–23024.

Coleman III, W.M., Lawrence, B.M., Cole, S.K., 2002. Semiquantitative determination of off-notes in mint oils by solid-phase microextraction. J. Chromatogr. Sci. 40, 133–139.

Coleman III, W.M., Lawrence, B.M., Craven, S.H., 2004. The use of a non-equilibrated solid phase microextraction method to quantitatively determine the off-notes in mint and other essential oils. J. Sci. Food Agric. 84, 1223–1228.

Converti, A., Perego, P., 2002. Use of carbon and energy balances in the study of the anaerobic metabolism of Enterobacter aerogenes at variable starting glucose concentrations. Appl. Microbiol. Biotechnol. 59, 303–309.

Covington, M.F., Maloof, J.N., Straume, M., Kay, S.A., Harmer, S.L., 2008. Global transcriptome analysis reveals circadian regulation of key pathways in plant growth and development. Genome Biol. 9, R130.

Cragg, G.M., Kingston, D.G.I., Newman, D.J., Kingston, D.G.I., Newman, D.J., 2011. Anticancer Agents from Natural Products. CRC Press.

Crocoll, C., Asbach, J., Novak, J., Gershenzon, J., Degenhardt, J., 2010. Terpene synthases of oregano (Origanum vulgare L.) and their roles in the pathway and regulation of terpene biosynthesis. Plant Mol. Biol. 73, 587–603.

Croteau, R., Alonso, W.R., Koepp, A.E., Johnson, M.A., 1994. Biosynthesis of monoterpenes: partial purification, characterization, and mechanism of action of 1,8-cineole synthase. Arch. Biochem. Biophys. 309, 184–192.

Croteau, R., Ketchum, R.E., Long, R.M., Kaspera, R., Wildung, M.R., 2006. Taxol biosynthesis and molecular genetics. Phytochem. Rev. 5, 75–97.

Croteau, R.B., Davis, E.M., Ringer, K.L., Wildung, M.R., 2005. (-)-Menthol biosynthesis and molecular genetics. Naturwissenschaften 92, 562.

Dauner, M., Sauer, U., 2000. GC-MS Analysis of Amino Acids Rapidly Provides Rich Information for Isotopomer Balancing. Biotechnol. Prog. 16, 642–649.

Davis, E.M., Ringer, K.L., McConkey, M.E., Croteau, R., 2005. Monoterpene metabolism. Cloning, expression, and characterization of menthone reductases from peppermint. Plant Physiol. 137, 873–881.

De Moraes, C.M., Mescher, M.C., Tumlinson, J.H., 2001. Caterpillar-induced nocturnal plant volatiles repel conspecific females. Nature 410, 577–580.

Dennis, J.E., Schnabel, R.B., 1983. Numerical methods for unconstrained optimization and nonlinear equations. Englewood Cliffs, N.J. : Prentice-Hall.

Dersch, L.M., Beckers, V., Wittmann, C., 2016. Green pathways: Metabolic network analysis of plant systems. Metab. Eng. 34, 1–24.

Dethloff, F., Orf, I., Kopka, J., 2017. Rapid in situ 13C tracing of sucrose utilization in Arabidopsis sink and source leaves. Plant Methods 13, 87.

Dicke, M., van Loon, J.J., 2000. Multitrophic effects of herbivore-induced plant volatiles in an evolutionary context. Entomol. Exp. Appl. 97, 237–249.

Dieuaide-Noubhani, M., Raffard, G., Canioni, P., Pradet, A., Raymond, P., 1995. Quantification of compartmented metabolic fluxes in maize root tips using isotope distribution from 13C- or 14C-labeled glucose. J. Biol. Chem. 270, 13147–13159.

Dreher, K., 2014. Putting The Plant Metabolic Network pathway databases to work: going offline to gain new capabilities. Methods Mol. Biol. Clifton NJ 1083, 151–171.

Dubey, V.S., Bhalla, R., Luthra, R., 2003. An overview of the non-mevalonate pathway for terpenoid biosynthesis in plants. J. Biosci. 28, 637–646.

Dudareva, N., Andersson, S., Orlova, I., Gatto, N., Reichelt, M., Rhodes, D., Boland, W., Gershenzon, J., 2005. The nonmevalonate pathway supports both monoterpene and sesquiterpene formation in snapdragon flowers. Proc. Natl. Acad. Sci. 102, 933–938.

Dudareva, N., Negre, F., Nagegowda, D.A., Orlova, I., 2006. Plant volatiles: recent advances and future perspectives. Crit. Rev. Plant Sci. 25, 417–440.

Dudareva, N., Pichersky, E., 2000. Biochemical and Molecular Genetic Aspects of Floral Scents. Plant Physiol. 122, 627–634.

Eastmond, P.J., Rawsthorne, S., 2000. Coordinate Changes in Carbon Partitioning and Plastidial Metabolism during the Development of Oilseed Rape Embryos. Plant Physiol. 122, 767–774.

Edwards, null, Nguyen, null, Do, null, Roberts, null, 1998. Contribution of malic enzyme, pyruvate kinase, phosphoenolpyruvate carboxylase, and the krebs cycle to respiration and biosynthesis and to intracellular pH

References

regulation during hypoxia in maize root tips observed by nuclear magnetic resonance imaging and gas chromatography-mass spectrometry. Plant Physiol. 116, 1073–1081.

Eisenreich, W., Sagner, S., Zenk, M.H., Bacher, A., 1997. Monoterpenoid essential oils are not of mevalonoid origin. Tetrahedron Lett. 38, 3889–3892.

Ettenhuber, C., Radykewicz, T., Kofer, W., Koop, H.-U., Bacher, A., Eisenreich, W., 2005a. Metabolic flux analysis in complex isotopolog space. Recycling of glucose in tobacco plants. Phytochemistry 66, 323–335.

Ettenhuber, C., Spielbauer, G., Margl, L., Hannah, L.C., Gierl, A., Bacher, A., Genschel, U., Eisenreich, W., 2005b. Changes in flux pattern of the central carbohydrate metabolism during kernel development in maize. Phytochemistry 66, 2632–2642.

Fagerquist, C.K., Neese, R.A., Hellerstein, M.K., 1999. Molecular ion fragmentation and its effects on mass isotopomer abundances of fatty acid methyl esters ionized by electron impact. J. Am. Soc. Mass Spectrom. 10, 430–439.

Fahn, A., 1979. Secretory tissues in plants. Academic Press, London ; New York.

Fatland, B.L., Ke, J., Anderson, M.D., Mentzen, W.I., Cui, L.W., Allred, C.C., Johnston, J.L., Nikolau, B.J., Wurtele, E.S., 2002. Molecular Characterization of a Heteromeric ATP-Citrate Lyase That Generates Cytosolic Acetyl-Coenzyme A in Arabidopsis. Plant Physiol. 130, 740–756.

Fellows, R.J., Geiger, D.R., 1974. Structural and Physiological Changes in Sugar Beet Leaves during Sink to Source Conversion. Plant Physiol. 54, 877–885.

Fernandez, C.A., Des Rosiers, C., Previs, S.F., David, F., Brunengraber, H., 1996. Correction of 13C mass isotopomer distributions for natural stable isotope abundance. J. Mass Spectrom. JMS 31, 255–262.

Fernie, A.R., Roscher, A., Ratcliffe, R.G., Kruger, N.J., 2001. Fructose 2,6-bisphosphate activates pyrophosphate: fructose-6-phosphate 1-phosphotransferase and increases triose phosphate to hexose phosphate cycling in heterotrophic cells. Planta 212, 250–263.

Fischer, E., Zamboni, N., Sauer, U., 2004. High-throughput metabolic flux analysis based on gas chromatography–mass spectrometry derived 13C constraints. Anal. Biochem. 325, 308–316.

Food and Drug Administration, 2018. Bioanalytical Method Validation: Guidance for Industry. US Dep. Health Hum. Serv. 44.

Friedman, M., Henika, P.R., Mandrell, R.E., 2002. Bactericidal activities of plant essential oils and some of their isolated constituents against Campylobacter jejuni, Escherichia coli, Listeria monocytogenes, and Salmonella enterica. J. Food Prot. 65, 1545–1560.

Gershenzon, J., Kreis, W., 1999. Biochemistry of terpenoids: monoterpenes, sesquiterpenes, diterpenes, sterols, cardiac glycosides and steroid saponins. Biochem. Plant Second. Metab. 2, 222–299.

Gershenzon, J., Maffei, M., Croteau, R., 1989. Biochemical and Histochemical Localization of Monoterpene Biosynthesis in the Glandular Trichomes of Spearmint (Mentha spicata). Plant Physiol. 89, 1351–1357.

Gershenzon, J., McCaskill, D., Rajaonarivony, J.I., Mihaliak, C., Karp, F., Croteau, R., 1992. Isolation of secretory cells from plant glandular trichomes and their use in biosynthetic studies of monoterpenes and other gland products. Anal. Biochem. 200, 130–138.

Gershenzon, J., McConkey, M.E., Croteau, R.B., 2000. Regulation of Monoterpene Accumulation in Leaves of Peppermint. Plant Physiol. 122, 205–214.

Glas, J.J., Schimmel, B.C.J., Alba, J.M., Escobar-Bravo, R., Schuurink, R.C., Kant, M.R., 2012. Plant Glandular Trichomes as Targets for Breeding or Engineering of Resistance to Herbivores. Int. J. Mol. Sci. 13, 17077–17103.

Goff, S.A., Klee, H.J., 2006. Plant volatile compounds: sensory cues for health and nutritional value? Science 311, 815–819.

Goffman, F.D., Alonso, A.P., Schwender, J., Shachar-Hill, Y., Ohlrogge, J.B., 2005. Light Enables a Very High Efficiency of Carbon Storage in Developing Embryos of Rapeseed. Plant Physiol. 138, 2269–2279.

Hamm, S., Bleton, J., Connan, J., Tchapla, A., 2005. A chemical investigation by headspace SPME and GC–MS of volatile and semi-volatile terpenes in various olibanum samples. Phytochemistry 66, 1499–1514.

Hammer, K.A., Carson, C.F., Riley, T.V., 2003. Antifungal activity of the components of Melaleuca alternifolia (tea tree) oil. J. Appl. Microbiol. 95, 853–860.

Hampel, D., Swatski, A., Mosandl, A., Wüst, M., 2007. Biosynthesis of monoterpenes and norisoprenoids in raspberry fruits (Rubus idaeus L.): the role of cytosolic mevalonate and plastidial methylerythritol phosphate pathway. J. Agric. Food Chem. 55, 9296–9304.

Harn, C., Khayat, E., Daie, J., 1993. Expression Dynamics of Genes Encoding Key Carbon Metabolism Enzymes during Sink to Source Transition of Developing Leaves. Plant Cell Physiol. 34, 1045–1053.

Hay, J.O., Shi, H., Heinzel, N., Hebbelmann, I., Rolletschek, H., Schwender, J., 2014. Integration of a constraint-based metabolic model of Brassica napus developing seeds with 13C-metabolic flux analysis. Front. Plant Sci. 5.

Heaps, N.A., Poulter, C.D., 2011. Type-2 isopentenyl diphosphate isomerase: evidence for a stepwise mechanism. J. Am. Chem. Soc. 133, 19017–19019.

Heinig, U., Gutensohn, M., Dudareva, N., Aharoni, A., 2013. The challenges of cellular compartmentalization in plant metabolic engineering. Curr. Opin. Biotechnol. 24, 239–246.

Heinrich, R., Schuster, S., 1996. The Regulation of Cellular Systems. Springer US.

Heinzle, E., Matsuda, F., Miyagawa, H., Wakasa, K., Nishioka, T., 2007. Estimation of metabolic fluxes, expression levels and metabolite dynamics of a secondary metabolic pathway in potato using label pulse-feeding experiments combined with kinetic network modelling and simulation. Plant J. Cell Mol. Biol. 50, 176–187.

Hemmerlin, A., Hoeffler, J.-F., Meyer, O., Tritsch, D., Kagan, I.A., Grosdemange-Billiard, C., Rohmer, M., Bach, T.J., 2003. Cross-talk between the cytosolic mevalonate and the plastidial methylerythritol phosphate pathways in tobacco bright yellow-2 cells. J. Biol. Chem. 278, 26666–26676.

Henry, L.K., Thomas, S.T., Widhalm, J.R., Lynch, J.H., Davis, T.C., Kessler, S.A., Bohlmann, J., Noel, J.P., Dudareva, N., 2018. Contribution of isopentenyl phosphate to plant terpenoid metabolism. Nat. Plants 4, 721.

Herold, A., 1980. Regulation of photosynthesis by sink activity–the missing link. New Phytol. 86, 131–144.

Hilker, M., Meiners, T., 2002. Induction of plant responses to oviposition and feeding by herbivorous arthropods: a comparison, in: Proceedings of the 11th International Symposium on Insect-Plant Relationships. Springer, pp. 181–192.

Hinkle, P.C., 2005. P/O ratios of mitochondrial oxidative phosphorylation. Biochim. Biophys. Acta 1706, 1–11.

Holm, Y., Hiltunen, R., Jokinen, K., Tormala, T., 1989. On the quality of the volatile oil in micropropagated peppermint. Flavour Fragr. J. 4, 81–84.

Iyer, V.V., Sriram, G., Fulton, D.B., Zhou, R., Westgate, M.E., Shanks, J.V., 2008. Metabolic flux maps comparing the effect of temperature on protein and oil biosynthesis in developing soybean cotyledons. Plant Cell Environ. 31, 506–517.

Jaiswal, D., Prasannan, C.B., Hendry, J.I., Wangikar, P.P., 2018. SWATH Tandem Mass Spectrometry Workflow for Quantification of Mass Isotopologue Distribution of Intracellular Metabolites and Fragments Labeled with Isotopic 13C Carbon. Anal. Chem. 90, 6486–6493.

Jeong, M.L., Jiang, H., Chen, H.-S., Tsai, C.-J., Harding, S.A., 2004. Metabolic profiling of the sink-to-source transition in developing leaves of quaking aspen. Plant Physiol. 136, 3364–3375.

Jin, J., Panicker, D., Wang, Q., Kim, M.J., Liu, J., Yin, J.-L., Wong, L., Jang, I.-C., Chua, N.-H., Sarojam, R., 2014. Next generation sequencing unravels the biosynthetic ability of spearmint (Mentha spicata) peltate glandular trichomes through comparative transcriptomics. BMC Plant Biol. 14, 292.

Johnson, C.B., Kazantzis, A., Skoula, M., Mitteregger, U., Novak, J., 2004. Seasonal, populational and ontogenic variation in the volatile oil content and composition of individuals of Origanum vulgare subsp. Hirtum, assessed by GC headspace analysis and by SPME sampling of individual oil glands. Phytochem. Anal. 15, 286–292.

Johnson, S.R., Lange, I., Srividya, N., Lange, B.M., 2017. Bioenergetics of Monoterpenoid Essential Oil Biosynthesis in Nonphotosynthetic Glandular Trichomes. Plant Physiol. 175, 681–695.

Juhnke, H., Krems, B., Kötter, P., Entian, K.-D., 1996. Mutants that show increased sensitivity to hydrogen peroxide reveal an important role for the pentose phosphate pathway in protection of yeast against oxidative stress. Mol. Gen. Genet. MGG 252, 456–464.

Junker, B.H., Klukas, C., Schreiber, F., 2006. VANTED: a system for advanced data analysis and visualization in the context of biological networks. BMC Bioinformatics 7, 109.

Junker, B.H., Lonien, J., Heady, L.E., Rogers, A., Schwender, J., 2007. Parallel determination of enzyme activities and in vivo fluxes in Brassica napus embryos grown on organic or inorganic nitrogen source. Phytochemistry, Dynamic Metabolic Networks 68, 2232–2242.

Kang, F., Rawsthorne, S., 1996. Metabolism of glucose-6-phosphate and utilization of multiple metabolites for fatty acid synthesis by plastids from developing oilseed rape embryos. Planta 199, 321–327.

Kasahara, H., Hanada, A., Kuzuyama, T., Takagi, M., Kamiya, Y., Yamaguchi, S., 2002. Contribution of the mevalonate and methylerythritol phosphate pathways to the biosynthesis of gibberellins in Arabidopsis. J. Biol. Chem. 277, 45188–45194.

Keeling, C.I., Bohlmann, J., 2006. Genes, enzymes and chemicals of terpenoid diversity in the constitutive and induced defence of conifers against insects and pathogens. New Phytol. 170, 657–675.

Kessler, A., Halitschke, R., Diezel, C., Baldwin, I.T., 2006. Priming of plant defense responses in nature by airborne signaling between Artemisia tridentata and Nicotiana attenuata. Oecologia 148, 280–292.

Kjonaas, R.B., Venkatachalam, K.V., Croteau, R., 1985. Metabolism of monoterpenes: oxidation of isopiperitenol to isopiperitenone, and subsequent isomerization to piperitenone by soluble enzyme preparations from peppermint (Mentha piperita) leaves. Arch. Biochem. Biophys. 238, 49–60.

102

References

Klapa, M.I., Aon, J.-C., Stephanopoulos, G., 2003a. Ion-trap mass spectrometry used in combination with gas chromatography for high-resolution metabolic flux determination. BioTechniques 34, 832–836, 838, 840 passim.

Klapa, M.I., Aon, J.-C., Stephanopoulos, G., 2003b. Systematic quantification of complex metabolic flux networks using stable isotopes and mass spectrometry. Eur. J. Biochem. 270, 3525–3542.

Koppisch, A.T., Fox, D.T., Blagg, B.S.J., Poulter, C.D., 2002. E. coli MEP Synthase: Steady-State Kinetic Analysis and Substrate Binding. Biochemistry 41, 236–243.

Kramer, D.M., Evans, J.R., 2011. The Importance of Energy Balance in Improving Photosynthetic Productivity. Plant Physiol. 155, 70–78.

Krüger, A., Grüning, N.-M., Wamelink, M.M.C., Kerick, M., Kirpy, A., Parkhomchuk, D., Bluemlein, K., Schweiger, M.-R., Soldatov, A., Lehrach, H., Jakobs, C., Ralser, M., 2011. The pentose phosphate pathway is a metabolic redox sensor and regulates transcription during the antioxidant response. Antioxid. Redox Signal. 15, 311–324.

Kruger, N.J., Huddleston, J.E., Le Lay, P., Brown, N.D., Ratcliffe, R.G., 2007. Network flux analysis: impact of 13C-substrates on metabolism in Arabidopsis thaliana cell suspension cultures. Phytochemistry 68, 2176–2188.

Kruger, N.J., Ratcliffe, R.G., 2015. Fluxes through plant metabolic networks: measurements, predictions, insights and challenges. Biochem. J. 465, 27–38.

Kulmala, M., 2003. How particles nucleate and grow. Science 302, 1000–1001.

KUNST, A., 1984. UV-methods with hexokinase and glucose-6-phosphate dehydrogenase. Methods Enzym. Anal. 163–172.

Lange, B.M., 2015. Biosynthesis and Biotechnology of High-Value p-Menthane Monoterpenes, Including Menthol, Carvone, and Limonene, in: Schrader, J., Bohlmann, J. (Eds.), Biotechnology of Isoprenoids, Advances in Biochemical Engineering/Biotechnology. Springer International Publishing, Cham, pp. 319–353.

Lange, B.M., Ghassemian, M., 2003. Genome organization in Arabidopsis thaliana: a survey for genes involved in isoprenoid and chlorophyll metabolism. Plant Mol. Biol. 51, 925–948.

Lange, B.M., Turner, G.W., 2013. Terpenoid biosynthesis in trichomes--current status and future opportunities. Plant Biotechnol. J. 11, 2–22.

Lange, B.M., Wildung, M.R., Stauber, E.J., Sanchez, C., Pouchnik, D., Croteau, R., 2000. Probing essential oil biosynthesis and secretion by functional evaluation of expressed sequence tags from mint glandular trichomes. Proc. Natl. Acad. Sci. 97, 2934–2939.

Langenheim, J.H., 1994. Higher plant terpenoids: a phytocentric overview of their ecological roles. J. Chem. Ecol. 20, 1223–1280.

Larson, P.R., Dickson, R.E., 1973. Distribution of imported 14C in developing leaves of eastern cottonwood according to phyllotaxy. Planta 111, 95–112.

Laule, O., Fürholz, A., Chang, H.-S., Zhu, T., Wang, X., Heifetz, P.B., Gruissem, W., Lange, M., 2003. Crosstalk between cytosolic and plastidial pathways of isoprenoid biosynthesis in Arabidopsis thaliana. Proc. Natl. Acad. Sci. 100, 6866–6871.

Lemoine, R., Camera, S.L., Atanassova, R., Dédaldéchamp, F., Allario, T., Pourtau, N., Bonnemain, J.-L., Laloi, M., Coutos-Thévenot, P., Maurousset, L., Faucher, M., Girousse, C., Lemonnier, P., Parrilla, J., Durand, M., 2013. Source-to-sink transport of sugar and regulation by environmental factors. Front. Plant Sci. 4.

Li, F.-S., Weng, J.-K., 2017. Demystifying traditional herbal medicine with modern approach. Nat. Plants 3, 17109.

Liao, Z.-H., Chen, M., Gong, Y.-F., 2006. Isoprenoid biosynthesis in plants: pathways, genes, regulation and metabolic engineering.

Libourel, I.G.L., Shachar-Hill, Y., 2008. Metabolic flux analysis in plants: from intelligent design to rational engineering. Annu. Rev. Plant Biol. 59, 625–650.

Lichtenthaler, H.K., 1987. [34] Chlorophylls and carotenoids: Pigments of photosynthetic biomembranes, in: Methods in Enzymology, Plant Cell Membranes. Academic Press, pp. 350–382.

Lichtenthaler, H.K., Schwender, J., Disch, A., Rohmer, M., 1997. Biosynthesis of isoprenoids in higher plant chloroplasts proceeds via a mevalonate-independent pathway. FEBS Lett. 400, 271–274.

Lonien, J., Schwender, J., 2009. Analysis of metabolic flux phenotypes for two Arabidopsis mutants with severe impairment in seed storage lipid synthesis. Plant Physiol. 151, 1617–1634.

Loreto, F., Mannozzi, M., Maris, C., Nascetti, P., Ferranti, F., Pasqualini, S., 2001. Ozone quenching properties of isoprene and its antioxidant role in leaves. Plant Physiol. 126, 993–1000.

Loreto, F., Pinelli, P., Manes, F., Kollist, H., 2004. Impact of ozone on monoterpene emissions and evidence for an isoprene-like antioxidant action of monoterpenes emitted by Quercus ilex leaves. Tree Physiol. 24, 361–367.

Loreto, F., Velikova, V., 2001. Isoprene produced by leaves protects the photosynthetic apparatus against ozone damage, quenches ozone products, and reduces lipid peroxidation of cellular membranes. Plant Physiol. 127, 1781–1787.

Lu, W., Clasquin, M.F., Melamud, E., Amador-Noguez, D., Caudy, A.A., Rabinowitz, J.D., 2010. Metabolomic Analysis via Reversed-Phase Ion-Pairing Liquid Chromatography Coupled to a Stand Alone Orbitrap Mass Spectrometer. Anal. Chem. 82, 3212–3221.

Lumbreras, V., Campos, N., Boronat, A., 1995. The use of an alternative promoter in the Arabidopsis thaliana HMG1 gene generates an mRNA that encodes a novel 3-hydroxy-3-methylglutaryl coenzyme A reductase isoform with an extended N-terminal region. Plant J. 8, 541–549.

Lupien, S., Karp, F., Wildung, M., Croteau, R., 1999. Regiospecific cytochrome P450 limonene hydroxylases from mint (Mentha) species: cDNA isolation, characterization, and functional expression of (-)-4S-limonene-3-hydroxylase and (-)-4S-limonene-6-hydroxylase. Arch. Biochem. Biophys. 368, 181–192.

Ma, F., Jazmin, L.J., Young, J.D., Allen, D.K., 2014. Isotopically nonstationary 13C flux analysis of changes in Arabidopsis thaliana leaf metabolism due to high light acclimation. Proc. Natl. Acad. Sci. 111, 16967–16972.

Mac Sweeney, A., Lange, R., Fernandes, R.P., Schulz, H., Dale, G.E., Douangamath, A., Proteau, P.J., Oefner, C., 2005. The crystal structure of E. coli 1-deoxy-D-xylulose-5-phosphate reductoisomerase in a ternary complex with the antimalarial compound fosmidomycin and NADPH reveals a tight-binding closed enzyme conformation. J. Mol. Biol. 345, 115–127.

Malinowski, R., 2013. Understanding of Leaf Development—the Science of Complexity. Plants 2, 396–415.

Malone, J.G., Mittova, V., Ratcliffe, R.G., Kruger, N.J., 2006. The response of carbohydrate metabolism in potato tubers to low temperature. Plant Cell Physiol. 47, 1309–1322.

Mandy, D.E., Goldford, J.E., Yang, H., Allen, D.K., Libourel, I.G.L., 2014. Metabolic flux analysis using 13C peptide label measurements. Plant J. 77, 476–486.

Martin, V.J., Pitera, D.J., Withers, S.T., Newman, J.D., Keasling, J.D., 2003. Engineering a mevalonate pathway in Escherichia coli for production of terpenoids. Nat. Biotechnol. 21, 796.

Masakapalli, S.K., Le Lay, P., Huddleston, J.E., Pollock, N.L., Kruger, N.J., Ratcliffe, R.G., 2010. Subcellular flux analysis of central metabolism in a heterotrophic Arabidopsis cell suspension using steady-state stable isotope labeling. Plant Physiol. 152, 602–619.

Masakapalli, S.K., Ritala, A., Dong, L., van der Krol, A.R., Oksman-Caldentey, K.-M., Ratcliffe, R.G., Sweetlove, L.J., 2014. Metabolic flux phenotype of tobacco hairy roots engineered for increased geraniol production. Phytochemistry 99, 73–85.

Matsuda, F., Morino, K., Ano, R., Kuzawa, M., Wakasa, K., Miyagawa, H., 2005. Metabolic flux analysis of the phenylpropanoid pathway in elicitor-treated potato tuber tissue. Plant Cell Physiol. 46, 454–466.

Matsuda, F., Morino, K., Miyashita, M., Miyagawa, H., 2003. Metabolic flux analysis of the phenylpropanoid pathway in wound-healing potato tuber tissue using stable isotope-labeled tracer and LC-MS spectroscopy. Plant Cell Physiol. 44, 510–517.

McCaskill, D., Croteau, R., 1995. Monoterpene and sesquiterpene biosynthesis in glandular trichomes of peppermint (Mentha x piperita) rely exclusively on plastid-derived isopentenyl diphosphate. Planta 197, 49–56.

McCaskill, D., Gershenzon, J., Croteau, R., 1992. Morphology and monoterpene biosynthetic capabilities of secretory cell clusters isolated from glandular trichomes of peppermint (Mentha piperita L.). Planta 187, 445–454.

McCloskey, D., Utrilla, J., Naviaux, R.K., Palsson, B.O., Feist, A.M., 2015. Fast Swinnex filtration (FSF): a fast and robust sampling and extraction method suitable for metabolomics analysis of cultures grown in complex media. Metabolomics 11, 198–209.

McCloskey, D., Young, J.D., Xu, S., Palsson, B.O., Feist, A.M., 2016. MID Max: LC–MS/MS Method for Measuring the Precursor and Product Mass Isotopomer Distributions of Metabolic Intermediates and Cofactors for Metabolic Flux Analysis Applications. Anal. Chem. 88, 1362–1370.

McConkey, M.E., Gershenzon, J., Croteau, R.B., 2000. Developmental regulation of monoterpene biosynthesis in the glandular trichomes of peppermint. Plant Physiol. 122, 215–224.

McGarvey, D.J., Croteau, R., 1995. Terpenoid metabolism. Plant Cell 7, 1015.

McNeil, S.D., Rhodes, D., Russell, B.L., Nuccio, M.L., Shachar-Hill, Y., Hanson, A.D., 2000. Metabolic modeling identifies key constraints on an engineered glycine betaine synthesis pathway in tobacco. Plant Physiol. 124, 153–162.

Mendoza-Poudereux, I., Kutzner, E., Huber, C., Segura, J., Eisenreich, W., Arrillaga, I., 2015. Metabolic cross-talk between pathways of terpenoid backbone biosynthesis in spike lavender. Plant Physiol. Biochem. PPB 95, 113–120.

Millard, P., Massou, S., Wittmann, C., Portais, J.-C., Létisse, F., 2014. Sampling of intracellular metabolites for stationary and non-stationary (13)C metabolic flux analysis in Escherichia coli. Anal. Biochem. 465, 38–49.

Morris, M.A., 2006. Mint: The Genus Mentha, ed BM Laurence. CRC Press, Boca Raton, FL.

104

References

Murashige, T., Skoog, F., 1962. A revised medium for rapid growth and bio assays with tobacco tissue cultures. Physiol. Plant. 15, 473–497.

Muyima, N.Y.O., Zulu, G., Bhengu, T., Popplewell, D., 2002. The potential application of some novel essential oils as natural cosmetic preservatives in an aqueous cream formulation. Flavour Fragr. J. 17, 258–266.

Nagegowda, D.A., 2010. Plant volatile terpenoid metabolism: biosynthetic genes, transcriptional regulation and subcellular compartmentation. FEBS Lett. 584, 2965–2973.

Nagegowda, D.A., Rhodes, D., Dudareva, N., 2010. The role of the methyl-erythritol-phosphate (MEP) pathway in rhythmic emission of volatiles, in: The Chloroplast. Springer, pp. 139–154.

Nakayama, N., Kuhlemeier, C., 2009. Leaf development: untangling the spirals. Curr. Biol. CB 19, R71-74.

Neuhaus, H.E., Emes, M.J., 2000. Nonphotosynthetic Metabolism in Plastids. Annu. Rev. Plant Physiol. Plant Mol. Biol. 51, 111–140.

Newman, J.D., Chappell, J., 1999. Isoprenoid Biosynthesis in Plants: Carbon Partitioning Within the Cytoplasmic Pathway. Crit. Rev. Biochem. Mol. Biol. 34, 95–106.

Olennikov, D.N., Tankhaeva, L.M., 2007. Lamiaceae carbohydrates. II. Water-soluble polysaccharides from Mentha x piperita. Chem. Nat. Compd. 43, 648–651.

Opitz, S., Nes, W.D., Gershenzon, J., 2014. Both methylerythritol phosphate and mevalonate pathways contribute to biosynthesis of each of the major isoprenoid classes in young cotton seedlings. Phytochemistry 98, 110–119.

Page, J.E., Hause, G., Raschke, M., Gao, W., Schmidt, J., Zenk, M.H., Kutchan, T.M., 2004. Functional analysis of the final steps of the 1-deoxy-D-xylulose 5-phosphate (DXP) pathway to isoprenoids in plants using virus-induced gene silencing. Plant Physiol. 134, 1401–1413.

Palancar, G.G., Toselli, B.M., 2004. Effects of meteorology and tropospheric aerosols on UV-B radiation: a 4-year study. Atmos. Environ. 38, 2749–2757.

Pan, S.-Y., Zhou, S.-F., Gao, S.-H., Yu, Z.-L., Zhang, S.-F., Tang, M.-K., Sun, J.-N., Ma, D.-L., Han, Y.-F., Fong, W.-F., Ko, K.-M., 2013. New Perspectives on How to Discover Drugs from Herbal Medicines: CAM's Outstanding Contribution to Modern Therapeutics. Evid.-Based Complement. Altern. Med. ECAM 2013, 627375.

Patterson, B.W., Carraro, F., Wolfe, R.R., 1993. Measurement of 15N enrichment in multiple amino acids and urea in a single analysis by gas chromatography/mass spectrometry. Biol. Mass Spectrom. 22, 518–523.

Paul, M.J., Driscoll, S.P., 1997. Sugar repression of photosynthesis: the role of carbohydrates in signalling nitrogen deficiency through source:sink imbalance. Plant Cell Environ. 20, 110–116.

Paul, M.J., Foyer, C.H., 2001. Sink regulation of photosynthesis. J. Exp. Bot. 52, 1383–1400.

Peñuelas, J., Llusià, J., 2003. BVOCs: plant defense against climate warming? Trends Plant Sci. 8, 105–109.

Piel, J., Donath, J., Bandemer, K., Boland, W., 1998. Mevalonate-Independent Biosynthesis of Terpenoid Volatiles in Plants: Induced and Constitutive Emission of Volatiles. Angew. Chem. Int. Ed Engl. 37, 2478–2481.

Placzek, S., Schomburg, I., Chang, A., Jeske, L., Ulbrich, M., Tillack, J., Schomburg, D., 2017. BRENDA in 2017: new perspectives and new tools in BRENDA. Nucleic Acids Res. 45, D380–D388.

Pollier, J., Moses, T., Goossens, A., 2011. Combinatorial biosynthesis in plants: a (p) review on its potential and future exploitation. Nat. Prod. Rep. 28, 1897–1916.

Proteau, P.J., 2004. 1-Deoxy-D-xylulose 5-phosphate reductoisomerase: an overview. Bioorganic Chem. 32, 483–493.

Quek, L.-E., Wittmann, C., Nielsen, L.K., Krömer, J.O., 2009. OpenFLUX: efficient modelling software for 13C-based metabolic flux analysis. Microb. Cell Factories 8, 25.

Ratcliffe, R.G., Shachar-Hill, Y., 2006. Measuring multiple fluxes through plant metabolic networks. Plant J. Cell Mol. Biol. 45, 490–511.

Ratcliffe, R.G., Shachar-Hill, Y., 2005. Revealing metabolic phenotypes in plants: inputs from NMR analysis. Biol. Rev. Camb. Philos. Soc. 80, 27–43.

Ray, D.K., Mueller, N.D., West, P.C., Foley, J.A., 2013. Yield Trends Are Insufficient to Double Global Crop Production by 2050. PLOS ONE 8, e66428.

Richard, S.B., Lillo, A.M., Tetzlaff, C.N., Bowman, M.E., Noel, J.P., Cane, D.E., 2004. Kinetic analysis of Escherichia coli 2-C-methyl-D-erythritol-4-phosphate cytidyltransferase, wild type and mutants, reveals roles of active site amino acids. Biochemistry 43, 12189–12197.

Ringer, K.L., Davis, E.M., Croteau, R., 2005. Monoterpene metabolism. Cloning, expression, and characterization of (-)-isopiperitenol/(-)-carveol dehydrogenase of peppermint and spearmint. Plant Physiol. 137, 863–872.

Ringer, K.L., McConkey, M.E., Davis, E.M., Rushing, G.W., Croteau, R., 2003. Monoterpene double-bond reductases of the (-)-menthol biosynthetic pathway: isolation and characterization of cDNAs encoding (-)-isopiperitenone reductase and (+)-pulegone reductase of peppermint. Arch. Biochem. Biophys. 418, 80–92.

Rippert, P., Puyaubert, J., Grisollet, D., Derrier, L., Matringe, M., 2009. Tyrosine and Phenylalanine Are Synthesized within the Plastids in Arabidopsis. Plant Physiol. 149, 1251–1260.

Rodríguez-Concepcíon, M., 2005. Early Steps in Isoprenoid Biosynthesis: Multilevel Regulation of the Supply of Common Precursors in Plant Cells. Phytochem. Rev. 5, 1–15.

Rodríguez-Concepción, M., Boronat, A., 2015. Breaking new ground in the regulation of the early steps of plant isoprenoid biosynthesis. Curr. Opin. Plant Biol. 25, 17–22.

Rohdich, F., Zepeck, F., Adam, P., Hecht, S., Kaiser, J., Laupitz, R., Gräwert, T., Amslinger, S., Eisenreich, W., Bacher, A., 2003. The deoxyxylulose phosphate pathway of isoprenoid biosynthesis: studies on the mechanisms of the reactions catalyzed by IspG and IspH protein. Proc. Natl. Acad. Sci. 100, 1586–1591.

Rohloff, J., 1999. Monoterpene Composition of Essential Oil from Peppermint (Mentha × piperita L.) with Regard to Leaf Position Using Solid-Phase Microextraction and Gas Chromatography/Mass Spectrometry Analysis. J. Agric. Food Chem. 47, 3782–3786.

Rohmer, M., 2003. Mevalonate-independent methylerythritol phosphate pathway for isoprenoid biosynthesis. Elucidation and distribution. Pure Appl. Chem. 75, 375–388.

Rohmer, M., Knani, M., Simonin, P., Sutter, B., Sahm, H., 1993. Isoprenoid biosynthesis in bacteria: a novel pathway for the early steps leading to isopentenyl diphosphate. Biochem. J. 295, 517–524.

Rohn, H., Hartmann, A., Junker, A., Junker, B.H., Schreiber, F., 2012. FluxMap: a VANTED add-on for the visual exploration of flux distributions in biological networks. BMC Syst. Biol. 6, 33.

Rontein, D., Dieuaide-Noubhani, M., Dufourc, E.J., Raymond, P., Rolin, D., 2002. The metabolic architecture of plant cells. Stability of central metabolism and flexibility of anabolic pathways during the growth cycle of tomato cells. J. Biol. Chem. 277, 43948–43960.

Roscher, A., Kruger, N.J., Ratcliffe, R.G., 2000. Strategies for metabolic flux analysis in plants using isotope labelling. J. Biotechnol. 77, 81–102.

Rühl, M., Rupp, B., Nöh, K., Wiechert, W., Sauer, U., Zamboni, N., 2012. Collisional fragmentation of central carbon metabolites in LC-MS/MS increases precision of ^{13}C metabolic flux analysis. Biotechnol. Bioeng. 109, 763–771.

Ruther, J., Kleier, S., 2005. Plant-plant signaling: ethylene synergizes volatile emission in Zea mays induced by exposure to (Z)-3-hexen-1-ol. J. Chem. Ecol. 31, 2217–2222.

Schellenberger, J., Zielinski, D.C., Choi, W., Madireddi, S., Portnoy, V., Scott, D.A., Reed, J.L., Osterman, A.L., Palsson, B.∅, 2012. Predicting outcomes of steady-state 13C isotope tracing experiments using Monte Carlo sampling. BMC Syst. Biol. 6, 9.

Schilmiller, A.L., Last, R.L., Pichersky, E., 2008. Harnessing plant trichome biochemistry for the production of useful compounds. Plant J. 54, 702–711.

Schmidt, C.O., Bouwmeester, H.J., Franke, S., König, W.A., 1999. Mechanisms of the biosynthesis of sesquiterpene enantiomers (+)-and (-)-germacrene D in Solidago canadensis. Chirality Pharmacol. Biol. Chem. Consequences Mol. Asymmetry 11, 353–362.

Schmidt, K., Carlsen, M., Nielsen, J., Villadsen, J., 1997. Modeling isotopomer distributions in biochemical networks using isotopomer mapping matrices. Biotechnol. Bioeng. 55, 831–840.

Schuhr, C.A., Radykewicz, T., Sagner, S., Latzel, C., Zenk, M.H., Arigoni, D., Bacher, A., Rohdich, F., Eisenreich, W., 2003. Quantitative assessment of crosstalk between the two isoprenoid biosynthesis pathways in plants by NMR spectroscopy. Phytochem. Rev. 2, 3–16.

Schwender, J., 2008. Metabolic flux analysis as a tool in metabolic engineering of plants. Curr. Opin. Biotechnol. 19, 131–137.

Schwender, J., Goffman, F., Ohlrogge, J.B., Shachar-Hill, Y., 2004. Rubisco without the Calvin cycle improves the carbon efficiency of developing green seeds. Nature 432, 779.

Schwender, J., Ohlrogge, J.B., Shachar-Hill, Y., 2003. A flux model of glycolysis and the oxidative pentosephosphate pathway in developing Brassica napus embryos. J. Biol. Chem. 278, 29442–29453.

Schwender, J., Shachar-Hill, Y., Ohlrogge, J.B., 2006. Mitochondrial metabolism in developing embryos of Brassica napus. J. Biol. Chem. 281, 34040–34047.

Selivanov, V.A., Marin, S., Lee, P.W.N., Cascante, M., 2006. Software for dynamic analysis of tracer-based metabolomic data: estimation of metabolic fluxes and their statistical analysis. Bioinforma. Oxf. Engl. 22, 2806–2812.

Shachar-Hill, Y., 2013. Metabolic network flux analysis for engineering plant systems. Curr. Opin. Biotechnol. 24, 247–255.

Shastri, A.A., Morgan, J.A., 2007. A transient isotopic labeling methodology for 13C metabolic flux analysis of photoautotrophic microorganisms. Phytochemistry 68, 2302–2312.

Shulaev, V., Silverman, P., Raskin, I., 1997. Airborne signalling by methyl salicylate in plant pathogen resistance. Nature 385, 718.

Skoog, D.A., Holler, F.J., Crouch, S.R., 2007. Instrumental analysis. Brooks/Cole, Cengage Learning Belmont.

References

Skorupinska-Tudek, K., Poznanski, J., Wojcik, J., Bienkowski, T., Szostkiewicz, I., Zelman-Femiak, M., Bajda, A., Chojnacki, T., Olszowska, O., Grunler, J., Meyer, O., Rohmer, M., Danikiewicz, W., Swiezewska, E., 2008. Contribution of the Mevalonate and Methylerythritol Phosphate Pathways to the Biosynthesis of Dolichols in Plants. J. Biol. Chem. 283, 21024–21035.

Sokol, S., Millard, P., Portais, J.-C., 2012. influx_s: increasing numerical stability and precision for metabolic flux analysis in isotope labelling experiments. Bioinforma. Oxf. Engl. 28, 687–693.

Spielbauer, G., Margl, L., Hannah, L.C., Römisch, W., Ettenhuber, C., Bacher, A., Gierl, A., Eisenreich, W., Genschel, U., 2006. Robustness of central carbohydrate metabolism in developing maize kernels. Phytochemistry 67, 1460–1475.

Sriram, G., Fulton, D.B., Iyer, V.V., Peterson, J.M., Zhou, R., Westgate, M.E., Spalding, M.H., Shanks, J.V., 2004. Quantification of compartmented metabolic fluxes in developing soybean embryos by employing biosynthetically directed fractional (13)C labeling, two-dimensional [(13)C, (1)H] nuclear magnetic resonance, and comprehensive isotopomer balancing. Plant Physiol. 136, 3043–3057.

Sriram, G., Fulton, D.B., Shanks, J.V., 2007. Flux quantification in central carbon metabolism of Catharanthus roseus hairy roots by 13C labeling and comprehensive bondomer balancing. Phytochemistry 68, 2243–2257.

Srour, O., Young, J.D., Eldar, Y.C., 2011. Fluxomers: a new approach for 13C metabolic flux analysis. BMC Syst. Biol. 5, 129.

Stincone, A., Prigione, A., Cramer, T., Wamelink, M.M.C., Campbell, K., Cheung, E., Olin-Sandoval, V., Grüning, N.-M., Krüger, A., Alam, M.T., Keller, M.A., Breitenbach, M., Brindle, K.M., Rabinowitz, J.D., Ralser, M., 2015. The return of metabolism: biochemistry and physiology of the pentose phosphate pathway. Biol. Rev. Camb. Philos. Soc. 90, 927–963.

Stitt, M., Wirtz, W., Heldt, H.W., 1983. Regulation of Sucrose Synthesis by Cytoplasmic Fructosebisphosphatase and Sucrose Phosphate Synthase during Photosynthesis in Varying Light and Carbon Dioxide. Plant Physiol. 72, 767–774.

Sweetlove, L.J., Fernie, A.R., 2013. The spatial organization of metabolism within the plant cell. Annu. Rev. Plant Biol. 64, 723–746.

Takabayashi, J., Dicke, M., 1996. Plant—carnivore mutualism through herbivore-induced carnivore attractants. Trends Plant Sci. 1, 109–113.

Tilman, D., Balzer, C., Hill, J., Befort, B.L., 2011. Global food demand and the sustainable intensification of agriculture. Proc. Natl. Acad. Sci. 108, 20260–20264.

Tissier, A., 2018. Plant secretory structures: more than just reaction bags. Curr. Opin. Biotechnol., Food biotechnology • Plant biotechnology 49, 73–79.

Tissier, A., 2012. Glandular trichomes: what comes after expressed sequence tags? Plant J. Cell Mol. Biol. 70, 51–68.

Tritsch, D., Hemmerlin, A., Bach, T.J., Rohmer, M., 2010. Plant isoprenoid biosynthesis via the MEP pathway: in vivo IPP/DMAPP ratio produced by (E)-4-hydroxy-3-methylbut-2-enyl diphosphate reductase in tobacco BY-2 cell cultures. Febs Lett. 584, 129–134.

Turgeon, R., 1989. The Sink-Source Transition in Leaves. Annu. Rev. Plant Physiol. Plant Mol. Biol. 40, 119–138.

Turgeon, R., Webb, J.A., 1975. Physiological and Structural Ontogeny of the Source Leaf, in: Aronoff, S., Dainty, J., Gorham, P.R., Srivastava, L.M., Swanson, C.A. (Eds.), Phloem Transport, NATO Advanced Study Institutes Series. Springer US, Boston, MA, pp. 297–326.

Turner, null, Gershenzon, null, Nielson, null, Froehlich, null, Croteau, null, 1999. Limonene synthase, the enzyme responsible for monoterpene biosynthesis in peppermint, is localized to leucoplasts of oil gland secretory cells. Plant Physiol. 120, 879–886.

Turner, G.W., Croteau, R., 2004. Organization of monoterpene biosynthesis in Mentha. Immunocytochemical localizations of geranyl diphosphate synthase, limonene-6-hydroxylase, isopiperitenol dehydrogenase, and pulegone reductase. Plant Physiol. 136, 4215–4227.

Turner, G.W., Gershenzon, J., Croteau, R.B., 2000. Development of Peltate Glandular Trichomes of Peppermint. Plant Physiol. 124, 665–680.

van Winden, W.A., Wittmann, C., Heinzle, E., Heijnen, J.J., 2002. Correcting mass isotopomer distributions for naturally occurring isotopes. Biotechnol. Bioeng. 80, 477–479.

Wang, P., Guo, L., Jaini, R., Klempien, A., McCoy, R.M., Morgan, J.A., Dudareva, N., Chapple, C., 2018. A 13C isotope labeling method for the measurement of lignin metabolic flux in Arabidopsis stems. Plant Methods 14, 51.

Weitzel, M., Wiechert, W., Nöh, K., 2007. The topology of metabolic isotope labeling networks. BMC Bioinformatics 8, 315.

Wiberley, A.E., Donohue, A.R., Westphal, M.M., Sharkey, T.D., 2009. Regulation of isoprene emission from poplar leaves throughout a day. Plant Cell Environ. 32, 939–947.

Wiechert, W., 2001. 13C metabolic flux analysis. Metab. Eng. 3, 195–206.

Wiechert, W., Möllney, M., Isermann, N., Wurzel, M., de Graaf, A.A., 1999. Bidirectional reaction steps in metabolic networks: III. Explicit solution and analysis of isotopomer labeling systems. Biotechnol. Bioeng. 66, 69–85.

Wiechert, W., Nöh, K., 2005. From stationary to instationary metabolic flux analysis. Adv. Biochem. Eng. Biotechnol. 92, 145–172.

Wiechert, W., Wurzel, M., 2001. Metabolic isotopomer labeling systems. Part I: global dynamic behavior. Math. Biosci. 169, 173–205.

Williams, T.C.R., Miguet, L., Masakapalli, S.K., Kruger, N.J., Sweetlove, L.J., Ratcliffe, R.G., 2008. Metabolic network fluxes in heterotrophic Arabidopsis cells: stability of the flux distribution under different oxygenation conditions. Plant Physiol. 148, 704–718.

Williams, T.C.R., Poolman, M.G., Howden, A.J.M., Schwarzlander, M., Fell, D.A., Ratcliffe, R.G., Sweetlove, L.J., 2010. A genome-scale metabolic model accurately predicts fluxes in central carbon metabolism under stress conditions. Plant Physiol. 154, 311–323.

Wright, L., Rohwer, J.M., Ghirardo, A., Hammerbacher, A., Ortíz, M., Raguschke, B., Schnitzler, J.-P., Gershenzon, J., Phillips, M.A., 2014. 1-Deoxyxylulose 5-phosphate synthase controls flux through the 2-C-methylerythritol 4-phosphate pathway in Arabidopsis thaliana. Plant Physiol. pp–114.

Yeung, D.Y.-H., Lee, T., Grant, G., Ma, M., Kwong, E., 2003. A SPME-GC procedure for monitoring peppermint flavor in tablets. J. Pharm. Biomed. Anal. 30, 1469–1477.

Young, J.D., 2014. INCA: a computational platform for isotopically non-stationary metabolic flux analysis. Bioinforma. Oxf. Engl. 30, 1333–1335.

Young, J.D., Walther, J.L., Antoniewicz, M.R., Yoo, H., Stephanopoulos, G., 2008. An elementary metabolite unit (EMU) based method of isotopically nonstationary flux analysis. Biotechnol. Bioeng. 99, 686–699.

Zager, J.J., Lange, B.M., 2018. Assessing Flux Distribution Associated with Metabolic Specialization of Glandular Trichomes. Trends Plant Sci. 23, 638–647.

Zamboni, N., Fendt, S.-M., Rühl, M., Sauer, U., 2009. (13)C-based metabolic flux analysis. Nat. Protoc. 4, 878–892.

Zamboni, N., Fischer, E., Sauer, U., 2005. FiatFlux--a software for metabolic flux analysis from 13C-glucose experiments. BMC Bioinformatics 6, 209.

Zulak, K.G., Bohlmann, J., 2010. Terpenoid biosynthesis and specialized vascular cells of conifer defense. J. Integr. Plant Biol. 52, 86–97.

Zupke, C., Stephanopoulos, G., 1994. Modeling of Isotope Distributions and Intracellular Fluxes in Metabolic Networks Using Atom Mapping Matrixes. Biotechnol. Prog. 10, 489–498.

Appendix

a

b

c

d

e

f

g

h

i

j

k

l
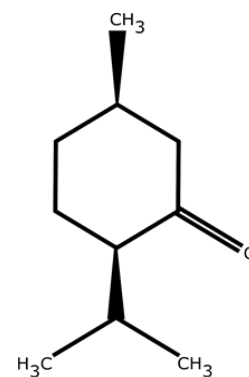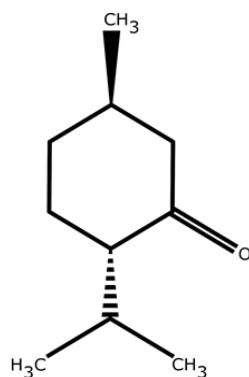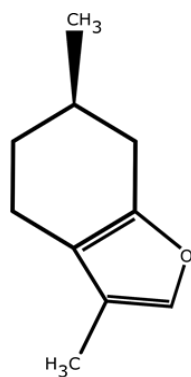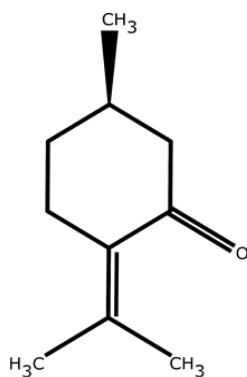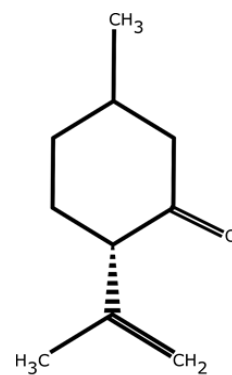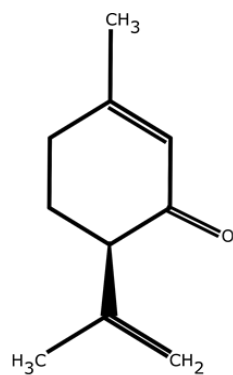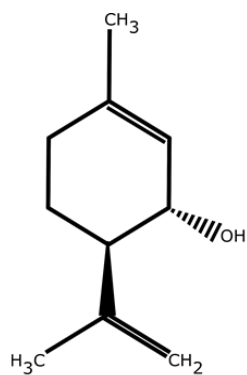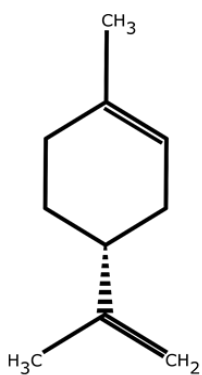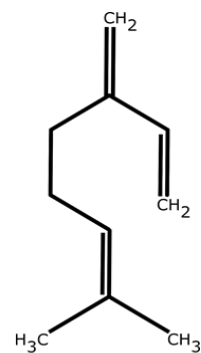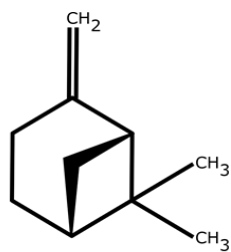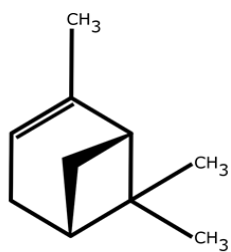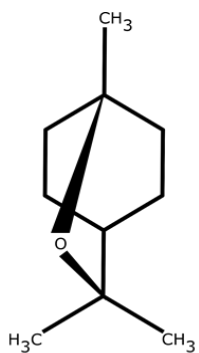
(Continue in the next page…)
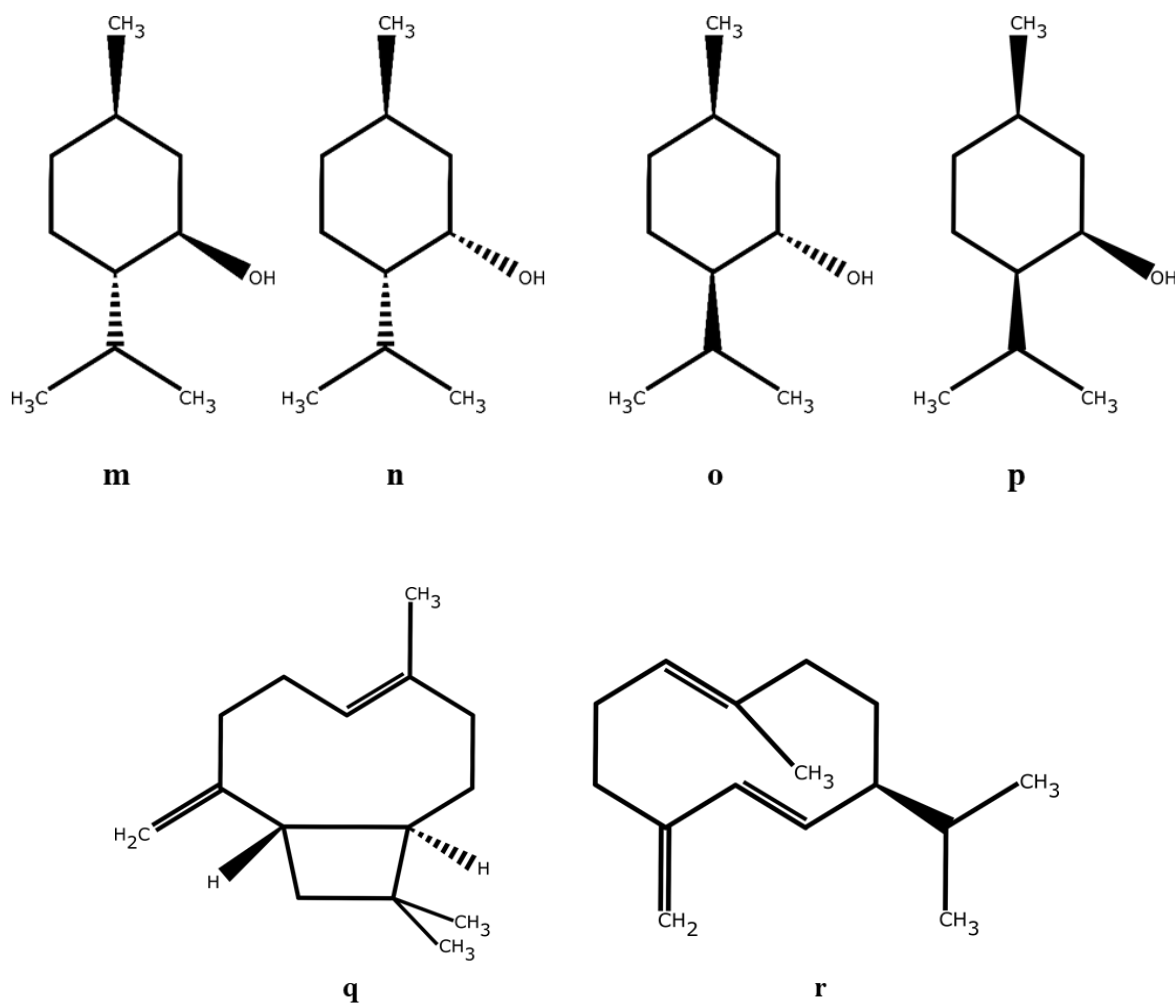
Figure S1. Different kinds of monoterpenes and sesquiterpenes produced in leaf of peppermint.

(a) Cineole, (b) α-pinene, (c) β-pinene, (d) myrcene, (e) limonene, (f) trans isopipertenol, (g) trans isopipertenone, (h) isopulegone, (i) pulegone, (j) menthofuran, (k) menthone, (l) isomenthone, (m) menthol, (n) neomenthol, (o) isomenthol, (p) neoisomenthol, (q) beta caryophyllene and (r) germacrene D.
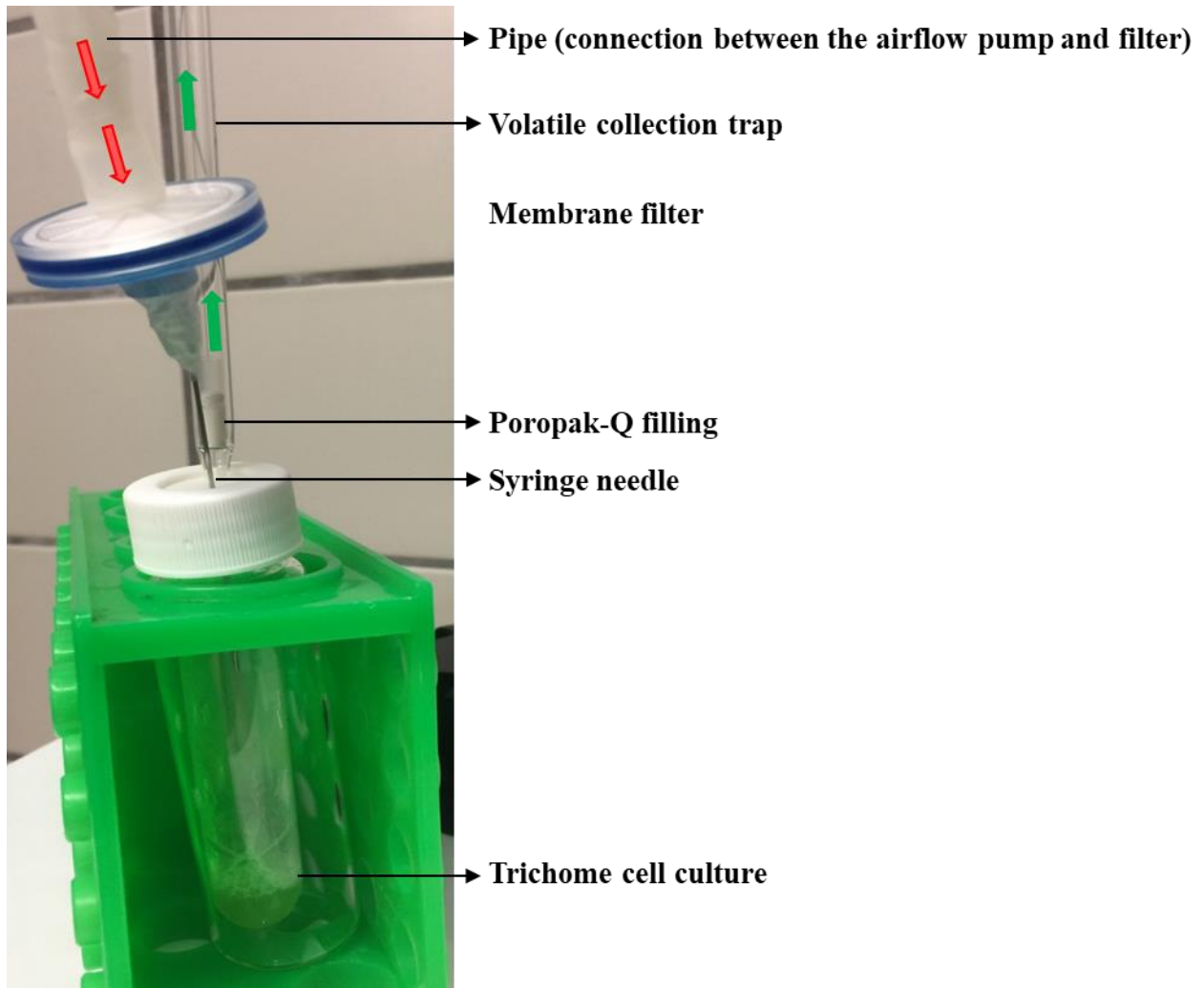
Figure S2. Photograph of trichome cell culture.

The red arrow shows the direction of incoming air, whereas green arrow presents the direction of outgoing air. The air came from the compressor CMC SC-400 (CMC Instruments GmbH, Eschborn; DE).
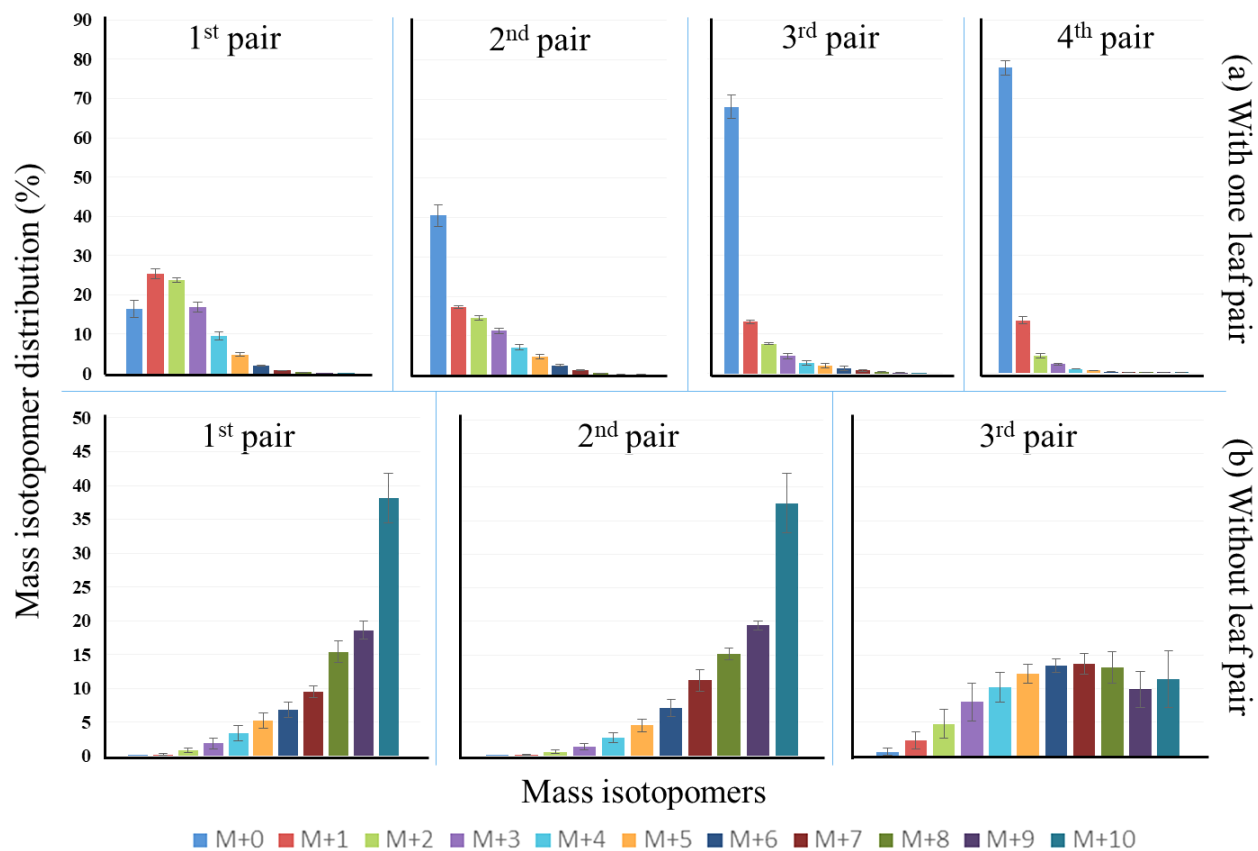
Figure S3. MID of isopulegone in each leaf pair at 30 μmol m⁻² s⁻¹ light intensity.

(a) Shoot-tip culture initiated with one developing leaf pair and at after 15 days of culture total four leaf pairs (older than 6 days) were observed. (b) Shoot-tip culture started without leaves and at 15 DALV total three leaf pairs (older than 6 days) were observed (mean ± standard error, n=5).
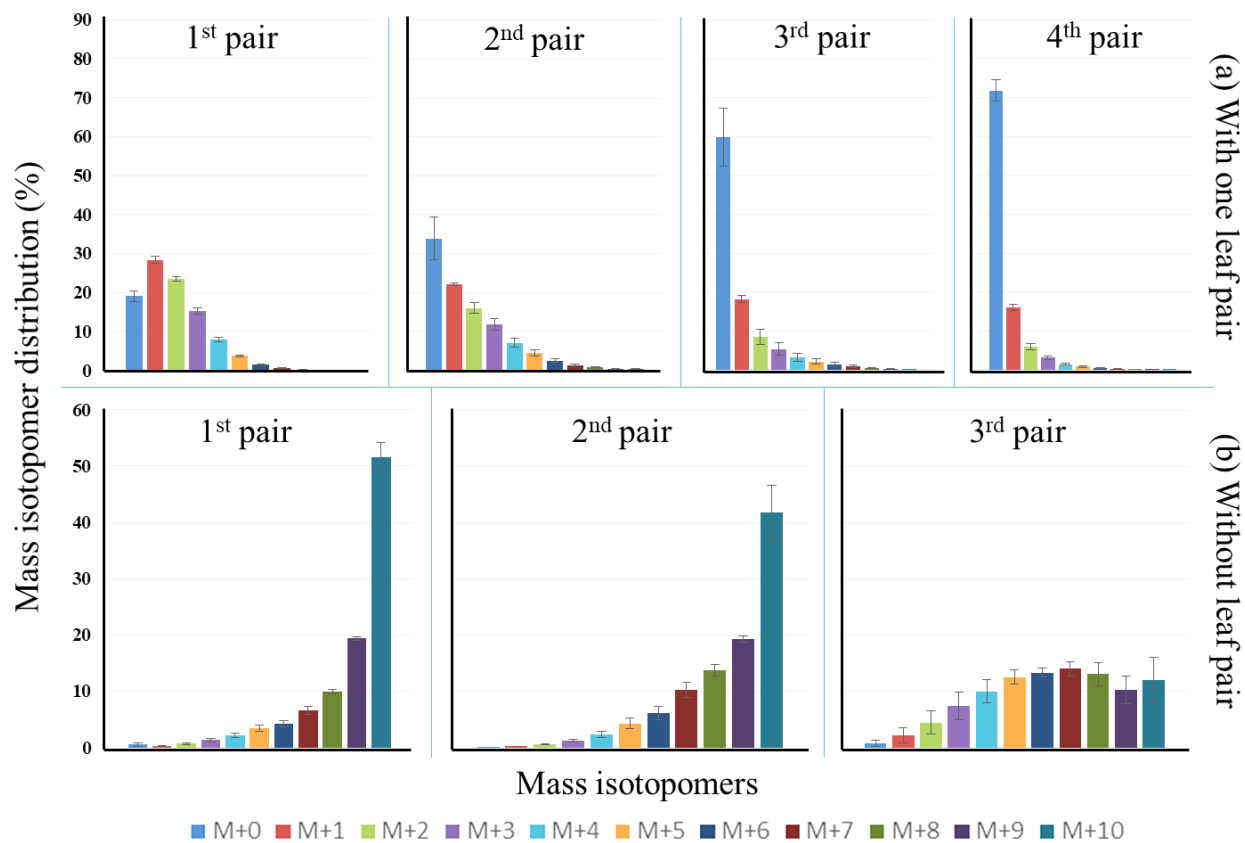
Figure S4. MID of menthofuran in each leaf pair at 30 μmol m⁻² s⁻¹ light intensity.

(a) Shoot-tip culture initiated with one developing leaf pair and at after 15 days of culture total four leaf pairs (older than 6 days) were observed. (b) Shoot-tip culture started without leaves and at 15 DALV total three leaf pairs (older than 6 days) were observed (mean ± standard error, n=5).
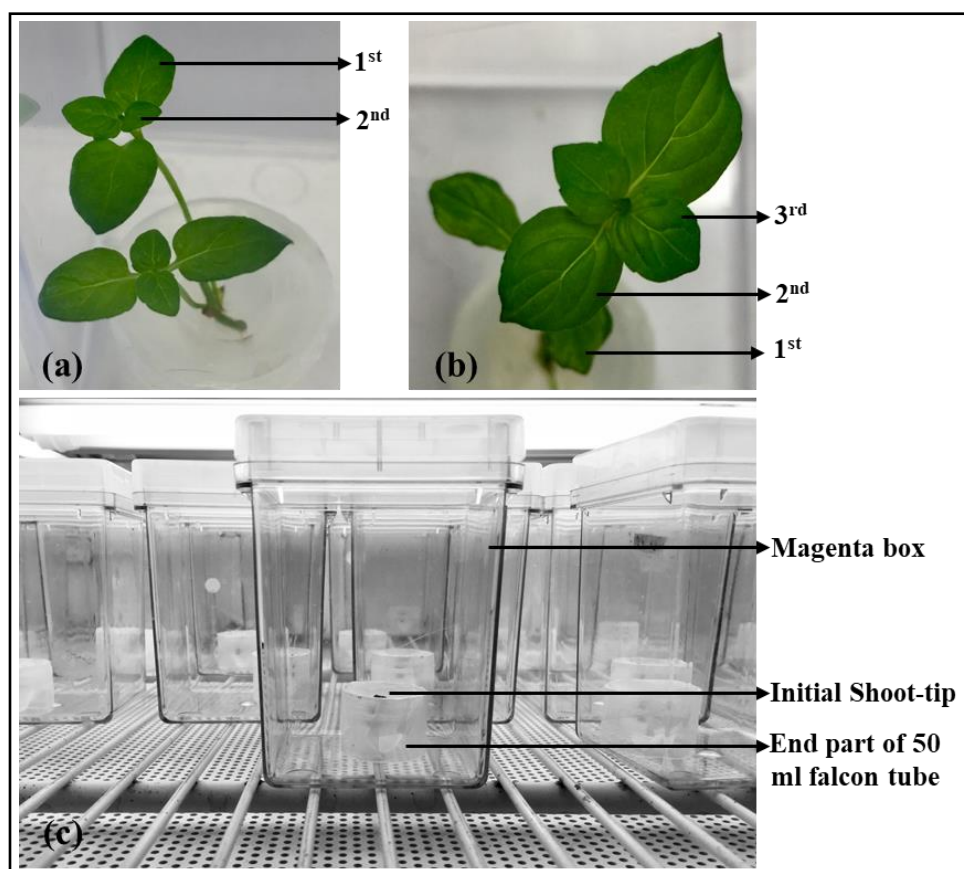
Figure S5. Photographs of shoot-tip culture.

(a) Shoot culture at 15 DALV under 5 μmol m^{-2} s^{-1} light intensity (b) shoot culture at 20 DALV under 5 μmol m^{-2} s^{-1} light intensity (c) Overview of shoot-tip culture system inside the growth chamber. Two and three leaf pairs (older than 6 days) were observed at 15 and 20 DALV, respectively.

Appendix
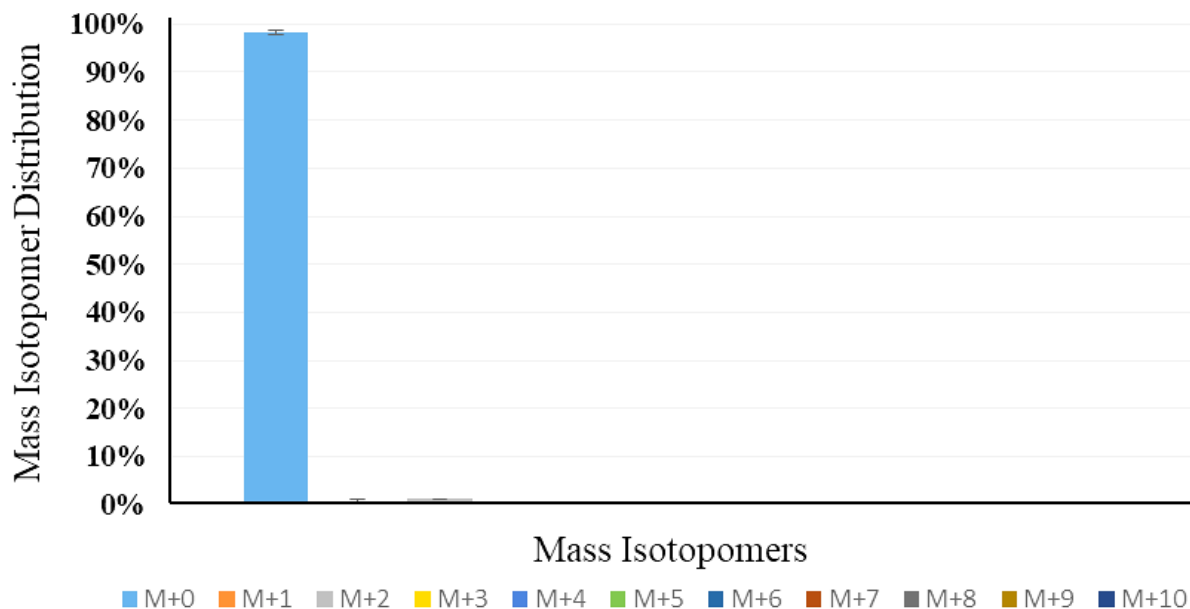
Figure S6. MID of pulegone from control culture.

This culture was nurtured with unlabeled glucose as the sole carbon source. Calculated label dilution in the control was 99.74% (after natural abundance correction) where negligible 0.26% ^{13}C was considered as experimental or measurement error (mean ± standard error, n=5). This result remained virtually similar for all other monoterpenes in control treatments at different age of the leaves under different light intensities.
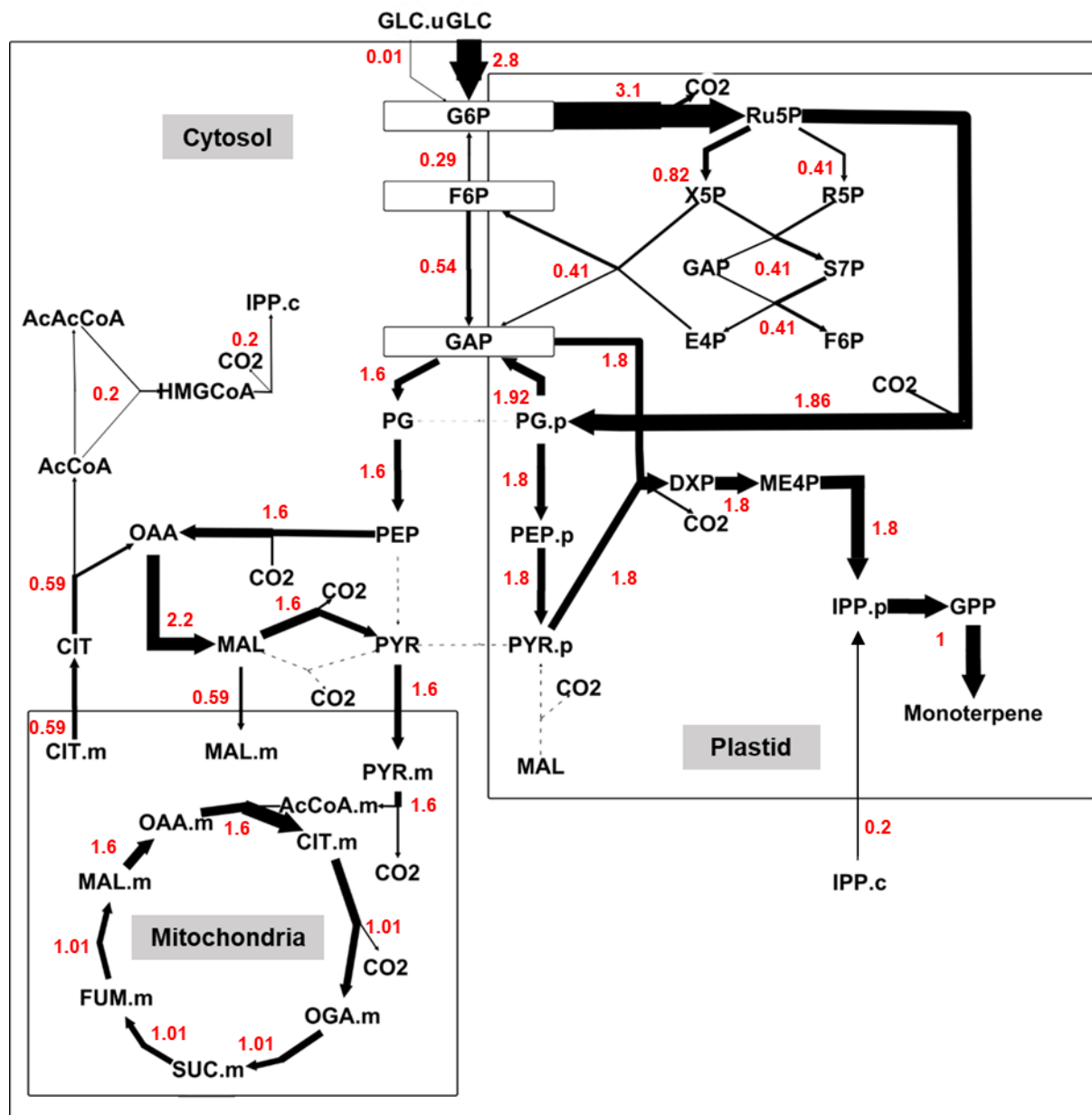
Figure S7. Advanced metabolic flux map of secretory cells in non-photosynthetic peppermint GTs during the secretory phase after skipping the redox import.

Parallel MFA (close_redox version) was assessed from ^{13}C labeling patterns of monoterpenes (pulegone, menthofuran and isopulegone) from $1\text{-}^{13}C_1$, $6\text{-}^{13}C_1$ and $1,6\text{-}^{13}C_2$ glucose incorporation (SEM, n = 3). Mol amount of fluxes (in red color) are presented after normalization to a net monoterpene production rate of 1 mol. Arrows indicate the direction of net flux, arrow widths are proportional to the magnitude of relative fluxes, and dashed arrows indicate zero flux value.
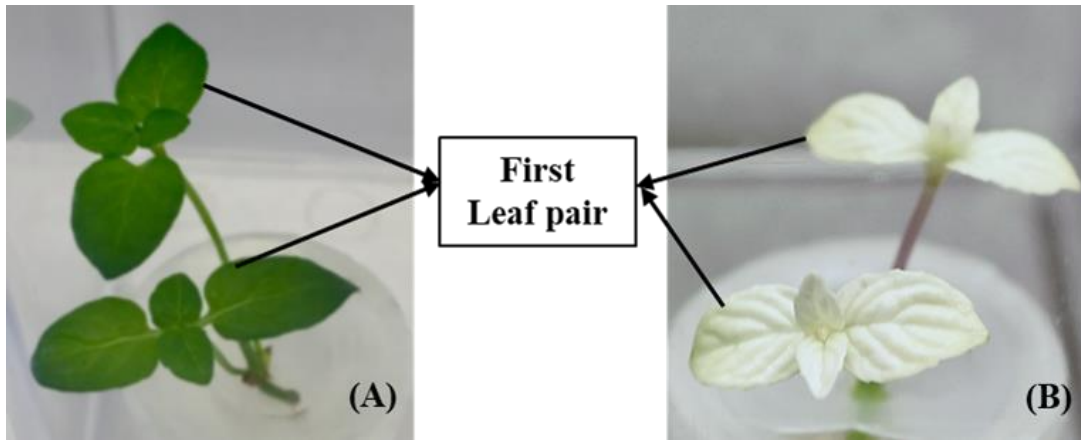
Figure S8. Phenotypical comparison between control and fosmidomycin treated shoot-tip.

(A) Control culture (untreated with FSM) and (B) Inhibitor treated culture (treated with 40 µM FSM). Due to inhibition of the DXP pathway by FSM, the leaf could not produce enough photosynthetic pigments, resulting in white color leaves. The picture was taken at 15 days age of first leaf pair.
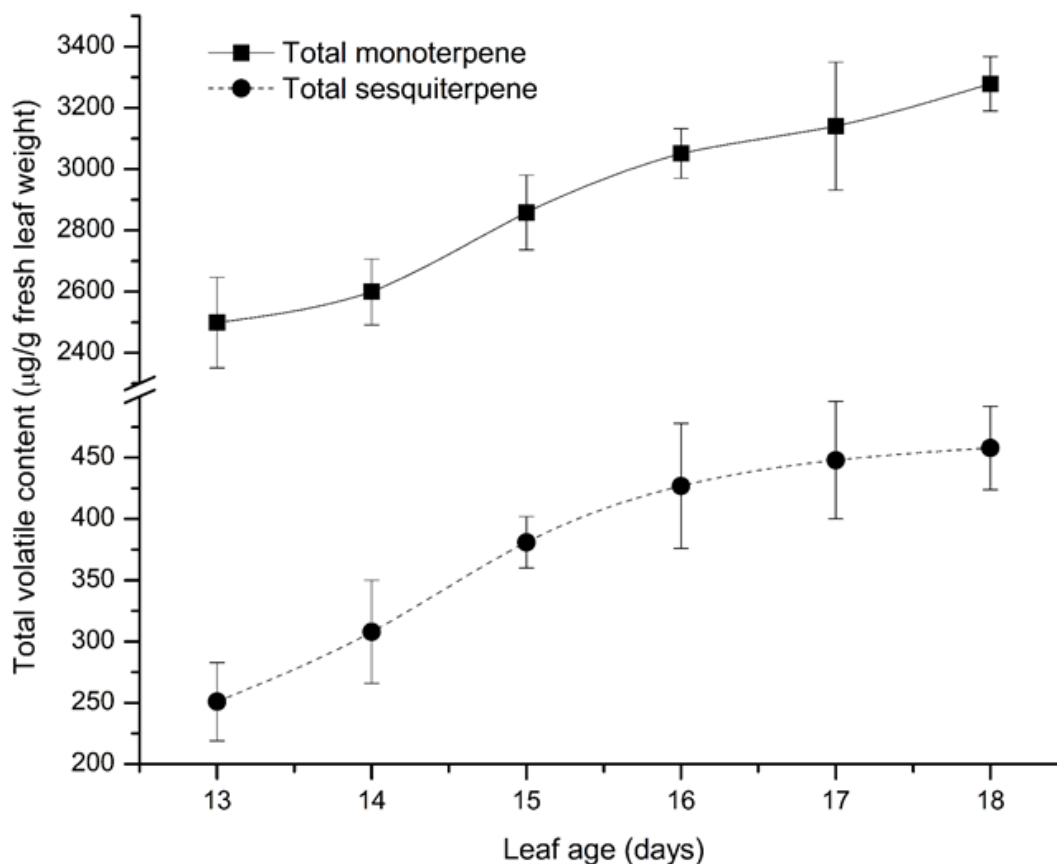
Figure S9. Metabolic steady-state determination in the first leaf pair of oregano shoot-tip culture.

The culture was grown under 10 µmol m^{-2}s^{-1} light intensity in the basal media containing unlabeled glucose (mean ± SE, n=5). The linear accumulation phase of monoterpene was observed between 14 to 16 days, whereas the linear accumulation phase of sesquiterpene was observed between 13 to 16 days. Finally, 15 days aged leaf was selected for further labeling study.
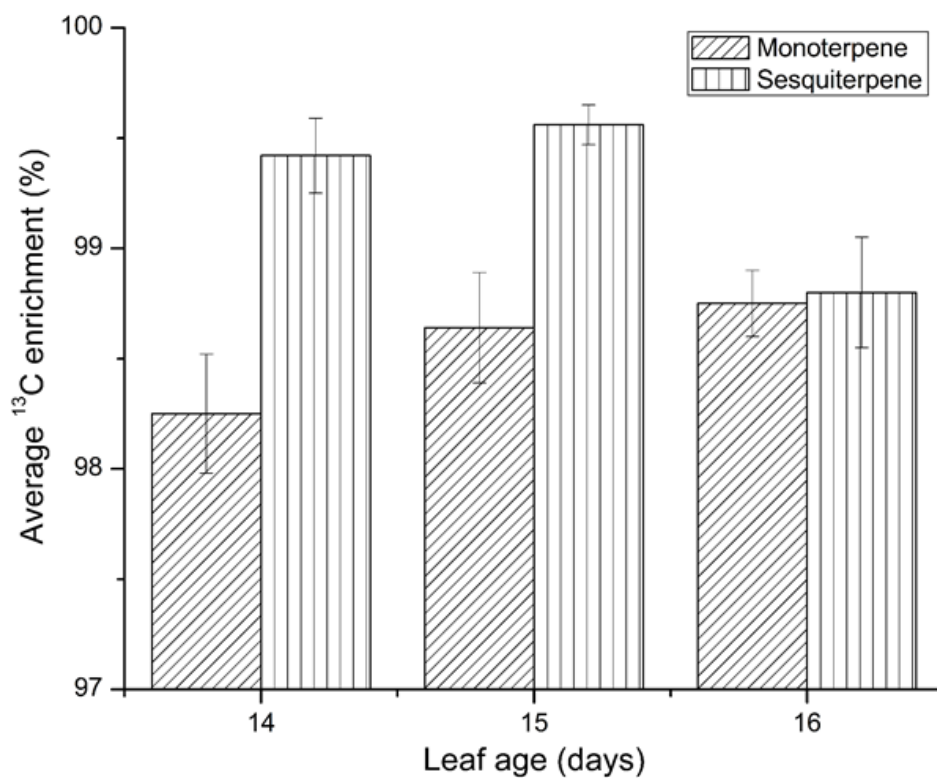
Figure S10. Isotopic steady-state determination in the first leaf pair of oregano shoot-tip culture.

The culture was grown under 10 µmol m^{-2} s^{-1} light intensity in the basal media containing U-^{13}C$_6$ glucose (mean ± SE, n=5). ^{13}C enrichment in volatiles deviated to less than 1% which defined the isotopic steady-state condition of the first leaf pair from oregano shoot-tip culture. Amount of sabinene hydrate and bisabolene was the highest among monoterpenes and sesquiterpenes, respectively and represent the isotopic status of their corresponding group.
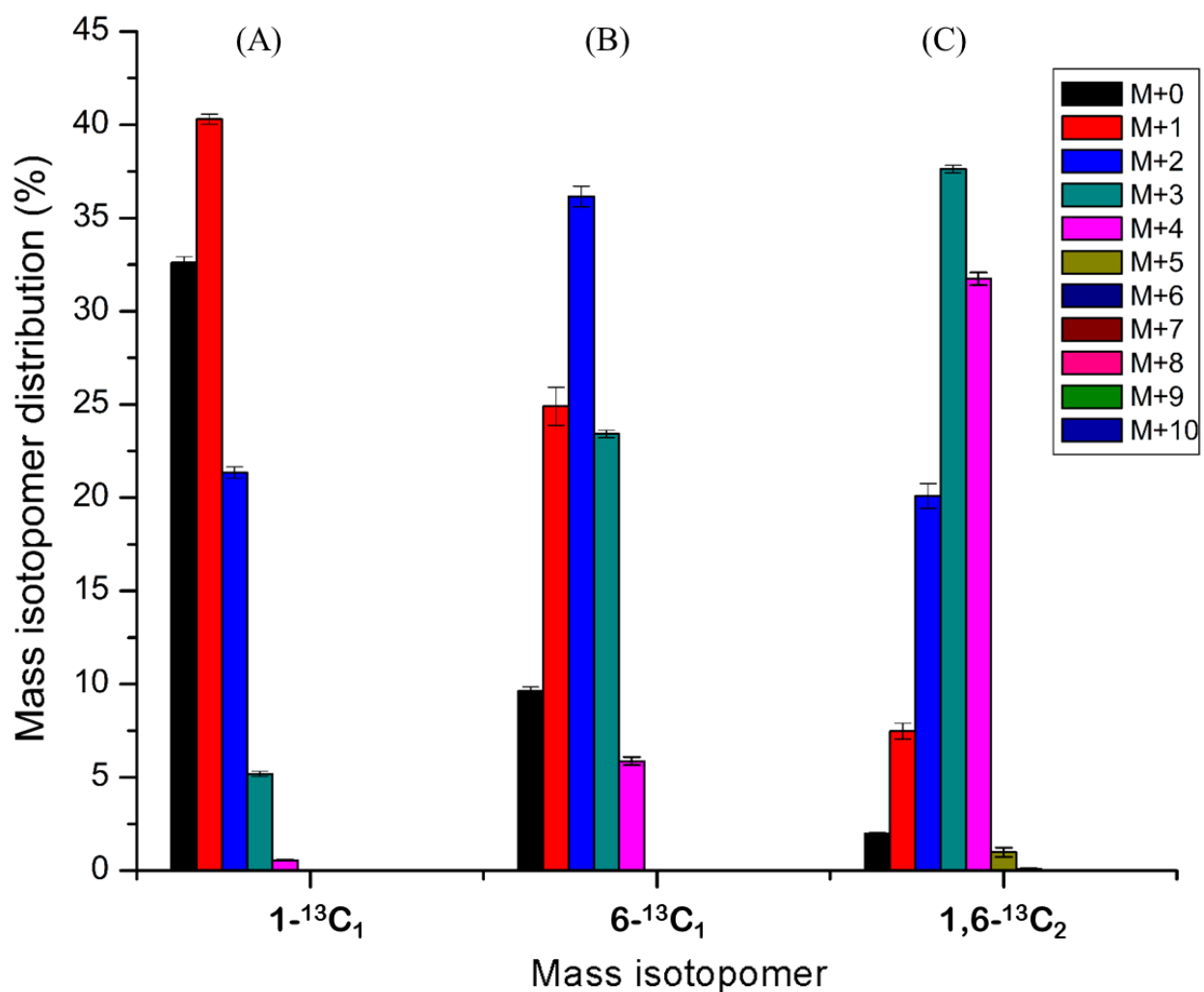
Figure S11. MID of sabinene hydrate in the first leaf pair from three different tracer analysis.

Oregano shoot-tip culture was grown under 10 μmol m^{-2} s^{-1} light intensity in the basal media containing (A) 1-^{13}C$_1$, (B) 6-^{13}C$_1$ and (C) 1,6-^{13}C$_2$ glucose as the sole carbon source (mean $\pm$ SE, n=3).
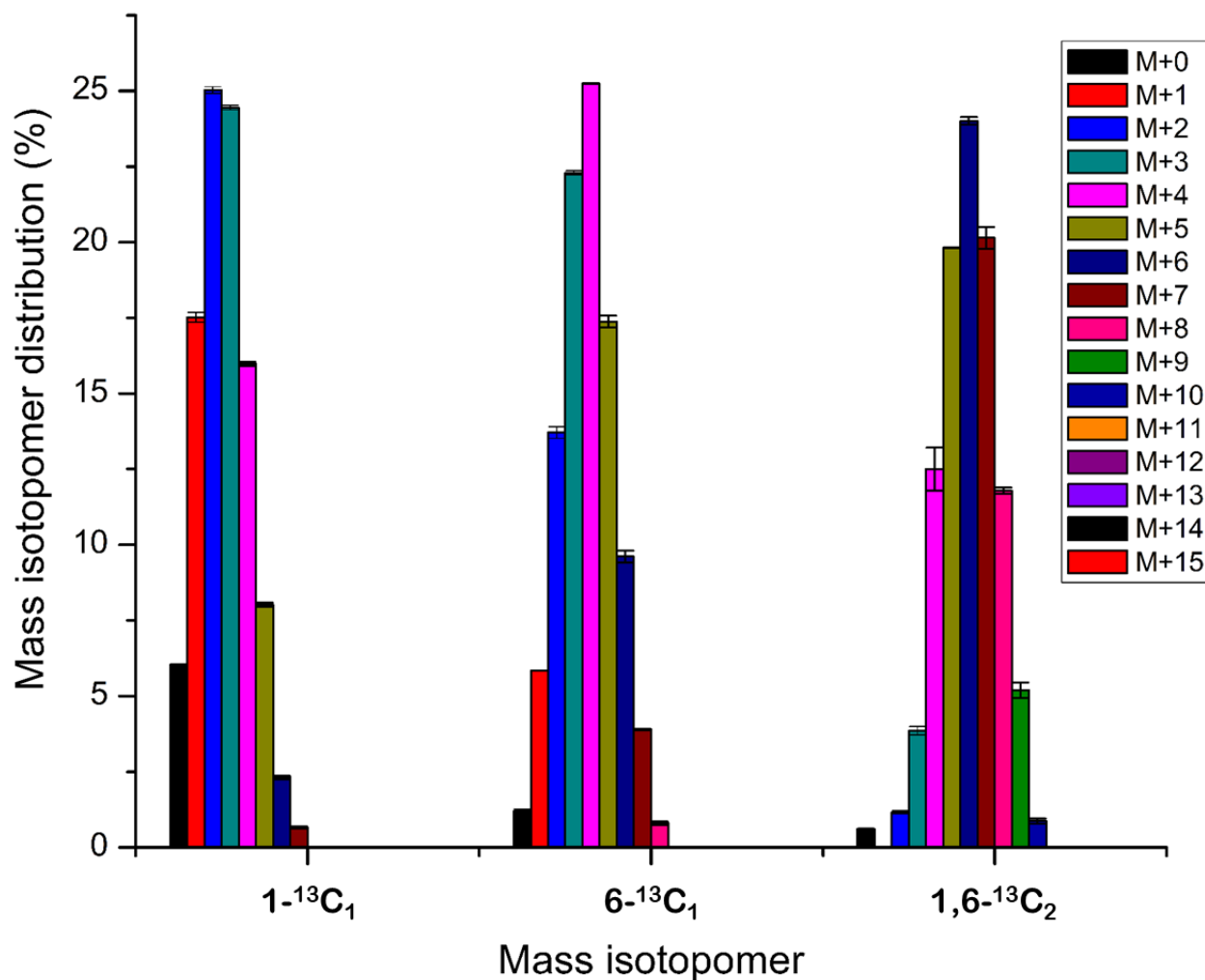
Figure S12. MID of bisabolene in the first leaf pair from three different tracer analysis.

Oregano shoot-tip culture was grown under 10 µmol m^{-2} s^{-1} light intensity in the basal media containing (A) 1-$^{13}C_1$, (B) 6-$^{13}C_1$ and (C) 1,6-$^{13}C_2$ glucose as the sole carbon source (mean ± SE, n=3).
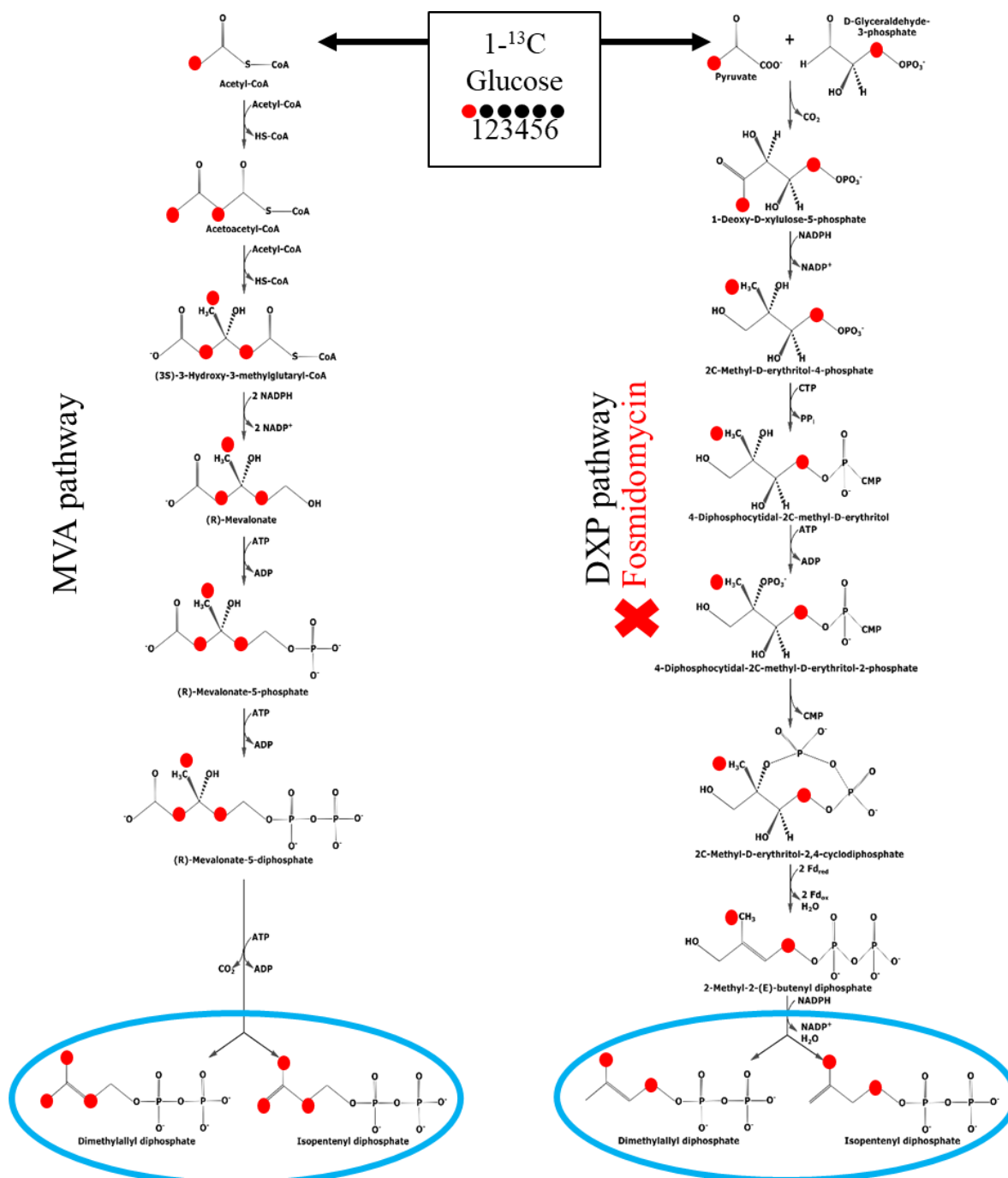
Figure S13. Carbon flow from 1-^{13}C glucose into DXP and MVA pathway via the glycolytic route.

This is a simplified scheme of ^{13}C flow where the maximum possibility of enrichment is considered for both the pathways, in case carbon is flown via glycolysis. Light blue color circle specifies two C_5 isoprene units which are IPP and DMAPP. Three and two label carbon were observed to be present by MVA and DXP pathway, respectively. In case, the DXP pathway is blocked, the altered isotope incorporation confirms the active role of the MVA pathway for monoterpene biosynthesis. Simultaneously, increasing ^{13}C enrichment could predict that precursor for the MVA pathway is mainly supplied from glycolysis.
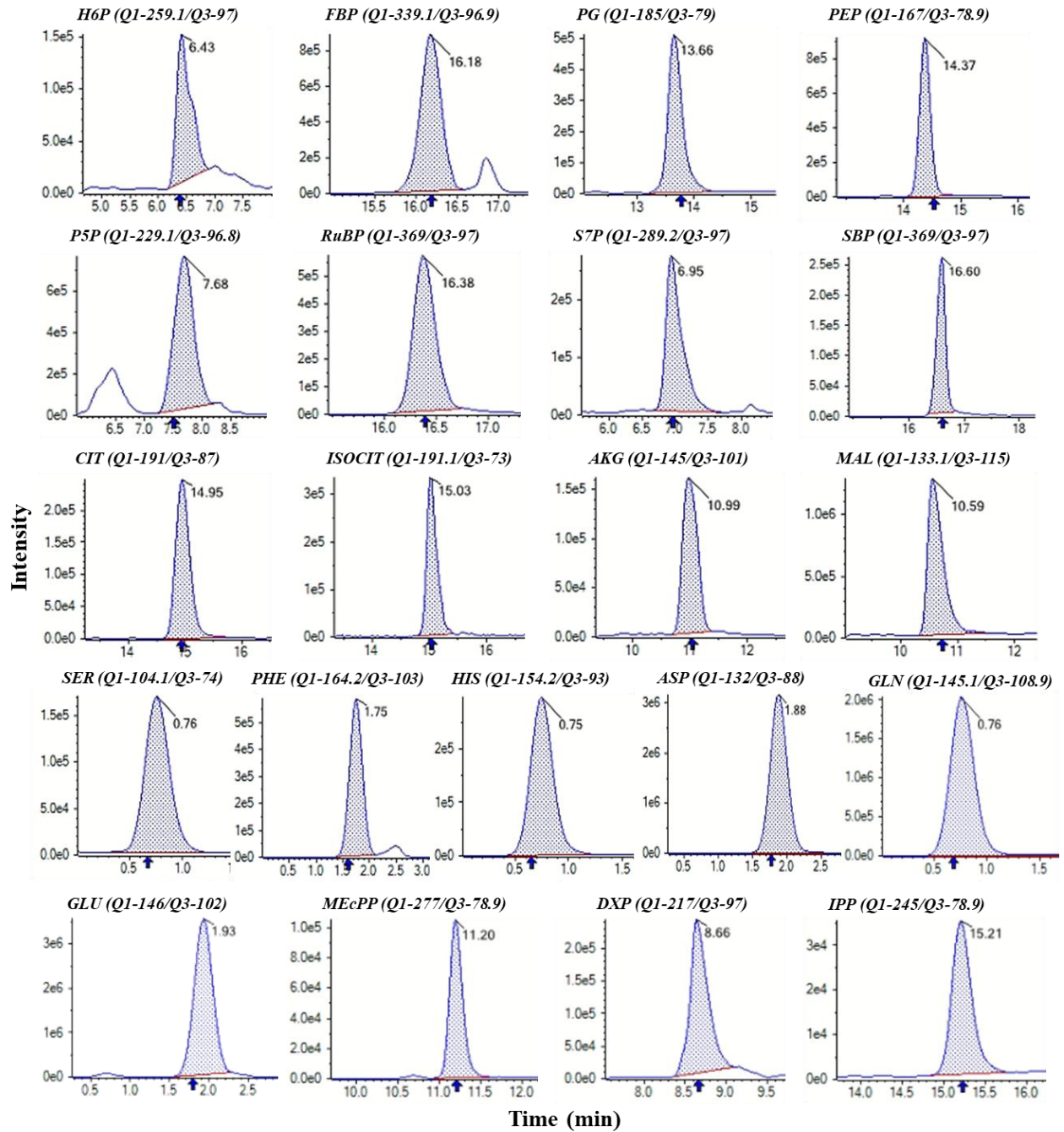
Figure S14. Chromatograph of precisely measured metabolites from peppermint shoot-tip culture in LCMS.

These metabolites were measured precisely and accurately from peppermint shoot-tip culture.
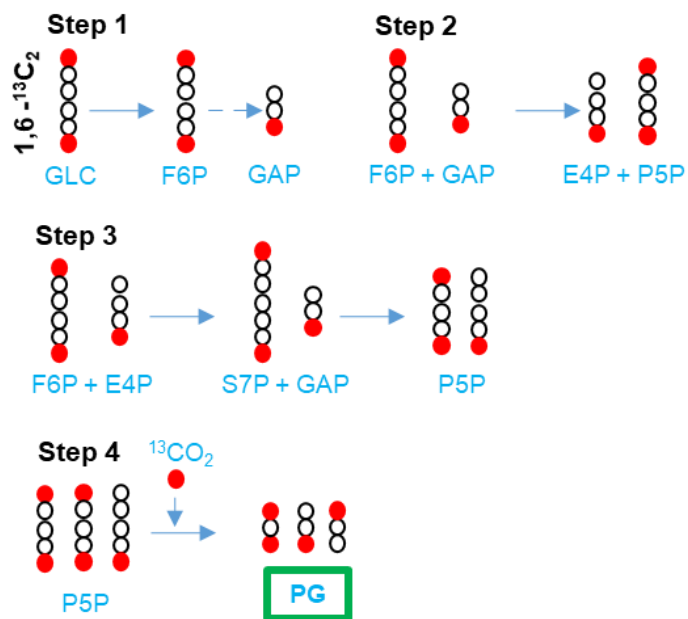
Figure S15. Theoretical overview of ^{13}C flow from 1,6-$^{13}C_2$ glucose to PG via reductive PPP.

This is a simplified scheme of ^{13}C flow where (M+2) mass isotopomer of PG is detected to be produced. White and red cycles denote ^{12}C and ^{13}C, respectively.

Appendix

Table S1. Total consumption of glucose by shoot-tip culture.

Glucose consumption was measured at 15 DALV growth of the shoot culture under different light intensities (mean ± standard error, n=5).

Light intensity (μmol m^{-2} s^{-1})	Total glucose needed (mg per shoot culture)
5	41.4 ± 1.8
10	47.1 ± 1.2
20	54.8 ± 2.6
30	46.3 ± 2.4

Table S2. Mass isotopomers of pulegone used for the peppermint GT model.

MIDs of three replications from three tracers after natural abundance correction was presented.

Mass isotopomer	Pulegone								
	1-^{13}C$_1$ glucose			6-^{13}C$_1$ glucose			1,6-^{13}C$_2$ glucose		
	Rep. 1	Rep. 2	Rep. 3	Rep. 1	Rep. 2	Rep. 3	Rep. 1	Rep. 2	Rep. 3
M+0	0.364	0.366	0.361	0.066	0.069	0.067	0.010	0.010	0.010
M+1	0.394	0.391	0.397	0.238	0.250	0.241	0.072	0.072	0.068
M+2	0.180	0.181	0.184	0.357	0.361	0.358	0.241	0.235	0.231
M+3	0.051	0.052	0.048	0.255	0.244	0.251	0.376	0.388	0.381
M+4	0.009	0.009	0.009	0.076	0.068	0.075	0.265	0.258	0.269
M+5	0.001	0.001	0.001	0.007	0.006	0.007	0.029	0.031	0.033
M+6	0.000	0.000	0.000	0.002	0.002	0.002	0.006	0.006	0.007
M+7	0.000	0.000	0.000	0.000	0.000	0.000	0.000	0.000	0.000
M+8	0.000	0.000	0.000	0.000	0.000	0.000	0.000	0.000	0.000
M+9	0.000	0.000	0.000	0.000	0.000	0.000	0.000	0.000	0.000
M+10	0.000	0.000	0.000	0.000	0.000	0.000	0.000	0.000	0.000

Table S3. Mass isotopomers of menthofuran used for the peppermint GT model.

MIDs of three replications from three tracers after natural abundance correction was presented.

Mass isotopomer	Menthofuran								
	$1\text{-}^{13}C_1$ glucose			$6\text{-}^{13}C_1$ glucose			$1,6\text{-}^{13}C_2$ glucose		
	Rep. 1	Rep. 2	Rep. 3	Rep. 1	Rep. 2	Rep. 3	Rep. 1	Rep. 2	Rep. 3
M+0	0.370	0.372	0.369	0.068	0.068	0.070	0.011	0.011	0.011
M+1	0.399	0.399	0.393	0.248	0.246	0.246	0.070	0.074	0.069
M+2	0.176	0.175	0.179	0.366	0.359	0.360	0.233	0.240	0.235
M+3	0.046	0.045	0.049	0.243	0.247	0.247	0.381	0.385	0.380
M+4	0.007	0.007	0.008	0.069	0.071	0.071	0.261	0.254	0.261
M+5	0.001	0.001	0.001	0.005	0.006	0.006	0.031	0.030	0.030
M+6	0.000	0.000	0.000	0.001	0.001	0.001	0.007	0.005	0.007
M+7	0.000	0.000	0.000	0.000	0.000	0.000	0.004	0.000	0.004
M+8	0.000	0.000	0.000	0.000	0.000	0.000	0.003	0.000	0.003
M+9	0.000	0.000	0.000	0.000	0.000	0.000	0.000	0.000	0.000
M+10	0.000	0.000	0.000	0.000	0.000	0.000	0.000	0.000	0.000

Table S4. Mass isotopomers of isopulegone used for the peppermint GT model.

MIDs of three replications from three tracers after natural abundance correction was presented.

Mass isotopomer	Isopulegone								
	$1\text{-}^{13}C_1$ glucose			$6\text{-}^{13}C_1$ glucose			$1,6\text{-}^{13}C_2$ glucose		
	Rep. 1	Rep. 2	Rep. 3	Rep. 1	Rep. 2	Rep. 3	Rep. 1	Rep. 2	Rep. 3
M+0	0.371	0.371	0.370	0.067	0.069	0.069	0.012	0.010	0.011
M+1	0.396	0.392	0.402	0.241	0.244	0.248	0.072	0.072	0.071
M+2	0.178	0.181	0.181	0.368	0.361	0.363	0.234	0.233	0.236
M+3	0.047	0.047	0.041	0.260	0.250	0.246	0.377	0.377	0.382
M+4	0.008	0.007	0.005	0.064	0.070	0.068	0.259	0.259	0.262
M+5	0.001	0.001	0.000	0.001	0.005	0.005	0.037	0.038	0.032
M+6	0.000	0.000	0.000	0.000	0.001	0.001	0.009	0.010	0.005
M+7	0.000	0.000	0.000	0.000	0.000	0.000	0.000	0.000	0.000
M+8	0.000	0.000	0.000	0.000	0.000	0.000	0.000	0.000	0.000
M+9	0.000	0.000	0.000	0.000	0.000	0.000	0.000	0.000	0.000
M+10	0.000	0.000	0.000	0.000	0.000	0.000	0.000	0.000	0.000

Table S5. A complete list of flux, reactions and carbon transitions for the open_redox MFA version of peppermint GTs.

Three uptake reactions were skipped for the **close_redox MFA** version of peppermint GTs, namely NADHim, NADPHim and ATPim. All other reactions were included in that modified version.

Pathway	Flux	Stoichiometry/Carbon transitions
Upper glycolysis	PGI	G6P (abcdef) ↔ F6P (abcdef)
	ALD	F6P (abcdef) + ATP ↔ GAP (cba) + GAP (def)
	GAPDH	GAP (abc) ↔ PG (abc) + ATP + NADH
	PGM	PG (abc) ↔ PEP (abc)
ANA	cME_NADPH	MAL (abcd) → PYR (abc) + CO2 (d) + NADPH
	cME_NADH	MAL (abcd) → PYR (abc) + CO2 (d) + NADH
	PK	PEP (abc) → PYR (abc) + ATP
	PEPC	PEP (abc) + CO2 (d) → OAA (abcd)
	MDH.c	MAL (abcd) ↔ OAA (abcd) + NADH
	pME_NADPH	MAL (abcd) → PYR.p (abc) + CO2 (d) + NADPH
Plastidic glycolysis	GAPDH.p	GAP (abc) ↔ PG.p (abc) + ATP + NADH
	PGM.p	PG.p (abc) ↔ PEP.p (abc)
	PK.p	PEP.p (abc) → PYR.p (abc) + ATP
PPP	oxPPP	G6P (abcdef) → Ru5P (bcdef) + CO2 (a) + 2*NADPH
	PPP1	Ru5P (abcde) ↔ X5P (abcde)
	PPP2	Ru5P (abcde) ↔ R5P (abcde)
	PPP3	X5P (abcde) + R5P (fghij) ↔ S7P (abfghij) + GAP (cde)
	PPP4	S7P (abcdefg) + GAP (hij) ↔ F6P (abchij) + E4P (defg)
	PPP5	X5P (abcde) + E4P (fghi) ↔ F6P (abfghi) + GAP (cde)
RUB	Rub	Ru5P (abcde) + CO2 (f) + ATP → PG.p (fba) + PG.p (cde)
TCA	PDH	PYR.m (abc) → AcCoA.m (bc) + CO2 (a) + NADH
	CS	OAA.m (abcd) + AcCoA.m (ef) → CIT.m (dcbfea)
	ISDH	CIT.m (abcdef) ↔ OGA.m (abcde) + CO2 (f) + NADH
	OGDH	OGA.m (abcde) → SUC.m (bcde) + CO2 (a) + NADH + ATP
	SDH	SUC.m (abcd) ↔ FUM.m (abcd)
	FUM	FUM.m (abcd) ↔ MAL.m (abcd)
	MDH.m	MAL.m (abcd) ↔ OAA.m (abcd) + NADH
MVA	ACL	CIT (dcbfea) + ATP → OAA (abcd) + AcCoA (ef)
	AACT	AcCoA (ab) + AcCoA (cd) → AcAcCoA (abcd)
	HMGCS	AcCoA (ef) + AcAcCoA (abcd) → HMGCoA (efcbad)
	DMD	HMGCoA (abcdef) + 3*ATP +2*NADPH → IPP.c (edcbf)+CO_2(a)
DXP	DXS	PYR.p (abc) + GAP (def) → DXP (cbdef) + CO2 (a)
	DXR	DXP (abcde) + NADPH → ME4P (cbdea)
	HMBPPR	ME4P (abcde) + 3*ATP + 2*NADPH → IPP.p (dcbae)

Pathway	Reaction	Stoichiometry/Carbon transitions
Monoterpene biosynthesis	GPPS	IPP.p (abcde) + IPP.p (fghij) → GPP (abcdfghiej)
	Mono	GPP (abcdefghij) + 2*NADPH →monoterpene (cbafedighj)+NADH
Uptake/export	NADHim	NADH.ext → NADH
	NADPHim	NADPH.ext → NADPH
	ATPim	ATP.ext → ATP
	upt	Gluc.ext (abcdef) + ATP → G6P (abcdef)
	upt_U	Gluc.u (abcdef) + ATP → G6P (abcdef)
	Ex_Mono	Monoterpene (abcdefghij) → Monoterpene.ext (abcdefghij)
	Ex_CO2	CO2 (a) → CO2.ext (a)
Transport	ATP	NADH → 2.5*ATP
	T_PYR.m	PYR (abc) ↔ PYR.m (abc)
	T_MAL.m	MAL (abcd) ↔ MAL.m (abcd)
	T_CIT	CIT.m (abcdef) ↔ CIT (abcdef)
	T_PYR.p	PYR (abc) ↔ PYR.p (abc)
	X_IPP	IPP.c (abcde) → IPP.p (abcde)

Table S6. Different level of confidence on the role of MVA for monoterpene production.

Lower bound (LB=0.19) and upper bound (UB=0.346) values at 95% confidence interval (CI) were obtained from open_redox MFA of peppermint, where SE of MVA flux was 0.0398. On the basis of 95% CI, LB and UB at 98%, 99% and 99.9% CI were calculated. Important parts of this calculation and the outcome are highlighted in bold.

MVA at different CI	Interval range (IR=UB-LB =SE×t×2)	LB calculation (Mean- IR/2)	LB value	UB calculation (Mean+ IR/2)	UB value
At **95%** CI (**t** value=1.960)	0.156	(Mean-0.078) = **X**	**X= 0.19** (9.5%)	(Mean+0.078) =**Y**	**Y= 0.346** (17.3%)
At **98%** CI (**t** value=2.326)	0.185	(Mean-0.093) = (**X-0.015**)	0.175 (**8.8%**)	(Mean+0.093) = (**Y+0.015**)	**Y**= 0.361 (**18.1%**)
At **99%** CI (**t** value=2.576)	0.205	(Mean-0.103) = (**X-0.025**)	0.165 (**8.3%**)	(Mean+0.103) = (**Y+0.025**)	0.371 (**18.6%**)
At **99.9%** CI (**t** value=3.291)	0.262	(Mean-0.131) = (**X-0.053**)	0.137 (**6.9%**)	(Mean+0.131) = (**Y+0.053**)	0.399 (**20%**)

Table S7. Estimated net fluxes from open_redox MFA version of peppermint GTs for monoterpene biosynthesis.

Estimated values were the medians of each flux at 95% flux confidence intervals, whereas UB95 and LB95 were the upper and lower bound of the fluxes, respectively. Standard errors (SE) were calculated as (UB95-LB95)/3.92. Abbrev: →: irreversible reaction; ↔: reversible reaction; .c: cytosolic metabolite; .p: plastidic metabolite; .m: mitochondrial metabolite.

Pathway	Stoichiometry	Flux	LB	UB	SE
Upper glycolysis	G6P ↔ F6P	0.883	0.050	1.026	0.249
	F6P + ATP ↔ GAP + GAP	0.726	0.481	0.827	0.088
	GAP ↔ PG + ATP + NADH	1.288	0.458	2.031	0.401
	PG ↔ PEP	1.288	0.458	2.031	0.401
ANA	MAL → PYR + CO2 + NADPH	1.288	0.000	2.025	0.517
	MAL → PYR + CO2 + NADH	0.000	0.000	1.612	0.411
	PEP → PYR + ATP	0.000	0.000	0.264	0.067
	PEP + CO2 → OAA	1.288	0.458	2.031	0.401
	MAL ↔ OAA + NADH	-2.061	-2.906	-1.062	0.470
	MAL → PYR.p + CO2 + NADPH	0.000	0.000	1.213	0.310
Plastidic glycolysis	GAP ↔ PG.p + ATP + NADH	-1.656	-2.619	-0.922	0.433
	PG.p ↔ PEP.p	1.742	0.000	2.065	0.527
	PEP.p → PYR.p + ATP	1.742	0.000	2.065	0.527
PPP	G6P → Ru5P + CO2 + 2*NADPH	1.464	1.365	2.531	0.297
	Ru5P ↔ X5P	-0.157	-0.369	0.428	0.203
	Ru5P ↔ R5P	-0.079	-0.185	0.214	0.102
	X5P + R5P ↔ S7P + GAP	-0.079	-0.185	0.214	0.102
	S7P + GAP ↔ F6P + E4P	-0.079	-0.185	0.214	0.102
	X5P + E4P ↔ F6P + GAP	-0.079	-0.185	0.214	0.102
RUB	Ru5P + CO2 + ATP → PG.p + PG.p	1.699	1.409	2.177	0.196
TCA	PYR.m → AcCoA.m + CO_2 + NADH	1.288	0.702	2.034	0.340
	OAA.m + AcCoA.m → CIT.m	1.288	0.702	2.034	0.340
	CIT.m ↔ OGA.m + CO2 + NADH	0.515	0.000	1.203	0.307
	OGA.m → SUC.m + CO2 + NADH + ATP	0.515	0.000	1.203	0.307
	SUC.m ↔ FUM.m	0.515	0.000	1.203	0.307
	FUM.m ↔ MAL.m	0.515	0.000	1.203	0.307
	MAL.m ↔ OAA.m + NADH	1.288	0.702	2.034	0.340
MVA	CIT + ATP → OAA + AcCoA	0.773	0.569	1.037	0.119
	AcCoA + AcCoA → AcAcCoA	0.258	0.190	0.346	0.040
	AcCoA + AcAcCoA → HMGCoA	0.258	0.190	0.346	0.040
	HMGCoA + 3*ATP + 2*NADPH → IPP.c + CO2	0.258	0.190	0.346	0.040

Pathway	Stoichiometry	Flux	LB	UB	SE
DXP	PYR.p + GAP → DXP + CO2	1.742	1.654	1.810	0.040
	DXP + NADPH → ME4P	1.742	1.654	1.810	0.040
	ME4P + 3*ATP + 2*NADPH → IPP.p	1.742	1.654	1.810	0.040
Monoterpene biosynthesis	IPP.p + IPP.p → GPP	1.000	1.000	1.000	0.000
	GPP + 2*NADPH → Monoterpene + NADH	1.000	1.000	1.000	0.000
Uptake /export	NADH.ext → NADH	1.670	0.000	4.134	1.055
	NADPH.ext → NADPH	3.527	1.009	3.715	0.690
	ATP.ext → ATP	0.041	0.000	11.831	3.018
	Gluc.ext + ATP → G6P	2.337	2.101	2.731	0.161
	Gluc.u + ATP → G6P	0.010	0.000	0.010	0.003
	Monoterpene → Monoterpene.ext	1.000	1.000	1.000	0.000
	CO2 → CO2.ext	4.082	2.668	6.448	0.964
Transport	PYR ↔ PYR.m	1.288	0.702	2.034	0.340
	NADH → 2.5*ATP	3.847	0.000	4.721	1.204
	MAL ↔ MAL.m	0.773	0.569	1.037	0.119
	CIT.m ↔ CIT	0.773	0.569	1.037	0.119
	PYR ↔ PYR.p	0.000	-0.264	0.892	0.295
	IPP.c → IPP.p	0.258	0.190	0.346	0.040

Table S8. Estimated net fluxes from close_redox MFA version of peppermint GTs for monoterpene biosynthesis.

Estimated values were the medians of the each flux at 95% flux confidence intervals, whereas UB95 and LB95 were the upper and lower bound of the fluxes, respectively. Standard errors (SE) were calculated as (UB95-LB95)/3.92. Abbrev: →: irreversible reaction; ↔: reversible reaction; .c: cytosolic metabolite; .p: plastidic metabolite; .m: mitochondrial metabolite.

Pathway	Stoichiometry	Flux	LB	UB	SE
Upper glycolysis	G6P ↔ F6P	-0.288	-1.233	-0.072	0.296
	F6P + ATP ↔ GAP + GAP	0.537	0.157	0.883	0.185
	GAP ↔ PG + ATP + NADH	1.605	0.163	1.928	0.450
	PG ↔ PEP	1.605	0.163	1.928	0.450
ANA	MAL → PYR + CO2 + NADPH	1.605	0.000	1.928	0.492
	MAL → PYR + CO2 + NADH	0.000	0.000	1.352	0.345
	PEP → PYR + ATP	0.000	0.000	0.698	0.178
	PEP + CO2 → OAA	1.605	0.175	1.928	0.447
	MAL ↔ OAA + NADH	-2.196	-2.577	-0.420	0.550
	MAL → PYR.p + CO2 + NADPH	0.000	0.000	0.250	0.064
Plastidic glycolysis	GAP ↔ PG.p + ATP + NADH	-1.922	-2.852	-0.165	0.686
	PG.p ↔ PEP.p	1.803	1.586	2.402	0.208
	PEP.p → PYR.p + ATP	1.803	1.586	2.402	0.208
PPP	G6P → Ru5P + CO2 + 2*NADPH	3.099	2.924	3.959	0.264
	Ru5P ↔ X5P	0.825	0.413	1.941	0.390
	Ru5P ↔ R5P	0.412	0.207	0.971	0.195
	X5P + R5P ↔ S7P + GAP	0.412	0.207	0.971	0.195
	S7P + GAP ↔ F6P + E4P	0.412	0.207	0.971	0.195
	X5P + E4P ↔ F6P + GAP	0.412	0.207	0.971	0.195
RUB	Ru5P + CO_2 + ATP → PG.p + PG.p	1.862	1.012	2.328	0.336
TCA	PYR.m → AcCoA.m + CO_2 + NADH	1.605	0.718	1.928	0.309
	OAA.m + AcCoA.m → CIT.m	1.605	0.718	1.928	0.309
	CIT.m ↔ OGA.m + CO2 + NADH	1.013	0.489	1.309	0.209
	OGA.m → SUC.m + CO_2 + NADH + ATP	1.013	0.489	1.309	0.209
	SUC.m ↔ FUM.m	1.013	0.489	1.309	0.209
	FUM.m ↔ MAL.m	1.013	0.489	1.309	0.209
	MAL.m ↔ OAA.m + NADH	1.605	0.718	1.928	0.309
MVA	CIT + ATP → OAA + AcCoA	0.592	0.257	0.774	0.132
	AcCoA + AcCoA → AcAcCoA	0.197	0.086	0.258	0.044
	AcCoA + AcAcCoA → HMGCoA	0.197	0.086	0.258	0.044
	HMGCoA + 3*ATP + 2*NADPH → IPP.c + CO2	0.197	0.086	0.258	0.044

Pathway	Stoichiometry	Flux	LB	UB	SE
DXP	PYR.p + GAP → DXP + CO2	1.803	1.742	1.915	0.044
	DXP + NADPH → ME4P	1.803	1.742	1.915	0.044
	ME4P + 3*ATP + 2*NADPH → IPP.p	1.803	1.742	1.915	0.044
Monoterpene biosynthesis	IPP.p + IPP.p → GPP	1.000	1.000	1.000	0.000
	GPP + 2*NADPH → Monoterpene + NADH	1.000	1.000	1.000	0.000
Uptake /export	Gluc.ext + ATP → G6P	2.801	2.725	2.854	0.033
	Gluc.u + ATP → G6P	0.010	0.000	0.010	0.003
	Monoterpene → Monoterpene.ext	1.000	1.000	1.000	0.000
	CO2 → CO2.ext	6.867	6.287	7.142	0.218
Transport	PYR ↔ PYR.m	1.605	0.718	1.928	0.309
	NADH → 2.5*ATP	3.721	3.189	3.981	0.202
	MAL ↔ MAL.m	0.592	0.257	0.774	0.132
	CIT.m ↔ CIT	0.592	0.257	0.774	0.132
	PYR ↔ PYR.p	0.000	-0.697	0.250	0.242
	IPP.c → IPP.p	0.197	0.086	0.258	0.044

Table S9. A complete list of flux, reactions and carbon transitions for performing MFA of oregano GTs.

Pathway	Flux	Stoichiometry/Carbon transitions
Upper glycolysis	PGI	G6P (abcdef) ↔ F6P (abcdef)
	ALD	F6P (abcdef) + ATP ↔ GAP (cba) + GAP (def)
	GAPDH	GAP (abc) ↔ PG (abc) + ATP + NADH
	PGM	PG (abc) ↔ PEP (abc)
ANA	cME_NADPH	MAL (abcd) → PYR (abc) + CO2 (d) + NADPH
	cME_NADH	MAL (abcd) → PYR (abc) + CO2 (d) + NADH
	PK	PEP (abc) → PYR (abc) + ATP
	PEPC	PEP (abc) + CO2 (d) → OAA (abcd)
	MDH.c	MAL (abcd) ↔ OAA (abcd) + NADH
	pME_NADPH	MAL (abcd) → PYR.p (abc) + CO2 (d) + NADPH
Plastidic glycolysis	GAPDH.p	GAP (abc) ↔ PG.p (abc) + ATP + NADH
	PGM.p	PG.p (abc) ↔ PEP.p (abc)
	PK.p	PEP.p (abc) → PYR.p (abc) + ATP
PPP	oxPPP	G6P (abcdef) → Ru5P (bcdef) + CO2 (a) + 2*NADPH
	PPP1	Ru5P (abcde) ↔ X5P (abcde)
	PPP2	Ru5P (abcde) ↔ R5P (abcde)
	PPP3	X5P (abcde) + R5P (fghij) ↔ S7P (abfghij) + GAP (cde)
	PPP4	S7P (abcdefg) + GAP (hij) ↔ F6P (abchij) + E4P (defg)
	PPP5	X5P (abcde) + E4P (fghi) ↔ F6P (abfghi) + GAP (cde)
RUB	Rub	Ru5P (abcde) + CO2 (f) + ATP → PG.p (fba) + PG.p (cde)
TCA	PDH	PYR.m (abc) → AcCoA.m (bc) + CO2 (a) + NADH
	CS	OAA.m (abcd) + AcCoA.m (ef) → CIT.m (dcbfea)
	ISDH	CIT.m (abcdef) ↔ OGA.m (abcde) + CO2 (f) + NADH
	OGDH	OGA.m (abcde) → SUC.m (bcde) + CO2 (a) + NADH + ATP
	SDH	SUC.m (abcd) ↔ FUM.m (abcd)
	FUM	FUM.m (abcd) ↔ MAL.m (abcd)
	MDH.m	MAL.m (abcd) ↔ OAA.m (abcd) + NADH
MVA	ACL	CIT (dcbfea) + ATP → OAA (abcd) + AcCoA (ef)
	AACT	AcCoA (ab) + AcCoA (cd) → AcAcCoA (abcd)
	HMGCS	AcCoA (ef) + AcAcCoA (abcd) → HMGCoA (efcbad)
	DMD	HMGCoA (abcdef) + 3*ATP +2*NADPH → IPP.c (edcbf)+CO$_2$(a)
DXP	DXS	PYR.p (abc) + GAP (def) → DXP (cbdef) + CO2 (a)
	DXR	DXP (abcde) + NADPH → ME4P (cbdea)
	HMBPPR	ME4P (abcde) + 3*ATP + 2*NADPH → IPP.p (dcbae)

Pathway	Reaction	Stoichiometry/Carbon transitions
Terpene biosynthesis	GPPS.p	IPPm.p (abcde) + IPPm.p (fghij) → GPP (abcdfghiej)
	Mono	GPP (abcdefghij) →monoterpene (cbafedighj)
	GPPS.c	IPPs.c (abcde) + IPPs.c (fghij) → GPP.c (abcdfghiej)
	FFPS	GPP.c (abcdefghij) + IPPs.c (klmno) → FPP (abcdefghklmnijo)
	BS	FPP (abcdefghijklmno) → sesquiterpene (cbafedghijklmno)
Uptake/export	NADHim	NADH.ext → NADH
	NADPHim	NADPH.ext → NADPH
	ATPim	ATP.ext → ATP
	upt	Gluc.ext (abcdef) + ATP → G6P (abcdef)
	upt_U	Gluc.u (abcdef) + ATP → G6P (abcdef)
	Ex_TERp	0.12*sesquiterpene (abcdefghijklmno) + 0.88*monoterpene (pqrstuvwxy) → terpene.ext (abcdefghijklmnopqrstuvwxy)
	Ex_CO2	CO2 (a) → CO2.ext (a)
Transport	ATP	NADH → 2.5*ATP
	T_PYR.m	PYR (abc) ↔ PYR.m (abc)
	T_MAL.m	MAL (abcd) ↔ MAL.m (abcd)
	T_CIT	CIT.m (abcdef) ↔ CIT (abcdef)
	T_PYR.p	PYR (abc) ↔ PYR.p (abc)
	Xcp	IPP.c (abcde) -> IPPm.p (abcde)
	Xpp	IPP.p (abcde) -> IPPm.p (abcde)
	Xpc	IPP.p (abcde) -> IPPs.c (abcde)
	Xcc	IPP.c (abcde) -> IPPs.c (abcde)

Table S10. Mass isotopomers of sabinene hydrate used for the oregano GT model.

MIDs from the biological replications of two tracers after natural abundance correction was presented.

Mass isotopomer	Sabinene hydrate				
	1-^{13}C$_1$ glucose			6-^{13}C$_1$ glucose	
	Rep. 1	Rep. 2	Rep. 3	Rep. 1	Rep. 2
M+0	0.320	0.327	0.331	0.097	0.092
M+1	0.406	0.398	0.406	0.267	0.249
M+2	0.214	0.219	0.208	0.352	0.362
M+3	0.055	0.051	0.050	0.230	0.236
M+4	0.005	0.006	0.005	0.054	0.060
M+5	0.000	0.000	0.000	0.000	0.000
M+6	0.000	0.000	0.000	0.000	0.000
M+7	0.000	0.000	0.000	0.000	0.000
M+8	0.000	0.000	0.000	0.000	0.000
M+9	0.000	0.000	0.000	0.000	0.000
M+10	0.000	0.000	0.000	0.000	0.000

Table S11. Mass isotopomers of bisabolene used for the oregano GT model.

MIDs from the biological replications of two tracers after natural abundance correction was presented.

Mass isotopomer	Bisabolene					
	1-^{13}C$_1$ glucose			6-^{13}C$_1$ glucose		
	Rep. 1	Rep. 2	Rep. 3	Rep. 1	Rep. 2	Rep. 3
M+0	0.060	0.061	0.060	0.013	0.011	0.012
M+1	0.173	0.174	0.178	0.059	0.058	0.059
M+2	0.252	0.248	0.251	0.140	0.133	0.138
M+3	0.246	0.243	0.245	0.224	0.222	0.223
M+4	0.160	0.161	0.158	0.253	0.252	0.253
M+5	0.081	0.081	0.079	0.171	0.178	0.173
M+6	0.022	0.024	0.023	0.093	0.100	0.095
M+7	0.006	0.007	0.006	0.039	0.039	0.039
M+8	0.000	0.000	0.000	0.009	0.007	0.008
M+9	0.000	0.000	0.000	0.000	0.000	0.000
M+10	0.000	0.000	0.000	0.000	0.000	0.000
M+11	0.000	0.000	0.000	0.000	0.000	0.000
M+12	0.000	0.000	0.000	0.000	0.000	0.000
M+13	0.000	0.000	0.000	0.000	0.000	0.000
M+14	0.000	0.000	0.000	0.000	0.000	0.000
M+15	0.000	0.000	0.000	0.000	0.000	0.000

Table S12. Estimated net fluxes of oregano GT's MFA for mono- and sesquiterpene biosynthesis.

Estimated values were the medians of each flux at 95% flux confidence intervals, whereas UB95 and LB95 were the upper and lower bound of the fluxes, respectively. Standard errors (SE) were calculated as (UB95-LB95)/3.92. Abbrev: →: irreversible reaction; ↔: reversible reaction; .c: cytosolic metabolite; .p: plastidic metabolite; .m: mitochondrial metabolite.

Pathway	Stoichiometry	Flux	LB	UB	SE
Upper glycolysis	G6P ↔ F6P	1.180	0.983	1.585	0.154
	F6P + ATP ↔ GAP + GAP	1.119	0.983	1.353	0.094
	GAP ↔ PG + ATP + NADH	2.394	1.917	2.559	0.164
	PG ↔ PEP	2.394	1.917	2.559	0.164
ANA	MAL → PYR + CO2 + NADPH	2.394	0.909	2.559	0.421
	MAL → PYR + CO2 + NADH	0.000	0.000	1.100	0.281
	PEP → PYR + ATP	0.000	0.000	0.883	0.225
	PEP + CO2 → OAA	2.394	1.147	2.559	0.360
	MAL ↔ OAA + NADH	-3.617	-3.944	-2.226	0.438
	MAL → PYR.p + CO2 + NADPH	0.000	0.000	0.205	0.052
Plastidic glycolysis	GAP ↔ PG.p + ATP + NADH	-1.898	-2.273	-1.071	0.307
	PG.p ↔ PEP.p	1.712	1.556	1.852	0.076
	PEP.p → PYR.p + ATP	1.712	1.556	1.852	0.076
PPP	G6P → Ru5P + CO2 + 2*NADPH	1.714	1.163	1.924	0.194
	Ru5P ↔ X5P	-0.061	-0.530	0.146	0.172
	Ru5P ↔ R5P	-0.031	-0.265	0.073	0.086
	X5P + R5P ↔ S7P + GAP	-0.031	-0.265	0.073	0.086
	S7P + GAP ↔ F6P + E4P	-0.031	-0.265	0.073	0.086
	X5P + E4P ↔ F6P + GAP	-0.031	-0.265	0.073	0.086
RUB	Ru5P + CO2 + ATP → PG.p + PG.p	1.805	1.415	2.023	0.155
TCA	PYR.m → AcCoA.m + CO_2 + NADH	2.394	1.917	2.558	0.164
	OAA.m + AcCoA.m → CIT.m	2.394	1.917	2.558	0.164
	CIT.m ↔ OGA.m + CO2 + NADH	1.171	0.832	1.326	0.126
	OGA.m → SUC.m + CO2 + NADH + ATP	1.171	0.832	1.326	0.126
	SUC.m ↔ FUM.m	1.171	0.832	1.326	0.126
	FUM.m ↔ MAL.m	1.171	0.832	1.326	0.126
	MAL.m ↔ OAA.m + NADH	2.394	1.917	2.558	0.164
MVA	CIT + ATP → OAA + AcCoA	1.223	0.804	1.419	0.157
	AcCoA + AcCoA → AcAcCoA	0.408	0.268	0.473	0.052
	AcCoA + AcAcCoA → HMGCoA	0.408	0.268	0.473	0.052
	HMGCoA + 3*ATP + 2*NADPH → IPP.c + CO2	0.408	0.268	0.473	0.052

Pathway	Stoichiometry	Flux	LB	UB	SE
DXP	PYR.p + GAP → DXP + CO2	1.712	1.647	1.852	0.052
	DXP + NADPH → ME4P	1.712	1.647	1.852	0.052
	ME4P + 3*ATP + 2*NADPH → IPP.p	1.712	1.647	1.852	0.052
Terpene biosynthesis	IPPm.p + IPPm.p → GPP.p	0.880	0.880	0.880	0.000
	GPP.p → monoterpene	0.880	0.880	0.880	0.000
	IPPs.c + IPPs.c → GPP.c	0.120	0.120	0.120	0.000
	GPP.c + IPPs.c → FPP	0.120	0.120	0.120	0.000
	FPP → sesquiterpene	0.120	0.120	0.120	0.000
Uptake /export	NADH.ext → NADH	0.000	0.000	1.100	0.281
	NADPH.ext → NADPH	0.132	0.000	2.373	0.605
	ATP.ext → ATP	0.000	0.000	2.751	0.702
	Gluc.ext + ATP → G6P	2.864	2.659	2.923	0.067
	Gluc.u + ATP → G6P	0.030	0.000	0.030	0.008
	0.12*sesquiterpene + 0.88*monoterpene → terpene.ext	1.000	1.000	1.000	0.000
	CO2 → CO2.ext	6.764	5.536	6.938	0.358
Transport	PYR ↔ PYR.m	2.394	1.917	2.558	0.164
	NADH → 2.5*ATP	4.009	2.947	4.151	0.307
	MAL ↔ MAL.m	1.223	0.804	1.419	0.157
	CIT.m ↔ CIT	1.223	0.804	1.419	0.157
	PYR ↔ PYR.p	0.000	-0.031	0.204	0.060
	IPP.c → IPPm.p	0.156	0.025	0.205	0.046
	IPP.p → IPPm.p	1.604	1.556	1.735	0.046
	IPP.p → IPPs.c	0.109	0.082	0.128	0.012
	IPP.c → IPPs.c	0.251	0.232	0.278	0.012

Table S13. Compound-dependent parameters of MRM acquisition method in LCMS.
Q1 and Q3 fragments of each mass isotopomer from every compound are listed. Retention time (RT), DP, CE, CXP and EP are specific for all mass isotopomers from one compound and listed as well.

Q1	Q3	RT	Compound name	DP	CE	CXP	EP
87.1	43	4.73	PYR	-40	-14	-1	-10
88.1	43	4.72	1-0X13C PYR	-40	-14	-1	-10
88.1	44	4.73	1-1X13C PYR	-40	-14	-1	-10
89.1	44	4.73	2-1X13C PYR	-40	-14	-1	-10
89.1	45	4.73	2-2X13C PYR	-40	-14	-1	-10
90.1	45	4.73	3-2X13C PYR	-40	-14	-1	-10
215	79.1	7.67	MEP	-26	-45	-18	-10
216	79.1	7.67	1-0x13C-MEP	-26	-45	-18	-10
217	79.1	7.67	2-0x13C-MEP	-26	-45	-18	-10
218	79.1	7.67	3-0x13C-MEP	-26	-45	-18	-10
219	79.1	7.67	4-0x13C-MEP	-26	-45	-18	-10
220	79.1	7.67	5-0x13C-MEP	-26	-45	-18	-10
213	97	8.63	DXP-1	-5	-16	-21	-10
214	97	8.63	1-0x13C-DXP	-5	-16	-21	-10
215	97	8.63	2-0x13C-DXP	-5	-16	-21	-10
216	97	8.63	3-0x13C-DXP	-5	-16	-21	-10
217	97	8.63	4-0x13C-DXP	-5	-16	-21	-10
218	97	8.63	5-0x13C-DXP	-5	-16	-21	-10
213	138.9	8.63	DXP-2	-26	-19	-24	-10
214	138.9	8.63	1-0x13C-DXP	-26	-19	-24	-10
214	140	8.63	1-1x13C-DXP	-26	-19	-24	-10
215	138.9	8.63	2-0x13C-DXP	-26	-19	-24	-10
215	140	8.63	2-1x13C-DXP	-26	-19	-24	-10
215	141	8.63	2-2x13C-DXP	-26	-19	-24	-10
216	138.9	8.63	3-0x13C-DXP	-26	-19	-24	-10
216	140	8.63	3-1x13C-DXP	-26	-19	-24	-10
216	141	8.63	3-2x13C-DXP	-26	-19	-24	-10
217	140	8.63	4-1x13C-DXP	-26	-19	-24	-10
217	141	8.63	4-2x13C-DXP	-26	-19	-24	-10
218	141	8.63	5-2x13C-DXP	-26	-19	-24	-10
169	97.1	7.21	GAP	-36	-19	-6	-10
170	97.1	7.21	1-0x13C-GAP	-36	-19	-6	-10
171	97.1	7.21	2-0x13C-GAP	-36	-19	-6	-10
172	97.1	7.21	3-0x13C-GAP	-36	-19	-6	-10
277	78.9	11.2	MEcPP	-43	-71	-17	-10
278	78.9	11.2	1-0x13C-MEcPP	-43	-71	-17	-10
279	78.9	11.2	2-0x13C-MEcPP	-43	-71	-17	-10
280	78.9	11.2	3-0x13C-MEcPP	-43	-71	-17	-10
281	78.9	11.2	4-0x13C-MEcPP	-43	-71	-17	-10
282	78.9	11.2	5-0x13C-MEcPP	-43	-71	-17	-10
227.1	97	13.32	MVA5P-1	-31	-18	-27	-10
228.1	97	13.32	1-0X13C MVA5P	-31	-18	-27	-10
229.1	97	13.32	2-0X13C MVA5P	-31	-18	-27	-10
230.1	97	13.32	3-0X13C MVA5P	-31	-18	-27	-10
231.1	97	13.32	4-0X13C MVA5P	-31	-18	-27	-10
232.1	97	13.32	5-0X13C MVA5P	-31	-18	-27	-10
233.1	97	13.32	6-0X13C MVA5P	-31	-18	-27	-10
227.1	165.2	13.32	MVA5P-2	-73	-22	-12	-10
228.1	165.2	13.32	1-0x13C-MVA5P	-73	-22	-12	-10
228.1	166.2	13.32	1-1x13C-MVA5P	-73	-22	-12	-10
229.1	166.2	13.32	2-1x13C-MVA5P	-73	-22	-12	-10
229.1	167.2	13.32	2-2x13C-MVA5P	-73	-22	-12	-10
230.1	167.2	13.32	3-2x13C-MVA5P	-73	-22	-12	-10
230.1	168.2	13.32	3-3x13C-MVA5P	-73	-22	-12	-10
231.1	168.2	13.32	4-3x13C-MVA5P	-73	-22	-12	-10
231.1	169.2	13.32	4-4x13C-MVA5P	-73	-22	-12	-10
232.1	169.2	13.32	5-4x13C-MVA5P	-73	-22	-12	-10
232.1	170.2	13.32	5-5x13C-MVA5P	-73	-22	-12	-10
233.1	170.2	13.32	6-5x13C-MVA5P	-73	-22	-12	-10
261	79	13.93	HMBPP	-40	-52	-9	-10
262	79	13.93	1-0x13C-HMBPP	-40	-52	-9	-10
263	79	13.93	2-0x13C-HMBPP	-40	-52	-9	-10
264	79	13.93	3-0x13C-HMBPP	-40	-52	-9	-10
265	79	13.93	4-0x13C-HMBPP	-40	-52	-9	-10
266	79	13.93	5-0x13C-HMBPP	-40	-52	-9	-10

Appendix

Q1	Q3	RT	Compound name	DP	CE	CXP	EP
245	78.9	15.23	IPP/DMAPP	-15	-44	-37	-10
246	78.9	15.23	1-0x13C-IPP/DMAPP	-15	-44	-37	-10
247	78.9	15.23	2-0x13C-IPP/DMAPP	-15	-44	-37	-10
248	78.9	15.23	3-0x13C-IPP/DMAPP	-15	-44	-37	-10
249	78.9	15.23	4-0x13C-IPP/DMAPP	-15	-44	-37	-10
250	78.9	15.23	5-0x13C-IPP/DMAPP	-15	-44	-37	-10
600	78.9	16.47	CDPMEP	-115	-126	-19	-10
601	78.9	16.47	1-0x13C-CDPMEP	-115	-126	-19	-10
602	78.9	16.47	2-0x13C-CDPMEP	-115	-126	-19	-10
603	78.9	16.47	3-0x13C-CDPMEP	-115	-126	-19	-10
604.1	78.9	16.47	4-0x13C-CDPMEP	-115	-126	-19	-10
605.1	78.9	16.47	5-0x13C-CDPMEP	-115	-126	-19	-10
307	78.9	16.62	MVAPP-1	-35	-75	-19	-10
308	78.9	16.62	1-0X13C MVAPP	-35	-75	-19	-10
309	78.9	16.62	2-0X13C MVAPP	-35	-75	-19	-10
310	78.9	16.62	3-0X13C MVAPP	-35	-75	-19	-10
311	78.9	16.62	4-0X13C MVAPP	-35	-75	-19	-10
312	78.9	16.62	5-0X13C MVAPP	-35	-75	-19	-10
313	78.9	16.62	6-0X13C MVAPP	-35	-75	-19	-10
307	165.2	16.62	MVAPP-2	-53	-23	-12	-10
308	165.2	16.62	1-0x13C-MVAPP	-53	-23	-12	-10
308	166.2	16.62	1-1x13C-MVAPP	-53	-23	-12	-10
309	166.2	16.62	2-1x13C-MVAPP	-53	-23	-12	-10
309	167.2	16.62	2-2x13C-MVAPP	-53	-23	-12	-10
310	167.2	16.62	3-2x13C-MVAPP	-53	-23	-12	-10
310	168.2	16.62	3-3x13C-MVAPP	-53	-23	-12	-10
311	168.2	16.62	4-3x13C-MVAPP	-53	-23	-12	-10
311	169.2	16.62	4-4x13C-MVAPP	-53	-23	-12	-10
312	169.2	16.62	5-4x13C-MVAPP	-53	-23	-12	-10
312	170.2	16.62	5-5x13C-MVAPP	-53	-23	-12	-10
313	170.2	16.62	6-5x13C-MVAPP	-53	-23	-12	-10
313.2	78.9	19.12	GPP	-34	-59	-22	-10
314.2	78.9	19.12	1-0X13C GPP	-34	-59	-22	-10
315.2	78.9	19.12	2-0X13C GPP	-34	-59	-22	-10
316.2	78.9	19.12	3-0X13C GPP	-34	-59	-22	-10
317.2	78.9	19.12	4-0X13C GPP	-34	-59	-22	-10
318.2	78.9	19.12	5-0X13C GPP	-34	-59	-22	-10
319.2	78.9	19.12	6-0X13C GPP	-34	-59	-22	-10
320.2	78.9	19.12	7-0X13C GPP	-34	-59	-22	-10
321.2	78.9	19.12	8-0X13C GPP	-34	-59	-22	-10
322.2	78.9	19.12	9-0X13C GPP	-34	-59	-22	-10
323.2	78.9	19.12	10-0X13C GPP	-34	-59	-22	-10
167	78.9	14.53	PEP-1	-30	-21	-9	-10
168	78.9	14.53	1-0x13C-PEP	-30	-21	-9	-10
169	78.9	14.53	2-0x13C-PEP	-30	-21	-9	-10
170	78.9	14.53	3-0x13C-PEP	-30	-21	-9	-10
167	139.1	14.53	PEP-2	-30	-10	-12	-10
168	139.1	14.53	1-0x13C-PEP	-30	-10	-12	-10
168	140.1	14.53	1-1x13C-PEP	-30	-10	-12	-10
169	140.1	14.53	2-1x13C-PEP	-30	-10	-12	-10
169	141.1	14.53	2-2x13C-PEP	-30	-10	-12	-10
170	141.1	14.53	3-2x13C-PEP	-30	-10	-12	-10
185	79.01	13.76	PG (2PGA + 3PGA)	-35	-20	-30	-10
186	79.01	13.76	1-0x13C-PG	-35	-20	-30	-10
187	79.01	13.76	2-0x13C-PG	-35	-20	-30	-10
188	79.01	13.76	3-0x13C-PG	-35	-20	-30	-10
259.1	97	6.37	H6P (G6P+F6P)-1	-50	-25	-15	-10
260.1	97	6.37	1-0x13C-H6P	-50	-25	-15	-10
261.1	97	6.37	2-0x13C-H6P	-50	-25	-15	-10
262.1	97	6.37	3-0x13C-H6P	-50	-25	-15	-10
263.1	97	6.37	4-0x13C-H6P	-50	-25	-15	-10
264.1	97	6.37	5-0x13C-H6P	-50	-25	-15	-10
265.1	97	6.37	6-0x13C-H6P	-50	-25	-15	-10
259.1	139	6.37	H6P (G6P+F6P)-2	-59	-22	-7	-10
260.1	139	6.37	1-0x13C-H6P	-59	-22	-7	-10
260.1	140	6.37	1-1x13C-H6P	-59	-22	-7	-10
261.1	139	6.37	2-0x13C-H6P	-59	-22	-7	-10
261.1	140	6.37	2-1x13C-H6P	-59	-22	-7	-10
261.1	141	6.37	2-2x13C-H6P	-59	-22	-7	-10

Q1	Q3	RT	Compound name	DP	CE	CXP	EP
262.1	139	6.37	3-0x13C-H6P	-59	-22	-7	-10
262.1	140	6.37	3-1x13C-H6P	-59	-22	-7	-10
262.1	141	6.37	3-2x13C-H6P	-59	-22	-7	-10
263.1	139	6.37	4-0x13C-H6P	-59	-22	-7	-10
263.1	140	6.37	4-1x13C-H6P	-59	-22	-7	-10
263.1	141	6.37	4-2x13C-H6P	-59	-22	-7	-10
264.1	140	6.37	5-1x13C-H6P	-59	-22	-7	-10
264.1	141	6.37	5-2x13C-H6P	-59	-22	-7	-10
265.1	141	6.37	6-2x13C-H6P	-59	-22	-7	-10
259.1	169.1	6.37	H6P (G6P+F6P)-3	-52	-15	-11	-10
260.1	169.1	6.37	1-0x13C-H6P	-52	-15	-11	-10
260.1	170.1	6.37	1-1x13C-H6P	-52	-15	-11	-10
261.1	169.1	6.37	2-0x13C-H6P	-52	-15	-11	-10
261.1	170.1	6.37	2-1x13C-H6P	-52	-15	-11	-10
261.1	171.1	6.37	2-2x13C-H6P	-52	-15	-11	-10
262.1	169.1	6.37	3-0x13C-H6P	-52	-15	-11	-10
262.1	170.1	6.37	3-1x13C-H6P	-52	-15	-11	-10
262.1	171.1	6.37	3-2x13C-H6P	-52	-15	-11	-10
262.1	172.1	6.37	3-3x13C-H6P	-52	-15	-11	-10
263.1	170.1	6.37	4-1x13C-H6P	-52	-15	-11	-10
263.1	171.1	6.37	4-2x13C-H6P	-52	-15	-11	-10
263.1	172.1	6.37	4-3x13C-H6P	-52	-15	-11	-10
264.1	171.1	6.37	5-2x13C-H6P	-52	-15	-11	-10
264.1	172.1	6.37	5-3x13C-H6P	-52	-15	-11	-10
265.1	172.1	6.37	6-3x13C-H6P	-52	-15	-11	-10
259.1	199.1	6.37	H6P (G6P+F6P)-4	-50	-15	-5	-10
260.1	199.1	6.37	1-0x13C-H6P	-50	-15	-5	-10
260.1	200.1	6.37	1-1x13C-H6P	-50	-15	-5	-10
261.1	199.1	6.37	2-0x13C-H6P	-50	-15	-5	-10
261.1	200.1	6.37	2-1x13C-H6P	-50	-15	-5	-10
261.1	201.1	6.37	2-2x13C-H6P	-50	-15	-5	-10
262.1	200.1	6.37	3-1x13C-H6P	-50	-15	-5	-10
262.1	201.1	6.37	3-2x13C-H6P	-50	-15	-5	-10
262.1	202.1	6.37	3-3x13C-H6P	-50	-15	-5	-10
263.1	201.1	6.37	4-2x13C-H6P	-50	-15	-5	-10
263.1	202.1	6.37	4-3x13C-H6P	-50	-15	-5	-10
263.1	203.1	6.37	4-4x13C-H6P	-50	-15	-5	-10
264.1	202.1	6.37	5-3x13C-H6P	-50	-15	-5	-10
264.1	203.1	6.37	5-4x13C-H6P	-50	-15	-5	-10
265.1	203.1	6.37	6-4x13C-H6P	-50	-15	-5	-10
289.2	97	6.96	S7P	-55	-25	-10	-10
290.2	97	6.96	1-0x13C-S7P	-55	-25	-10	-10
291.2	97	6.96	2-0x13C-S7P	-55	-25	-10	-10
292.2	97	6.96	3-0x13C-S7P	-55	-25	-10	-10
293.2	97	6.96	4-0x13C-S7P	-55	-25	-10	-10
294.2	97	6.96	5-0x13C-S7P	-55	-25	-10	-10
295.2	97	6.96	6-0x13C-S7P	-55	-25	-10	-10
296.2	97	6.96	7-0x13C-S7P	-55	-25	-10	-10
369	97	16.61	SBP	-35	-22	-11	-10
370	97	16.61	1-0x13C-SBP	-35	-22	-11	-10
371	97	16.61	2-0x13C-SBP	-35	-22	-11	-10
372	97	16.61	3-0x13C-SBP	-35	-22	-11	-10
373	97	16.61	4-0x13C-SBP	-35	-22	-11	-10
374	97	16.61	5-0x13C-SBP	-35	-22	-11	-10
375	97	16.61	6-0x13C-SBP	-35	-22	-11	-10
376	97	16.61	7-0x13C-SBP	-35	-22	-11	-10
339.1	96.9	16.17	FBP-1	-69	-52	-11	-10
340.1	96.9	16.17	1-0x13C-FBP	-69	-52	-11	-10
341.1	96.9	16.17	2-0x13C-FBP	-69	-52	-11	-10
342.1	96.9	16.17	3-0x13C-FBP	-69	-52	-11	-10
343.1	96.9	16.17	4-0x13C-FBP	-69	-52	-11	-10
344.1	96.9	16.17	5-0x13C-FBP	-69	-52	-11	-10
345.1	96.9	16.17	6-0x13C-FBP	-69	-52	-11	-10
339.1	138.9	16.17	FBP-2	-69	-30	-17	-10
340.1	138.9	16.17	1-0x13C-FBP	-69	-30	-17	-10
340.1	139.9	16.17	1-1x13C-FBP	-69	-30	-17	-10
341.1	138.9	16.17	2-0x13C-FBP	-69	-30	-17	-10
341.1	139.9	16.17	2-1x13C-FBP	-69	-30	-17	-10
341.1	140.9	16.17	2-2x13C-FBP	-69	-30	-17	-10

Appendix

Q1	Q3	RT	Compound name	DP	CE	CXP	EP
342.1	138.9	16.17	3-0x13C-FBP	-69	-30	-17	-10
342.1	139.9	16.17	3-1x13C-FBP	-69	-30	-17	-10
342.1	140.9	16.17	3-2x13C-FBP	-69	-30	-17	-10
343.1	138.9	16.17	4-0x13C-FBP	-69	-30	-17	-10
343.1	139.9	16.17	4-1x13C-FBP	-69	-30	-17	-10
343.1	140.9	16.17	4-2x13C-FBP	-69	-30	-17	-10
344.1	139.9	16.17	5-1x13C-FBP	-69	-30	-17	-10
344.1	140.9	16.17	5-2x13C-FBP	-69	-30	-17	-10
345.1	140.9	16.17	6-2x13C-FBP	-69	-30	-17	-10
309.1	97	16.39	RuBP	-35	-20	-27	-10
310.1	97	16.39	1-0x13C-RuBP	-35	-20	-27	-10
311.1	97	16.39	2-0x13C-RuBP	-35	-20	-27	-10
312.1	97	16.39	3-0x13C-RuBP	-35	-20	-27	-10
313.1	97	16.39	4-0x13C-RuBP	-35	-20	-27	-10
314.1	97	16.39	5-0x13C-RuBP	-35	-20	-27	-10
191	87	14.93	CIT-1	-40	-22	-15	-10
192	87	14.93	1-0x13C-CIT	-40	-22	-15	-10
192	88	14.93	1-1x13C-CIT	-40	-22	-15	-10
193	87	14.93	2-0x13C-CIT	-40	-22	-15	-10
193	88	14.93	2-1x13C-CIT	-40	-22	-15	-10
193	89	14.93	2-2x13C-CIT	-40	-22	-15	-10
194	87	14.93	3-0x13C-CIT	-40	-22	-15	-10
194	88	14.93	3-1x13C-CIT	-40	-22	-15	-10
194	89	14.93	3-2x13C-CIT	-40	-22	-15	-10
194	90	14.93	3-3x13C-CIT	-40	-22	-15	-10
195	88	14.93	4-1x13C-CIT	-40	-22	-15	-10
195	89	14.93	4-2x13C-CIT	-40	-22	-15	-10
195	90	14.93	4-3x13C-CIT	-40	-22	-15	-10
196	89	14.93	5-2x13C-CIT	-40	-22	-15	-10
196	90	14.93	5-3x13C-CIT	-40	-22	-15	-10
197	90	14.93	6-3x13C-CIT	-40	-22	-15	-10
191	84.9	14.93	CIT-2	-40	-25	-20	-10
192	84.9	14.93	1-0x13C-CIT	-40	-25	-20	-10
192	85.9	14.93	1-1x13C-CIT	-40	-25	-20	-10
193	84.9	14.93	2-0x13C-CIT	-40	-25	-20	-10
193	85.9	14.93	2-1x13C-CIT	-40	-25	-20	-10
193	86.9	14.93	2-2x13C-CIT	-40	-25	-20	-10
194	85.9	14.93	3-1x13C-CIT	-40	-25	-20	-10
194	86.9	14.93	3-2x13C-CIT	-40	-25	-20	-10
194	87.9	14.93	3-3x13C-CIT	-40	-25	-20	-10
195	86.9	14.93	4-2x13C-CIT	-40	-25	-20	-10
195	87.9	14.93	4-3x13C-CIT	-40	-25	-20	-10
195	88.9	14.93	4-4x13C-CIT	-40	-25	-20	-10
196	87.9	14.93	5-3x13C-CIT	-40	-25	-20	-10
196	88.9	14.93	5-4x13C-CIT	-40	-25	-20	-10
197	88.9	14.93	6-4x13C-CIT	-40	-25	-20	-10
191	172.9	14.93	CIT-3	-40	-12	-10	-10
192	173.9	14.93	1-1x13C-CIT	-40	-12	-10	-10
193	174.9	14.93	2-2x13C-CIT	-40	-12	-10	-10
194	175.9	14.93	3-3x13C-CIT	-40	-12	-10	-10
195	176.9	14.93	4-4x13C-CIT	-40	-12	-10	-10
196	177.9	14.93	5-5x13C-CIT	-40	-12	-10	-10
197	178.9	14.93	6-6x13C-CIT	-40	-12	-10	-10
191	67	14.93	CIT-4	-40	-30	-12	-10
192	67	14.93	1-0x13C-CIT	-40	-30	-12	-10
192	68	14.93	1-1x13C-CIT	-40	-30	-12	-10
193	67	14.93	2-0x13C-CIT	-40	-30	-12	-10
193	68	14.93	2-1x13C-CIT	-40	-30	-12	-10
193	69	14.93	2-2x13C-CIT	-40	-30	-12	-10
194	68	14.93	3-1x13C-CIT	-40	-30	-12	-10
194	69	14.93	3-2x13C-CIT	-40	-30	-12	-10
194	70	14.93	3-3x13C-CIT	-40	-30	-12	-10
195	69	14.93	4-2x13C-CIT	-40	-30	-12	-10
195	70	14.93	4-3x13C-CIT	-40	-30	-12	-10
195	71	14.93	4-4x13C-CIT	-40	-30	-12	-10
196	70	14.93	5-3x13C-CIT	-40	-30	-12	-10
196	71	14.93	5-4x13C-CIT	-40	-30	-12	-10
197	71	14.93	6-4x13C-CIT	-40	-30	-12	-10
191	130.9	14.93	CIT-5	-40	-17	-7	-10

Q1	Q3	RT	Compound name	DP	CE	CXP	EP
192	130.9	14.93	1-0x13C-CIT	-40	-17	-7	-10
192	131.9	14.93	1-1x13C-CIT	-40	-17	-7	-10
193	130.9	14.93	2-0x13C-CIT	-40	-17	-7	-10
193	131.9	14.93	2-1x13C-CIT	-40	-17	-7	-10
193	132.9	14.93	2-2x13C-CIT	-40	-17	-7	-10
194	131.9	14.93	3-1x13C-CIT	-40	-17	-7	-10
194	132.9	14.93	3-2x13C-CIT	-40	-17	-7	-10
194	133.9	14.93	3-3x13C-CIT	-40	-17	-7	-10
195	132.9	14.93	4-2x13C-CIT	-40	-17	-7	-10
195	133.9	14.93	4-3x13C-CIT	-40	-17	-7	-10
195	134.9	14.93	4-4x13C-CIT	-40	-17	-7	-10
196	133.9	14.93	5-3x13C-CIT	-40	-17	-7	-10
196	134.9	14.93	5-4x13C-CIT	-40	-17	-7	-10
197	134.9	14.93	6-4x13C-CIT	-40	-17	-7	-10
191.1	73	15.03	ISOCIT	-45	-28	-31	-10
192.1	73	15.03	1-0x13C-ISOCIT	-45	-20	-5	-10
192.1	74	15.03	1-1x13C-ISOCIT	-45	-20	-5	-10
193.1	73	15.03	2-0x13C-ISOCIT	-45	-20	-5	-10
193.1	74	15.03	2-1x13C-ISOCIT	-45	-20	-5	-10
193.1	75	15.03	2-2x13C-ISOCIT	-45	-20	-5	-10
194.1	73	15.03	3-0x13C-ISOCIT	-45	-20	-5	-10
194.1	74	15.03	3-1x13C-ISOCIT	-45	-20	-5	-10
194.1	75	15.03	3-2x13C-ISOCIT	-45	-20	-5	-10
195.1	73	15.03	4-0x13C-ISOCIT	-45	-20	-5	-10
195.1	74	15.03	4-1x13C-ISOCIT	-45	-20	-5	-10
195.1	75	15.03	4-2x13C-ISOCIT	-45	-20	-5	-10
196.1	74	15.03	5-1x13C-ISOCIT	-45	-20	-5	-10
196.1	75	15.03	5-2x13C-ISOCIT	-45	-20	-5	-10
197.1	75	15.03	6-2x13C-ISOCIT	-45	-20	-5	-10
173.1	84.9	14.04	ACT	-30	-18	-7	-10
174.1	84.9	14.04	1-0x13C-ACT	-30	-18	-7	-10
174.1	86	14.04	1-1x13C-ACT	-30	-18	-7	-10
175.1	84.9	14.04	2-0x13C-ACT	-30	-18	-7	-10
175.1	86	14.04	2-1x13C-ACT	-30	-18	-7	-10
175.1	87	14.04	2-2x13C-ACT	-30	-18	-7	-10
176.1	86	14.04	3-1x13C-ACT	-30	-18	-7	-10
176.1	87	14.04	3-2x13C-ACT	-30	-18	-7	-10
176.1	88	14.04	3-3x13C-ACT	-30	-18	-7	-10
177.1	87	14.04	4-2x13C-ACT	-30	-18	-7	-10
177.1	88	14.04	4-3x13C-ACT	-30	-18	-7	-10
177.1	89	14.04	4-4x13C-ACT	-30	-18	-7	-10
178.1	88	14.04	5-3x13C-ACT	-30	-18	-7	-10
178.1	89	14.04	5-4x13C-ACT	-30	-18	-7	-10
179.1	89	14.04	6-4x13C-ACT	-30	-18	-7	-10
145.01	101	11.03	AKG	-10	-12	-13	-10
146.01	101	11.03	1-0x13C-AKG	-10	-12	-13	-10
146.01	102	11.03	1-1x13C-AKG	-10	-12	-13	-10
147.01	102	11.03	2-1x13C-AKG	-10	-12	-13	-10
147.01	103	11.03	2-2x13C-AKG	-10	-12	-13	-10
148.01	103	11.03	3-2x13C-AKG	-10	-12	-13	-10
148.01	104	11.03	3-3x13C-AKG	-10	-12	-13	-10
149.01	104	11.03	4-3x13C-AKG	-10	-12	-13	-10
149.01	105	11.03	4-4x13C-AKG	-10	-12	-13	-10
150.01	105	11.03	5-4x13C-AKG	-10	-12	-13	-10
117.11	99	10.16	SUC	-32	-14	-5	-10
118.11	100	10.16	1-1x13C-SUC	-32	-14	-5	-10
119.11	101	10.16	2-2x13C-SUC	-32	-14	-5	-10
120.11	102	10.16	3-3x13C-SUC	-32	-14	-5	-10
121.11	103	10.16	4-4x13C-SUC	-32	-14	-5	-10
131.1	87	11.19	OXA	-25	-10	-5	-10
132.1	87	11.19	1-0x13C-OXA	-25	-10	-5	-10
132.1	88	11.19	1-1x13C-OXA	-25	-10	-5	-10
133.1	88	11.19	2-1x13C-OXA	-25	-10	-5	-10
133.1	89	11.19	2-2x13C-OXA	-25	-10	-5	-10
134.1	89	11.19	3-2x13C-OXA	-25	-10	-5	-10
134.1	90	11.19	3-3x13C-OXA	-25	-10	-5	-10
135.1	90	11.19	4-3x13C-OXA	-25	-10	-5	-10
173.2	131	0.62	ARG	-50	-18	-7	-10
174.2	131	0.62	1-0X13C ARG	-50	-18	-7	-10

Appendix

Q1	Q3	RT	Compound name	DP	CE	CXP	EP
174.2	132	0.62	1-1X13C ARG	-50	-18	-7	-10
175.2	132	0.62	2-1X13C ARG	-50	-18	-7	-10
175.2	133	0.62	2-2X13C ARG	-50	-18	-7	-10
176.2	133	0.62	3-2X13C ARG	-50	-18	-7	-10
176.2	134	0.62	3-3X13C ARG	-50	-18	-7	-10
177.2	134	0.62	4-3X13C ARG	-50	-18	-7	-10
177.2	135	0.62	4-4X13C ARG	-50	-18	-7	-10
178.2	135	0.62	5-4X13C ARG	-50	-18	-7	-10
178.2	136	0.62	5-5X13C ARG	-50	-18	-7	-10
179.2	136	0.62	6-5X13C ARG	-50	-18	-7	-10
132	88	1.77	ASP	-40	-18	-10	-10
133	88	1.77	1-0X13C ASP	-40	-18	-10	-10
133	89	1.77	1-1X13C ASP	-40	-18	-10	-10
134	89	1.77	2-1X13C ASP	-40	-18	-10	-10
134	90	1.77	2-2X13C ASP	-40	-18	-10	-10
135	90	1.77	3-2X13C ASP	-40	-18	-10	-10
135	91	1.77	3-3X13C ASP	-40	-18	-10	-10
136	91	1.77	4-3X13C ASP	-40	-18	-10	-10
146	102	1.79	GLU	-72	-18	-9	-10
147	102	1.79	1-0X13C GLU	-72	-18	-9	-10
147	103	1.79	1-1X13C GLU	-72	-18	-9	-10
148	103	1.79	2-1X13C GLU	-72	-18	-9	-10
148	104	1.79	2-2X13C GLU	-72	-18	-9	-10
149	104	1.79	3-2X13C GLU	-72	-18	-9	-10
149	105	1.79	3-3X13C GLU	-72	-18	-9	-10
150	105	1.79	4-3X13C GLU	-72	-18	-9	-10
150	106	1.79	4-4X13C GLU	-72	-18	-9	-10
151	106	1.79	5-4X13C GLU	-72	-18	-9	-10
145.1	108.9	0.68	GLN	-30	-18	-5	-10
146.1	109.9	0.68	1-1X13C GLN	-30	-18	-5	-10
147.1	110.9	0.68	2-2X13C GLN	-30	-18	-5	-10
148.1	111.9	0.68	3-3X13C GLN	-30	-18	-5	-10
149.1	112.9	0.68	4-4X13C GLN	-30	-18	-5	-10
150.1	113.9	0.68	5-5X13C GLN	-30	-18	-5	-10
154.2	93	0.65	HIS	-40	-24	-3	-10
155.2	93	0.65	1-0X13C HIS	-40	-24	-3	-10
155.2	94	0.65	1-1X13C HIS	-40	-24	-3	-10
156.2	94	0.65	2-1X13C HIS	-40	-24	-3	-10
156.2	95	0.65	2-2X13C HIS	-40	-24	-3	-10
157.2	95	0.65	3-2X13C HIS	-40	-24	-3	-10
157.2	96	0.65	3-3X13C HIS	-40	-24	-3	-10
158.2	96	0.65	4-3X13C HIS	-40	-24	-3	-10
158.2	97	0.65	4-4X13C HIS	-40	-24	-3	-10
159.2	97	0.65	5-4X13C HIS	-40	-24	-3	-10
159.2	98	0.65	5-5X13C HIS	-40	-24	-3	-10
160.2	98	0.65	6-5X13C HIS	-40	-24	-3	-10
261.3	130.2	0.95	LEU+ILE	-30	-10	-1	-10
262.3	130.2	0.95	1-0X13C LEU+ILE	-30	-10	-1	-10
262.3	131.2	0.95	1-1X13C LEU+ILE	-30	-10	-1	-10
263.3	130.2	0.95	2-0X13C LEU+ILE	-30	-10	-1	-10
263.3	131.2	0.95	2-1X13C LEU+ILE	-30	-10	-1	-10
263.3	132.2	0.95	2-2X13C LEU+ILE	-30	-10	-1	-10
264.3	130.2	0.95	3-0X13C LEU+ILE	-30	-10	-1	-10
264.3	131.2	0.95	3-1X13C LEU+ILE	-30	-10	-1	-10
264.3	132.2	0.95	3-2X13C LEU+ILE	-30	-10	-1	-10
264.3	133.2	0.95	3-3X13C LEU+ILE	-30	-10	-1	-10
265.3	130.2	0.95	4-0X13C LEU+ILE	-30	-10	-1	-10
265.3	131.2	0.95	4-1X13C LEU+ILE	-30	-10	-1	-10
265.3	132.2	0.95	4-2X13C LEU+ILE	-30	-10	-1	-10
265.3	133.2	0.95	4-3X13C LEU+ILE	-30	-10	-1	-10
265.3	134.2	0.95	4-4X13C LEU+ILE	-30	-10	-1	-10
266.3	130.2	0.95	5-0X13C LEU+ILE	-30	-10	-1	-10
266.3	131.2	0.95	5-1X13C LEU+ILE	-30	-10	-1	-10
266.3	132.2	0.95	5-2X13C LEU+ILE	-30	-10	-1	-10
266.3	133.2	0.95	5-3X13C LEU+ILE	-30	-10	-1	-10
266.3	134.2	0.95	5-4X13C LEU+ILE	-30	-10	-1	-10
266.3	135.2	0.95	5-5X13C LEU+ILE	-30	-10	-1	-10
267.3	130.2	0.95	6-0X13C LEU+ILE	-30	-10	-1	-10
267.3	131.2	0.95	6-1X13C LEU+ILE	-30	-10	-1	-10

Q1	Q3	RT	Compound name	DP	CE	CXP	EP
267.3	132.2	0.95	6-2X13C LEU+ILE	-30	-10	-1	-10
267.3	133.2	0.95	6-3X13C LEU+ILE	-30	-10	-1	-10
267.3	134.2	0.95	6-4X13C LEU+ILE	-30	-10	-1	-10
267.3	135.2	0.95	6-5X13C LEU+ILE	-30	-10	-1	-10
267.3	136.2	0.95	6-6X13C LEU+ILE	-30	-10	-1	-10
268.3	131.2	0.95	7-1X13C LEU+ILE	-30	-10	-1	-10
268.3	132.2	0.95	7-2X13C LEU+ILE	-30	-10	-1	-10
268.3	133.2	0.95	7-3X13C LEU+ILE	-30	-10	-1	-10
268.3	134.2	0.95	7-4X13C LEU+ILE	-30	-10	-1	-10
268.3	135.2	0.95	7-5X13C LEU+ILE	-30	-10	-1	-10
268.3	136.2	0.95	7-6X13C LEU+ILE	-30	-10	-1	-10
269.3	132.2	0.95	8-2X13C LEU+ILE	-30	-10	-1	-10
269.3	133.2	0.95	8-3X13C LEU+ILE	-30	-10	-1	-10
269.3	134.2	0.95	8-4X13C LEU+ILE	-30	-10	-1	-10
269.3	135.2	0.95	8-5X13C LEU+ILE	-30	-10	-1	-10
269.3	136.2	0.95	8-6X13C LEU+ILE	-30	-10	-1	-10
270.3	133.2	0.95	9-3X13C LEU+ILE	-30	-10	-1	-10
270.3	134.2	0.95	9-4X13C LEU+ILE	-30	-10	-1	-10
270.3	135.2	0.95	9-5X13C LEU+ILE	-30	-10	-1	-10
270.3	136.2	0.95	9-6X13C LEU+ILE	-30	-10	-1	-10
271.3	134.2	0.95	10-4X13C LEU+ILE	-30	-10	-1	-10
271.3	135.2	0.95	10-5X13C LEU+ILE	-30	-10	-1	-10
271.3	136.2	0.95	10-6X13C LEU+ILE	-30	-10	-1	-10
272.3	135.2	0.95	11-5X13C LEU+ILE	-30	-10	-1	-10
272.3	136.2	0.95	11-6X13C LEU+ILE	-30	-10	-1	-10
273.3	137.2	0.95	12-6X13C LEU+ILE	-30	-10	-1	-10
145.2	101	0.68	LYS	-65	-14	-5	-10
146.2	101	0.68	1-0X13C LYS	-65	-14	-5	-10
146.2	102	0.68	1-1X13C LYS	-65	-14	-5	-10
147.2	102	0.68	2-1X13C LYS	-65	-14	-5	-10
147.2	103	0.68	2-2X13C LYS	-65	-14	-5	-10
148.2	103	0.68	3-2X13C LYS	-65	-14	-5	-10
148.2	104	0.68	3-3X13C LYS	-65	-14	-5	-10
149.2	104	0.68	4-3X13C LYS	-65	-14	-5	-10
149.2	105	0.68	4-4X13C LYS	-65	-14	-5	-10
150.2	105	0.68	5-4X13C LYS	-65	-14	-5	-10
150.2	106	0.68	5-5X13C LYS	-65	-14	-5	-10
151.2	106	0.68	6-5X13C LYS	-65	-14	-5	-10
148.2	47	0.87	MET	-80	-28	-5	-10
149.2	47	0.87	1-0X13C MET	-80	-28	-5	-10
149.2	48	0.87	1-1X13C MET	-80	-28	-5	-10
150.2	48	0.87	2-1X13C MET	-80	-28	-5	-10
151.2	48	0.87	3-1X13C MET	-80	-28	-5	-10
152.2	48	0.87	4-1X13C MET	-80	-28	-5	-10
153.2	48	0.87	5-1X13C MET	-80	-28	-5	-10
164.2	103	1.6	PHE	-55	-24	-5	-10
165.2	103	1.6	1-0X13C PHE	-55	-24	-5	-10
165.2	104	1.6	1-1X13C PHE	-55	-24	-5	-10
166.2	104	1.6	2-1X13C PHE	-55	-24	-5	-10
166.2	105	1.6	2-2X13C PHE	-55	-24	-5	-10
167.2	105	1.6	3-2X13C PHE	-55	-24	-5	-10
167.2	106	1.6	3-3X13C PHE	-55	-24	-5	-10
168.2	106	1.6	4-3X13C PHE	-55	-24	-5	-10
168.2	107	1.6	4-4X13C PHE	-55	-24	-5	-10
169.2	107	1.6	5-4X13C PHE	-55	-24	-5	-10
169.2	108	1.6	5-5X13C PHE	-55	-24	-5	-10
170.2	108	1.6	6-5X13C PHE	-55	-24	-5	-10
170.2	109	1.6	6-6X13C PHE	-55	-24	-5	-10
171.2	109	1.6	7-6X13C PHE	-55	-24	-5	-10
171.2	110	1.6	7-7X13C PHE	-55	-24	-5	-10
172.2	110	1.6	8-7X13C PHE	-55	-24	-5	-10
172.2	111	1.6	8-8X13C PHE	-55	-24	-5	-10
173.2	111	1.6	9-8X13C PHE	-55	-24	-5	-10
114.1	86	0.69	PRO	-55	-18	-3	-10
115.1	86	0.69	1-0X13C PRO	-55	-18	-3	-10
115.1	87	0.69	1-1X13C PRO	-55	-18	-3	-10
116.1	87	0.69	2-1X13C PRO	-55	-18	-3	-10
116.1	88	0.69	2-2X13C PRO	-55	-18	-3	-10
117.1	88	0.69	3-2X13C PRO	-55	-18	-3	-10

144

Appendix

Q1	Q3	RT	Compound name	DP	CE	CXP	EP
117.1	89	0.69	3-3X13C PRO	-55	-18	-3	-10
118.1	89	0.69	4-3X13C PRO	-55	-18	-3	-10
118.1	90	0.69	4-4X13C PRO	-55	-18	-3	-10
119.1	90	0.69	5-4X13C PRO	-55	-18	-3	-10
104.1	74	0.67	SER	-20	-16	-3	-10
105.1	74	0.67	1-0X13C SER	-20	-16	-3	-10
105.1	75	0.67	1-1X13C SER	-20	-16	-3	-10
106.1	75	0.67	2-1X13C SER	-20	-16	-3	-10
106.1	76	0.67	2-2X13C SER	-20	-16	-3	-10
107.1	76	0.67	3-2X13C SER	-20	-16	-3	-10
118.1	73.9	0.68	THR	-25	-14	-7	-10
119.1	73.9	0.68	1-0X13C THR	-25	-14	-7	-10
119.1	74.9	0.68	1-1X13C THR	-25	-14	-7	-10
120.1	73.9	0.68	2-0X13C THR	-25	-14	-7	-10
120.1	74.9	0.68	2-1X13C THR	-25	-14	-7	-10
120.1	75.9	0.68	2-2X13C THR	-25	-14	-7	-10
121.1	74.9	0.68	3-1X13C THR	-25	-14	-7	-10
121.1	75.9	0.68	3-2X13C THR	-25	-14	-7	-10
122.1	75.9	0.68	4-2X13C THR	-25	-14	-7	-10
203.2	116.2	2.49	TRP	-50	-22	-7	-10
204.2	116.2	2.49	1-0X13C TRP	-50	-22	-7	-10
204.2	117.2	2.49	1-1X13C TRP	-50	-22	-7	-10
205.2	116.2	2.49	2-0X13C TRP	-50	-22	-7	-10
205.2	117.2	2.49	2-1X13C TRP	-50	-22	-7	-10
205.2	118.2	2.49	2-2X13C TRP	-50	-22	-7	-10
206.2	116.2	2.49	3-0X13C TRP	-50	-22	-7	-10
206.2	117.2	2.49	3-1X13C TRP	-50	-22	-7	-10
206.2	118.2	2.49	3-2X13C TRP	-50	-22	-7	-10
206.2	119.2	2.49	3-3X13C TRP	-50	-22	-7	-10
207.2	117.2	2.49	4-1X13C TRP	-50	-22	-7	-10
207.2	118.2	2.49	4-2X13C TRP	-50	-22	-7	-10
207.2	119.2	2.49	4-3X13C TRP	-50	-22	-7	-10
207.2	120.2	2.49	4-4X13C TRP	-50	-22	-7	-10
208.2	118.2	2.49	5-2X13C TRP	-50	-22	-7	-10
208.2	119.2	2.49	5-3X13C TRP	-50	-22	-7	-10
208.2	120.2	2.49	5-4X13C TRP	-50	-22	-7	-10
208.2	121.2	2.49	5-5X13C TRP	-50	-22	-7	-10
209.2	119.2	2.49	6-3X13C TRP	-50	-22	-7	-10
209.2	120.2	2.49	6-4X13C TRP	-50	-22	-7	-10
209.2	121.2	2.49	6-5X13C TRP	-50	-22	-7	-10
209.2	122.2	2.49	6-6X13C TRP	-50	-22	-7	-10
210.2	120.2	2.49	7-4X13C TRP	-50	-22	-7	-10
210.2	121.2	2.49	7-5X13C TRP	-50	-22	-7	-10
210.2	122.2	2.49	7-6X13C TRP	-50	-22	-7	-10
210.2	123.2	2.49	7-7X13C TRP	-50	-22	-7	-10
211.2	121.2	2.49	8-5X13C TRP	-50	-22	-7	-10
211.2	122.2	2.49	8-6X13C TRP	-50	-22	-7	-10
211.2	123.2	2.49	8-7X13C TRP	-50	-22	-7	-10
211.2	124.2	2.49	8-8X13C TRP	-50	-22	-7	-10
212.2	122.2	2.49	9-6X13C TRP	-50	-22	-7	-10
212.2	123.2	2.49	9-7X13C TRP	-50	-22	-7	-10
212.2	124.2	2.49	9-8X13C TRP	-50	-22	-7	-10
213.2	123.2	2.49	10-7X13C TRP	-50	-22	-7	-10
213.2	124.2	2.49	10-8X13C TRP	-50	-22	-7	-10
214.2	124.2	2.49	11-8X13C TRP	-50	-22	-7	-10
259.1	240.8	6.17	G1P	-54	-19	-9	-10
260.1	241.8	6.17	1-1X13C G1P	-54	-19	-9	-10
261.1	242.8	6.17	2-2X13C G1P	-54	-19	-9	-10
262.1	243.8	6.17	3-3X13C G1P	-54	-19	-9	-10
263.1	244.8	6.17	4-4X13C G1P	-54	-19	-9	-10
264.1	245.8	6.17	5-5X13C G1P	-54	-19	-9	-10
265.1	246.8	6.17	6-6X13C G1P	-54	-19	-9	-10
115.1	71	10.5	FUM	-5	-12	-13	-10
116.1	71	10.5	1-0x13C-FUM	-5	-12	-13	-10
116.1	72	10.5	1-1x13C-FUM	-5	-12	-13	-10
117.1	72	10.5	2-1x13C-FUM	-5	-12	-13	-10
117.1	73	10.5	2-2x13C-FUM	-5	-12	-13	-10
118.1	73	10.5	3-2x13C-FUM	-5	-12	-13	-10
118.1	74	10.5	3-3x13C-FUM	-5	-12	-13	-10

Q1	Q3	RT	Compound name	DP	CE	CXP	EP
119.1	74	10.5	4-3x13C-FUM	-5	-12	-13	-10
133.1	115	10.72	MAL-1	-52	-16	-5	-10
134.1	116	10.72	1-1x13C-MAL	-52	-16	-5	-10
135.1	117	10.72	2-2x13C-MAL	-52	-16	-5	-10
136.1	118	10.72	3-3x13C-MAL	-52	-16	-5	-10
137.1	119	10.72	4-4x13C-MAL	-52	-16	-5	-10
133.1	71	10.72	MAL-2	-52	-20	-10	-10
134.1	71	10.72	1-0x13C-MAL	-52	-20	-10	-10
134.1	72	10.72	1-1x13C-MAL	-52	-20	-10	-10
135.1	72	10.72	2-1x13C-MAL	-52	-20	-10	-10
135.1	73	10.72	2-2x13C-MAL	-52	-20	-10	-10
136.1	73	10.72	3-2x13C-MAL	-52	-20	-10	-10
136.1	74	10.72	3-3x13C-MAL	-52	-20	-10	-10
137.1	74	10.72	4-3x13C-MAL	-52	-20	-10	-10
133.1	73	10.72	MAL-3	-52	-22	-15	-10
134.1	73	10.72	1-0x13C-MAL	-52	-22	-15	-10
134.1	74	10.72	1-1x13C-MAL	-52	-22	-15	-10
135.1	73	10.72	2-0x13C-MAL	-52	-22	-15	-10
135.1	74	10.72	2-1x13C-MAL	-52	-22	-15	-10
135.1	75	10.72	2-2x13C-MAL	-52	-22	-15	-10
136.1	74	10.72	3-1x13C-MAL	-52	-22	-15	-10
136.1	75	10.72	3-2x13C-MAL	-52	-22	-15	-10
137.1	75	10.72	4-2x13C-MAL	-52	-22	-15	-10
133.1	87.1	10.72	MAL-4	-52	-18	-10	-10
134.1	87.1	10.72	1-0x13C-MAL	-52	-18	-10	-10
134.1	88.1	10.72	1-1x13C-MAL	-52	-18	-10	-10
135.1	88.1	10.72	2-1x13C-MAL	-52	-18	-10	-10
135.1	89.1	10.72	2-2x13C-MAL	-52	-18	-10	-10
136.1	89.1	10.72	3-2x13C-MAL	-52	-18	-10	-10
136.1	90.1	10.72	3-3x13C-MAL	-52	-18	-10	-10
137.1	90.1	10.72	4-3x13C-MAL	-52	-18	-10	-10
133.1	89.1	10.72	MAL-5	-52	-18	-15	-10
134.1	89.1	10.72	1-0x13C-MAL	-52	-18	-15	-10
134.1	90.1	10.72	1-1x13C-MAL	-52	-18	-15	-10
135.1	90.1	10.72	2-1x13C-MAL	-52	-18	-15	-10
135.1	91.1	10.72	2-2x13C-MAL	-52	-18	-15	-10
136.1	91.1	10.72	3-2x13C-MAL	-52	-18	-15	-10
136.1	92.1	10.72	3-3x13C-MAL	-52	-18	-15	-10
137.1	92.1	10.72	4-3x13C-MAL	-52	-18	-15	-10
381.3	78.9	19.86	FPP	-43	-65	-21	-10
382.3	78.9	19.86	1-0X13C FPP	-43	-65	-21	-10
383.3	78.9	19.86	2-0X13C FPP	-43	-65	-21	-10
384.3	78.9	19.86	3-0X13C FPP	-43	-65	-21	-10
385.3	78.9	19.86	4-0X13C FPP	-43	-65	-21	-10
386.3	78.9	19.86	5-0X13C FPP	-43	-65	-21	-10
387.3	78.9	19.86	6-0X13C FPP	-43	-65	-21	-10
388.3	78.9	19.86	7-0X13C FPP	-43	-65	-21	-10
389.3	78.9	19.86	8-0X13C FPP	-43	-65	-21	-10
390.3	78.9	19.86	9-0X13C FPP	-43	-65	-21	-10
391.3	78.9	19.86	10-0X13C FPP	-43	-65	-21	-10
392.3	78.9	19.86	11-0X13C FPP	-43	-65	-21	-10
393.3	78.9	19.86	12-0X13C FPP	-43	-65	-21	-10
394.3	78.9	19.86	13-0X13C FPP	-43	-65	-21	-10
395.3	78.9	19.86	14-0X13C FPP	-43	-65	-21	-10
396.3	78.9	19.86	15-0X13C FPP	-43	-65	-21	-10
449.069	78.8	19.12	GGPP	-41	-85	-17	-10
450.069	78.8	19.12	1-0X13C GGPP	-41	-85	-17	-10
451.069	78.8	19.12	2-0X13C GGPP	-41	-85	-17	-10
452.069	78.8	19.12	3-0X13C GGPP	-41	-85	-17	-10
453.069	78.8	19.12	4-0X13C GGPP	-41	-85	-17	-10
454.069	78.8	19.12	5-0X13C GGPP	-41	-85	-17	-10
455.069	78.8	19.12	6-0X13C GGPP	-41	-85	-17	-10
456.069	78.8	19.12	7-0X13C GGPP	-41	-85	-17	-10
457.069	78.8	19.12	8-0X13C GGPP	-41	-85	-17	-10
458.069	78.8	19.12	9-0X13C GGPP	-41	-85	-17	-10
459.069	78.8	19.12	10-0X13C GGPP	-41	-85	-17	-10
460.069	78.8	19.12	11-0X13C GGPP	-41	-85	-17	-10
461.069	78.8	19.12	12-0X13C GGPP	-41	-85	-17	-10
462.069	78.8	19.12	13-0X13C GGPP	-41	-85	-17	-10

Appendix

Q1	Q3	RT	Compound name	DP	CE	CXP	EP
463.069	78.8	19.12	14-0X13C GGPP	-41	-85	-17	-10
464.069	78.8	19.12	15-0X13C GGPP	-41	-85	-17	-10
465.069	78.8	19.12	16-0X13C GGPP	-41	-85	-17	-10
466.069	78.8	19.12	17-0X13C GGPP	-41	-85	-17	-10
467.069	78.8	19.12	18-0X13C GGPP	-41	-85	-17	-10
468.069	78.8	19.12	19-0X13C GGPP	-41	-85	-17	-10
469.069	78.8	19.12	20-0X13C GGPP	-41	-85	-17	-10
229.1	96.8	7.5	P5P (RIBU5P + XU5P)	-42	-18	-10	-10
230.1	96.8	7.5	1-0x13C-P5P	-42	-18	-10	-10
231.1	96.8	7.5	2-0x13C-P5P	-42	-18	-10	-10
232.1	96.8	7.5	3-0x13CP5P	-42	-18	-10	-10
233.1	96.8	7.5	4-0x13C-P5P	-42	-18	-10	-10
234.1	96.8	7.5	5-0x13C-P5P	-42	-18	-10	-10
275	96.9	13	PG6	-57	-24	-5	-10
276	96.9	13	1-0x13C-PG6	-57	-24	-5	-10
277	96.9	13	2-0x13C-PG6	-57	-24	-5	-10
278	96.9	13	3-0x13C-PG6	-57	-24	-5	-10
279	96.9	13	4-0x13C-PG6	-57	-24	-5	-10
280	96.9	13	5-0x13C-PG6	-57	-24	-5	-10
281	96.9	13	6-0x13C-PG6	-57	-24	-5	-10
147.2	59.1	5	MVA-1	-45	-20	-7	-10
148.2	59.1	5	1-0X13C MVA	-45	-20	-7	-10
149.2	59.1	5	2-0X13C MVA	-45	-20	-7	-10
150.2	59.1	5	3-0X13C MVA	-45	-20	-7	-10
151.2	59.1	5	4-0X13C MVA	-45	-20	-7	-10
152.2	59.1	5	5-0X13C MVA	-45	-20	-7	-10
153.2	59.1	5	6-0X13C MVA	-45	-20	-7	-10
147.2	99.1	5	MVA-2	-29	-19	-5	-10
148.2	99.1	5	1-0x13C-MVA	-29	-19	-5	-10
148.2	100.1	5	1-1x13C-MVA	-29	-19	-5	-10
149.2	100.1	5	2-1x13C-MVA	-29	-19	-5	-10
149.2	101.1	5	2-2x13C-MVA	-29	-19	-5	-10
150.2	101.1	5	3-2x13C-MVA	-29	-19	-5	-10
150.2	102.1	5	3-3x13C-MVA	-29	-19	-5	-10
151.2	102.1	5	4-3x13C-MVA	-29	-19	-5	-10
151.2	103.1	5	4-4x13C-MVA	-29	-19	-5	-10
152.2	103.1	5	5-4x13C-MVA	-29	-19	-5	-10
152.2	104.1	5	5-5x13C-MVA	-29	-19	-5	-10
153.2	104.1	5	6-5x13C-MVA	-29	-19	-5	-10

Table S14. List of compounds and sum formula of their fragments.

All of these metabolites were initially included in the acquisition method for peppermint sample analysis and screened on the basis of peak abundance and their quality. Abbreviation: H6P- Hexose 6 phosphate (glucose 6-phosphate and fructose 6-phosphate); FBP- fructose bisphosphate; GAP- glyceraldehyde phosphate; PG- phosphoglycerate (2-phosphoglycerate and 3-phosphoglycerate); PEP- phosphoenolpyruvate; PYR- pyruvate; G1P- glucose 1-phosphate; PG6- 6-phosphogluconate; P5P- pentose 5-phosphate (ribulose 5-phosphate and xylulose 5-phosphate); S7P- sedoheptulose 7-phosphate; RuBP- ribulose bisphosphate; SBP- sedoheptulose bisphosphate; CIT- citrate; ISOCIT- isocitrate; ACT- aconitate; AKG- alpha-ketoglutarate; SUC- succinate; FUM- fumarate; MAL- malate; OXA- oxaloacetate; ARG- arginine; ASP- aspartate; GLU- glutamate; GLN- glutamine; HIS- histidine; LEU+ILE- leucine and isoleucine; LYS- lysine; MET- methionine; PHE- phenylalanine; PRO- proline; SER- serine; THR- threonine; TRP- tryptophan; MVA- mevalonate; MVA5P- mevalonate 5-phosphate; MVAPP- mevalonate pyrophosphate; FPP- farnesyl pyrophosphate; DXP- deoxy xylulose phosphate; MEP- methylerythritol phosphate; CDPMEP- cytidyldiphospho methyl erythritol phosphate; MEcPP- methyl erythritol cyclodiphosphate; HMBPP- Hydroxymethyl-but-2-enyl pyrophosphate; IPP/DMAPP- isopentenyl pyrophosphate and dimethylallyl pyrophosphate; GPP- geranyl pyrophosphate; GGPP- geranylgeranyl pyrophosphate.

Compound name	Q1	Q1 formula	Q3	Q3 formula	Peak quality from peppermint sample
H6P (G6P+F6P)-1			97	$H_2O_4P^-$	High abundance
H6P (G6P+F6P)-2			139	$C_2H_4O_5P^-$	Bad peak
H6P (G6P+F6P)-3	259.1	$C_6H_{12}O_9P^-$	169.1	$C_3H_6O_6P^-$	High abundance
H6P (G6P+F6P)-4			199.1	$C_4H_8O_7P^-$	Bad peak
FBP-1	339.1	$C_6H_{13}O_{12}P_2^-$	96.9	$H_2O_4P^-$	High abundance
FBP-2			138.9	$C_2H_4O_5P^-$	High abundance
GAP	169	$C_3H_6O_6P^-$	97.1	$H_2O_4P^-$	High abundance
PG (2PGA + 3PGA)	185	$C_3H_6O_7P^-$	79	O_3P^-	High abundance
PEP-1	167	$C_3H_4O_6P^-$	78.9	O_3P^-	High abundance
PEP-2			139.1	$C_2H_4O_5P^-$	High abundance
PYR	87.1	$C_3H_3O_3^-$	43	$C_2H_3O^-$	Bad peak
G1P	259.1	$C_6H_{12}O_9P^-$	240.8	$C_6H_{10}O_8P^-$	No peak found
PG6	275	$C_6H_{12}O_{10}P^-$	96.9	$H_2O_4P^-$	Low abundance
P5P (RIBU5P + XU5P)	229.1	$C_5H_{10}O_8P^-$	96.8	$H_2O_4P^-$	High abundance
S7P	289.2	$C_7H_{14}O_{10}P^-$	97	$H_2O_4P^-$	High abundance
RuBP	309.1	$C_5H_{11}O_{11}P_2^-$	97	$H_2O_4P^-$	High abundance
SBP	369	$C_7H_{15}O_{13}P_2^-$	97	$H_2O_4P^-$	High abundance
CIT-1			87	$C_3H_3O_3^-$	High abundance
CIT-2			84.9	$C_4H_5O_2^-$	Bad peak
CIT-3	191	$C_6H_7O_7^-$	172.9	$C_6H_5O_6^-$	High abundance
CIT-4			67	$C_4H_3O^-$	High abundance
CIT-5			130.9	$C_4H_3O_5^-$	High abundance

Appendix

Compound name	Q1	Q1 formula	Q3	Q3 formula	Peak quality from peppermint sample
ISOCIT	191.1	$C_6H_7O_7^-$	73	$C_2HO_3^-$	High abundance
ACT	173.1	$C_6H_5O_6^-$	84.9	$C_4H_5O_2^-$	High abundance
AKG	145	$C_5H_5O_5^-$	101	$C_4H_5O_3^-$	High abundance
SUC	117.11	$C_4H_5O_4^-$	99	$C_4H_3O_3^-$	Bad peak
FUM	115.1	$C_4H_3O_4^-$	71	$C_3H_3O_2^-$	Bad peak
MAL-1			115	$C_4H_3O_4^-$	High abundance
MAL-2			71	$C_3H_3O_2^-$	High abundance
MAL-3	133.1	$C_4H_5O_5^-$	73	$C_3H_5O_2^-$	Bad peak
MAL-4			87.1	$C_3H_3O_3^-$	High abundance
MAL-5			89.1	$C_3H_5O_3^-$	Bad peak
OAA	131.1	$C_4H_3O_5^-$	87	$C_3H_3O_3^-$	Bad peak
ARG	173.2	$C_6H_{13}N_4O_2^-$	131	$C_5H_{11}N_2O_2^-$	High abundance
ASP	132	$C_4H_6NO_4^-$	88	$C_3H_6NO_2^-$	High abundance
GLU	146	$C_5H_8NO_4^-$	102	$C_4H_8NO_2^-$	High abundance
GLN	145.1	$C_5H_9N_2O_3^-$	108.9	$C_5H_5N_2O^-$	High abundance
HIS	154.2	$C_6H_8N_3O_2^-$	93	$C_5H_5N_2^-$	High abundance
LEU+ILE	261.3	$C_{12}H_{25}N_2O_4^-$	130.2	$C_6H_{12}NO_2^-$	Bad peak
LYS	145.2	$C_6H_{13}N_2O_2^-$	101	$C_5H_{13}N_2^-$	High abundance
MET	148.2	$C_5H_{10}NO_2S^-$	47	CH_3S^-	Bad peak
PHE	164.2	$C_9H_{10}NO_2^-$	103	$C_8H_7^-$	High abundance
PRO	114.1	$C_5H_8NO_2^-$	86	$C_4H_6NO^-$	Low abundance
SER	104.1	$C_3H_6NO_3^-$	74	$C_2H_4NO_2^-$	High abundance
THR	118.1	$C_4H_8NO_3^-$	73.9	$C_2H_4NO_2^-$	Bad peak
TRP	203.2	$C_{11}H_{11}N_2O_2^-$	116.2	$C_8H_6N^-$	High abundance
MVA-1	147.2	$C_6H_{11}O_4^-$	59.1	$H_{11}O_3^-$	Bad peak
MVA-2			99.1	$C_5H_7O_2^-$	No peak found
MVA5P-1	227.1	$C_6H_{12}O_7P^-$	97	$H_2O_4P^-$	Low abundance
MVA5P-2			165.2	$C_5H_{10}O_4P^-$	No peak found
MVAPP-1	307	$C_6H_{13}O_{10}P_2^-$	78.9	O_3P^-	High abundance
MVAPP-2			165.2	$C_5H_{10}O_4P^-$	No peak found
FPP	381.3	$C_{15}H_{27}O_7P_2^-$	78.9	O_3P^-	No peak found
DXP-1	213	$C_5H_{10}O_7P^-$	97	$H_2O_4P^-$	High abundance
DXP-2			138.9	$C_2H_4O_5P^-$	Low abundance
MEP	215	$C_5H_{12}O_7P^-$	79.1	O_3P^-	No peak found
CDPMEP	600	$C_{14}H_{25}N_3O_{17}P_3^-$	78.9	O_3P^-	No peak found
MEcPP	277	$C_5H_{11}O_9P_2^-$	78.9	O_3P^-	High abundance
HMBPP	261	$C_5H_{11}O_8P_2^-$	79	O_3P^-	No peak found
IPP/DMAPP	245	$C_5H_{11}O_7P_2^-$	78.9	O_3P^-	High abundance
GPP	313.2	$C_{10}H_{19}O_7P_2^-$	78.9	O_3P^-	Low abundance
GGPP	449.069	$C_{20}H_{35}O_7P_2^-$	78.8	O_3P^-	No peak found

Data S1. Isotopomer network and MFA in oregano GTs.

Likewise, peppermint GTs, steady-state ^{13}C-MFA in oregano GTs was performed with similar network based on the isotope labeling measurement of sabinene hydrate (monoterpene) and bisabolene (sesquiterpene) from two parallel tracer studies (1-^{13}C$_1$ and 6-^{13}C$_1$). Although a third tracer experiment using 1,6-^{13}C$_2$ glucose was performed, the respective labeling data was not used for ^{13}C-MFA due to the detection of insufficient data quality for parallel MFA. All tracer experiments were replicated thrice and the replicate data sets were used for flux estimation. In total 5 monoterpene fragments (1 replicate of the 6-^{13}C$_1$ tracer experiment was not used due to insufficient data quality) and 6 sesquiterpene fragments resulting into 151 MID signals were used for parallel ^{13}C-MFA (Appendix table). The standard deviation of all mass isotopomers of each replicate was assigned based on linear scaling of the machine precision (0.3%) as formulated by Young et al., 2014 and reported in the user guidelines of INCA (Jazmin et al., 2014).

Isotopic steady-state ^{13}C-MFA was performed as described in section 2.3.7. (Peppermint model) with some modifications like follows.

1. All flux estimations were done by normalizing the terpene excretion rate to 1 (arbitrary unit). Unlike peppermint GT flux analysis, the upper bound of the ^{13}C-Glucose uptake was constrained to 4 (arbitrary unit) based on preliminary flux balance analysis computations which predicted a minimal requirement of 1.74 mol glucose for the biosynthesis of 1 mol terpene.

2. The ratio between monoterpene and sesquiterpene production was fixed to 88% to 12%, respectively. This was constrained according to the experimental outcome from 15 days aged leaf.

3. The maximum average ^{13}C enrichment into these two groups of volatiles from 15 days old leaves was 1.4%, the upper bound of the unlabeled glucose uptake was constrained to 0.03.

4. The estimated fluxes from the global best-fit solution were considered acceptable when the obtained variance-weighted sum of squared residuals (SSR) was below the χ^2 at a 95% confidence level ($\chi2\ 95\%,109 = 139.8$).

Data S2. Model reconstruction for oregano GTs.

Metabolic network of oregano GTs was built on the base of a compartmentalized model for peppermint GTs. The ^{13}C-MFA model was extended by the cytosolic biosynthetic pathway of sesquiterpene production. To quantify the cross-talk between MVA and DXP pathway with respect to mono- and sesquiterpene biosynthesis the model integrates the exchange of DXP- and MVA specific IPP between the cytosol and plastid, respectively. For the sake of simplicity, IPP was assumed to be the most important terpene precursor exchanged between the cytosol and plastid. The final metabolic network model used for ^{13}C-MFA comprises 40 biochemical reactions and 15 transport processes across four different compartments (i.e. cytosol, mitochondria, leucoplast, extracellular media). The reaction list of the oregano GT model is provided in the Appendix.

Data S3. Isotopic status of released CO_2 from CIT to AKG.

This is simplified theoretical calculation when the metabolic condition is assumed to be in steady-state and AKG is not produced from any unknown sources except the TCA cycle. Furthermore, the isotopic status of GLU or GLN suggested that there would not be any changes in the isotopic status when AKG is produced from these amino acids.

Average ^{13}C enrichment in CIT and ISOCIT = 45 mol%

Total ^{13}C enrichment in CIT and ISOCIT = 45 mol% × 6 = 270 mol%

Possible average ^{13}C enrichment in AKG, in the case of loss of $^{12}CO_2$ = 270 mol% ÷ 5 = 54 mol%

Actual average ^{13}C enrichment in AKG = 49.5 mol%

Therefore, isotopic status of released CO_2 = (49.5%-45%)^{12}C : (54%-49.5%)^{13}C = 1:1 (^{12}C:^{13}C)

Acknowledgement

For a rock to get shape into a fine structure, it needs to be molded by many hands. In the same manner, this thesis was made possible with the co-operation and guidance of many people. I would thus feel privileged to thank everyone who, knowingly or otherwise, has provided support, encouragement and assistance along the way.

First and foremost, I express my profound gratitude to my supervisor, Prof. Dr. Björn Junker, for his guidance and constant encouragement throughout the journey of my PhD work. I enjoyed every bit of discussion with him which helped me a lot to gain insight into the subject. He always motivated me and provided special attention in completing this academic exercise. I am very grateful to Prof. Dr. Degenhardt, an outstanding scientist who I admire, for allowing me to accomplish many of my analytical works in his lab. I also owe gratitude to the referees for their kind agreement to be the referee of this thesis.

I would like to express my thanks to Erasmus Mundus BRAVE program for financially supporting my research with a scholarship for 3 years. International office of Martin Luther University and Fazit foundation also supported me generously by providing thesis writing fellowship.

Especially my sincere and special thanks to Dr. Grafahrend-Belau, without whom the project would not have reached to this dimension. Her input and useful discussions have increased a lot of my understanding and knowledge of this project. I am deeply indebted to Dr. Noack and Dr. Raorane for their constant encouragement, inspiration and support. Dr. Raorane spent his time graciously to review this thesis and offer the invaluable suggestion for completing this seemingly never-ending task in a resplendent way. I would like to extend my sincere thanks to Dr. Lindemann and Mr. Mondal for all their help to learn about the terpenoid measurement in GCMS.

I am privileged to have a group of colleagues who are always ready to offer any help when needed. I thank Ms. Ernst, Ms. Aue, Ms. Junghanns, Mr. Richter and Ms. Biehain.

Lastly, but certainly not the least, I owe all my success to my family members. I would like to express my heartfelt gratitude to them for their enormous support and encouragement which kept me motivated for every aspect of my research not only during the time I worked on the thesis but all along the journey.

Curriculum Vitae

Name: Somnath Koley

Date of birth: 18/07/1991

Nationality: Indian

Personal address: Vill. P.O.: Joypur, District: Bankura, State: West Bengal, Pin code: 722138, India

Institutional affiliation: AG Biosynthese von Wirkstoffen, Institute of Pharmacy, Hoher Weg 8, 06120 Halle, Germany

Email: somnath.koley@pharmazie.uni-halle.de; somnathkoley5@gmail.com

Education

2008-2012	Palli Siksha Bhavana, Visva-Bharati University, WestBengal, India Bachelor of Science in Agriculture (Hons.)
2012-2014	Orissa University of Agriculture and Technology, Orissa, India Master of Science in Agriculture

Academic positions

2015-	PhD Student Department of Pharmaceutical Biology

Research Interests

Quantifying the plant metabolic network to understand the biochemical bottleneck and to improve the productivity of plant products.

Research Experience

- Completed M.Sc. dissertation on the topic: *"Studies on etiology and management of Alternaria leaf blight disease of tomato in Odisha"*
- Interpreting the contribution of two terpene biosynthetic pathways for volatile production and characterizing subcellular metabolism in trichome cell.
- Analysis of different intermediates of glycolytic, pentose phosphate, TCA, mevalonate and non-mevalonate pathway as well as amino acids, chlorophylls, carotenoids and terpenoids
- Designing, performing and depicting isotope labeling study
- Tissue and cell culture

Technical skills

- Analysis of metabolites in GCMS and LCMS
- In-depth analytical software knowledge and troubleshooting skills of LCMS machine
- Sample drying in speed vac, nitrogen evaporator and freeze dryer
- Basic knowledge in VANTED software for visualization and correlation of the metabolites
- Basic knowledge in fluorescence, phase contrast and stereomicroscopy
- Designing, establishing and management of *in vitro* experiments
- Phytopigment analysis in spectrophotometer
- Soil physicochemical analysis

Research grants and academic achievements

2019   Post-doctoral bursary from Donald Danforth Plant Science Center (St. Louis, U.S.A.)

2019   PhD thesis writing grant from Fazit-Stiftung

2017   PhD finalization grant from DAAD

2014   PhD funding scholarship from ERASMUS MUNDUS action 2 programme (BRAVE project)

2010   Outstanding student award in class 10th (1st rank) and B.Sc. (3rd rank)

Publications

2019   Koley S, Raorane ML and Junker BH. Shoot-tip culture: a step towards 13C metabolite flux analysis of sink leaf metabolism. Plant Methods, 15(1): 48, 2019.

2019   Koley S, Grafahrend-Belau E, Raorane ML and Junker BH. Monoterpenes in peppermint: a cytosolic route to its production in glandular trichome. Preparation.

2016   Koley S and Mahapatra SS. In vitro efficacy of systemic and non-systemic chemicals on the growth inhibition of Alternaria solani causing early leaf blight of tomato. International journal of scientific research, 5(5): 312-314, 2016.

2015   Koley S and Mahapatra SS. Evaluation of Culture Media for Growth Characteristics of Alternaria solani, Causing Early Blight of Tomato. Journal of plant pathology and microbiology, S1: 005, 2015.

2015   Koley S and Mahapatra SS. Studies on nutritional requirements of Alternaria solani causing early blight of tomato in Richard's broth medium. Journal of plant protection and environment, 12(1): 114-119, 2015.

2015   Koley S, Mahapatra SS and Kole PC. In vitro efficacy of bio-control agents and botanicals on the growth inhibition of Alternaria solani causing early leaf blight of tomato. International journal of bio-resource, environment and agricultural sciences, 1(3): 114-118, 2015.
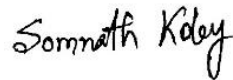
Conference participation

2018   4th Leibniz Plant Biochemistry Symposium, Germany (Participated)

2017   13th International Meeting on Biosynthesis, Function and Synthetic Biology of Isoprenoids, China (Poster presentation)

2015   11th Plant Science Student Conference, Germany (Oral talk)

Eigenständigkeitserklärung

Hiermit erkläre ich, dass diese Arbeit bisher weder bei der Naturwissenschaftlichen Fakultät I Biowissenschaften der Martin-Luther-Universität Halle-Wittenberg noch einer anderen wissenschaftlichen Einrichtung zum Zweck der Promotion vorgelegt wurde.

Darüber hinaus erkläre ich, dass ich die vorliegende Arbeit eigenständig und ohne fremde Hilfe verfasst sowie keine anderen als die im Text angegebenen Quellen und Hilfsmittel verwendet habe. Textstellen, welche aus verwendeten Werken wörtlich oder inhaltlich übernommen wurden, wurden von mir als solche kenntlich gemacht.

Ich erkläre weiterhin, dass ich mich bisher noch nie um einen Doktorgrad beworben habe.

Somnath Koley

Halle (Saale), 12.08.2019